05-4506832 pustaka.upsi.edu.my Perpustakaan Tuanku Bainun Kampus Sultan Abdul Jalil Shah PustakaTBainun ptbupsi

STRUCTURAL, INTENSITY PARAMETERS AND LUMINESCENCE ANALYSIS OF rGO-/ CNTs-COATED TELLURITE GLASS DOPED WITH ERBIUM NANOPARTICLES

05-4506832 pustaka.upsi.edu.my Perpustakaan Tuanku Bainun Kampus Sultan Abdul Jalil Shah PustakaTBainun ptbupsi

AZLINA BINTI YAHYA

UNIVERSITI PENDIDIKAN SULTAN IDRIS

2023

05-4506832 pustaka.upsi.edu.my Perpustakaan Tuanku Bainun Kampus Sultan Abdul Jalil Shah PustakaTBainun ptbupsi

05-4506832 pustaka.upsi.edu.my Perpustakaan Tuanku Bainun Kampus Sultan Abdul Jalil Shah PustakaTBainun ptbupsi

STRUCTURAL, INTENSITY PARAMETERS AND LUMINESCENCE ANALYSIS OF rGO-/ CNTs-COATED TELLURITE GLASS DOPED WITH ERBIUM NANOPARTICLES

AZLINA BINTI YAHYA

05-4506832 pustaka.upsi.edu.my Perpustakaan Tuanku Bainun Kampus Sultan Abdul Jalil Shah PustakaTBainun ptbupsi

THESIS SUBMITTED IN FULFILLMENT OF THE REQUIREMENT
FOR THE DEGREE OF DOCTOR OF PHILOSOPHY

FACULTY OF SCIENCE AND MATHEMATICS
UNIVERSITI PENDIDIKAN SULTAN IDRIS

2023

05-4506832 pustaka.upsi.edu.my Perpustakaan Tuanku Bainun Kampus Sultan Abdul Jalil Shah PustakaTBainun ptbupsi

UPSI/IPS-3/BO 32
Pind : 00 m/s: 1/1

UNIVERSITI PENDIDIKAN SULTAN IDRIS
SULTAN IDRIS EDUCATION UNIVERSITY

Please tick (√)

Project Paper	
Masters by Research	
Master by Mixed Mode	
PhD	√

INSTITUTE OF GRADUATE STUDIES

DECLARATION OF ORIGINAL WORK

This declaration is made on the 25th day of August 2023

i. Student's Declaration:

I, **AZLINA BINTI YAHYA, P20201000831, FACULTY OF SCIENCE AND MATHEMATICS** hereby declare that the work entitled **STRUCTURAL, INTENSITY PARAMETERS AND LUMINESCENCE ANALYSIS OF rGO-/CNTs-COATED TELLURITE GLASS DOPED WITH ERBIUM NANOPARTICLES** is my original work. I have not copied from any other students' work or from any other sources except where due reference or acknowledgement is made explicitly in the text, nor has any part been written for me by another person.

Azlina
Signature of the student

ii. Supervisor's Declaration:

I, **Ts. DR. MUHAMMAD NOORAZLAN BIN ABD AZIS** hereby certifies that the work entitled **STRUCTURAL, INTENSITY PARAMETERS AND LUMINESCENCE ANALYSIS OF rGO-/CNTs-COATED TELLURITE GLASS DOPED WITH ERBIUM NANOPARTICLES** was prepared by the above-named student, and was submitted to the Institute of Graduate Studies as a * ~~partial~~/full fulfillment for the conferment of **DOCTOR OF PHILOSOPHY (PHYSICS)**, and the aforementioned work, to the best of my knowledge, is the said student's work.

13/09/2023
Date

Signature of the Supervisor

DR. MUHAMMAD NOORAZLAN BIN ABD AZIS
Senior Lecturer
Faculty of Science and Mathematics
Sultan Idris Education University
35900, Tanjung Malim,
Perak, Malaysia

UPSI/IPS-3/BO 31
Pind.: 01 m/s:1/1

UNIVERSITI PENDIDIKAN SULTAN IDRIS
SULTAN IDRIS EDUCATION UNIVERSITY

INSTITUT PENGAJIAN SISWAZAH /
INSTITUTE OF GRADUATE STUDIES

BORANG PENGESAHAN PENYERAHAN TESIS/DISERTASI/LAPORAN KERTAS PROJEK
DECLARATION OF THESIS/DISSERTATION/PROJECT PAPER FORM

Tajuk / *Title*: STRUCTURAL, INTENSITY PARAMETERS AND LUMINESCENCE ANALYSIS OF rGO-/ CNTs-COATED TELLURITE GLASS DOPED WITH ERBIUM NANOPARTICLES

No. Matrik /*Matric No.*: P20201000831

Saya / *I* : AZLINA BINTI YAHYA

(Nama pelajar / *Student's Name*)

mengaku membenarkan Tesis/Disertasi/Laporan Kertas Projek (Kedoktoran/Sarjana)* ini disimpan di Universiti Pendidikan Sultan Idris (Perpustakaan Tuanku Bainun) dengan syarat-syarat kegunaan seperti berikut:-
acknowledged that Universiti Pendidikan Sultan Idris (Tuanku Bainun Library) reserves the right as follows:-

1. Tesis/Disertasi/Laporan Kertas Projek ini adalah hak milik UPSI.
   The thesis is the property of Universiti Pendidikan Sultan Idris
2. Perpustakaan Tuanku Bainun dibenarkan membuat salinan untuk tujuan rujukan dan penyelidikan.
   Tuanku Bainun Library has the right to make copies for the purpose of reference and research.
3. Perpustakaan dibenarkan membuat salinan Tesis/Disertasi ini sebagai bahan pertukaran antara Institusi Pengajian Tinggi.
   The Library has the right to make copies of the thesis for academic exchange.
4. Sila tandakan (√) bagi pilihan kategori di bawah / *Please tick (√) from the categories below:-*

☐	**SULIT/*CONFIDENTIAL***	Mengandungi maklumat yang berdarjah keselamatan atau kepentingan Malaysia seperti yang termaktub dalam Akta Rahsia Rasmi 1972. /*Contains confidential information under the Official Secret Act 1972*
☐	**TERHAD/*RESTRICTED***	Mengandungi maklumat terhad yang telah ditentukan oleh organisasi/badan di mana penyelidikan ini dijalankan. / *Contains restricted information as specified by the organization where research was done.*
☑	**TIDAK TERHAD / *OPEN ACCESS***	

azlina

(Tandatangan Pelajar/ Signature)

Tarikh: 13/09/2023

DR. MUHAMMAD NOORAZLAN BIN ABD AZIS
Senior Lecturer
Faculty of Science and Mathematics
Sultan Idris Education University
35900, Tanjung Malim,
Perak, Malaysia

(Tandatangan Penyelia / *Signature of Supervisor*)
(Nama & Cop Rasmi / *Name & Official Stamp*)

Catatan: Jika Tesis/Disertasi ini **SULIT @ TERHAD**, sila lampirkan surat daripada pihak berkuasa/organisasi berkenaan dengan menyatakan sekali sebab dan tempoh laporan ini perlu dikelaskan sebagai **SULIT** dan **TERHAD**.

Notes: If the thesis is CONFIDENTAL or RESTRICTED, please attach with the letter from the related authority/organization mentioning the period of confidentiality and reasons for the said confidentiality or restriction.

05-4506832 pustaka.upsi.edu.my Perpustakaan Tuanku Bainun Kampus Sultan Abdul Jalil Shah PustakaTBainun ptbupsi

ACKNOWLEDGEMENT

First and foremost, I would like to extend my thankfulness and greatest glory to the Almighty Allah S.W.T, for giving me the strength, good health, and blessing to pursue and complete my Ph.D. study successfully.

I would like to express my genuine appreciation to my supervisor, Ts. Dr. Muhammad Noorazlan Abd Azis for his invaluable help and tremendous encouragement throughout this study. I am most grateful for his supervision and invaluable advice, and my Ph.D. research would not have been accomplished without all the support that I have always received from him. Also, my precious thanks to my co-supervisor, Prof. Dr. Suriani Abu Bakar for her kindness and good support throughout my Ph.D. journey.

Then, I would like to expand my deepest gratitude to the Nanotechnology Research Centre's lab members, Hafizah Rajaa, Rosmanisah, and Dr. Muqoyyanah for guiding and giving me moral support to complete my Ph.D. research. Also, I would like to extend my appreciation to team members from the Centre for Research and Instrumentation Management (*i*-CRIM, UKM) including, Madam. Norhashimah Ramli, Mr. Mohamad Hasnul Naim Abd Hamid, Mr. Mohd Riduan Mt Said, and Tc. Mohamad Sazuan Sahrom, assistant science officer, Mr. Mohd Shukri Abd. Aziz from FESEM Laboratory, Chemistry Department, Faculty of Science, UM, Dr. Abdul Hafidz Yusoff from Faculty of Bioengineering and Technology, Jeli Campus, UMK, Ts. Dr. Mohd Firdaus Malek from NANO-SciTech Centre (NST), UiTM, Madam Radiah Idris, and other staff members from the Chemistry Department, Faculty of Science and Mathematics, UPSI for helping me in my research analyses. Besides, many thanks and appreciation to my friend, Dr. Nurul Hila, and members from UiTM, UTM, and USM for their support and prayers. May Allah S.W.T grants all of you great success.

My sincere appreciation goes to the Ministry of Education for providing Skim Geran Penyelidikan Fundamental (FRGS) Fasa 1/2018 (Grant code: 2019-0006-102-02) and I am so grateful for giving me an opportunity to carry out the research. Last but not least, a special credit and appreciation to my beloved parents, Yahya Abdullah and Ku Zainab Ku Ain, and also family members, for their love, prayers, sacrifices, and encouragement during my research period. Lastly, I offer my regards and blessings to all of those who supported me in any aspect to complete this thesis successfully.

05-4506832 pustaka.upsi.edu.my Perpustakaan Tuanku Bainun Kampus Sultan Abdul Jalil Shah PustakaTBainun ptbupsi

05-4506832 pustaka.upsi.edu.my Perpustakaan Tuanku Bainun Kampus Sultan Abdul Jalil Shah PustakaTBainun ptbupsi

ABSTRACT

This study aimed to improve the optical properties of reduced graphene oxide- and carbon nanotubes-coated tellurite glass doped with erbium oxide nanoparticles denoted as ZBTEr(NPs)-rGO and ZBTEr(NPs)-CNTs. Two sets of glass series were synthesized by melt-quenched technique with chemical composition of $(0.47(1-y))TeO_2+(0.2(1-y))B_2O_3+(0.29(1-y))+ZnO+Er_2O_3(y)$ wherein, y = 0.005, 0.01, 0.02, 0.03, 0.04, and 0.05 mol% Er_2O_3 nanoparticles. Tellurite-based glass was deposited with rGO and CNTs onto the glass surfaces by spray-coated technique. The physical, morphological, structural, and optical properties of ZBTEr(NPs)-rGO and ZBTEr(NPS)-CNTs glasses were characterized via densimeter, scanning electron microscopy (SEM), energy dispersive X-ray (EDX), transmission electron microscopy (TEM), X-ray diffraction (XRD), Fourier transform-infrared (FT-IR), micro-Raman spectroscopy, ultraviolet-visible (UV-Vis) spectrophotometer, and photoluminescence. SEM micrographs revealed morphological structures of rGO and CNTs on the glass surfaces meanwhile, EDX spectra disclosed elemental composition of rGO and CNTs. TEM images proved existence of Er(NPs) with average size (~23.53 nm) in glass matrix. XRD pattern verified amorphous nature of glasses. FT-IR spectra evaluated the presence of non-bridging oxygens (NBOs) with TeO_4, TeO_3, and BO_3 functional groups meanwhile, Raman spectra demonstrated good quality of rGO and CNTs. The refractive index value was increased (2.402-2.775) for ZBTEr(NPs)-rGO meanwhile, (2.432-2.542) for ZBTEr(NPs)-CNTs. The optical bandgap energy value was improved (1.913-2.931 eV) for ZBTEr(NPs)-rGO and (2.513-2.875 eV) ZBTEr(NPs)-CNTs meanwhile, non-linear trend of Urbach energy (0.118-0.408 eV) for ZBTEr(NPs)-rGO and (0.158-0.375 eV) for ZBTEr(NPs)-CNTs. Judd-Ofelt's intensity parameters showed $\Omega_2>\Omega_6>\Omega_4$ trend for ZBTEr(NPs)-rGO whilst, $\Omega_2>\Omega_4>\Omega_6$ trend for ZBTEr(NPs)-CNTs. Radiative parameters and branching ratio proved $^2H_{11/2}\rightarrow{}^4I_{15/2}$ transition showed highest radiative transition value, resulting in a strong green emission. Luminescence spectra exhibited two emission peaks assigned to $^2H_{11/2}\rightarrow{}^4I_{15/2}$ and $^4S_{3/2}\rightarrow{}^4I_{15/2}$ transitions. In conclusion, the rGO and CNTs deposition enhanced the optical properties of glass materials. Implication of this study offers a new milestone in the glass coatings field for improving current fiber optics.

05-4506832 pustaka.upsi.edu.my Perpustakaan Tuanku Bainun Kampus Sultan Abdul Jalil Shah PustakaTBainun ptbupsi

05-4506832 pustaka.upsi.edu.my Perpustakaan Tuanku Bainun Kampus Sultan Abdul Jalil Shah PustakaTBainun ptbupsi

STRUKTUR, PARAMETER KEAMATAN, DAN ANALISIS PENDARCAHAYAAN BAGI KACA TELLURIT DISALUT rGO/CNTs TERDOP DENGAN NANOZARAH ERBIUM

ABSTRAK

Kajian ini bertujuan untuk meningkatkan sifat optik kaca tellurit disalut grafin oksida terkurang (rGO)/nanotiub karbon (CNTs) terdop dengan nanozarah erbium oksida (ZBTEr(NPs)-rGO/-CNTs). Dua set siri kaca berasaskan tellurit telah disintesis dengan teknik lebur lindap konvensional berdasarkan komposisi kimia $(0.47(1-y))TeO_2+(0.2(1-y))B_2O_3+(0.29(1-y))+ZnO+Er_2O_3(y)$ iaitu, y = 0.005, 0.01, 0.02, 0.03, 0.04, and 0.05 mol% nanozarah Er_2O_3. Kaca berasaskan tellurit telah disalut dengan rGO dan CNTs atas permukaan kaca dengan teknik salutan semburan. Sifat fizikal, morfologi, struktur, dan optik bagi kaca ZBTEr(NPs)-rGO/-CNTs dicirikan dengan menggunakan densimeter, mikroskop pengimbasan elektron (SEM), penyebaran tenaga sinar-X (EDX), mikroskop penghantaran elektron (TEM), pembelauan sinar-X (XRD), transformasi Fourier inframerah (FT-IR), spektroskopi mikro-Raman, spektrofotometer cahaya nampak ultralembayung (UV-Vis), dan kefotopendarcahayaan. Mikrograf SEM mendedahkan struktur morfologi rGO dan CNTs pada permukaan kaca manakala, spektrum EDX mendedahkan komposisi unsur rGO dan CNTs. Imej TEM membuktikan kewujudan Er(NPs) dengan saiz purata (~23.53 nm) dalam matriks kaca. Corak XRD megesahkan sifat amorfus bagi kaca. Spektrum FT-IR mengesahkan kehadiran oksigen bukan penitian (NBO) dengan kumpulan berfungsi TeO_4, TeO_3, dan BO_3 manakala, spektrum Raman menunjukkan kualiti rGO dan CNTs yang baik. Nilai indeks biasan meningkat (2.402-2.775) bagi ZBTEr (NPs)-rGO manakala, (2.432-2.542) bagi ZBTEr(NPs)-CNTs. Nilai tenaga jurang jalur optik meningkat (1.913-2.931 eV) bagi ZBTEr(NPs)-rGO dan (2.513-2.875 eV) bagi ZBTEr(NPs)-CNTs manakala, trend tidak linear tenaga Urbach (0.118-0.408 eV) bagi ZBTEr (NPs)-rGO dan (0.158-0.375 eV) bagi ZBTEr(NPs)-CNTs. Parameter keamatan Judd-Ofelt menunjukkan trend $\Omega_2>\Omega_6>\Omega_4$ bagi ZBTEr(NPs)-rGO manakala, trend $\Omega_2>\Omega_4>\Omega_6$ bagi ZBTEr(NPs)-CNTs. Parameter sinaran dan nisbah percabangan membuktikan peralihan $^2H_{11/2}\rightarrow{}^4I_{15/2}$ mempunyai nilai peralihan sinaran tertinggi yang menghasilkan pancaran hijau yang kuat. Spektrum pendarcahayaan menunjukkan dua puncak pancaran yang diberikan kepada peralihan $^2H_{11/2}\rightarrow{}^4I_{15/2}$ dan $^4S_{3/2}\rightarrow{}^4I_{15/2}$. Kesimpulannya, salutan rGO/CNTs meningkatkan sifat optik bahan kaca. Implikasi kajian ini adalah menawarkan pencapaian yang baru dalam bidang salutan kaca untuk penambahbaikan gentian optik semasa.

05-4506832 pustaka.upsi.edu.my Perpustakaan Tuanku Bainun Kampus Sultan Abdul Jalil Shah PustakaTBainun ptbupsi

05-4506832 pustaka.upsi.edu.my Perpustakaan Tuanku Bainun Kampus Sultan Abdul Jalil Shah PustakaTBainun ptbupsi

TABLE OF CONTENTS

		Page
DECLARATION OF ORIGINAL WORK		ii
DECLARATION OF THESIS		iii
ACKNOWLEDGEMENT		iv
ABSTRACT		v
ABSTRAK		vi
TABLE OF CONTENTS		vii
LIST OF TABLES		xiv
LIST OF FIGURES		xix
LIST OF SYMBOLS AND ACRONYMS		xxvii
LIST OF APPENDICES		xxx
CHAPTER 1	**INTRODUCTION**	
	1.1 Introduction	1
	1.2 Research Background	2
	1.3 Research Problems	8
	1.4 Research Objectives	11
	1.5 Scope and Limitations of Study	12
	1.6 Significance of Research	14
	1.7 Thesis Overview	15

05-4506832 pustaka.upsi.edu.my Perpustakaan Tuanku Bainun Kampus Sultan Abdul Jalil Shah PustakaTBainun ptbupsi

05-4506832 pustaka.upsi.edu.my Perpustakaan Tuanku Bainun Kampus Sultan Abdul Jalil Shah PustakaTBainun ptbupsi

CHAPTER 2 LITERATURE REVIEW

2.1 Introduction 17

2.2 Tellurite-based Glass Structure 18

2.3 Erbium Nanoparticles Rare-earth Ions (REIs) Doped Glass System 22

2.4 Carbon-based Nanomaterials (CBNs) 25

2.4.1 Overview of Graphene 26

2.4.2 Graphene Oxide and Atomic Structures 32

2.5 Properties of Graphene Oxide and Reduced Graphene Oxide 39

2.5.1 Optical Properties 39

2.5.2 Thermal Properties 41

2.6 Synthesis Methods of Graphene Oxide and Reduced Graphene Oxide 42

2.6.1 Chemical Oxidation Process 44

2.6.1.1 Brodie and Staudenmaier Method 44

2.6.1.2 Hummers and Modified Hummers Method 44

2.6.2 Chemical Reduction Process 46

2.6.2.1 Chemical Reagent Reduction 46

2.6.2.2 Thermal Annealing for Reduction 49

2.7 Overview of Carbon Nanotubes 51

2.7.1 Structures of Carbon Nanotubes 51

05-4506832 pustaka.upsi.edu.my Perpustakaan Tuanku Bainun Kampus Sultan Abdul Jalil Shah PustakaTBainun ptbupsi

05-4506832 pustaka.upsi.edu.my Perpustakaan Tuanku Bainun Kampus Sultan Abdul Jalil Shah PustakaTBainun ptbupsi

2.8	Properties of Carbon Nanotubes	56
	2.8.1 Optical and Electronic Properties	56
	2.8.2 Thermal Properties	57
2.9	Synthesis Methods of Carbon Nanotubes	58
	2.9.1 Arc Discharge	59
	2.9.2 Chemical Vapor Deposition (CVD)	60
2.10	Physical Properties Characterization	62
	2.10.1 Density and Molar Volume	62
	2.10.2 Rare-earth Ion Concentration, Inter-ionic Distance, and Polaron Radius	64
	2.10.3 Oxygen Packing Density and Field Strength	66
2.11	Morphological Properties Characterization	67
2.12	Structural Network Arrangement and Interatomic Bonding Characterization	69
2.13	Optical Properties Characterization	72
	2.13.1 Optical Absorption Spectra	72
	2.13.2 Optical Bandgap Energy	76
	2.13.3 Urbach Energy	79
	2.13.4 Refractive Index	81
	2.13.5 Reflection Loss, Transmission Coefficient, and Dielectric Constant	83
	2.13.6 Electronegativity	84
	2.13.7 Judd-Ofelt's Theoretical Study	87
	2.13.8 Photoluminescence	92

05-4506832 pustaka.upsi.edu.my Perpustakaan Tuanku Bainun Kampus Sultan Abdul Jalil Shah PustakaTBainun ptbupsi

05-4506832 pustaka.upsi.edu.my Perpustakaan Tuanku Bainun Kampus Sultan Abdul Jalil Shah PustakaTBainun ptbupsi

2.14 Applications on Glass Fiber/ GO/ rGO/ CNTs-coated Glass 99

2.15 Summary 104

CHAPTER 3 RESEARCH METHODOLOGY

3.1 Introduction 105

3.2 Glass Fabrication 106

3.2.1 Melt-quenching Technique 106

3.3 Synthesis of Graphene Oxide and Reduced Graphene Oxide 110

3.3.1 Electrochemical Exfoliation Method 110

3.3.2 Reduction of GO to rGO 111

3.4 Dispersion of Carbon Nanotubes 112

3.5 Glass Deposition Process 113

3.5.1 Spray Coating Technique 113

3.6 Physical Properties Characterization 115

3.6.1 Density and Molar Volume Measurement 115

3.7 Structural Properties Characterization 115

3.7.1 Field Emission Scanning Electron Microscopy and Energy Dispersive X-ray 115

3.7.2 High Resolution Transmission Electron Microscopy 117

3.7.3 X-ray Diffraction 117

3.7.4 Fourier Transform Infrared Spectroscopy 119

3.7.5 Micro-Raman Spectroscopy 120

05-4506832 pustaka.upsi.edu.my Perpustakaan Tuanku Bainun Kampus Sultan Abdul Jalil Shah PustakaTBainun ptbupsi

05-4506832 pustaka.upsi.edu.my Perpustakaan Tuanku Bainun Kampus Sultan Abdul Jalil Shah PustakaTBainun ptbupsi

3.8 Optical Properties Characterization 121

3.8.1 Ultraviolet-Visible Spectroscopy 121

3.8.2 Photoluminescence 122

3.9 Brief Description of Experimental Work 123

3.10 Summary 126

CHAPTER 4 RESULTS AND DISCUSSION

4.1 Introduction 127

4.2 Physical and Structural Properties of Tellurite Glass Doped with Erbium Nanoparticles (ZBTEr (NPs)-uncoated) 128

4.2.1 Density and Molar Volume 128

4.2.2 Erbium Inter-ionic Distance, Polaron Radius, Field Strength, and Oxygen Packing Density 131

4.2.3 X-ray Diffraction of ZBTEr (NPs)-uncoated Glass 136

4.2.4 Fourier Transform Infrared Analysis of ZBTEr (NPs)-uncoated Glass 137

4.2.5 High Resolution Transmission Electron Microscopy Analysis of ZBTEr (NPs)-uncoated Glass 141

4.3 Structural Properties of Reduced Graphene Oxide-coated Tellurite Glass Doped with Erbium Nanoparticles (ZBTEr (NPs)-rGO) 143

4.3.1 Field Emission Scanning Electron Microscopy and Energy Dispersive X-ray Analyses of ZBTEr (NPs)-rGO Glass 143

4.3.2 Micro-Raman Analysis of rGO 153

05-4506832 pustaka.upsi.edu.my Perpustakaan Tuanku Bainun Kampus Sultan Abdul Jalil Shah PustakaTBainun ptbupsi

05-4506832 pustaka.upsi.edu.my Perpustakaan Tuanku Bainun Kampus Sultan Abdul Jalil Shah PustakaTBainun ptbupsi

4.4	Optical Properties of Reduced Graphene Oxide-coated Tellurite Glass Doped with Erbium Nanoparticles (ZBTEr (NPs)-rGO)		157
	4.4.1	Optical Absorption Spectra	157
	4.4.2	Optical Bandgap Energy	161
	4.4.3	Urbach Energy	168
	4.4.4	Refractive Index	172
	4.4.5	Reflection Loss, Transmission Coefficient, and Dielectric Constant	176
	4.4.6	Electronegativity	178
	4.4.7	Judd-Ofelt's Analysis	185
	4.4.8	Luminescence Analysis	200
4.5	Structural Properties of Carbon Nanotubes-coated Tellurite Glass Doped with Erbium Nanoparticles (ZBTEr (NPs)-CNTs)		204
	4.5.1	Field Emission Scanning Electron Microscopy and Energy Dispersive X-ray Analyses of ZBTEr (NPs)-CNTs)	204
	4.5.5	Micro-Raman Analysis of CNTs	213
4.6	Optical Properties of Carbon Nanotubes-coated Tellurite Glass Doped with Erbium Nanoparticles (ZBTEr (NPs)-CNTs)		215
	4.6.1	Optical Absorption Spectra	215
	4.6.2	Optical Bandgap Energy	219
	4.6.3	Urbach Energy	225
	4.6.4	Refractive Index	230
	4.6.5	Reflection Loss, Transmission Coefficient, and Dielectric Constant	234

05-4506832 pustaka.upsi.edu.my Perpustakaan Tuanku Bainun Kampus Sultan Abdul Jalil Shah PustakaTBainun ptbupsi

05-4506832 pustaka.upsi.edu.my Perpustakaan Tuanku Bainun Kampus Sultan Abdul Jalil Shah PustakaTBainun ptbupsi

4.6.6 Electronegativity 236

4.6.7 Judd-Ofelt's Analysis 243

4.6.8 Luminescence Analysis 258

4.7 Comparative Studies of the ZBTEr (NPs)-rGO and ZBTEr (NPs)-CNTs Glasses 263

4.7.1 Optical Properties Characterization 263

4.8 Summary 271

CHAPTER 5 CONCLUSION AND FUTURE WORKS

5.1 Introduction 273

5.2 Conclusion 274

5.3 Suggestions for Future Outlook 280

REFERENCES 282

APPENDICES 310

05-4506832 pustaka.upsi.edu.my Perpustakaan Tuanku Bainun Kampus Sultan Abdul Jalil Shah PustakaTBainun ptbupsi
05-4506832 pustaka.upsi.edu.my Perpustakaan Tuanku Bainun Kampus Sultan Abdul Jalil Shah PustakaTBainun ptbupsi

05-4506832 pustaka.upsi.edu.my Perpustakaan Tuanku Bainun Kampus Sultan Abdul Jalil Shah PustakaTBainun ptbupsi

LIST OF TABLES

Table No.		Pages
1.1	Summary of the research problems and research questions that relate to this study	10
2.1	The comparison between SWCNTs and MWCNTs (Iijima & Ichihashi, 1993)	55
2.2	Summarization of the previous studies on tellurite-based (uncoated) glass and glass fiber/GO/rGO/CNTs-coated glass	102
3.1	The details of high purity raw chemical powders	107
4.1	Density and molar volume with the different Er_2O_3 nanoparticles concentration for ZBTEr (NPs)-uncoated glasses	131
4.2	Erbium ion concentration (N), erbium inter-ionic distance (R_i), polaron radius (R_P), erbium field strength (F), and oxygen packing density (OPD) with the different Er_2O_3 nanoparticles concentration for ZBTEr (NPs)-uncoated glasses	135
4.3	Assignments of transmission bands of ZBTEr (NPs)-uncoated glasses	140
4.4	The weight and atomic percentages, % of elements content with the different spectrum of rGO solution sample	152
4.5	Micro-Raman peaks position and I_D/I_G ratio of GO and rGO samples	156
4.6	Comparison of optical bandgap energy (E_{opt}) value between ZBTEr (NPs)-uncoated and ZBTEr (NPs)-rGO glasses	163

05-4506832 pustaka.upsi.edu.my Perpustakaan Tuanku Bainun Kampus Sultan Abdul Jalil Shah PustakaTBainun ptbupsi

05-4506832 pustaka.upsi.edu.my Perpustakaan Tuanku Bainun Kampus Sultan Abdul Jalil Shah PustakaTBainun ptbupsi

4.7	Comparison of Urbach energy (ΔE) value between ZBTEr (NPs)-uncoated and ZBTEr (NPs)-rGO glasses	171
4.8	Comparison of refractive index (n) values between ZBTEr (NPs)-uncoated and ZBTEr (NPs)-rGO glasses	175
4.9	Variation of reflection loss (R_L), transmission coefficient (T), and dielectric constant (ϵ) for ZBTEr (NPs)-rGO glasses	177
4.10	Pauling electronegativity (χ_i), average electronegativity (χ_{av}), and average electronegativity-based oxide ion polarizability α_0^{2-} (χ_{nav}), n = 1, 2, 3 of the ZBTEr (NPs)-rGO glasses	178
4.11	Average electronegativity (χ_{av}), average electronegativity-based oxide ion polarizability, α_0^{2-} (χ_{nav}), n = 1, 2, 3, and refractive index-based oxide ion polarizability, α_0^{2-} (n) of ZBTEr (NPs)-rGO glasses	180
4.12	Optical energy bandgap-based optical electronegativity $\Delta\chi^*(E_{opt})$, refractive index-based optical electronegativity $\Delta\chi^*$ (n), energy bandgap optical electronegativity-based oxide ion polarizability α_0^{2-} ($\Delta\chi^*(E_{opt})$), and refractive index optical electronegativity-based oxide ion polarizability $\alpha_0^{2-}(\Delta\chi^*(n))$ of ZBTEr (NPs)-rGO glasses	182
4.13	The experimental ($f_{exp} \times 10^{-6}$) and calculated oscillator strength ($f_{cal} \times 10^{-6}$) along with the root mean square deviation ($\delta_{rms} \times 10^{-6}$) of ZBTEr (NPs)-rGO glasses	187
4.14	Judd-Ofelt's intensity parameters ($\Omega_\lambda \times 10^{-20}$ cm^2) and spectroscopic quality factor, $\chi = \frac{\Omega_4}{\Omega_6}$ of ZBTEr (NPs)-rGO glasses	191
4.15	The magnetic dipole and electric dipole radiative transition probabilities (A_{MD}, A_{ED}), emission branching ratio (β_R), and radiative lifetime (t_r) of 0.005 mol% ZBTEr (NPs)-rGO glass	194

05-4506832 pustaka.upsi.edu.my Perpustakaan Tuanku Bainun Kampus Sultan Abdul Jalil Shah PustakaTBainun ptbupsi

05-4506832 pustaka.upsi.edu.my Perpustakaan Tuanku Bainun Kampus Sultan Abdul Jalil Shah PustakaTBainun ptbupsi

05-4506832 pustaka.upsi.edu.my Perpustakaan Tuanku Bainun Kampus Sultan Abdul Jalil Shah PustakaTBainun ptbupsi

4.16	The magnetic dipole and electric dipole radiative transition probabilities (A_{MD}, A_{ED}), emission branching ratio (β_R), and radiative lifetime (t_r) of 0.01 mol% ZBTEr (NPs)-rGO glass	195
4.17	The magnetic dipole and electric dipole radiative transition probabilities (A_{MD}, A_{ED}), emission branching ratio (β_R), and radiative lifetime (t_r) of 0.02 mol% ZBTEr (NPs)-rGO glass	196
4.18	The magnetic dipole and electric dipole radiative transition probabilities (A_{MD}, A_{ED}), emission branching ratio (β_R), and radiative lifetime (t_r) of 0.03 mol% ZBTEr (NPs)-rGO glass	197
4.19	The magnetic dipole and electric dipole radiative transition probabilities (A_{MD}, A_{ED}), emission branching ratio (β_R), and radiative lifetime (t_r) of 0.04 mol% ZBTEr (NPs)-rGO glass	198
4.20	The magnetic dipole and electric dipole radiative transition probabilities (A_{MD}, A_{ED}), emission branching ratio (β_R), and radiative lifetime (t_r) of 0.05 mol% ZBTEr (NPs)-rGO glass	199
4.21	The weight and atomic percentages, % of elements content with the different spectrum of CNTs solution sample	213
4.22	Micro-Raman peaks position and I_D/I_G ratio of CNTs sample	215
4.23	Comparison of optical bandgap energy (E_{opt}) value between ZBTEr (NPs)-uncoated and ZBTEr (NPs)-CNTs glasses	222
4.24	Comparison of Urbach energy (ΔE) value between ZBTEr (NPs)-uncoated and ZBTEr (NPs)-CNTs glasses	229
4.25	Comparison of refractive index (n) values between ZBTEr (NPs)-uncoated and ZBTEr (NPs)-CNTs glasses	233

05-4506832 pustaka.upsi.edu.my Perpustakaan Tuanku Bainun Kampus Sultan Abdul Jalil Shah PustakaTBainun ptbupsi

05-4506832 pustaka.upsi.edu.my Perpustakaan Tuanku Bainun Kampus Sultan Abdul Jalil Shah PustakaTBainun ptbupsi

4.26	Variation of reflection loss (R_L), transmission coefficient (T), and dielectric constant (ϵ) for ZBTEr (NPs)-CNTs glasses	235
4.27	Pauling electronegativity (χ_i), average electronegativity (χ_{av}), and average electronegativity-based oxide ion polarizability α_0^{2-} (χ_{nav}), n = 1, 2, 3 of the ZBTEr (NPs)-CNTs glasses	237
4.28	Average electronegativity (χ_{av}), average electronegativity-based oxide ion polarizability, α_0^{2-} (χ_{nav}), n = 1, 2, 3, and refractive index-based oxide ion polarizability, α_0^{2-} (n) of ZBTEr (NPs)-CNTs glasses	238
4.29	Optical energy bandgap-based optical electronegativity $\Delta\chi^*(E_{opt})$, refractive index-based optical electronegativity $\Delta\chi^*$ (n), energy bandgap optical electronegativity-based oxide ion polarizability $\alpha_0^{2-}(\Delta\chi^*(E_{opt}))$, and refractive index optical electronegativity-based oxide ion polarizability $\alpha_0^{2-}(\Delta\chi^*(n))$ of ZBTEr (NPs)-CNTs glasses	240
4.30	The experimental ($f_{exp} \times 10^{-6}$) and calculated oscillator strength ($f_{cal} \times 10^{-6}$) along with the root mean square deviation ($\delta_{rms} \times 10^{-6}$) of ZBTEr (NPs)-CNTs glasses	245
4.31	Judd-Ofelt's intensity parameter ($\Omega_\lambda \times 10^{-20}$ cm^2) and spectroscopic quality factor $\chi = \frac{\Omega_4}{\Omega_6}$ of ZBTEr (NPs)-CNTs glasses	249
4.32	The magnetic dipole and electric dipole radiative transition probabilities (A_{MD}, A_{ED}), emission branching ratio (β_R), and radiative lifetime (t_r) of 0.005 mol% ZBTEr (NPs)-CNTs glass	252
4.33	The magnetic dipole and electric dipole radiative transition probabilities (A_{MD}, A_{ED}), emission branching ratio (β_R), and radiative lifetime (t_r) of 0.01 mol% ZBTEr (NPs)-CNTs glass	253
4.34	The magnetic dipole and electric dipole radiative transition probabilities (A_{MD}, A_{ED}), emission branching ratio (β_R), and radiative lifetime (t_r) of 0.02 mol% ZBTEr (NPs)-CNTs glass	254

05-4506832 pustaka.upsi.edu.my Perpustakaan Tuanku Bainun Kampus Sultan Abdul Jalil Shah PustakaTBainun ptbupsi

05-4506832 pustaka.upsi.edu.my Perpustakaan Tuanku Bainun Kampus Sultan Abdul Jalil Shah PustakaTBainun ptbupsi

4.35	The magnetic dipole and electric dipole radiative transition probabilities (A_{MD}, A_{ED}), emission branching ratio (β_R), and radiative lifetime (t_r) of 0.03 mol% ZBTEr (NPs)-CNTs glass	255
4.36	The magnetic dipole and electric dipole radiative transition probabilities (A_{MD}, A_{ED}), emission branching ratio (β_R), and radiative lifetime (t_r) of 0.04 mol% ZBTEr (NPs)-CNTs glass	256
4.37	The magnetic dipole and electric dipole radiative transition probabilities (A_{MD}, A_{ED}), emission branching ratio (β_R), and radiative lifetime (t_r) of 0.05 mol% ZBTEr (NPs)-CNTs glass	257
4.38	The summarized results of optical bandgap energy, E_{opt} and refractive index, *n* for ZBTEr (NPs)-rGO, ZBTEr (NPs)-CNTs, and previous studies	267
4.39	The summarized results of Judd-Ofelt's intensity parameters, Ω_t (t = 2, 4, 6) for ZBTEr (NPs)-rGO, ZBTEr (NPs)-CNTs, and previous studies	269

05-4506832 pustaka.upsi.edu.my Perpustakaan Tuanku Bainun Kampus Sultan Abdul Jalil Shah PustakaTBainun ptbupsi

05-4506832 pustaka.upsi.edu.my Perpustakaan Tuanku Bainun Kampus Sultan Abdul Jalil Shah PustakaTBainun ptbupsi

LIST OF FIGURES

Figure No.		Pages
1.1	Basic atomic structure of an amorphous silica (a) Schematic representation of two tetrahedra displaying nominal distance between neighboring Si-O and O-O atoms, and a bridging oxygen (BO) between two tetrahedra and (b) Subsection of an amorphous silica simulation which shows the random arrangement of silica tetrahedral unit (Lunt et al., 2018)	4
2.1	Tellurite-based glass structures found in the x = 0.20, x = 0.33, and x = 0.50 sodium tellurite crystals. Noticed that each structural unit is identified in term of Q_m^n, whereby m = 3, 4 and shows the total number of oxygens bonded to the tellurium atom, and $n = 0-4$ is denoted as the number of bridging oxygen (BO) bonded to the tellurium atom (Mclaughlin et al., 2000)	19
2.2	Ball and stick representation of structural units existing in tellurite glass system. (a) Trigonal bipyramid, TeO_4, (b) Distorted trigonal bipyramid, TeO_{3+1}, and (c) Trigonal pyramid, TeO_3 (Manning et al., 2012)	21
2.3	Basic vectors in the hexagonal lattice of graphene with the corresponding Brillouin zone (Dubois et al., 2009)	27
2.4	Graphitic forms of carbon family materials consist of (a) 0-D Buckyballs of fullerene, (b) 1-D Roll of carbon nanotube, and (c) 3-D Stack of graphite (Geim & Novoselov, 2007)	28
2.5	The electronic bands of π and π^* with respect to valence and the other of conduction bands at the six corners in the Dirac cones which meet at the Dirac points and indicate that zero-band gap of graphene (Dubois et al., 2009)	30
2.6	The schematic representation of different graphene-based nanomaterials including, (a) Single-layer graphene, (b)	35

05-4506832 pustaka.upsi.edu.my Perpustakaan Tuanku Bainun Kampus Sultan Abdul Jalil Shah PustakaTBainun ptbupsi

05-4506832 pustaka.upsi.edu.my Perpustakaan Tuanku Bainun Kampus Sultan Abdul Jalil Shah PustakaTBainun ptbupsi

	Multilayer graphene sheets, (c) GO, (d) rGO, (e) GOQD, and (f) GQD (Cheng et al., 2017)	
2.7	Schematic representation of (a) lattice structure and corresponding energy band diagrams of graphene, GO, and rGO; and electronic transitions in (b) GO and (c) rGO (Abid et al., 2018)	37
2.8	The development timeline of graphene history (Dreyer et al., 2010)	38
2.9	(a) The π orbitals of a C = C bond, (b) The π* orbitals of a C = C bond, and (c) Energy diagram of π, π*, and *n* orbitals and transitions (Naumov, 2017)	40
2.10	Schematic illustration of graphene synthesis methods and 'top-down' and 'bottom-up' graphene synthesis (Edwards & Coleman, 2013; Lee et al., 2018)	43
2.11	Schematic representation of common methods used to synthesize the GO (Marcano et al., 2010)	45
2.12	Schematic representation of (a) formation of SWCNTs by rolling of a graphene sheet along lattice vectors which leads to armchair, zigzag, and chiral tubes (b) the three forms of CNTs (Madani et al., 2013)	54
2.13	Schematic diagram of an arc-discharge set up (Arora & Sharma, 2014)	60
2.14	Schematic representation of CVD process (Zaytseva & Neumann, 2016)	61
2.15	Schematic diagram of TEM instrument	68
2.16	Schematic diagram of Bragg diffraction from the lattice plane when subjected to X-rays	70
2.17	Schematic illustration in states of conduction and valence bands (Morigaki & Ogihara, 2006)	73
2.18	Schematic illustration of the photon emission processes (a) direct and (b) indirect bandgap semiconductors (Sun, 2010)	77

05-4506832 pustaka.upsi.edu.my Perpustakaan Tuanku Bainun Kampus Sultan Abdul Jalil Shah PustakaTBainun ptbupsi

05-4506832 pustaka.upsi.edu.my Perpustakaan Tuanku Bainun Kampus Sultan Abdul Jalil Shah PustakaTBainun ptbupsi

2.19	Flow diagram of Judd-Ofelt's intensity parameters calculation	91
2.20	Schematic illustration of photoluminescence band diagram (McSherry et al., 2004)	93
2.21	Schematic diagram of energy transfer and exchange interaction between two ions via Coulomb interaction (Ronda, 2007)	97
2.22	Schematic diagram of cross-relaxation between two Tb^{3+} ions (Ronda, 2007)	98
3.1	Schematic representation for synthesis and deposition of rGO and CNTs onto tellurite-based glass surfaces	108
3.2	Flow diagram of glass fabrication and deposition process for ZBTEr (NPs)-rGO and ZBTEr (NPs)-CNTs glasses	109
3.3	Experimental set up to synthesize GO via electrochemical exfoliation technique	110
3.4	Experimental set up for reduction process of GO to rGO	111
3.5	Experimental set up to disperse the MWCNTs	112
3.6	Experimental procedure of rGO-coated and CNTs-coated glass samples via spray coating technique	113
3.7	Schematic diagram of rGO-coated and CNTs-coated glass via spray coating technique	114
3.8	Experimental set up of the annealing process for rGO-coated and CNTs-coated glass samples via 2-zone tube furnace	114
3.9	FESEM was used to investigate the microstructure surfaces onto the rGO-coated and CNTs-coated glasses	116
3.10	XRD measurement (Bruker, D2 Phaser) used for investigation of the amorphous nature of rGO- and CNTs-coated glass samples	118
3.11	Micro-Raman spectroscopy was used to identify the nature of defects in GO, rGO, and CNTs samples	121

05-4506832 pustaka.upsi.edu.my Perpustakaan Tuanku Bainun Kampus Sultan Abdul Jalil Shah PustakaTBainun ptbupsi

05-4506832 pustaka.upsi.edu.my Perpustakaan Tuanku Bainun Kampus Sultan Abdul Jalil Shah PustakaTBainun ptbupsi

3.12	UV-Vis spectrophotometer (The Cary 5000) was applied to analyze the optical absorption spectra of rGO-coated and CNTs-coated tellurite glass samples	122
3.13	Photoluminescence (PL) spectrometer was used to determine the optical emission characterization of rGO- and CNTs-coated tellurite glass samples	123
3.14	Research flow chart of overall experimental study	125
4.1	Variation of density and molar volume as a function of Er_2O_3 nanoparticles concentration of the ZBTEr (NPs)-uncoated glass	130
4.2	Variation of erbium ion concentration (N), erbium inter-ionic distance (R_i), and polaron radius (R_p) as a function of Er_2O_3 nanoparticles concentration for ZBTEr (NPs)-uncoated glasses	134
4.3	Variation of oxygen packing density (OPD) and field strength (F) as a function of Er_2O_3 nanoparticles concentration for ZBTEr (NPs)-uncoated glasses	134
4.4	XRD spectra of ZBTEr (NPs)-uncoated glasses	136
4.5	FT-IR spectra of ZBTEr (NPs)-uncoated glasses	139
4.6	TEM images of the ZBTEr (NPs)-rGO glass matrix displaying Er (NPs) distribution at 0.05 mol% Er_2O_3 NPs concentration with the magnification of 150 K X	142
4.7	The possible mechanism of growth of nanoparticles in the ZBTEr (NPs)-rGO glass matrix system whereby, (a) stage 1 indicates the assembly of differently sized particles, (b) stage 2 shows the particles exchange into atoms to form the bigger particles, and (c) stage 3 presents the formation of a bigger particle through Oswald's ripening effect	143
4.8	SEM micrographs of the ZBTEr (NPs)-rGO glass showing the different of rGO structures at 0.03 mol% Er_2O_3 nanoparticles concentration with the magnification of (a) 50 K X, (b) - (c) 30 K X, and (d) 70 K X	147
4.9	Schematic illustration of rGO layer-coated onto the ZBTEr (NPs) glass surfaces	148

05-4506832 pustaka.upsi.edu.my Perpustakaan Tuanku Bainun Kampus Sultan Abdul Jalil Shah PustakaTBainun ptbupsi

05-4506832 pustaka.upsi.edu.my Perpustakaan Tuanku Bainun Kampus Sultan Abdul Jalil Shah PustakaTBainun ptbupsi

4.10	The EDX spectra with supported microstructure images of the ZBTEr (NPs)-rGO glass surfaces followed by two different regions at (a) 25 μm and (b) 10 μm	150
4.11	The EDX elemental mappings of (a) carbon (C), (b) nitrogen (N), (c) oxygen (O), (d) sodium (Na), and (e) sulphur (S) with the magnification of 20 K X	151
4.12	Micro-Raman spectra of GO and rGO with supported microstructure image of the ZBTEr (NPs)-rGO glass surfaces at 50 μm	156
4.13	Optical absorption spectra of ZBTEr (NPs)-rGO glasses	160
4.14	Optical absorption spectra of ZBTEr (NPs)-uncoated glasses	160
4.15	Tauc's plot of $(\alpha\hbar\omega)^{1/2}$ against photon energy, $\hbar\omega$ of ZBTEr (NPs)-rGO glasses	162
4.16	Variation of optical bandgap energy as a function of Er_2O_3 nanoparticles concentration for ZBTEr (NPs)-uncoated and ZBTEr (NPs)-rGO glasses	162
4.17	The possible mechanism of photon excitation on the ZBTEr (NPs)-rGO glass system with the presence of UV light leading to the excitation of electrons from valence band (VB) to conduction band (CB)	165
4.18	Plotted graph of log (α) against photon energy, $\hbar\omega$ of ZBTEr (NPs)-rGO glasses	170
4.19	Variation of Urbach energy as a function of Er_2O_3 nanoparticles concentration for ZBTEr (NPs)-uncoated and ZBTEr (NPs)-rGO glasses	170
4.20	Variation of refractive index as a function of Er_2O_3 nanoparticles concentration for ZBTEr (NPs)-uncoated and ZBTEr (NPs)-rGO glasses	174
4.21	Variation of reflection loss, transmission coefficient, and dielectric constant as a function of Er_2O_3 nanoparticles concentration for ZBTEr (NPs)-rGO glasses	177
4.22	Least square plot of refractive index-based oxide ion polarizability, α_0^{2-} (n) against average electronegativity-	181

05-4506832 pustaka.upsi.edu.my Perpustakaan Tuanku Bainun Kampus Sultan Abdul Jalil Shah PustakaTBainun ptbupsi

05-4506832 pustaka.upsi.edu.my Perpustakaan Tuanku Bainun Kampus Sultan Abdul Jalil Shah PustakaTBainun ptbupsi

	based oxide ion polarizability, $\alpha_0^{2-}(\chi_{3av})$ of ZBTEr (NPs)-rGO glasses	
4.23	Least square plot of energy bandgap optical electronegativity-based oxide ion polarizability, $\alpha_0^{2-}(\Delta\chi^*(E_{opt}))$ with energy bandgap-based oxide ion polarizability, $\alpha_0^{2-}(E_{opt})$ of ZBTEr (NPs)-rGO glasses	183
4.24	Least square plot of refractive index optical electronegativity-based oxide ion polarizability, $\alpha_0^{2-}(\Delta\chi^*(n))$ with refractive index-based oxide ion polarizability, $\alpha_0^{2-}(n)$ of ZBTEr (NPs)-rGO glasses	184
4.25	Variation of the Judd-Ofelt's intensity parameters, Ω_t (t = 2, 4, 6) as a function of Er_2O_3 nanoparticles concentration for ZBTEr (NPs)-rGO glasses	190
4.26	Luminescence spectra of ZBTEr (NPs)-rGO glasses	201
4.27	Luminescence spectra of ZBTEr (NPs)-uncoated glasses	202
4.28	Schematic energy levels diagram of Er^{3+} nanoparticles of ZBTEr (NPs)-rGO and ZBTEr (NPs)-uncoated glasses	203
4.29	SEM micrographs of the ZBTEr (NPs)-CNTs glass showing the different of CNTs nanostructures at 0.04 mol% Er_2O_3 nanoparticles concentration with the magnification of (a), (c) 20 K X, (b) 2 K X, and (d) 50 K X	208
4.30	Schematic illustration of CNTs layer-coated on the ZBTEr (NPs) glass surfaces	209
4.31	The EDX spectra with supported microstructure images of the ZBTEr (NPs)-CNTs glass surfaces followed by two different regions at (a) 5 μm and (b) 10 μm	211
4.32	The EDX elemental mappings of (a) carbon (C), (b) iron (Fe), and (c) oxygen (O) with the magnification of 20 K X	212
4.33	Micro-Raman spectra of CNTs with supported microstructure image of the ZBTEr (NPs)-CNTs glass surfaces at 50 μm	214
4.34	Optical absorption spectra of ZBTEr (NPs)-CNTs glasses	218

05-4506832 pustaka.upsi.edu.my Perpustakaan Tuanku Bainun Kampus Sultan Abdul Jalil Shah PustakaTBainun ptbupsi

05-4506832 pustaka.upsi.edu.my Perpustakaan Tuanku Bainun Kampus Sultan Abdul Jalil Shah PustakaTBainun ptbupsi

4.35	Optical absorption spectra of ZBTEr (NPs)-uncoated glasses	219
4.36	Tauc's plot of $(\alpha\hbar\omega)^{1/2}$ against photon energy, $\hbar\omega$ of ZBTEr (NPs)-CNTs glasses	221
4.37	Variation of optical bandgap energy as a function of Er_2O_3 nanoparticles concentration for ZBTEr (NPs)-uncoated and ZBTEr (NPs)-CNTs glasses	221
4.38	The possible mechanism of photon excitation on the ZBTEr (NPs)-CNTs glass system with the presence of UV light leading to the excitation of electrons from valence band (VB) to conduction band (CB)	224
4.39	Plotted graph of log (α) against photon energy, $\hbar\omega$ of ZBTEr (NPs)-CNTs glasses	228
4.40	Variation of Urbach energy as a function of Er_2O_3 nanoparticles concentration for ZBTEr (NPs)-uncoated and ZBTEr (NPs)-CNTs glasses	228
4.41	Variation of refractive index as a function of Er_2O_3 nanoparticles concentration for ZBTEr (NPs)-uncoated and ZBTEr (NPs)-CNTs glasses	232
4.42	Variation of reflection loss, transmission coefficient and dielectric constant as a function of Er_2O_3 nanoparticles concentration for ZBTEr (NPs)-CNTs glasses	235
4.43	Least square plot of refractive index-based oxide ion polarizability, $\alpha_0^{2-}(n)$ against average electronegativity-based oxide ion polarizability, $\alpha_0^{2-}(\chi_{3av})$ of ZBTEr (NPs)-CNTs glasses	239
4.44	Least-square plot of energy bandgap optical electronegativity-based oxide ion polarizability, $\alpha_0^{2-}(\Delta\chi^*(E_{opt}))$ with energy bandgap-based oxide ion polarizability, $\Delta\chi^*(E_{opt})$ of ZBTEr (NPs)-CNTs glasses	242
4.45	Least-square plot of refractive index optical electronegativity-based oxide ion polarizability, $\alpha_0^{2-}(\Delta\chi^*(n))$ with refractive index-based oxide ion polarizability, $\Delta\chi^*(n)$ of ZBTEr (NPs)-CNTs glasses	242

05-4506832 pustaka.upsi.edu.my Perpustakaan Tuanku Bainun Kampus Sultan Abdul Jalil Shah PustakaTBainun ptbupsi
05-4506832 pustaka.upsi.edu.my Perpustakaan Tuanku Bainun Kampus Sultan Abdul Jalil Shah PustakaTBainun ptbupsi

05-4506832 pustaka.upsi.edu.my Perpustakaan Tuanku Bainun Kampus Sultan Abdul Jalil Shah PustakaTBainun ptbupsi

4.46	Variation of the Judd-Ofelt intensity parameters, Ω_t (t = 2, 4, 6) as a function of Er_2O_3 nanoparticles concentration for ZBTEr (NPs)-CNTs glasses	248
4.47	Luminescence spectra of ZBTEr (NPs)-CNTs glasses	260
4.48	Luminescence spectra of ZBTEr (NPs)-uncoated glasses	260
4.49	Schematic energy levels diagram of Er^{3+} nanoparticles of ZBTEr (NPs)-CNTs and ZBTEr (NPs)-uncoated glasses	262

05-4506832 pustaka.upsi.edu.my Perpustakaan Tuanku Bainun Kampus Sultan Abdul Jalil Shah PustakaTBainun ptbupsi
05-4506832 pustaka.upsi.edu.my Perpustakaan Tuanku Bainun Kampus Sultan Abdul Jalil Shah PustakaTBainun ptbupsi

05-4506832 pustaka.upsi.edu.my Perpustakaan Tuanku Bainun Kampus Sultan Abdul Jalil Shah PustakaTBainun ptbupsi

LIST OF SYMBOLS AND ACRONYMS

α	-	Absorption Coefficient	cm^{-1}
α_0^{2-}	-	Oxide Ion Polarizability	Å
A	-	Area	m^2
A_{ed}	-	Electric Dipole Transition Probability	s^{-1}
A_{md}	-	Magnetic Dipole Transition Probability	s^{-1}
β_R	-	Branching Ratio	%
c	-	Speed of Light	ms^{-1}
d	-	Thickness	m
δ_{rms}	-	Root Mean Square Deviation	-
e	-	Electronic Charge	C
ε	-	Molar Extinction Coefficient	$Lmol^{-1}cm^{-1}$
ϵ	-	Dielectric Constant	-
E_{opt}	-	Optical Bandgap Energy	Joule (J)/eV
ΔE	-	Urbach Energy	Joule (J)/eV
F	-	Field Strength	cm^3
f_{cal}	-	Calculated Oscillator Strength	-
f_{exp}	-	Experimental Oscillator Strength	-
h	-	Plank's Constant	m^2kgs^{-1}
ħω	-	Photon Energy	Joule (J)/eV

05-4506832 pustaka.upsi.edu.my Perpustakaan Tuanku Bainun Kampus Sultan Abdul Jalil Shah PustakaTBainun ptbupsi

05-4506832 pustaka.upsi.edu.my Perpustakaan Tuanku Bainun Kampus Sultan Abdul Jalil Shah PustakaTBainun ptbupsi

J	-	Angular Momentum	kgm^2s^{-1}
M_W	-	Molecular Weight	g/mol
m	-	Mass of Electron	g
N_A	-	Avogadro's Number	-
N	-	Ionic Concentration of Rare-earth	$ions/cm^3$
η	-	Refractive Index	-
OPD	-	Oxygen Packing Density	g.atom/L
ρ	-	Density	kg/m^3
Ω_t	-	Judd-Ofelt's Intensity Parameter	-
R_i	-	Inter-ionic Distance	Å
R_L	-	Reflection Loss	-
R_P	-	Polaron Radius	Å
S_{ed}	-	Electric Dipole Line Strength	-
S_{md}	-	Magnetic Dipole Line Strength	-
$S\|aj'\rangle\|^2$	-	Manifold State of Elements	-
T	-	Transmission Coefficient	-
t_r	-	Radiative Lifetime	ms
$\|\langle U^{(\lambda)}\rangle\|^2$	-	Reduced Matrix Elements	-
V_m	-	Molar Volume	m^3/mol
v	-	Wavenumber	cm^{-1}
ω	-	Radian Frequency	Fm^{-1}
λ	-	Wavelength	m
χ	-	Electronegativity	-

05-4506832 pustaka.upsi.edu.my Perpustakaan Tuanku Bainun Kampus Sultan Abdul Jalil Shah PustakaTBainun ptbupsi

05-4506832 pustaka.upsi.edu.my Perpustakaan Tuanku Bainun Kampus Sultan Abdul Jalil Shah PustakaTBainun ptbupsi

B_2O_3	-	Boron (III) Oxide
BOs	-	Bridging Oxygens
CNTs	-	Carbon Nanotubes
EDX	-	Energy Dispersive X-ray
Er_2O_3	-	Erbium (III) Oxide
FESEM	-	Field Emission Scanning Electron Microscopy
FT-IR	-	Fourier Transform Infrared
GO	-	Graphene Oxide
HR-TEM	-	High Resolution Transmission Electron Microscopy
NBOs	-	Non-bridging Oxygens
rGO	-	Reduced Graphene Oxide
REIs	-	Rare-earth Ions
SDS	-	Sodium Dodecyl Sulphate
TeO_2	-	Tellurium (II) Oxide
tbp	-	Trigonal Bipyramidal
tp	-	Trigonal Pyramidal
XRD	-	X-ray Diffraction
UV-Vis	-	Ultraviolet Visible
ZnO	-	Zinc Oxide

05-4506832 pustaka.upsi.edu.my Perpustakaan Tuanku Bainun Kampus Sultan Abdul Jalil Shah PustakaTBainun ptbupsi

05-4506832 pustaka.upsi.edu.my Perpustakaan Tuanku Bainun Kampus Sultan Abdul Jalil Shah PustakaTBainun ptbupsi

LIST OF APPENDICES

A Academic Journals

B Presentations

C Awards

05-4506832 pustaka.upsi.edu.my Perpustakaan Tuanku Bainun Kampus Sultan Abdul Jalil Shah PustakaTBainun ptbupsi

05-4506832 pustaka.upsi.edu.my Perpustakaan Tuanku Bainun Kampus Sultan Abdul Jalil Shah PustakaTBainun ptbupsi

05-4506832 pustaka.upsi.edu.my Perpustakaan Tuanku Bainun Kampus Sultan Abdul Jalil Shah PustakaTBainun ptbupsi

CHAPTER 1

INTRODUCTION

05-4506832 pustaka.upsi.edu.my Perpustakaan Tuanku Bainun Kampus Sultan Abdul Jalil Shah PustakaTBainun ptbupsi

1.1 Introduction

This chapter outlines a brief introduction on the research studies and background. The objectives, research problems, scopes, limitations, and significance of the research work are presented in this chapter. The last part of this chapter elucidates the summary of the thesis.

05-4506832 pustaka.upsi.edu.my Perpustakaan Tuanku Bainun Kampus Sultan Abdul Jalil Shah PustakaTBainun ptbupsi

05-4506832 pustaka.upsi.edu.my Perpustakaan Tuanku Bainun Kampus Sultan Abdul Jalil Shah PustakaTBainun ptbupsi

1.2 Research Background

The discovery of a breakthrough in glass-making was initiated in 5000 BC during the Mesopotamia era when they found a natural glass known as “fulgurites” that has been formed from the strike of lightning. The early efforts of glassmaking were inspired from the Egyptian era when glass production was initially invented from a substantial amount of sand-based silica. Then, it was followed by the evolution of glass manufacturing during the Roman Empire via the glass blowing technique and has been extended to the production of stained-glass windows. The commercial products from glasses in this era were mainly covered the ornaments and small containers for cosmetics.

In the early 1900s, glass development and production began to increase rapidly since the invention of machinery and thereafter the revolution of glass production was initiated by Sir Alastair Pilkington. In addition, the innovation of glass manufacturing is undoubtedly one of the most extensively high-demanding due to the continuous research in the field of glass science and technology. Consequently, the widespread use and broad commercialization in glass applications were utilized in optical lenses, light-emitting devices, optical fiber amplifiers, optoelectronics, solid-state high-power lasers for telecommunications, and many other fields. The rare-earth ions (REIs) doped glasses recently have been a great interest in the field of photonic materials in terms of multifunctional applications particularly, for upconversion luminescence temperature sensors.

05-4506832 pustaka.upsi.edu.my Perpustakaan Tuanku Bainun Kampus Sultan Abdul Jalil Shah PustakaTBainun ptbupsi

05-4506832 pustaka.upsi.edu.my Perpustakaan Tuanku Bainun Kampus Sultan Abdul Jalil Shah PustakaTBainun ptbupsi

Commonly, glass belongs to solid materials which can be classified into crystalline and amorphous solids. In Greek, the term glass can be defined as an amorphous or "shapeless" or non-crystalline solid material from a fusion process. Moreover, glass can be formed from silica sand, soda ash, limestone, dolomite, lead oxide, and borate oxide. The amorphous glasses possess a short-range periodic arrangement and does not consist of a well-shaped or geometrical shape in contrast with the crystalline solids. Typically, glass materials have several essential properties, such as high transparency, excellent refractive index, high hardness, rust resistance, and low manufacturing costs. In addition, glass can be easily customized to different shapes or sizes and altered its properties especially to produce high-quality optical glasses (Al-Hadeethi et al., 2019; Gupta et al., 2020; Sayyed et al., 2020).

05-4506832 pustaka.upsi.edu.my Perpustakaan Tuanku Bainun Kampus Sultan Abdul Jalil Shah PustakaTBainun ptbupsi

Glass system is occupied by a continuous random network due to the disappearance of any crystalline structure meanwhile, the amorphous silica consists of two tetrahedral that shows the relation between the Si-O and O-O atoms and bridging oxygen existing between the two tetrahedral, as presented in Figure 1.1. The network structure showed the short-range order which is compatible with the absence of long-range order.

05-4506832 pustaka.upsi.edu.my Perpustakaan Tuanku Bainun Kampus Sultan Abdul Jalil Shah PustakaTBainun ptbupsi

05-4506832 pustaka.upsi.edu.my Perpustakaan Tuanku Bainun Kampus Sultan Abdul Jalil Shah PustakaTBainun ptbupsi

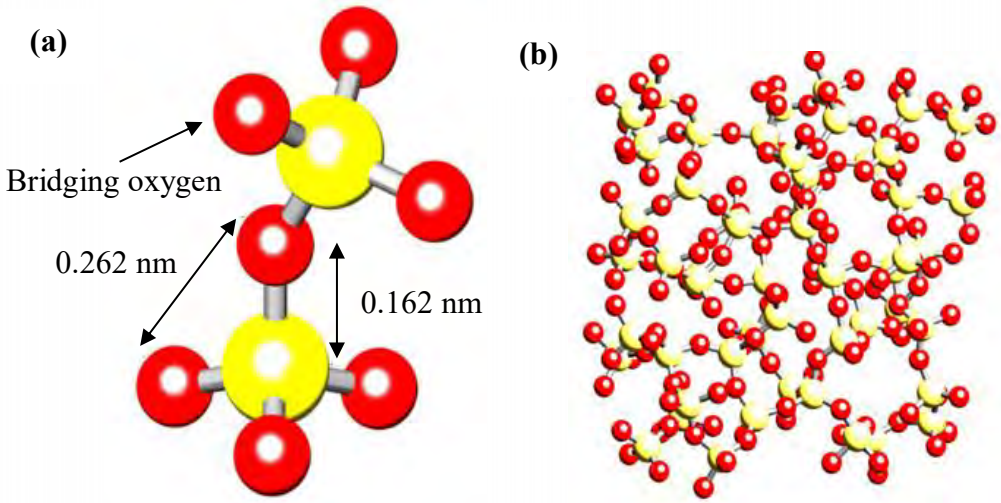


Figure 1.1. Basic atomic structure of an amorphous silica (a) Schematic representation of two tetrahedra displaying nominal distance between neighboring Si-O and O-O atoms, and a bridging oxygen (BO) between two tetrahedra and (b) Subsection of an amorphous silica simulation which shows the random arrangement of silica tetrahedral unit (Lunt et al., 2018)

05-4506832 pustaka.upsi.edu.my Perpustakaan Tuanku Bainun Kampus Sultan Abdul Jalil Shah PustakaTBainun ptbupsi

The formation of glass usually occurs by a rapid cooling when the molten continuously hardens into the solid state without the crystallization of materials. According to the studies on glass formation by Zachariasen, natural glass can be formed based on the following rules as outlined below (Zachariasen, 1932):

1. No oxygen atom may be linked to more than two cations
2. Cation coordination number is small either 3 or 4
3. Oxygen polyhedral share corners, not edges, or faces
4. For 3D networks, at least three corners must be shared

05-4506832 pustaka.upsi.edu.my Perpustakaan Tuanku Bainun Kampus Sultan Abdul Jalil Shah PustakaTBainun ptbupsi

05-4506832 pustaka.upsi.edu.my Perpustakaan Tuanku Bainun Kampus Sultan Abdul Jalil Shah PustakaTBainun ptbupsi

The constituents of glass can be comprised to three components which are glass former, glass intermediate, and glass modifier. The glass former forms a highly cross-linked network of chemical bonds and possesses high electronegativity which can produce good glass-forming. Commonly, silicon oxide has been used as a network-forming in glass network rather than the other oxides such as germanium and boron oxides. Meanwhile, the glass modifier can be added in the glass network as it may alter the glass properties and break up all the bonds in the glass structure which attributes to the formation of non-bridging oxygen (NBO) atoms in the glassy matrix.

Additionally, the glass modifier can only participate in glass network modification which form highly ionic bonds with oxygen and reducing network connectivity. The glass intermediate usually possesses the intermediate electronegativity value between the glass former and the glass modifier. Due to that, the glass intermediate is not able to form the glass network by itself however, can be formed when the glass intermediate is mixed with another glass former. This behavior depends on the single bond strength value. Moreover, a high single bond strength value may potentially improve the glass formation (Dimitrov & Komatsu, 2013).

The extensive research on silicate glasses is significantly received good attentions when trivalent rare-earth ions is introduced in silicate glass network which gives excellent fluorescence efficiency in photoluminescence properties (Wang et al., 2020). The use of borate glasses are demanding due to high chemical durability and thermal shock resistance which usually has been added to silicate glasses (Bengisu, 2015). In addition, recent studies

05-4506832 pustaka.upsi.edu.my Perpustakaan Tuanku Bainun Kampus Sultan Abdul Jalil Shah PustakaTBainun ptbupsi

05-4506832 pustaka.upsi.edu.my Perpustakaan Tuanku Bainun Kampus Sultan Abdul Jalil Shah PustakaTBainun ptbupsi

suggested that germanate glasses possess low-phonon energy, and strong chemical and mechanical stability which is useful for optical fiber drawing (Pisarski et al., 2020). Meanwhile, the phosphate glasses captured an interest among the researchers due to their intense green light emission which is suitable to be used as optical fiber amplifiers (Taherunnisa et al., 2019). Fortunately, the tellurite-based glasses are non-crystalline solids that shows many advantages which have been extensively studied for their numerous optical, photonics, and laser applications (Azlan et al., 2019; Umar et al., 2017).

In comparison with these glasses, tellurite-based glass provides superior properties such as low melting point, high refractive index, high dielectric constant, and excellent infrared transmission (Pepe et al., 2019; Usman et al., 2018; Yuliantini et al., 2019; Zaitizila et al., 2018). Furthermore, tellurite glasses possess good chemical durability, excellent mechanical strength, and allow a wide spectral in the range of 3-18 μm which attribute to the high possibility of fabricating stable glass (Gomes et al., 2017).

Tellurium oxide, TeO_2 and zinc oxide, ZnO can be a good combination and excellent compatibility to form stable glasses. Thus, these glasses have been widely explored for potential applications in optical fiber. The inclusion of ZnO in tellurite-based glasses may provide superior mechanical properties, low ability to crystallize, low optical bandgap energy, as well as high refractive index than other oxide materials (Faznny et al., 2016). Additionally, the addition of borate oxide, B_2O_3 in tellurite-based glass matrix had been developed that might potentially enhance the glass transparency, possess good stability, and rare-earth ion solubility.

05-4506832 pustaka.upsi.edu.my Perpustakaan Tuanku Bainun Kampus Sultan Abdul Jalil Shah PustakaTBainun ptbupsi

05-4506832 pustaka.upsi.edu.my Perpustakaan Tuanku Bainun Kampus Sultan Abdul Jalil Shah PustakaTBainun ptbupsi

Rare-earth ions (REIs) doped glasses have grabbed attention due to their outstanding characteristics to improve the optical properties. In this research, the lanthanide oxide nanoparticles have been selected to be doped in the glass system to achieve higher optical performance and specifically, obtain a good impact on the fiber optics technology. Moreover, erbium, Er^{3+} nanoparticles are often chosen among researchers which act as the most remarkable candidate in the development of broadband erbium-doped fiber amplifier (EDFA) due to its emission of about 1.53 μm and thus, suitable to be used as a lasing glass material.

The technology of carbon-based nanomaterials (CBNs) is growing rapidly in recent years. CBNs have extraordinary characteristics and multifunctionality which importance in many applications such as optoelectronics, biomedical, and photonics devices. Owing to such characteristics, the CBNs sparked immense interest among the researchers for upcoming applications in optical sensors (Li et al., 2019), ultrafast lasers (Ma et al., 2019), and optoelectronic devices (Wang et al., 2019). Hence, due to these properties, the CBNs have high potential to enhance the optical properties of the glass materials.

Considerable research studies on glass coatings have been continuously investigated by utilizing the CBNs as coating materials on the glass surfaces. Notably, the fiber optics are usually made from glass materials. The deposition of graphene oxide (GO) and carbon nanotubes (CNTs) on glass materials may give insights the effect of these materials on optical fiber. Based on the current studies, the optical fiber can be coated with graphene oxide via simple and low-cost technique. The previous research on optical fiber

05-4506832 pustaka.upsi.edu.my Perpustakaan Tuanku Bainun Kampus Sultan Abdul Jalil Shah PustakaTBainun ptbupsi

05-4506832 pustaka.upsi.edu.my Perpustakaan Tuanku Bainun Kampus Sultan Abdul Jalil Shah PustakaTBainun ptbupsi

coated with GO shows outstanding optical properties and can be applied for multifunctional fiber devices, highly sensitive sensors, and flexible optical electronics (Fang, Xiong, Hao, Zhang, & Wang, 2019; Ishtiaq et al., 2022). The studies of CBNs coated-glass fibers are still on-going and may contribute to wide optical applications such as light-weight electromagnetic shielding, optical sensors, and optoelectronics device performances.

1.3 Research Problems

The applications of glass materials especially in fiber optics were initiated many years ago. Cao et al., (2016) investigated the spectroscopic properties of rare-earth ions (REIs) namely, Er^{3+}/ Ho^{3+} co-doped silicate glasses, which is useful in improving the Ho^{3+} 2.0 µm fiber laser performance and mid-infrared laser materials. Taking over the advantages of silicate glasses, they have achieved an excellent transmittance, which acts as a key to fast communications. The silicate glasses was significantly used in the production of highly non-linear fibers, high-concentration rare-earth ions doped fibers, ultrafast lasers, and optical fiber communications (Liang et al., 2021).

Nevertheless, the problems encountered with these glasses are due to the relatively high loss and high melting temperature of around 2100 °C, as proposed in the previous study (Kasik et al., 2020). In addition, the low optical loss of glass materials is aimed especially for mid-IR applications. Therefore, these limitations need to be overcome and

05-4506832 pustaka.upsi.edu.my Perpustakaan Tuanku Bainun Kampus Sultan Abdul Jalil Shah PustakaTBainun ptbupsi

05-4506832 pustaka.upsi.edu.my Perpustakaan Tuanku Bainun Kampus Sultan Abdul Jalil Shah PustakaTBainun ptbupsi

progressive research work is still required to find a suitable glass material with lower melting point and low transmission loss.

Over the years, tellurite-based glasses have been extensively introduced due to their unique advantages over silicate glasses, as reported in previous studies (Azlan et al., 2019). Shen, et al. (2020) proposed that tellurite glass fiber possesses an efficient low-loss and outstanding candidate for mid-infrared laser emission applications. Subsequently, the tellurite glass has good solubility with rare-earth ions (REIs). Furthermore, the tellurite glasses are well-known as the most stable glass former than the other types of glass, such as germanate, borate, phosphate, and silicate glasses.

In addition, the lanthanide oxide nanoparticles such as erbium nanoparticles can be used as a dopant to improve the optical properties of tellurite-based glass system which is beneficial to be applied in photonic devices. Despite extensive studies on tellurite glasses doped with erbium ions, the optical properties of tellurite glasses are still limited. Tellurite glass with refractive index (>2.0) is aimed to meet the criteria for optical fiber.

Therefore, the research on glass coatings can be adopted to overcome these limitations. The deposition of carbon-based nanomaterials (CBNs) on glass surfaces is expected to achieve excellent optical properties. The investigation of reduced graphene oxide (rGO) and carbon nanotubes (CNTs) coated on glass surfaces is still limited in number. Therefore, rGO and CNTs deposited on the tellurite-based glass surfaces via a simple spray coating technique can be a first step to achieve high functionality of optical

05-4506832 pustaka.upsi.edu.my Perpustakaan Tuanku Bainun Kampus Sultan Abdul Jalil Shah PustakaTBainun ptbupsi

05-4506832 pustaka.upsi.edu.my Perpustakaan Tuanku Bainun Kampus Sultan Abdul Jalil Shah PustakaTBainun ptbupsi

fiber. Hence, the outcome of this research is believed to contribute to the new glass technology especially, in the application of fiber optics. In summary, the research problems proposed in the present study are summarized in Table 1.1.

Table 1.1

Summary of the research problems and research solutions that relate to this study

Research problems	Research solutions
• The commercial fiber optics used silicate glasses as a key to fast communication however, the problems encountered with these glasses are due to the high loss and high melting temperature of around 2100 °C (Kasik et al., 2020)	• Tellurite-based glasses has been introduced to reduce high loss and melting temperature; and possess high-solubility of rare-earth (RE) ions
• The extensive studies on tellurite-based glasses doped with erbium, Er^{3+} ions nevertheless, these glasses are still lacking to achieve a significant refractive index value (>2.0) especially, for fiber optics application	• Novel research on glass coatings can be adopted to enhance the optical efficiency and overcome the limitations of current glass materials

(Continue)

05-4506832 pustaka.upsi.edu.my Perpustakaan Tuanku Bainun Kampus Sultan Abdul Jalil Shah PustakaTBainun ptbupsi

05-4506832 pustaka.upsi.edu.my Perpustakaan Tuanku Bainun Kampus Sultan Abdul Jalil Shah PustakaTBainun ptbupsi

Table 1.1 *(Continue)*

Research problems	Research solutions
• A recent study proposed the GO coating prominently improves the optical properties by balancing the oxygen functional (Wang et al., 2020) however, the investigation of rGO and CNTs towards glass coatings has not been reported yet	• The rGO and CNTs can be deposited on the tellurite-based glass surfaces via a simple spray coating technique to compare the optical properties of the glass materials

05-4506832 pustaka.upsi.edu.my Perpustakaan Tuanku Bainun Kampus Sultan Abdul Jalil Shah PustakaTBainun ptbupsi

1.4 Research Objectives

The objectives of this work are outlined as follows:

i. To synthesize the two-glass series by using melt-quenched and spray coating techniques with composition of {(0.47(1-y)) TeO_2 + (0.2 (1-y)) B_2O_3 + (0.29 (1-y)) ZnO + (y) Er_2O_3 (nanoparticles)} -rGO/-CNTs (coated), (y = 0.005, 0.01, 0.02, 0.03, 0.04, and 0.05 mol%) denoted as ZBTEr (NPs)-rGO and ZBTEr (NPs)-CNTs.

ii. To investigate the surface morphology, particle size, and bonding parameters of ZBTEr (NPs)-rGO and ZBTEr (NPs)-CNTs glasses by using FESEM, FT-IR, TEM, XRD, Raman, and EDX spectroscopy.

05-4506832 pustaka.upsi.edu.my Perpustakaan Tuanku Bainun Kampus Sultan Abdul Jalil Shah PustakaTBainun ptbupsi

05-4506832 pustaka.upsi.edu.my Perpustakaan Tuanku Bainun Kampus Sultan Abdul Jalil Shah PustakaTBainun ptbupsi

iii. To determine the absorption spectra, refractive index, optical bandgap energy, and Urbach energy of ZBTEr (NPs)-rGO and ZBTEr (NPs)-CNTs glasses by using UV-Vis spectroscopy.

iv. To analyze the intensity parameters, emission lifetime, and luminescence properties of ZBTEr (NPs)-rGO and ZBTEr (NPs)-CNTs glasses by using Judd-Ofelt theory and luminescence spectroscopy.

1.5 Scope and Limitations of Study

This study attempts to identify the structural and optical properties of erbium nanoparticles doped tellurite-based glasses coated with reduced graphene oxide (rGO) and carbon nanotubes (CNTs). The two sets of glass series with chemical composition of {(0.47(1-y))TeO_2 + (0.2(1-y))B_2O_3 + (0.29(1-y))ZnO + (y)Er_2O_3 (nanoparticles)} -rGO/-CNTs (coated) were prepared via conventional melt-quenching technique. Subsequently, the rGO and CNTs were deposited on the tellurite-based glasses surface using a simple and low-cost spray coating technique.

The physical properties of the prepared glasses including, density, molar volume, rare-earth inter-ionic distance, polaron radius, field strength, and oxygen packing density (OPD) were calculated by Archimedes' principle. Then, several analysis methods were carried out for glass characterizations such as Field Emission Scanning Electron

05-4506832 pustaka.upsi.edu.my Perpustakaan Tuanku Bainun Kampus Sultan Abdul Jalil Shah PustakaTBainun ptbupsi

05-4506832 pustaka.upsi.edu.my Perpustakaan Tuanku Bainun Kampus Sultan Abdul Jalil Shah PustakaTBainun ptbupsi

Microscopy (FESEM), High-Resolution Transmission Electron Microscopy (HR-TEM), X-ray Diffraction (XRD), Fourier Transform Infrared Spectrometer (FT-IR), micro-Raman, and X-ray Energy Dispersive X-ray (EDX) spectroscopy to investigate the structural and morphological properties of the glasses. The FESEM analysis was conducted to confirm the existence of rGO and CNTs morphology on the glass surfaces meanwhile, the elemental compositions that exists in rGO and CNTs were evaluated by using EDX analysis. HR-TEM analysis was performed to determine the particles' size of erbium oxide in the amorphous matrix system. Next, XRD was analyzed to confirm amorphous nature of the tellurite-based glasses. FT-IR analysis was used to determine the structural bonding, functional groups, stretching vibrational modes, and the presence of non-bridging oxygens (NBOs). Lastly, the micro-Raman analysis was utilized to determine the characteristics vibrational modes of GO, rGO, and CNTs that attached on the glass surfaces.

Meanwhile, the study on optical properties of ZBTEr (NPs)-rGO and ZBTEr (NPs)-CNTs glasses were identified via Ultra-violet Visible (UV-Vis) spectrophotometer to obtain the optical absorption spectra, optical bandgap energy, Urbach energy, refractive index, reflection loss, transmission coefficient, dielectric constant, and electronegativity. The theoretical analysis of optical parameters was performed by using Judd-Ofelt's theory to identify the intensity spectral parameters (Ω_2, Ω_4, Ω_6), oscillator strength (f_{exp}), radiative transition probabilities (A_{rad}), branching ratio (β_R), as well as excited-state radiative lifetime (τ_r). The investigation of luminescence spectra of of ZBTEr (NPs)-rGO and ZBTEr (NPs)-CNTs glasses was studied by using photoluminescence spectroscopy to analyze the emission and excitation state.

05-4506832 pustaka.upsi.edu.my Perpustakaan Tuanku Bainun Kampus Sultan Abdul Jalil Shah PustakaTBainun ptbupsi

05-4506832 pustaka.upsi.edu.my Perpustakaan Tuanku Bainun Kampus Sultan Abdul Jalil Shah PustakaTBainun ptbupsi

Understanding the CBNs characteristics is important to determine the suitability of CBNs as coating materials on glass surfaces. The association between the CBNs and glass materials promotes a novel glass especially to be used in fiber optics. The current focus of this study is to determine the optical properties of coated glasses.

1.6 Significance of Research

In this study, the characterization of glasses can be determined based on their physical, structural, and optical properties. Moreover, these properties are essential for optical fiber applications and optoelectronic devices. Hence, the main purpose of this work is to improve the optical properties of the tellurite-based glass via coating the GO and CNTs on the glass surfaces. The fabrication and spectroscopic studies of the ZBTEr (NPs)-rGO and ZBTEr (NPs)-CNTs glasses may attribute to a novel approach to improve the optical properties of the tellurite-based glass.

Taking advantage of CBNs in the glass technology development, rGO and CNTs are potential candidates as the coating materials due to high demand in industry. In this work, optical glasses can be significantly improved by using rGO and CNTs as the coating materials.

To the best of our knowledge, this work will lead to excellent improvement, especially for fiber optics technology. It has been known that broadband of the optical fiber

05-4506832 pustaka.upsi.edu.my Perpustakaan Tuanku Bainun Kampus Sultan Abdul Jalil Shah PustakaTBainun ptbupsi

05-4506832 pustaka.upsi.edu.my Perpustakaan Tuanku Bainun Kampus Sultan Abdul Jalil Shah PustakaTBainun ptbupsi

transmits the optical data via infra-red spectrum at the "speed of light" about 3.0×10^8 m/s. This research will upgrade the current fiber optics with "coated-fiber optics" which may allow the optical data to transmit faster from one destination to another. Thus, the present research was completely done to explore more understanding of the glass coatings whereby, a clearer understanding of the effects of CBNs on the glass surfaces was employed. Particularly, the interest in rGO and CNTs coating layer was absolutely exploited which is closely associated with the attached oxygens functionalization on the glass surfaces.

1.7 Thesis Overview

This thesis consists of five chapters that describe the overall presentation of the present study which comprises two glass series namely, erbium nanoparticles doped tellurite glass coated with reduced graphene oxide (ZBTEr (NPs)-rGO) and erbium nanoparticles doped tellurite glass coated with carbon nanotubes (ZBTEr (NPs)-CNTs). Therefore, the outlines of the thesis in this study are described as follows:

Chapter 1 introduces the research purpose including the background of the study, research problems, research objectives, scopes, limitations, and significance of the research. The summarization of the thesis has been well described, with provided research aims, respective analysis, and the main contribution in this work.

05-4506832 pustaka.upsi.edu.my Perpustakaan Tuanku Bainun Kampus Sultan Abdul Jalil Shah PustakaTBainun ptbupsi

05-4506832 pustaka.upsi.edu.my Perpustakaan Tuanku Bainun Kampus Sultan Abdul Jalil Shah PustakaTBainun ptbupsi

Chapter 2 presents a discussion of the literature review, including tellurite-based glass structure, the role of the dopant in the glass matrix, as well as the history of the carbon-based materials (CBNs) with their properties and synthesis techniques. Importantly, this chapter highlights the fundamental theory and calculation of the optical properties, including optical bandgap, Urbach energy, refractive index, Judd-Ofelt's theoretical study, as well as other optical parameters.

The research methodology, procedures, and experimental techniques which involved the glass fabrication, synthesis of rGO and CNTs, and the spray coating technique are comprehensively presented in Chapter 3. Furthermore, the physical, structural, and optical properties characterizations are briefly described, and this chapter summarizes the research work in flowchart diagram.

Chapter 4 discusses the results of the physical, morphological, structural, and optical properties of the ZBTEr (NPs)-rGO and ZBTEr (NPs)-CNTs glasses. Taking advantage of the deposition of rGO and CNTs on the glass surfaces, this chapter presents in-depth discussion on the effects and interaction between the coating materials and ZBTEr (NPs) glasses. Theoretical optical parameters of the ZBTEr (NPs)-rGO and ZBTEr (NPs)-CNTs glasses are carried out by using Judd-Ofelt's analysis. In addition, the luminescence analysis is analyzed to support the Judd-Ofelt's analysis.

Finally, Chapter 5 summarizes the conclusion in this study and provides several future works.

05-4506832 pustaka.upsi.edu.my Perpustakaan Tuanku Bainun Kampus Sultan Abdul Jalil Shah PustakaTBainun ptbupsi

05-4506832 pustaka.upsi.edu.my Perpustakaan Tuanku Bainun Kampus Sultan Abdul Jalil Shah PustakaTBainun ptbupsi

CHAPTER 2

LITERATURE REVIEW

05-4506832 pustaka.upsi.edu.my Perpustakaan Tuanku Bainun Kampus Sultan Abdul Jalil Shah PustakaTBainun ptbupsi

2.1 Introduction

This chapter presents a brief discussion on previous literatures of the glass system including, the tellurite glass structure, the role of erbium nanoparticles, atomic properties, and the synthesis process of carbon-based nanomaterials (CBNs) such as graphene oxide (GO), reduced graphene oxide (rGO), and carbon nanotubes (CNTs). The optical properties characterization consists of literatures on the absorption spectra including, optical bandgap energy, Urbach energy, and Judd-Ofelt's theoretical study. Meanwhile, the structural properties cover the morphological analysis, structural arrangement, and network formation.

05-4506832 pustaka.upsi.edu.my Perpustakaan Tuanku Bainun Kampus Sultan Abdul Jalil Shah PustakaTBainun ptbupsi

05-4506832 pustaka.upsi.edu.my Perpustakaan Tuanku Bainun Kampus Sultan Abdul Jalil Shah PustakaTBainun ptbupsi

2.2 Tellurite-based Glass Structure

Tellurite-based glasses are fascinating material due to their outstanding properties as compared to other oxide glasses such as silicate, borate, germanate, as well as phosphate. Moreover, tellurite glass exhibits excellent chemical durability, chemical resistance, good solubility of rare-earth ions (REIs), high electrical conductivity, high refractive index (2.0 – 2.5), low melting points (733 °C), low cut-off phonon energy (~700 cm^{-1}), wide spectral transparency range approximately (0.3 – 5.0 μm), low vibrational frequencies (800 cm^{-1}), wideband infrared transmittance, large dielectric constant, and good glass stability (Ding et al., 2020; Effendy et al., 2021; Konstantinidis et al., 2021; Lalla et al., 2020; Machado et al., 2019; Pepe et al., 2019; Zaitizila et al., 2018).

05-4506832 pustaka.upsi.edu.my Perpustakaan Tuanku Bainun Kampus Sultan Abdul Jalil Shah PustakaTBainun ptbupsi

Tellurite-based glass is mainly composed of TeO_4 trigonal bipyramid units (tbp) and TeO_3 trigonal pyramid units (tp), as can be seen in Figure 2.1. For TeO_4 (tbp) units, one equatorial site of the sp^3d hybrid orbitals is occupied by a lone pair of electrons, and the other two equatorial and axial sites are occupied by oxygen atoms. Meanwhile, for TeO_3 (tp) units, one of the Te sp^3 hybrid orbitals is occupied by a lone pair of electrons (Lee et al., 2008; Noguera et al., 2003).

05-4506832 pustaka.upsi.edu.my Perpustakaan Tuanku Bainun Kampus Sultan Abdul Jalil Shah PustakaTBainun ptbupsi

05-4506832 pustaka.upsi.edu.my Perpustakaan Tuanku Bainun Kampus Sultan Abdul Jalil Shah PustakaTBainun ptbupsi

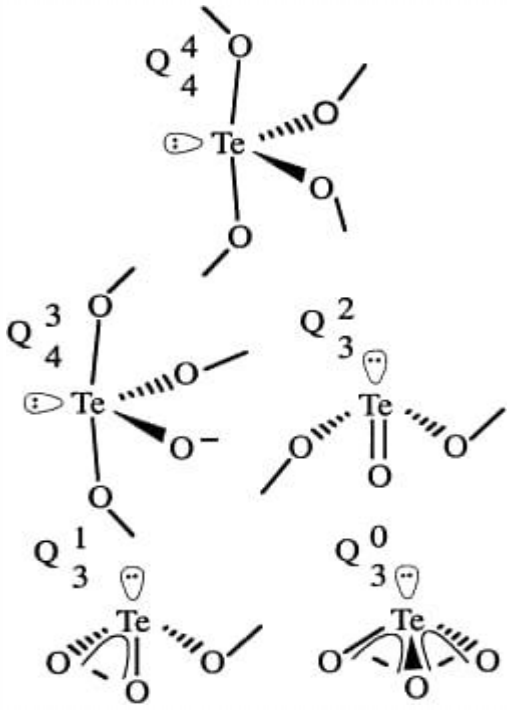


Figure 2.1. Tellurite-based glass structures found in the x = 0.20, x = 0.33, and x = 0.50 sodium tellurite crystals. Noticed that each structural unit is identified in term of Q_m^n, whereby m = 3, 4 and shows the total number of oxygens bonded to the tellurium atom, and n = 0−4 is denoted as the number of bridging oxygen (BO) bonded to the tellurium atom (Mclaughlin et al., 2000)

In an effort to form stable oxide glasses, Stanworth, (1952) proposed that the tellurite glasses possess the physical properties value including, a cation radius of Te^{4+} (0.84 Å) whereby, the partial refractivity of tellurium oxide, TeO_2 is high and thus, resulting in a higher refractive index comparable to other glasses. In particular, the combination of three components such as TeO_2, PbO, and BaO showed an improvement in expansion coefficients, deformation of temperature, and densities than usual oxide glasses. This improvement is attributable to a higher refractive index which become an interest in optical fibers.

05-4506832 pustaka.upsi.edu.my Perpustakaan Tuanku Bainun Kampus Sultan Abdul Jalil Shah PustakaTBainun ptbupsi

05-4506832 pustaka.upsi.edu.my Perpustakaan Tuanku Bainun Kampus Sultan Abdul Jalil Shah PustakaTBainun ptbupsi

The research on tellurite glasses as a key role might be potentially applied for producing the tunable yellow to orange-reddish phosphor based on the applications in light emitting diodes (LEDs) technology (Alvarez-Ramos et al., 2018). Along with the advantages of commercial diode that have been produced, tellurite glasses normally possess low energy consumption, good longevity, and reduction in its size. Therefore, the use of tellurite glass in diodes is significant for saving the energy and environmental-friendly.

Boron oxide is one of the well-known modifier candidates for the glass forming materials and the most appropriate for a new design of optical devices due to good rare-earth solubility, high melting point, good thermal stability, high-quality transparency, and the most cost-effective properties compared to other glasses (Munisudhakar et al., 2019). The addition of boron oxide into the tellurite glass system may attribute for enhancing the good stability and performance of the glass due to its excellent characteristics.

The interest in zinc oxide, ZnO has been progressively explored among researchers and can be considered as stable glass modifier in tellurite-based glass networks. It is known that the inclusion of ZnO in glass can create low rates of crystallization and enhance the glassmaking ability (Pavani et al., 2011). Besides, the addition of ZnO might significantly modify the coordination of tellurium oxide from TeO_4 (trigonal bipyramidal) to TeO_{3+1} polyhedron or (known as distorted TeO_4) and TeO_3 (trigonal pyramid), as shown in Figure 2.2.

05-4506832 pustaka.upsi.edu.my Perpustakaan Tuanku Bainun Kampus Sultan Abdul Jalil Shah PustakaTBainun ptbupsi

05-4506832 pustaka.upsi.edu.my Perpustakaan Tuanku Bainun Kampus Sultan Abdul Jalil Shah PustakaTBainun ptbupsi

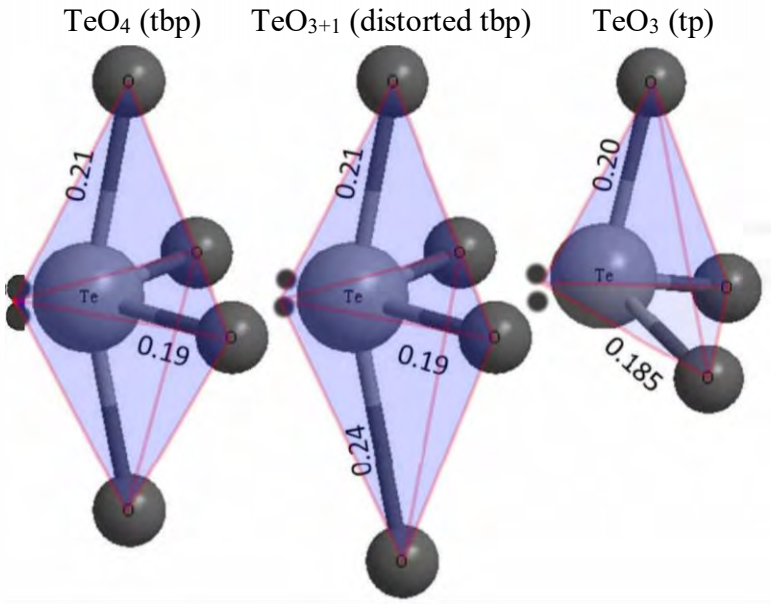


Figure 2.2. Ball and stick representation of structural units existing in tellurite glass system. (a) Trigonal bipyramid, TeO_4, (b) Distorted trigonal bipyramid, TeO_{3+1}, and (c) Trigonal pyramid, TeO_3 (Manning et al., 2012)

05-4506832 pustaka.upsi.edu.my Perpustakaan Tuanku Bainun Kampus Sultan Abdul Jalil Shah PustakaTBainun ptbupsi

The previous research on the incorporation of ZnO can be demonstrated as the dual properties occurred in the amorphous glass materials lattice network where ZnO can acts as a modifier network during the lower concentration and as a host former on the higher concentration (Bachvarova-nedelcheva et al., 2018). Moreover, it was proposed that the open network created at lower content of ZnO and its connectivity can be beneficial to tellurite lattice network.

Effendy et al., (2021) reported that the substitution of glass modifiers such as alkali earth oxide into the base glass network former may result in a rearrangement of the internal glass structure which leads to the creation of NBOs and thereby, improves the optical properties of glass materials. Furthermore, the research on ZnO and tellurite-based glass

05-4506832 pustaka.upsi.edu.my Perpustakaan Tuanku Bainun Kampus Sultan Abdul Jalil Shah PustakaTBainun ptbupsi

05-4506832 pustaka.upsi.edu.my Perpustakaan Tuanku Bainun Kampus Sultan Abdul Jalil Shah PustakaTBainun ptbupsi

network has been appropriated for investigation of the good features of optical properties (Nazrin et al., 2018). Hence, many studies have been reported for different kinds of optical applications such as optical fibers, optical sensors, optical switching mechanical devices, and optical laser glasses (Alalawi et al., 2020; El-Mallawany et al., 2021; Elkhoshkhany et al., 2019; Hussein et al., 2022).

2.3 Erbium Nanoparticles Rare-earth Ions (REIs) Doped Glass System

Erbium oxide belongs to the rare-earth materials classified into the lanthanides group whereby, the element comprises the *5s* and *5p* outermost electrons. Generally, the majority of lanthanides, Ln^{3+} are paramagnetic and exhibit a strong magnetic field and optical properties due to the unpaired electrons existing in the *f*-orbitals (Kurzen et al., 2013). The inclusion of Er^{3+} ions be considered as the ability for the generation in the laser technology due to much extensive research that has been accomplished to fabricate a new optical laser amplifier device.

In particular, the nanoparticles are known to possess a unique quantum nature efficiency which can improve the properties of the glass materials (Azlan & Halimah, 2018). Another important factor is that the incorporation of nanoparticles into the glass matrix-assisted the localized surface plasmon resonance (LSPR) with the presence of REIs and subsequently, the localized field attributes to the alteration of the optical characteristics in the amorphous glass matrix (Yusof, Ghoshal, & Azlan, 2017). Nazhirah et al., (2021)

05-4506832 pustaka.upsi.edu.my Perpustakaan Tuanku Bainun Kampus Sultan Abdul Jalil Shah PustakaTBainun ptbupsi

05-4506832 pustaka.upsi.edu.my Perpustakaan Tuanku Bainun Kampus Sultan Abdul Jalil Shah PustakaTBainun ptbupsi

investigated the effects of bimetallic nanoparticles for self-cleaning in the tellurite glass system which was supported to provide significant results on the physical, structural, thermal, and mechanical properties.

Erbium-doped fiber (EDF) is a powerful candidate as the potential medium which emerged the desirable properties including, a large gain bandwidth and EDF may provide the optical amplification signals in the range of wavelength at 1.53 μm without having any special effects involved in the gain contraction (Al-azzawi et al., 2019; Taherunnisa et al., 2019).

Differently from the other rare-earth oxide, erbium requires a significant interest among the researchers because of its interesting materials as it can attribute to the favorable emissions at blue, green, and red colors of about 1.5 μm, which possess applications in the technology of telecommunication optics. The inclusion of nanoparticles is strongly required to extend the research on nanoparticles doped glass to obtain excellent properties in photonic devices and give the potential performance on laser glass (Azlan, Halimah, Suriani, Azlina, Umar, et al., 2019).

The advancement of broadband in optical systems correlates with the high capacity existing in broad transmission and optical amplifiers which rapidly increasing in a variety of wavelengths of telecommunication dimensions. In addition, Sadik et al., (2020) developed an interest in up-conversion luminescence in erbium ions especially for expanding the erbium-doped fiber amplifier (EDFA). The integration of REIs into several

05-4506832 pustaka.upsi.edu.my Perpustakaan Tuanku Bainun Kampus Sultan Abdul Jalil Shah PustakaTBainun ptbupsi

05-4506832 pustaka.upsi.edu.my Perpustakaan Tuanku Bainun Kampus Sultan Abdul Jalil Shah PustakaTBainun ptbupsi

kinds of host glasses elucidated the impressive new performance for waveguide device applications.

Similarly, Yuan et al., (2021) fabricated the Yb^{3+}/ Er^{3+} co-doped tungsten tellurite glasses to form broadband near-infrared optical fiber amplifiers and tunable fiber lasers for the optical telecommunication window. The association of dopants material into host glasses whereby, a strong 1.5 μm emission with full width at a high maximum (FWHM) of 64 nm, attributed to a highly efficient resonance energy transfer process from Yb^{3+}: $^2F_{5/2}$ to Er^{3+}: $^2I_{11/2}$ energy state level. Consequently, these results demonstrated a long lifetime of Er^{3+}: $^4I_{13/2}$ energy level (3.96 ms), strong emission cross section (1.06×10^{-20} cm^2), and gain coefficient (4.07 cm^{-1}) which is near 1.5 μm and thus, attributing in the higher gain bandwidth of 6.78×10^{-26} cm^3. Therefore, it was believed that the optical properties can be improved by taking the advantages of REIs.

The investigation of erbium ions doped glasses plays a vital role as it has the large possibility to be applied in a wider band internet due to the non-uniform broadening for the glass network system. Furthermore, the studies on EDFA may definitely attribute in a laser system by correlating the Er^{3+} ions which possess $^4I_{13/2} \rightarrow {}^4I_{15/2}$ transition excited state at the infrared region around 1550 nm wavelength and the green region around 550 nm which possess $^4S_{3/2} \rightarrow {}^4I_{15/2}$ transition (Halimah et al., 2019).

05-4506832 pustaka.upsi.edu.my Perpustakaan Tuanku Bainun Kampus Sultan Abdul Jalil Shah PustakaTBainun ptbupsi

05-4506832 pustaka.upsi.edu.my Perpustakaan Tuanku Bainun Kampus Sultan Abdul Jalil Shah PustakaTBainun ptbupsi

2.4 Carbon-based Nanomaterials (CBNs)

Carbon-based nanomaterials (CBNs) have revealed a rich polymorphism of numerous allotropes indicating each possible dimensionality including, fullerene molecule (0D), nanotubes, graphene ribbons (1D), graphite platelets (2D), and nano-diamond (3D) derivatives (Gaur et al., 2021; Ibrahim et al., 2021). The nanomaterials exhibit different physical, chemical, thermal, and optical properties and hence, carbon nanostructures play a vital role until the recent development in the field of nanoscience and nanotechnology.

Since the researchers Konstantin Novoselov and Andre Geim were successfully awarded the Nobel Prize in 2010 (Novoselov et al., 2004), graphene (GE) has attained much interest and attention among the frontier issues of scientific research in optics, electronics, materials science, and biotechnology. By virtue of both exceptional linear and nonlinear optical properties, GE has been considered a wondrous and extraordinary material. The primary advantage of graphene is that it has high conductivity and shows remarkable optical properties which attracted the researchers to the potential applications of graphene such as light-emitting diodes, liquid crystal displays (LCD), and touchscreen devices due to its excellent and outstanding features (Bonaccorso et al., 2010). Due to the high transparency in the visible, graphene is envisioned to act in the form of transparent conductive electrodes (Woo, 2019).

05-4506832 pustaka.upsi.edu.my Perpustakaan Tuanku Bainun Kampus Sultan Abdul Jalil Shah PustakaTBainun ptbupsi

05-4506832 pustaka.upsi.edu.my Perpustakaan Tuanku Bainun Kampus Sultan Abdul Jalil Shah PustakaTBainun ptbupsi

2.4.1 Overview of Graphene

Graphene is an atomically-thin, two-dimensional (2D) nanomaterial sheet that acts as a monolayer formed by sp^2 carbon atoms possessing a honeycomb lattice structure and has attracted great interest among researchers which exhibits outstanding photonic and optoelectronic properties (Smith et al., 2019; Wang et al., 2019). Despite the benefits of using graphene in electronic devices, graphene is primarily possessed as a passive non-emissive element due to its shortcoming dictated by the electronic band structures (Naumov, 2017). Such graphene electronically is a zero-bandgap semiconductor in which the electrons relax non-radiatively when excited to the higher energy state levels.

Furthermore, the graphene plane is an ideal bidimensional (2D) allotropic form of carbon in which the atoms are periodically arranged in an infinite hexagonal network with two atoms per unit cell (indicated by A and B), as shown in Figure 2.3. The atomic structure is characterized by two types of bonds which demonstrates the planar sp^2 hybridization. In addition, the symmetry of graphene and the presence of both A-B sublattices possess a strong influence on the transport properties of the 2D system. Indeed, when the atoms are positioned onto the graphene hexagonal lattice, the electronic wavefunctions from different atoms overlap and thus, resulting in the electrons of π bonds in the graphene reacting independently from the other valence electrons.

05-4506832 pustaka.upsi.edu.my Perpustakaan Tuanku Bainun Kampus Sultan Abdul Jalil Shah PustakaTBainun ptbupsi

05-4506832 pustaka.upsi.edu.my Perpustakaan Tuanku Bainun Kampus Sultan Abdul Jalil Shah PustakaTBainun ptbupsi

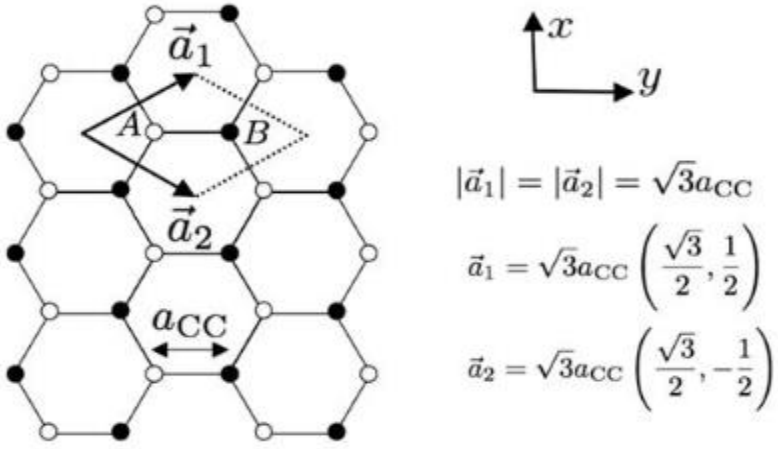


Figure 2.3. Basic vectors in the hexagonal lattice of graphene with the corresponding Brillouin zone (Dubois et al., 2009)

According to Dubois et al., (2009), the fundamental of the building block existing in the carbon nanostructures relies on the theoretical concept of the graphene sheet. Graphene undoubted can be referred to as a perfect infinite single layer with densely packed into a benzene-ring structure. Indeed, graphene has been widely used to ascribe the properties of various CBNs such as large fullerenes (graphene is cut into strips), carbon nanotube (graphene sheets are rolled up into nanometer-sized cylinders), and graphite (a large number of graphene sheets are stacked), as depicted in Figure 2.4.

05-4506832 pustaka.upsi.edu.my Perpustakaan Tuanku Bainun Kampus Sultan Abdul Jalil Shah PustakaTBainun ptbupsi

05-4506832 pustaka.upsi.edu.my Perpustakaan Tuanku Bainun Kampus Sultan Abdul Jalil Shah PustakaTBainun ptbupsi

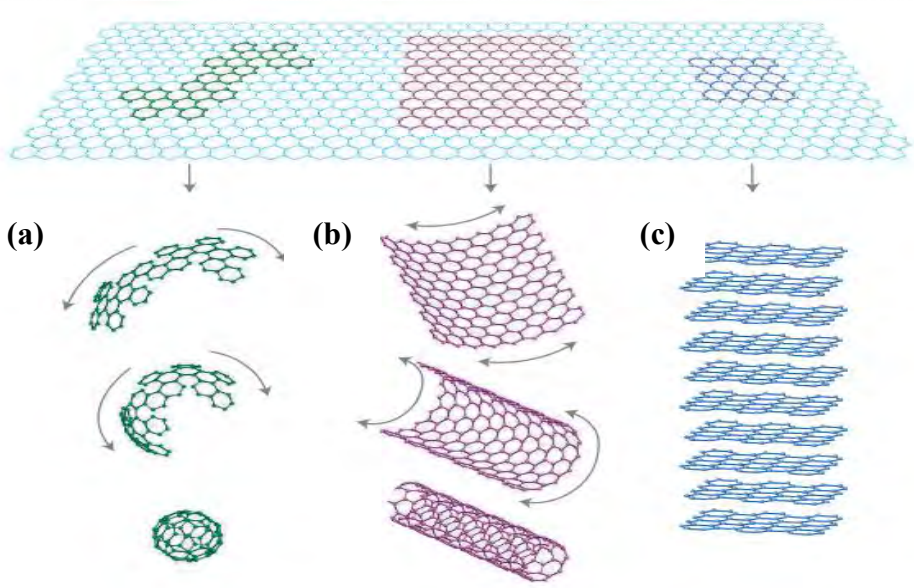


Figure 2.4. Graphitic forms of carbon family materials consist of (a) 0-D Buckyballs of fullerene, (b) 1-D Roll of carbon nanotube, and (c) 3-D Stack of graphite (Geim & Novoselov, 2007)

05-4506832 pustaka.upsi.edu.my Perpustakaan Tuanku Bainun Kampus Sultan Abdul Jalil Shah PustakaTBainun ptbupsi

Additionally, graphene has many desirable characteristics including, sufficient mechanical strength (Mohan et al., 2018), high electrical conductivity (Mun et al., 2017), known as a perfect barrier ability (Bunch et al., 2008), and other astonishing properties. For these reasons, graphene has been chosen as the goal of countless research efforts to incorporate graphene into advanced coating applications, as has been proposed by previous studies (Ba et al., 2020; Mao et al., 2021; Mu et al., 2021).

Nevertheless, the use of pristine graphene has been proved challenging due to its limitation in the optical absorption characteristics caused by the strong van der Waals interactions, poor solubility, and more agglomeration structures. These features contribute to the gapless semiconductor or having zero-bandgap energy whereby, the valence and

05-4506832 pustaka.upsi.edu.my Perpustakaan Tuanku Bainun Kampus Sultan Abdul Jalil Shah PustakaTBainun ptbupsi

05-4506832 pustaka.upsi.edu.my Perpustakaan Tuanku Bainun Kampus Sultan Abdul Jalil Shah PustakaTBainun ptbupsi

conduction bands physically contact each other at Dirac points that exists in the Brillouin zone (Sahu & Rout, 2017). According to the Fermi level, E_F which can be said as the change neutrality point, the Fermi surface is defined by the set of *K* and *K'* points which are connected by the time-reversal symmetry. The graphene is therefore displaying a zero bandgap which acts as a metallic character when the occupied and unoccupied bands cross on each other at the Dirac points. However, in the other case, the term overlap or zero-gap semiconductor is often used since the Fermi surface is reduced to a finite set of points.

Particularly, the π-band electronic dispersion for graphene near the six corners of the 2D hexagonal Brillouin zone is found to be linear whereby, the electronic properties of graphene can be described by an effective massless Dirac fermion model in the existing charge neutrality point, which is linear dispersion and electron-hole symmetry. These "Dirac cones" feature which containing the holes and electrons appear in the corners of the 2D Brillouin zone whereby, the points touch at the Fermi energy and thereby, the six points on the Dirac cones are referred to as the Dirac points, as illustrated in Figure 2.5.

05-4506832 pustaka.upsi.edu.my Perpustakaan Tuanku Bainun Kampus Sultan Abdul Jalil Shah PustakaTBainun ptbupsi

05-4506832 pustaka.upsi.edu.my Perpustakaan Tuanku Bainun Kampus Sultan Abdul Jalil Shah PustakaTBainun ptbupsi

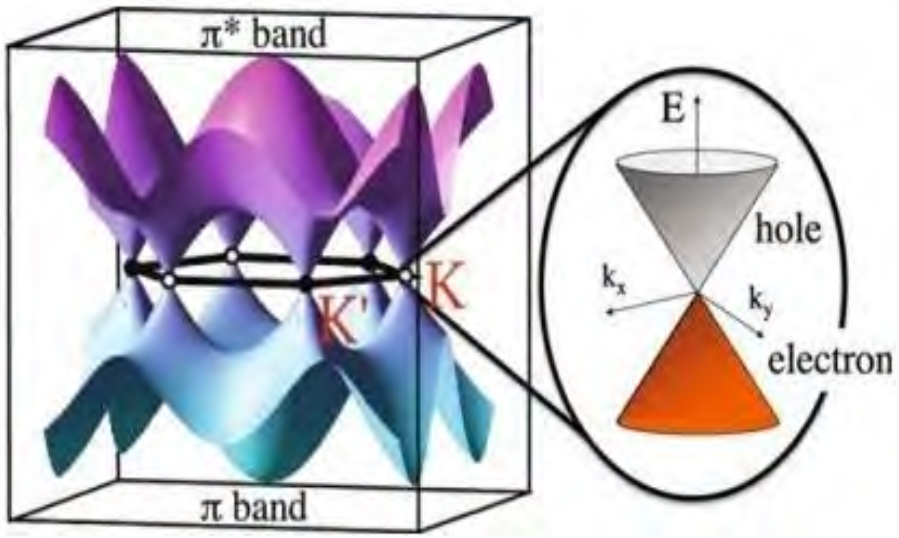


Figure 2.5. The electronic bands of π and π^* with respect to valence and the other of conduction bands at the six corners in the Dirac cones which meet at the Dirac points and indicate that zero-band gap of graphene (Dubois et al., 2009)

05-4506832 pustaka.upsi.edu.my Perpustakaan Tuanku Bainun Kampus Sultan Abdul Jalil Shah PustakaTBainun ptbupsi

Furthermore, pure graphene is naturally semi-metal consisting of a zero-band gap, and thus, graphene which possesses the oxygen functionalization groups can cause the opening up of bandgap (Gupta et al., 2017). In particular, the lack of the zero-band gap energy of graphene makes it difficult and remains challenging to achieve high performance in some practical applications due to its optical properties which are limited by the weaker optical absorption (Li et al., 2019).

On the other hand, a similar structure to graphene can be synthesized based on graphite or any other carbon sources in an effort to achieve the desirable advantages of pristine graphene while influencing the surface with the functionalized oxygen-containing groups. As an alternative, graphene has been synthesized from graphite using a chemical exfoliation method to produce graphene oxide (GO). This is attributed to the opening of

05-4506832 pustaka.upsi.edu.my Perpustakaan Tuanku Bainun Kampus Sultan Abdul Jalil Shah PustakaTBainun ptbupsi

05-4506832 pustaka.upsi.edu.my Perpustakaan Tuanku Bainun Kampus Sultan Abdul Jalil Shah PustakaTBainun ptbupsi

bandgap energy of GO due to the pristine lattice of graphene which has been stimulated via an oxidation process (Nourbakhsh et al., 2010). Moreover, limited particle size and complexity in production usually hinder potential applications of graphene nanostructures in larger-scale optoelectronics. Thus, more applicable graphene-based structures with a specified set of optical properties could be compromised to overcome those limitations. Specifically, the functionalized graphene which can be said as a common form of graphene such as GO may appear to be more suitable for many applications.

Recently, a new class of graphene derivatives has emerged which take advantage of graphene oxide (GO), reduced graphene oxide (rGO), and graphene quantum dots (GQDs) whereby, these nanomaterials have proven to be effective in nanocomposite materials due to their properties and dispersibility in the polymer matrices, which has attributed to various applications (Cheng et al., 2017).

A typical application of graphene involves further high-performance flexible supercapacitors which have been widely recognized as an active electrode material due to the graphene possessing a highly-exposed surface area, high electrical conductivity, and superior chemical stability characteristics (Purkait et al., 2018; Sahoo et al., 2022; Suriani et al., 2017; Yang et al., 2019; Zhou et al., 2021). Similarly, Xiao et al., (2020) used graphene-based nanoporous materials to investigate high-capacity ion electrosorption electrodes for potential supercapacitors.

05-4506832 pustaka.upsi.edu.my Perpustakaan Tuanku Bainun Kampus Sultan Abdul Jalil Shah PustakaTBainun ptbupsi

05-4506832 pustaka.upsi.edu.my Perpustakaan Tuanku Bainun Kampus Sultan Abdul Jalil Shah PustakaTBainun ptbupsi

2.4.2 Graphene Oxide and Atomic Structures

The major concern of the carbon-based nanomaterials (CBNs) such as graphene oxide (GO) from the oxidation of graphite which mainly exhibits a large amount of oxygen-containing functional groups which is considered to be beneficial for the glass materials industry especially, for enhancing the optical characteristics of the glass network system (Papadakis et al., 2020). Primarily, the functionalization by oxygen-containing groups gives results in a gap between the valence and conduction bands in GO which in turn transforms into a semiconductor, or even an insulator based on the degree of derivatization (Afroozeh, 2021; Necolau & Pandele, 2020; Sharma et al., 2020; Wang et al., 2020). Similarly, Tang et al., (2017) reported that the opening of optical bandgap existing in glass materials may be caused by an abundant content of oxygen groups in the active layer of GO sheets.

Taking advantage of GO over graphene in terms of the presence of oxygen-containing functionality in GO edges, therefore GO itself has very interesting with appreciable attention due to it can exhibit the absorption of oxygenated functionality groups in the optical characteristics (Hasan et al., 2017). Such variability demonstrates that the GO has a significant superiority since its structure can be tailored for a specific optoelectronic application by using the additional functionalization through the oxidation process (Sharma et al., 2019). Therefore, a simple and cost-effective production of GO from graphite with the large size variability and adjustable electronics properties make GO an attractive candidate for modern electronics devices (Hummers & Offeman, 1958).

05-4506832 pustaka.upsi.edu.my Perpustakaan Tuanku Bainun Kampus Sultan Abdul Jalil Shah PustakaTBainun ptbupsi

05-4506832 pustaka.upsi.edu.my Perpustakaan Tuanku Bainun Kampus Sultan Abdul Jalil Shah PustakaTBainun ptbupsi

Unlike graphene, rich oxygenated containing functional groups in the basal plane are consists of epoxy and hydroxyl bonds, whereas the carboxylic acid, carbonyl, and lactol groups positioned at the edges of GO structures (Shin et al., 2017). The structures of GO are composed mainly form carbons, which consist of sp^2 graphitic basal plane that covalently bond on a homogeneous (Pirouz et al., 2018). Furthermore, the interest in GO development among researchers due to the ability of GO exhibit remarkable characteristics including, the high electrical conductivity, high specific surface area, good thermal properties, containing high mobility of charge carriers, and specific optical properties which suitable to be applied in sensing applications (Augustine et al., 2017).

The synthesis of graphene and its derivatives can be attributed to the preferred structure and properties which largely depend on the size, shape, and functional groups connected on the surface of the material (Smith et al., 2019). The ideal structures are composed of graphene nanosheets and few-layered graphene consisting of fully carbon structure with minimum defects, respectively. In addition, GO, which was ultimately manufactured into a single and few layers of graphene, which developed from oxygen, is functionalized with epoxy and hydroxyl groups (Sundaram et al., 2010).

GO can be dispersible mainly in aqueous solutions with the presence of oxygen functional groups in which carbon atoms are transformed from sp^2 to sp^3 hybrid in the GO structure by oxidation of graphene sheets (Ikram et al., 2020). The modification of functional groups in the existing graphene structures demonstrates a broad variety of applications especially in the mechanical, thermal, optical, and electrical applications. In

05-4506832 pustaka.upsi.edu.my Perpustakaan Tuanku Bainun Kampus Sultan Abdul Jalil Shah PustakaTBainun ptbupsi

05-4506832 pustaka.upsi.edu.my Perpustakaan Tuanku Bainun Kampus Sultan Abdul Jalil Shah PustakaTBainun ptbupsi

fact, GO is defined as a highly oxidized form of graphene that simultaneously exhibits the hydrophobic sp^2- and sp^3-bonded carbon and abundant hydrophilic hydroxyl, epoxide, and carboxylic acid groups on the edge and defects of the nanosheets (Cheng et al., 2017). GO is capable of π-π interactions with aromatic molecules with assisted hydrophilic groups and abundant residual sp^2-bonded carbon on the GO basal plane (Akbari et al., 2019; Mohammed et al., 2020; Tian et al., 2019).

Extensive research has been done to remove the oxygen-containing functional groups of GO due to an effort to produce materials with properties as close to pristine graphene. As a result, reduced graphene oxide (rGO) can be obtained by reducing GO whereby, rGO exhibits more balanced physical and chemical properties regarding the solvent dispersibility, surface chemical groups, and superior electrical, optical, mechanical, and thermal performances (Azizighannad & Mitra, 2018; Tarcan et al., 2020). Apart from that, the GO reduction includes the C/O ratio of the end of the product, selectivity in removing the single type of oxygen group such as hydroxyl, carboxylic acid, and epoxy, healing of the surface defects of GO based on the oxidation process, and choice of reducing agents, as well as, improving the optical properties, mechanical strength, and dispersibility of nanosheets (De Silva et al., 2017; Smith et al., 2019).

Meanwhile, graphene quantum dots (GQDs) and graphene oxide quantum dots (GOQD) are defined as nanometer-sized single layer-fragments of graphene and GO which are essentially produced through “cutting” of graphene or GO nanosheets and thus, resulting in a size-dimension smaller than 20 nm in diameter which exclusively take

05-4506832 pustaka.upsi.edu.my Perpustakaan Tuanku Bainun Kampus Sultan Abdul Jalil Shah PustakaTBainun ptbupsi

05-4506832 pustaka.upsi.edu.my Perpustakaan Tuanku Bainun Kampus Sultan Abdul Jalil Shah PustakaTBainun ptbupsi

advantage from the graphene effects (Afroozeh, 2021; Smith et al., 2019). The considerable of graphene derivatives takes place when the desired structure and properties are extremely dependent upon the size, shape, and functional groups attached to the surface of the material. Due to these unique features, the different graphene-based nanomaterials involve in the family of graphene derivatives including, single-layer graphene that consists of single-atom-thin fully sp^2 hybridized carbon structure, a multi-layered structure of graphene with a highly-favorable stacking of graphene sheets, a highly oxidized form of GO with both sp^2 and sp^3 carbon containing abundant of oxygen groups, most of the oxygen groups and sp^3 carbon are eliminated to generate graphene-"like" material, as well as, both of GOQD and GQD, are illustrated as shown in Figure 2.6.

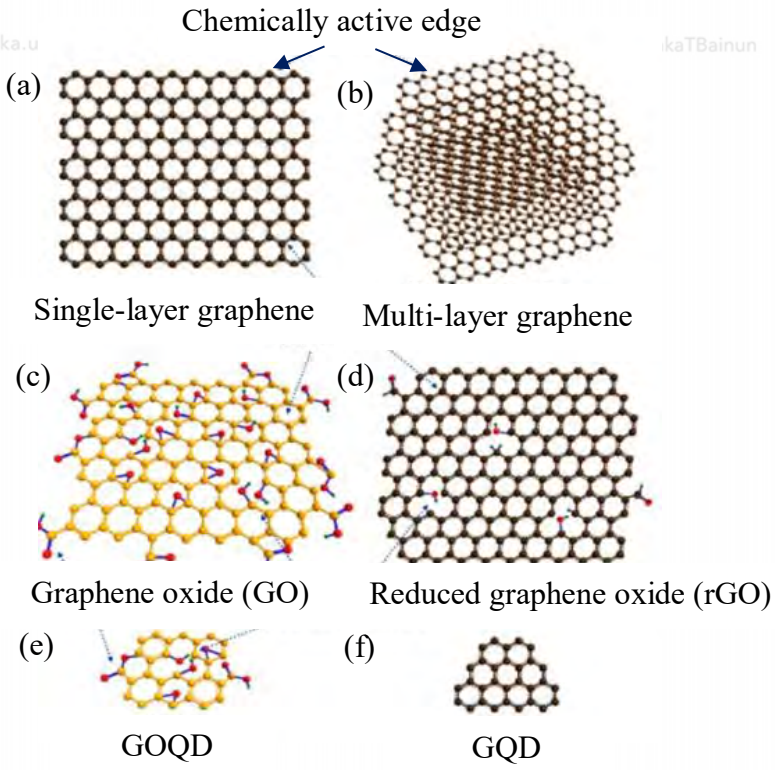


Figure 2.6. Schematic representation of different graphene-based nanomaterials including, (a) Single-layer graphene, (b) Multi-layer graphene sheets, (c) GO, (d) rGO, (e) GOQD, and (f) GQD (Cheng et al., 2017)

05-4506832 pustaka.upsi.edu.my Perpustakaan Tuanku Bainun Kampus Sultan Abdul Jalil Shah PustakaTBainun ptbupsi

05-4506832 pustaka.upsi.edu.my Perpustakaan Tuanku Bainun Kampus Sultan Abdul Jalil Shah PustakaTBainun ptbupsi

The understanding of lattice and electronic band structure of graphene, GO, and rGO is crucial for identifying the transformation of GO to rGO which attributes to a remarkable photoexcitation response. The atomic structure of GO consisted of the graphene basal plane possessing the dispersed oxygen-containing functional groups resulting in the sp^3 matrix which makes it an electronic insulator (Dideikin & Vul', 2019). Additionally, the ordered hexagonal lattice of graphene becomes disordered by oxygens defects produced via the chemical oxidation method. The electronic properties of carbon nanomaterials present a combination of sp^2 and sp^3 bonding which is primarily controlled by π and π^* states and thus, resulting in σ-σ^* bandgap (Chien et al., 2012). By characterizing these features, it is possible that the various disorder-induced localized states may imply within the two-dimensional (2D) network of GO production. Accordingly, the structural disorder-induced localized states should be present in the band tail of π and π^* bandgap, demonstrating in the optical transitions which cause broad absorption or emission bands (Chien et al., 2012; Smith et al., 2019).

By the reduction process to form deoxygenation, the structural modification is attributed to the removal of oxygenous functional groups and recovery of the conjugations between carbon atoms. Consequently, the carbon lattices from the initial distorted sp^2 domains may generate the additional graphitic domains of sp^2 clusters. Due to these characteristics, the reduction process leads to increased carrier mobility, higher absorption, tunable bandgap energy whereby, the photoresponsivity may be controlled via controlling the oxygen groups and defects. Subsequently, the lattice structure and variation of the bandgap of graphene, GO, and rGO is presented in Figure 2.7 meanwhile, the development

05-4506832 pustaka.upsi.edu.my Perpustakaan Tuanku Bainun Kampus Sultan Abdul Jalil Shah PustakaTBainun ptbupsi

05-4506832 pustaka.upsi.edu.my Perpustakaan Tuanku Bainun Kampus Sultan Abdul Jalil Shah PustakaTBainun ptbupsi

timeline of graphene-based nanomaterials (GBNs) history is illustrated in Figure 2.8.

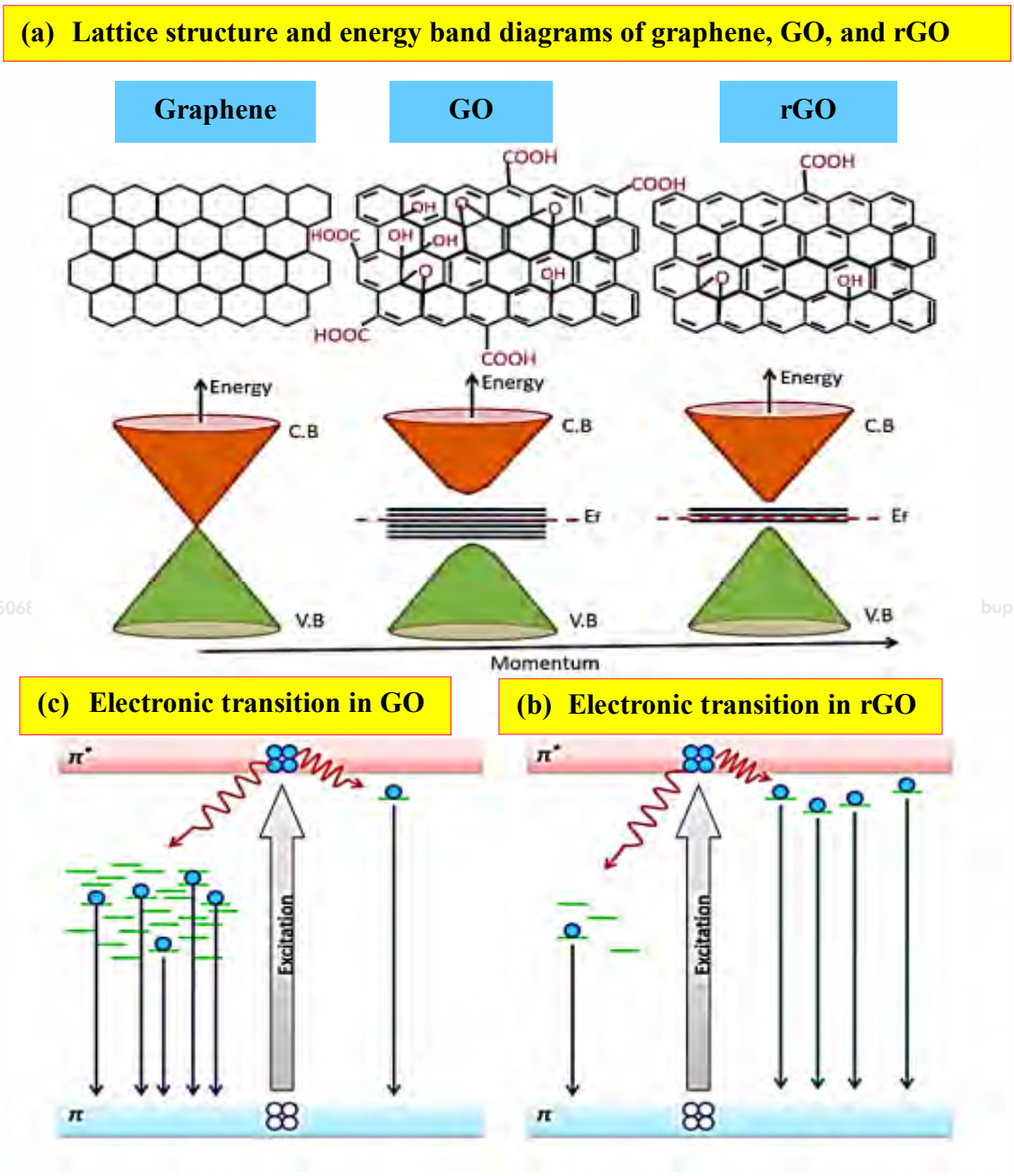


Figure 2.7. Schematic representation of (a) lattice structure and corresponding energy band diagrams of graphene, GO, and rGO; and electronic transitions in (b) GO and (c) rGO (Abid et al., 2018)

05-4506832 pustaka.upsi.edu.my Perpustakaan Tuanku Bainun Kampus Sultan Abdul Jalil Shah PustakaTBainun ptbupsi

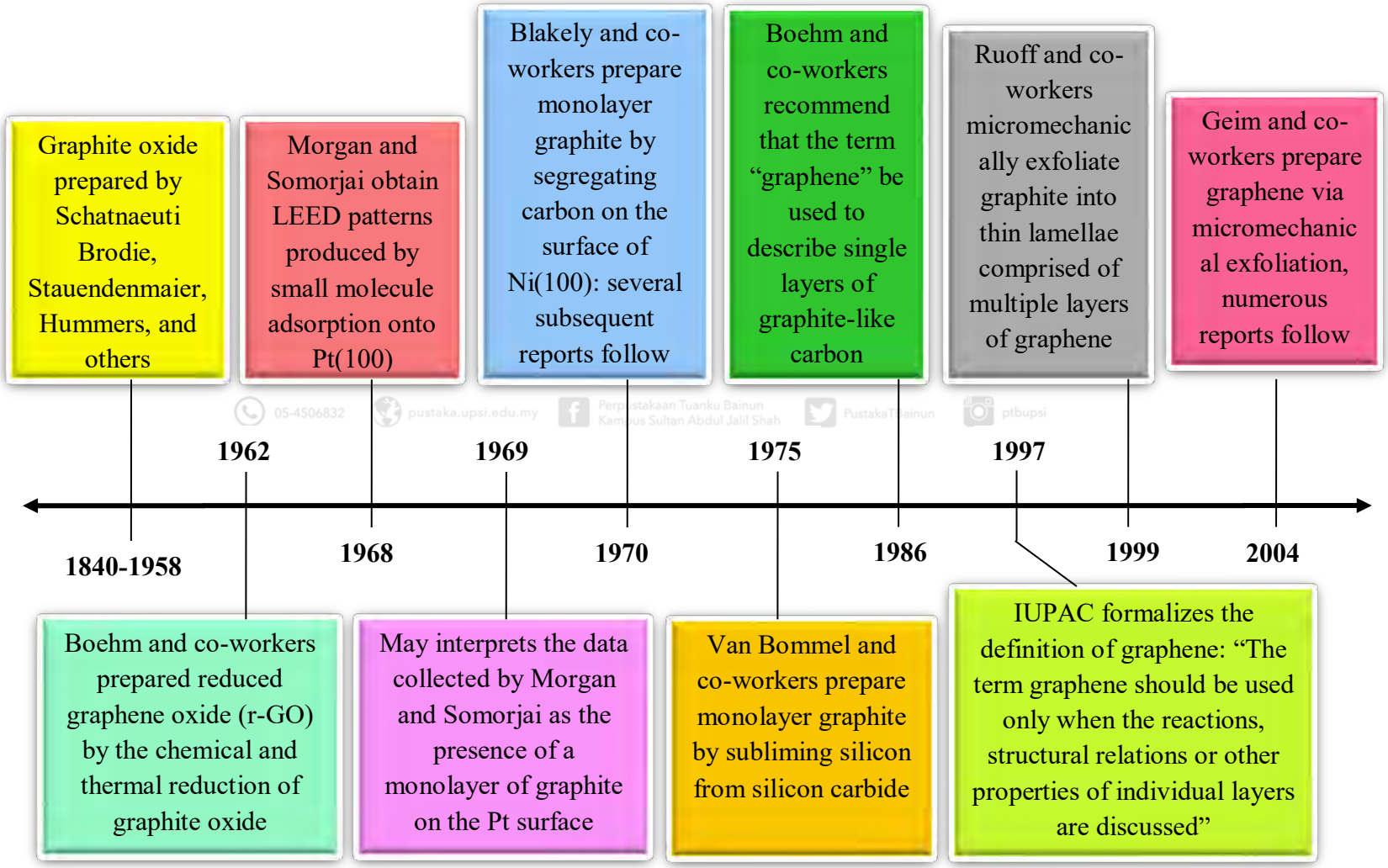


Figure 2.8. The development timeline of graphene history (Dreyer et al., 2010)

05-4506832 pustaka.upsi.edu.my Perpustakaan Tuanku Bainun Kampus Sultan Abdul Jalil Shah PustakaTBainun ptbupsi

2.5 Properties of Graphene Oxide and Reduced Graphene Oxide

2.5.1 Optical Properties

Graphene oxide (GO) has emerged as a potential alternative to graphene via the introduction of adsorption of oxygen functional groups whereby, these functional characteristics not only open up the bandgap but, may provide an option to tune the optical properties by means of controlled oxidation process (Johari & Shenoy, 2011).

The desirable optical properties of GO are well reported in which the optical absorption spectra of GO are dictated by the electronic transitions from the ultraviolet (UV) based on the band tail extending into the visible. The most prominent absorption feature in the GO nanolayer is a $\pi \rightarrow \pi^*$ transition, commonly known as the aromatic C = C bonds. The *p* orbitals of carbon may be combined either in-phase or out of phase (refer to Figure 2.9), which produces the bonding and antibonding combinations. This is eventually demonstrated in π and π^*orbitals whereby, the π orbital is lower in energy compared to the π^* and thus, allowing for a photon-induced transition between the π and π^*. Usually, the transition of GO dominates the absorption spectrum within the range of ~230 nm, as previously reported (Kochmann et al., 2012; Shang et al., 2012; Zhang et al., 2012).

Typically, the absorption spectrum of GO prepared by the modified Hummers method can be attributed to the $n \rightarrow \pi^*$ transition in the C = O bonds of oxygen-containing functional groups and then, promoting an electron from a lone-pair non-bonding *n* orbital to the antibonding π^* orbital through the photon absorption. As a result, the non-bonding

05-4506832 pustaka.upsi.edu.my Perpustakaan Tuanku Bainun Kampus Sultan Abdul Jalil Shah PustakaTBainun ptbupsi

05-4506832 pustaka.upsi.edu.my Perpustakaan Tuanku Bainun Kampus Sultan Abdul Jalil Shah PustakaTBainun ptbupsi

orbital is between the π and π* (refer Figure to 2.9 (c)) whereby, the $n \rightarrow \pi^*$ transition is less energetic and shifted from the $\pi \rightarrow \pi^*$ absorption feature.

On the contrary, the sp^2 domains in the existing GO with the smaller bandgap energy were presented to show a single-photon absorption. Therefore, the difference in the ratio of sp^2 to sp^3 domains in GO via a controlled oxidation or reduction process may allow the alteration of nonlinear optical properties, which is highly presentable for nanotechnology generation applications. In addition, the oxidation or reduction process is involved to modify the sp^2/sp^3 structure which could be interesting to introduce the optical changes and shifted absorption.

05-4506832 ptbupsi

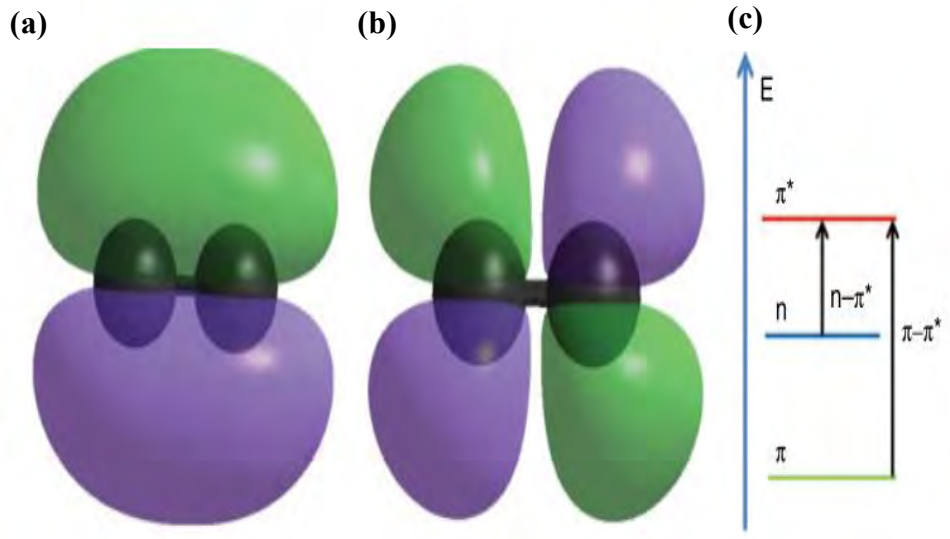


Figure 2.9. (a) The π orbitals of a C = C bond, (b) The π* orbitals of a C = C bond, and (c) Energy diagram of π, π*, and *n* orbitals and transitions (Naumov, 2017)

05-4506832 pustaka.upsi.edu.my Perpustakaan Tuanku Bainun Kampus Sultan Abdul Jalil Shah PustakaTBainun ptbupsi

05-4506832 pustaka.upsi.edu.my Perpustakaan Tuanku Bainun Kampus Sultan Abdul Jalil Shah PustakaTBainun ptbupsi

2.5.2 Thermal Properties

The synthesized GO from graphite possesses a low thermal conductivity ranging from 0.5 to 1.0 W m^{-1} K^{-1} which these values require for good thermal properties for many applications (Renteria et al., 2015). On the other hand, graphene possesses the highest in-plane thermal conductivity approximately ~3000 to 5000 W m^{-1} K^{-1} (Stankovich et al., 2007) whereas, Kim et al., (2018) suggested that the GO reduction has been shown to improve the thermal conductivity based on the selected materials. In addition to this, Renteria et al., (2015) studied that the produced rGO films from annealing GO at high temperatures up to 1000 °C may substantially enhance the in-plane thermal conductivity, resulting in an improvement ranging from ~3 to 61 W m^{-1} K^{-1}, respectively that useful for applications in the directional heat conduction.

The incorporation of rGO into the nanocomposites gives the improvement in the thermal conductivity which was believed to be a result of high conductivity, providing a lower thermal resistance of traveling phonon (Smith et al., 2019). Another essential factor for improved thermal conductivity is the high orientation of the rGO sheets which limits the thermal transfer within the boundaries including, rGO has been shown to improve the thermal properties of many nanocomposite applications including, epoxy, polymer, and poly(vinyl) alcohol (PVA).

05-4506832 pustaka.upsi.edu.my Perpustakaan Tuanku Bainun Kampus Sultan Abdul Jalil Shah PustakaTBainun ptbupsi

05-4506832 pustaka.upsi.edu.my Perpustakaan Tuanku Bainun Kampus Sultan Abdul Jalil Shah PustakaTBainun ptbupsi

2.6 Synthesis Methods of Graphene Oxide and Reduced Graphene Oxide

The considerable research on the synthesis of graphene and its derivatives, the desired structure, and properties since the last decade is highly dependent upon the size, shape, and functionalization groups on the surface of the nanomaterial. Among many fabrication techniques used, mechanical exfoliation synthesis is an efficient and handful process to generate graphene which was first explored by Novoselov et al., (2004). Furthermore, the high interest in graphite has increased that the exfoliation method may provide a simpler, cheaper, and more efficient, as well as may emphasize a variety of commercial product evolution.

The synthesis of GO can be essentially classified into two main categories namely, top-down (destruction) and bottom-up (construction) synthesis methods, as displayed in Figure 2.10. The top-down approach comprises the structural breakdown of precursor which is first extracted from a carbon source, typically the exfoliated graphite into the interlayer separation of graphene nanolayers (Chua & Pumera, 2014), particularly for use in nanocomposite materials (Lee et al., 2018). The top-down possesses several examples in this approach to produce graphitic forms including, mechanical or chemical exfoliation (Huang et al., 2015; Park & Ruoff, 2009), arc discharge (Zhang et al., 2017), oxidative exfoliation, and reduction of GO (Emiru & Ayele, 2016), liquid-phase exfoliation (LPE) (Wan et al., 2018), and unzipping of carbon nanotubes (CNTs) (Silva et al., 2018).

05-4506832 pustaka.upsi.edu.my Perpustakaan Tuanku Bainun Kampus Sultan Abdul Jalil Shah PustakaTBainun ptbupsi

05-4506832 pustaka.upsi.edu.my Perpustakaan Tuanku Bainun Kampus Sultan Abdul Jalil Shah PustakaTBainun ptbupsi

Meanwhile, the bottom-up synthesis was utilized by alternative sources of carbon material which require a high temperature to build the hexagonal structure of the graphene sheets (Price et al., 2019). Due to these, several methods were implemented in this approach including, chemical vapor deposition (CVD) (Shen et al., 2018), epitaxial growth (Kruskopf et al., 2018), substrate-free gas-phase synthesis (Dato & Frenklach, 2010), template route (Yang et al., 2015), and total organic system (Singh et al., 2011). Nevertheless, the bottom-up synthesis brings a graphene product with defect free and large-scale area which exhibits several shortcomings of the time-consuming, as well as faces some challenges to scalability (Wang et al., 2017). Hence, high demand in the nanotechnology field has been focused on the top-down synthesis approaches which were discovered as convenient works to generate the GO-based materials.

05-4506832 pustaka.upsi.edu.my Perpustakaan Tuanku Bainun Kampus Sultan Abdul Jalil Shah PustakaTBainun ptbupsi

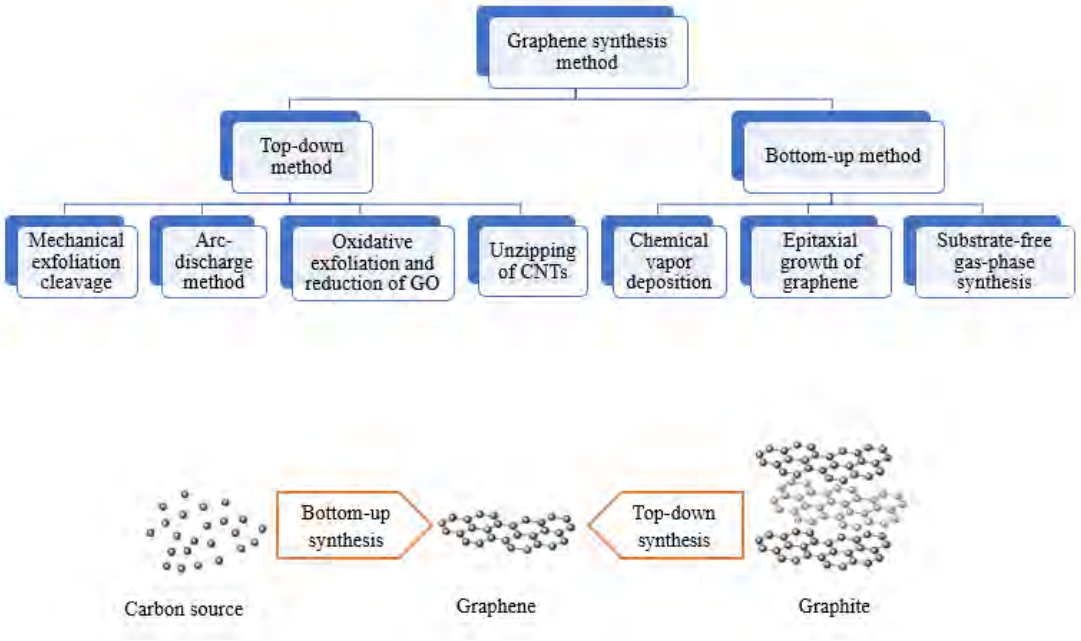


Figure 2.10. Schematic illustration of graphene synthesis methods and 'top-down' and 'bottom-up' graphene synthesis (Edwards & Coleman, 2013; Lee et al., 2018)

05-4506832 pustaka.upsi.edu.my Perpustakaan Tuanku Bainun Kampus Sultan Abdul Jalil Shah PustakaTBainun ptbupsi

05-4506832 pustaka.upsi.edu.my Perpustakaan Tuanku Bainun Kampus Sultan Abdul Jalil Shah PustakaTBainun ptbupsi

2.6.1 Chemical Oxidation Process

2.6.1.1 Brodie and Staudenmaier Method

The first approach for GO synthesis was constantly attributed by Brodie, (1859) in which his work proposed the first manufacturing of GO and introduced an oxidization mixture whereby, the graphite was combined with the potassium chloride, $KClO_3$ and solubilized in the nitric acid, HNO_3. Subsequently, a further approach for deriving the graphite oxide was followed by Staudenmaier, (1898) who improved Brodie's method through the incorporation of sulphuric acid, H_2SO_4 in order to increase the acidity of the mixture. Nonetheless, Brodie and Staudenmaier's method evolve more outcome hazards such as toxic ClO_2 gases which attribute to oxidized graphitic material.

05-4506832 pustaka.upsi.edu.my Perpustakaan Tuanku Bainun Kampus Sultan Abdul Jalil Shah PustakaTBainun ptbupsi

2.6.1.2 Hummers and Modified Hummers Method

Years later, Hummers & Offeman, (1958) proposed an alternative technique via replacing the HNO_3, $KClO_3$ with potassium permanganate, $KMnO_4$ as an oxidizer, and the use of sodium nitrate to form nitric acid in situ rather than using nitric acid as a solvent whereby, these chemical substances may improve the condition with a drastic manufacturing time less than 2h with a lower temperature, as well as, to produce less hazardous compared to the previous work. Therefore, this approach is generally used to generate the GO due to the safer and more scalable nature of Hummer's method.

05-4506832 pustaka.upsi.edu.my Perpustakaan Tuanku Bainun Kampus Sultan Abdul Jalil Shah PustakaTBainun ptbupsi

05-4506832 pustaka.upsi.edu.my Perpustakaan Tuanku Bainun Kampus Sultan Abdul Jalil Shah PustakaTBainun ptbupsi

Another popular modification that changes or improves the synthesis method proposed by Hummers is regarded as a "modified Hummer's method" whereby, this approach gets rid of the sodium nitride, $NaNO_3$ by adding up phosphoric acid, H_3PO_4 and thus, enlarged the amount of $KMnO_4$. The resulting mixture can be attributed to no toxic gases, easy to control the temperature, and more production of GO powder with a higher oxidation degree (Marcano et al., 2010). Alternatively, the researchers should acknowledge modifying Hummer's method to suit their desired applications by considering the carbon source, pre-treatment techniques, oxidizing agent, and choice of the solvent, as these considerations may give the beneficial impact of carbon to oxygen atomic (C/O) ratio for the final GO products. Last but not least, an overview of the popular methods which was successfully accomplished for the synthesis of GO are presented in Figure 2.11.

05-4506832 pustaka.upsi.edu.my Perpustakaan Tuanku Bainun Kampus Sultan Abdul Jalil Shah PustakaTBainun ptbupsi

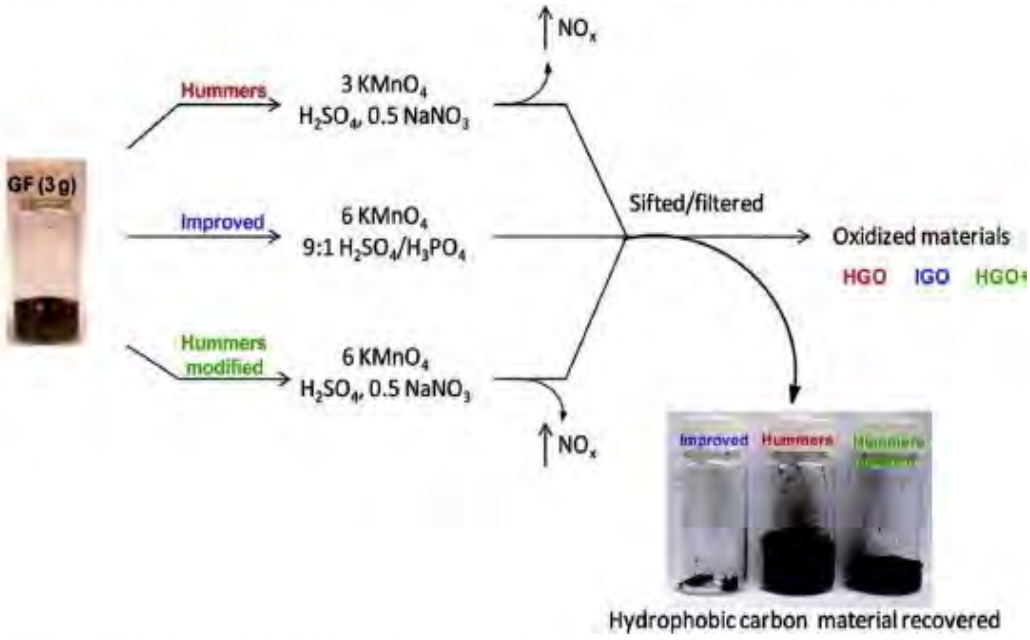


Figure 2.11. Schematic representation of common methods used to synthesize the GO (Marcano et al., 2010)

05-4506832 pustaka.upsi.edu.my Perpustakaan Tuanku Bainun Kampus Sultan Abdul Jalil Shah PustakaTBainun ptbupsi

05-4506832 pustaka.upsi.edu.my Perpustakaan Tuanku Bainun Kampus Sultan Abdul Jalil Shah PustakaTBainun ptbupsi

2.6.2 Chemical Reduction Process

2.6.2.1 Chemical Reagent Reduction

The reduction process by chemical reagents is referred to the chemical reactions with the produced GO. Normally, the reduction of GO can be accomplished at room temperature or by using moderate heating. Consequently, the requirement for the equipment to reduce the GO is not as critical compared to thermal reduction treatment, which attributes the chemical reduction as cheaper and easy to handle for the mass production of graphene.

Alternatively, the researchers have been done many efforts to produce the materials with the desired properties as close to the pristine graphene by removing the oxygen functional groups of GO using the chemical reduction method (De Silva et al., 2017; Stankovich et al., 2007). This reduction approach can be implied from the thermal to chemical to electrochemical whereby, each of these leads to the differences in the morphological, electrical, and other properties. Commonly, the reduction of GO can be comprised of important factors including, the C/O ratio of the final product, selectivity of removing a single type of oxygen group (hydroxyl, carboxylic acid, and epoxy), surface defects of the GO based on the oxidation process, the use of reducing agents (hydrazine hydrate), as well as important to maintain the desired physical or chemical properties of the GO for instances, electrical conductivity, mechanical strength, optical properties, solubility or dispersibility of the GO nanosheets (Smith et al., 2019).

05-4506832 pustaka.upsi.edu.my Perpustakaan Tuanku Bainun Kampus Sultan Abdul Jalil Shah PustakaTBainun ptbupsi

05-4506832 pustaka.upsi.edu.my Perpustakaan Tuanku Bainun Kampus Sultan Abdul Jalil Shah PustakaTBainun ptbupsi

The electrochemical reduction of GO is essential due to the use of chemical agents which are exclusively driven by the electron exchange between GO surfaces and electrodes of a typical electrochemical cell (Yang et al., 2016). Recently, numerous green reducing agents have been reported to be effective in synthesizing rGO solutions including, ascorbic acids, sugars, amino acids, and microorganisms, as well (De Silva et al., 2017). These reducing agents were selectively attributed to the different techniques used for fabricating the rGO due to their superior advantages in scalability (the capacity to be changed in size or scale), energy usage, and amount of chemical waste produced.

In addition to this approach, the reduction of graphite oxide by using the hydrazine hydrate has been applied to the discovery of graphene meanwhile, the use of hydrazine to prepare chemically the derived graphene was first explored by Stankovich et al., (2007). These investigations present the open approach for the convenient mass production of graphene. Consequently, the hydrazine hydrate has been accepted as a high-demand which acts as the chemical reagent to successfully reduce the GO. Furthermore, the reduction process of graphene and its derivatives by using the hydrazine hydrate and dimethylhydrazine can be significantly achieved by adding up these liquid reagents into a GO aqueous dilution and thus, resulting in the agglomerated structures of graphene-based nanomaterials due to a higher of hydrophobility effects (Pei & Cheng, 2012).

In an effort to fulfill the applications of graphene, some researchers had proposed solutions to reduce the GO and at the same time, retain the colloidal state in water through the incorporation of soluble polymers as surfactants, or ammonia in order to alter the charge

05-4506832 pustaka.upsi.edu.my Perpustakaan Tuanku Bainun Kampus Sultan Abdul Jalil Shah PustakaTBainun ptbupsi

05-4506832 pustaka.upsi.edu.my Perpustakaan Tuanku Bainun Kampus Sultan Abdul Jalil Shah PustakaTBainun ptbupsi

state of the rGO nanosheets. Due to these advantages, the graphene sheets produced in the colloidal solutions can be subsequently used for macroscopic structures via a simple solution process such as the filtration method.

Other than that, metal hydrides such as sodium hydride, sodium borohydride ($NaBH_4$), and lithium aluminium hydride have been recommended as the strong reducing agents in organic chemistry however, these chemical agents possessed a slight to very strong reactivity with the water which becomes the main solvent for the exfoliation and dispersion of GO samples. Shin et al., (2009) proposed that $NaBH_4$ was exhibited as an effective reductant than the hydrazine hydrate for the reduction process even though, it is slowly hydrolyzed by the water and thus, effectively can reduce C = O species during the reduction process. As an improvement, an additional dehydration approach has been suggested by using the concentrated sulphuric acid of about 98% H_2SO_4 after the reduction by $NaBH_4$ in order to further enhance the reduction process of GO (Gao et al., 2009).

Other strong reductants have been reported by Moon et al., (2010) whereby, the hydroiodic acid (HI) was used for the reduction of GO. This approach can be realized by using the GO in the form of a colloid, powder, or film in a gas or solution environment and placed at room temperature. In comparison with the reducing agents as has been stated earlier, the GO film which was reduced by HI possessed good flexibility and improved tensile strength. As a result, the HI shows a better reducing effect than the hydrazine hydrate and is suitable to be used for the reduction of GO films.

05-4506832 pustaka.upsi.edu.my Perpustakaan Tuanku Bainun Kampus Sultan Abdul Jalil Shah PustakaTBainun ptbupsi

05-4506832 pustaka.upsi.edu.my Perpustakaan Tuanku Bainun Kampus Sultan Abdul Jalil Shah PustakaTBainun ptbupsi

On the contrary to the chemical reagent used, another method that promises the reduction of GO is rely on the electrochemical removal of oxygen functionalization groups (Zhou et al., 2009). Usually, the electrochemical reduction of GO sheets can be performed using an aqueous buffer solution at room temperature along with the supported absence of chemical reductant and especially caused via the electron exchange between the electrodes and GO sheets. Consequently, the reduction process could inhibit dangerous chemical reductants such as hydrazine hydrate.

2.6.2.2 Thermal Annealing for Reduction

Reduction of GO via a thermal treatment depends on the decomposition of oxygen functional groups into CO and CO_2 gases at the elevated temperature (Pei & Cheng, 2012; Slobodian et al., 2018) whereby, these gases are applied to exfoliate an individual GO nanosheets. Due to these advantages, a thermal reduction can be accomplished by thermal annealing at an elevated temperature in an oxygen-free environment or via less-conventional techniques such as microwaving the GO powder and flash reduction of GO films by using a high-intensity light. The inclusion of chemical reducing agents including, hydrazine hydrate (Stankovich et al., 2007), metal hydrides, and hydrohalic acids (Pei & Cheng, 2012) to produce the GO solutions is commonly used by many techniques which were supported in the previous literature.

05-4506832 pustaka.upsi.edu.my Perpustakaan Tuanku Bainun Kampus Sultan Abdul Jalil Shah PustakaTBainun ptbupsi

05-4506832 pustaka.upsi.edu.my Perpustakaan Tuanku Bainun Kampus Sultan Abdul Jalil Shah PustakaTBainun ptbupsi

In the initial stages of graphene exploration, GO can be significantly reduced by heat treatment whereby, the rapid heating of more than 2000 °C/min was normally used to exfoliate the graphite oxide for graphene production. Typically, the exfoliated nanosheets namely, the chemical graphene derivatives underwent the rapid heating process and reduces the functionalized graphene sheets via decomposing the oxygen-containing groups at an elevated temperature. Notably, the effect of thermal exfoliation is that, the structural damage to graphene sheets is caused by the release of carbon dioxide (Kudin et al., 2008). As a result, the electrical conductivity of the graphene sheets possesses a typical mean value of 10-23 S/cm which was much lower compared to the perfect graphene and thus, indicating the weak effect on the reduction and restoration of an electronic structure of a carbon plane (Schniepp et al., 2006). Therefore, Schniepp et al., (2006) demonstrated that the if the temperature was less than 500 °C then, the resulting C/O ratio was not more than 7 meanwhile, if the temperature reached 750 °C then, the C/O ratio should be higher than 13. Consequently, these results of heating temperature significantly affect the reduction of GO.

In addition to the interesting topic on the annealing temperature, the annealing atmosphere is essential for the thermal annealing reduction of GO. The oxygen gas should be excluded during the annealing process because of the etching of oxygen that will be dramatically increased at high temperatures. Usually, the annealing reduction method is performed in a vacuum with inert gases, and reducing atmosphere (Becerril et al., 2008; Wang et al., 2008).

05-4506832 pustaka.upsi.edu.my Perpustakaan Tuanku Bainun Kampus Sultan Abdul Jalil Shah PustakaTBainun ptbupsi

05-4506832 pustaka.upsi.edu.my Perpustakaan Tuanku Bainun Kampus Sultan Abdul Jalil Shah PustakaTBainun ptbupsi

2.7 Overview of Carbon Nanotubes

Carbon nanotubes (CNTs) are completely carbon-based hollow tubes with nanometer-sized diameters. Particularly, nanotubes are intriguing candidates for nanoscale light emitters and many other optical applications including, in the region of interest for infrared wavelength applications such as optical communication. In addition to this, nanotubes exhibit a variety of highly remarkable characteristics depending on their diameter and "twist" feature which makes them either metallic or semiconductors.

2.7.1 Structures of Carbon Nanotubes

05-4506832 pustaka.upsi.edu.my Perpustakaan Tuanku Bainun Kampus Sultan Abdul Jalil Shah PustakaTBainun ptbupsi

CNTs are well known as a one-atom-thick sheet of graphite called graphene, rolled up into seamless cylinders with a diameter of the order of nanometers. Since the initial report was proposed by Iijima in 1991, CNTs have evolved into the forefront in the nanotechnology research fields. However, it was believed that the history of CNTs has been explored since the 1950s when researchers started the discovery of CNTs structures in the range of 50 to 100 nm diameters. The development of CNTs was continued when Iijima observed the needle-shaped material which appeared on the fullerene via the arc-discharge method. These unique needle-shaped materials were then officially converted to the name of "carbon nanotube" by Iijima after considering the CNTs possess the nanometers size and tubular shape. Since then, Iijima's discovery of CNTs has become a turning point for further

05-4506832 pustaka.upsi.edu.my Perpustakaan Tuanku Bainun Kampus Sultan Abdul Jalil Shah PustakaTBainun ptbupsi

05-4506832 pustaka.upsi.edu.my Perpustakaan Tuanku Bainun Kampus Sultan Abdul Jalil Shah PustakaTBainun ptbupsi

exploration of CNTs due to its great significance for applications as well as excellent properties, including optical, electrical, mechanical, and thermal characterizations.

CNTs are theoretically an allotrope of carbon fabricated by rolling up graphene sheets. Based on the number of concentrically rolled-up graphene sheets, CNTs can be categorized into single-walled (SWCNTs) and multi-walled (MWCNTs). The SWCNTs are described as a single graphitic sheet wrapped into a cylinder tube meanwhile, MWCNTs are intrinsically comprised of concentric sheets covered with graphite multilayers.

In addition, the structure of SWCNTs can be visualized as a rolled-up tubular shell of graphene sheet made up of benzene-type hexagonal rings of carbon atoms. The MWCNTs is the stack of graphene sheets rolled-up whereby, each nanotube is a single molecule composed of millions of atoms and the length of this molecule can be tens of micrometers long with diameters as small as 0.7 nm (Meyyappan et al., 2003). Typically, the SWCNTs contain only 10 atoms around the circumference and the thickness of the tube is only one atom thick. Meanwhile, the MWCNTs are larger than SWCNTs and consist of many single-walled stacked ones inside each other.

Dependent on the wrapping of graphene into a cylinder shape during its creation process, there are three different possible forms of SWCNTs including, armchair, zigzag, and chiral (refer to Figure 2.12). The SWCNTs structure is well-characterized by a pair of indices (n, m) which ascribe the chiral vector and have an effect on the electrical properties of nanotubes. As a common opinion, when $m = 0$, the nanotubes are called “zigzag”

05-4506832 pustaka.upsi.edu.my Perpustakaan Tuanku Bainun Kampus Sultan Abdul Jalil Shah PustakaTBainun ptbupsi

05-4506832 pustaka.upsi.edu.my Perpustakaan Tuanku Bainun Kampus Sultan Abdul Jalil Shah PustakaTBainun ptbupsi

nanotubes, when $n = m$, the nanotubes are called "armchair" nanotubes, and the other state is called "chiral" nanotubes.

The chiral vector $C = na_1 + ma_2$ (a_1 and a_2 are the base cell vectors of graphite) identifies the tube diameter d, and finds out the direction of a rolling graphene sheet. Thus, the diameter of a carbon tube can be derived by the following expression:

$$d = \frac{a\sqrt{m^2+mn+n^2}}{\pi} \quad (2.1)$$

where $a = 1.42 \times \sqrt{3}$ which refers to the lattice constant in the graphite sheet. When $n - m$ is a multiple of 3, the nanotube can be described as 'metallic' or highly conducting nanotubes, and if not, therefore, the nanotube is a semi-metallic or semiconductor. Wholly, the armchair nanotube is metallic, whereas other forms of nanotubes will form a semiconductor. The parameters and vectors attribute to an effect on nanotube structures are as follows (Ali et al., 2014):

1. Translational vector = $T = t1a1 + t2a2 >> (t1, t2)$
2. Chiral vector = Ch = na1 + na2 >> (n, m)
3. Length of chiral vector = $L = a\ \sqrt{(n^2 + m^2 + n * m)}$

   where a is the lattice constant
4. Chiral angle = $cos\ \theta = (2n + m) / (2* \sqrt{(n^2 + m^2 + n * m)})$
5. Number of hexagons in the unit cell = $N = (2 * (n^2 + m^2 + n * m) / dR)$

05-4506832 pustaka.upsi.edu.my Perpustakaan Tuanku Bainun Kampus Sultan Abdul Jalil Shah PustakaTBainun ptbupsi

05-4506832 pustaka.upsi.edu.my Perpustakaan Tuanku Bainun Kampus Sultan Abdul Jalil Shah PustakaTBainun ptbupsi

6. Diameter = $dt = L/\pi$
7. Rotation angle of the symmetry vector = $\psi = 2\pi/ N$ (in radians)
8. Symmetry vector = $R = p\text{a}1 + q\text{a}2 >> (p, q)$
9. Pitch of the symmetry vector = $\tau = ((\text{m} * p\text{-}n * q) * T) / N$

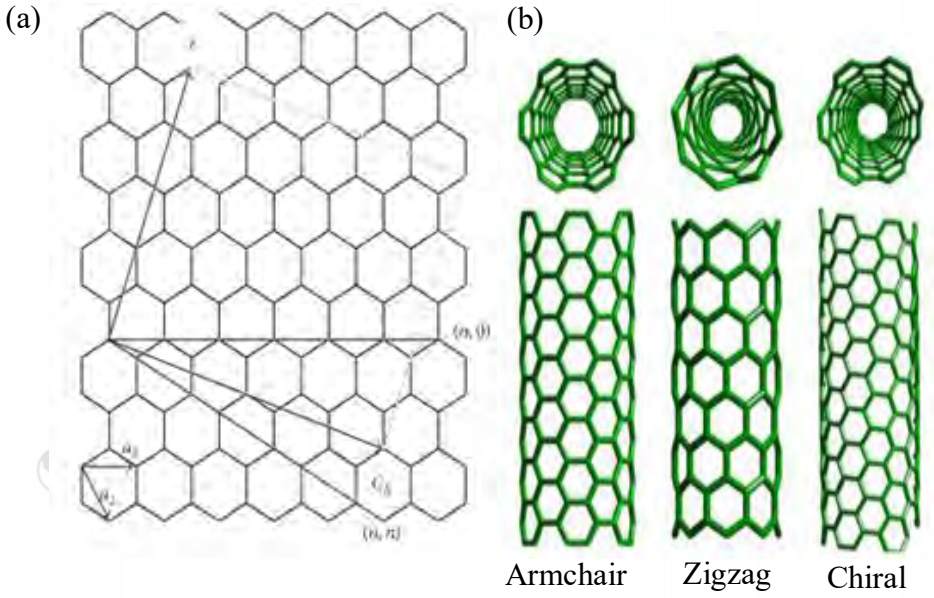


Figure 2.12. Schematic representation of (a) formation of SWCNTs by rolling of a graphene sheet along lattice vectors which leads to armchair, zigzag, and chiral tubes, (b) the three forms of CNTs (Madani et al., 2013)

MWCNTs can be formed into two structural models including, the Russian Doll model and the Parchment model. When a carbon nanotube contains another carbon nanotube inside it then, the outer nanotube has a greater diameter than the thinner nanotube, which is known as the Russian Doll model. On the other hand, when a single graphene sheet is wrapped around itself manifold times then, it is called the Parchment model. Both SWCNTs and MWCNTs exhibit similar properties, and due to the multilayer nature of

05-4506832 pustaka.upsi.edu.my Perpustakaan Tuanku Bainun Kampus Sultan Abdul Jalil Shah PustakaTBainun ptbupsi

05-4506832 pustaka.upsi.edu.my Perpustakaan Tuanku Bainun Kampus Sultan Abdul Jalil Shah PustakaTBainun ptbupsi

MWCNTs, the outer walls are not be able to shield the inner carbon nanotubes however, the MWCNTs present the high tensile strength properties which only exist partially in the SWCNTs. Briefly, the comparison between both SWCNTs and MWCNTs is summarized in Table 2.1.

Table 2.1

The comparison between SWCNTs and MWCNTs (Iijima & Ichihashi, 1993)

SWCNTs	MWCNTs
• Single layer of graphene	• Multiple layers of graphene
• Catalyst is required for synthesis	• Can be produced without catalyst
• Bulk synthesis is difficult as it requires proper control over atmospheric condition	• Bulk synthesis is easy
• Purity is poor	• Purity is high
• A chance of defect is more during functionalization	• A chance of defect is less but once occurred it is difficult to improve
• Can be easily twisted	• Can be easily twisted

Carbon has different approaches in order to build bond structures with their completely different properties. The sp^2 hybridization of carbon shows a strong layered construction with weak out-of-plane bonding of the van der Waals form and excellent in-plane bounds (Ali et al., 2014). In addition, the strong sp^2 individual carbon bonds possess a higher tensile strength compared to steel and Kevlar. In fact, this bond is even stronger

05-4506832 pustaka.upsi.edu.my Perpustakaan Tuanku Bainun Kampus Sultan Abdul Jalil Shah PustakaTBainun ptbupsi

05-4506832 pustaka.upsi.edu.my Perpustakaan Tuanku Bainun Kampus Sultan Abdul Jalil Shah PustakaTBainun ptbupsi

than the sp^3 bond existing in a diamond whereby, the SWCNTs have tensile strength hundreds of times than steel. The highest measured tensile strength or known as breaking strain for a carbon nanotube was up to 63 GPa which is around 50 times higher than steel (Yu et al., 2000) and even the weakest types of CNTs have strengths of several GPa (Xie et al., 2000). Other than that, the CNTs possess good chemical and environmental stability and high thermal conductivity (~3000 W/m/K), comparable to a diamond. Thus, the applications of CNTs encompass many fields and disciplines including, nanotechnology, manufacturing, electronics, and biomedical (Ali et al., 2014).

2.8 Properties of Carbon Nanotubes

05-4506832 pustaka.upsi.edu.my Perpustakaan Tuanku Bainun Kampus Sultan Abdul Jalil Shah PustakaTBainun ptbupsi

As stated in the early introduction, CNTs originated based on graphite sheets with the presence of new properties by the effects of quantum confinement. Therefore, a brief introduction focusing on the basic properties of CNTs, followed by a discussion on the related optical and electronic properties of CNTs, as well as other thermal properties will be discussed in the next subsection.

2.8.1 Optical and Electronic Properties

The electronic properties of CNTs are essential due to their high electrical conductivity which promises the CNTs to be either metallic or semiconducting properties. The rolling

05-4506832 pustaka.upsi.edu.my Perpustakaan Tuanku Bainun Kampus Sultan Abdul Jalil Shah PustakaTBainun ptbupsi

05-4506832 pustaka.upsi.edu.my Perpustakaan Tuanku Bainun Kampus Sultan Abdul Jalil Shah PustakaTBainun ptbupsi

action in the CNTs breaks the symmetry of the planar system and reveals a different direction along with the hexagonal lattice network and axial direction which reforms the nanotubes to behave electrically either as metallic or semiconductor properties. Taking advantage of the CNTs, the semiconducting CNTs usually possess the optical bandgap energy ranging from approximately 1.8 eV on very small diameter tubes to transform into 0.18 eV for the largest possible diameter tubes (Saifuddin et al., 2013). As a result, some of the nanotubes possess electrical conductivities higher than copper, resulting in the possibility of electronic devices.

In addition to this, CNTs comprised of two kinds of bonds by the factor of sp^2 hybridization including, σ bonds located on the cylinder walls and attribute to the formation of the hexagonal network, as well as the π bonds which may interact between the nanotubes with existing of van der Waals force (Norizan et al., 2020). Unfortunately, σ bonds in-plane are unable to attribute to electronic properties such as the role in optical absorption or electronic characteristics due to the σ bonds being positioned far away from the Fermi level (Khosravi et al., 2021). On the contrary, π bonds with the energies are located near to Fermi level.

2.8.2 Thermal Properties

Recently, the measurement of thermal conductivity demonstrates higher conductivity of about 2000 W/m/K for a single nanotube meanwhile, the multi nanotubes possess

05-4506832 pustaka.upsi.edu.my Perpustakaan Tuanku Bainun Kampus Sultan Abdul Jalil Shah PustakaTBainun ptbupsi

05-4506832 pustaka.upsi.edu.my Perpustakaan Tuanku Bainun Kampus Sultan Abdul Jalil Shah PustakaTBainun ptbupsi

approximately ~3000 W/m/K as compared to diamond however, both types of nanotubes are greater than graphite and carbon material. Furthermore, the thermal conductivity of CNTs is significantly dependent on several factors including, chirality and diameter of CNTs, morphology, defects, and size of the CNTs. Therefore, it can be concluded that the graphitization process of CNTs is required to produce lower defects, uniform structures of CNTs, as well as a good value of thermal conductivity (Han & Fina, 2011).

2.9 Synthesis Methods of Carbon Nanotubes

The number of patents on the synthesis of CNTs is increasing rapidly however, there are many challenges remaining that must be resolved regarding the synthesis of CNTs. Currently, the main challenges in the field of nanotube synthesis include mass production which relates to the low-cost, large-scale production of high-quality nanotubes, selective production whereby, it controls the structure and electronic properties of produced nanotubes, the organization that controls the orientation of produced nanotubes, and the development of mechanism during the formation of CNTs.

There are several techniques that have been developed for producing nanotube structures and different morphology which mostly involve the gas phases. Commonly, there are three procedures used to synthesize the CNTs including, the carbon arc-discharge, the laser ablation technique, and the chemical vapor deposition (CVD) technique. Furthermore, high-temperature preparation techniques for laser-ablation or arc-discharge

05-4506832 pustaka.upsi.edu.my Perpustakaan Tuanku Bainun Kampus Sultan Abdul Jalil Shah PustakaTBainun ptbupsi

05-4506832 pustaka.upsi.edu.my Perpustakaan Tuanku Bainun Kampus Sultan Abdul Jalil Shah PustakaTBainun ptbupsi

were the first techniques used to synthesize CNTs, however, these techniques have been replaced by low-temperature CVD method (<800 °C), whereby the length, diameter, alignment, purity, density, and orientation of CNTs can be accurately controlled by the low CVD method (Ganesh, 2013). Basically, the raw elements in the formation of CNTs are catalysts, a source of carbon, and sufficient energy. The features of all of these techniques act as the addition of energy to a carbon source in order to produce the fragments (single C atoms or groups) which may recombine to generate CNTs (Saifuddin et al., 2013).

2.9.1 Arc Discharge

Arc-discharge was the first technique introduced by Bacon (1960) that allowed the synthesis of SWCNTs in relatively large amount (gram). Afterward, the utilization for the production of CNTs was carried out by Iijima and co-workers (1991). This technique uses a higher temperature above 1700 °C for the synthesis of CNTs which typically causes the production of CNTs with fewer structural defects, compared with other techniques, as shown in Figure 2.13. Commonly, the utilized arc-discharge technique uses the high-purity graphite (6 to 10 mm optical density (OD)) electrodes whereby, the electrodes are water-cooled electrodes with diameters between 6 and 12 mm as well as, separated by 1 to 2 mm in a chamber filled with helium (500 torrs) at sub-atmospheric pressure (Grobert, 2007). To date, many modifications to the arc-discharge process have been suggested due to the different applied in gas, current, and pressure to induce the reorganization of carbon atoms into CNTs (Chaudhary et al., 2013).

05-4506832 pustaka.upsi.edu.my Perpustakaan Tuanku Bainun Kampus Sultan Abdul Jalil Shah PustakaTBainun ptbupsi

05-4506832 pustaka.upsi.edu.my Perpustakaan Tuanku Bainun Kampus Sultan Abdul Jalil Shah PustakaTBainun ptbupsi

Generally, there are two main different approaches which are, the CNTs synthesis using the different catalyst precursors and without the use of catalyst precursors in the arc-discharge deposition procedure and production of CNTs. The synthesis of MWCNTs can be conducted without the use of catalyst precursors however, the synthesis of SWCNTs uses the varying catalyst precursors for expansion of CNTs, by a composition of graphite and metal, as well. The previous studies have proposed that Ni-Y-graphite mixtures can generate high yields (<90 %) of SWCNTs with an average diameter in the range of 1.0 to 1.4 nm, respectively (Saito et al., 1998).

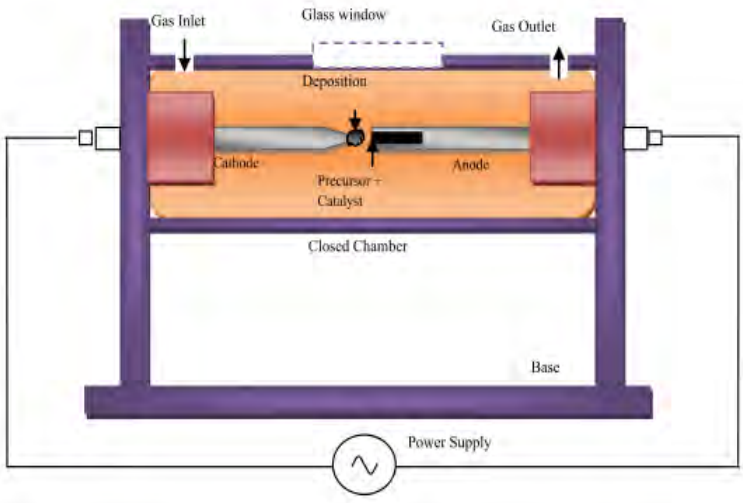


Figure 2.13. Schematic diagram of an arc-discharge set up (Arora & Sharma, 2014)

2.9.2 Chemical Vapor Deposition (CVD)

In contrast with both previous techniques, the CVD method involves the decomposition of a gaseous or volatile compound of carbon that is catalyzed by metallic nanoparticles, and

05-4506832 pustaka.upsi.edu.my Perpustakaan Tuanku Bainun Kampus Sultan Abdul Jalil Shah PustakaTBainun ptbupsi

05-4506832 pustaka.upsi.edu.my Perpustakaan Tuanku Bainun Kampus Sultan Abdul Jalil Shah PustakaTBainun ptbupsi

thus, served as the nucleation site for the initiation of carbon nanotube growth, as presented in Figure 2.14. This technique eventually allows CNTs to expand on different materials and involves the chemical breakdown of a hydrocarbon on a substrate. The main process of growing CNTs in this technique is similar to an arc-discharge technique whereby, the carbon atoms are in contact with the metallic catalyst particles.

Fortunately, the CVD has been proven to be a preferred technique for a purpose of large quantities production of CNTs due to the structures, diameter, length, and alignment can be well controlled during the CVD process. Therefore, the main advantages of this technique consist of a relatively low cost, mild operation, and controllable process. As compared with laser ablation, CVD is an economically practical technique for large-scale and pure production of CNTs, as well.

05-4506832 pustaka.upsi.edu.my Perpustakaan Tuanku Bainun Kampus Sultan Abdul Jalil Shah PustakaTBainun ptbupsi

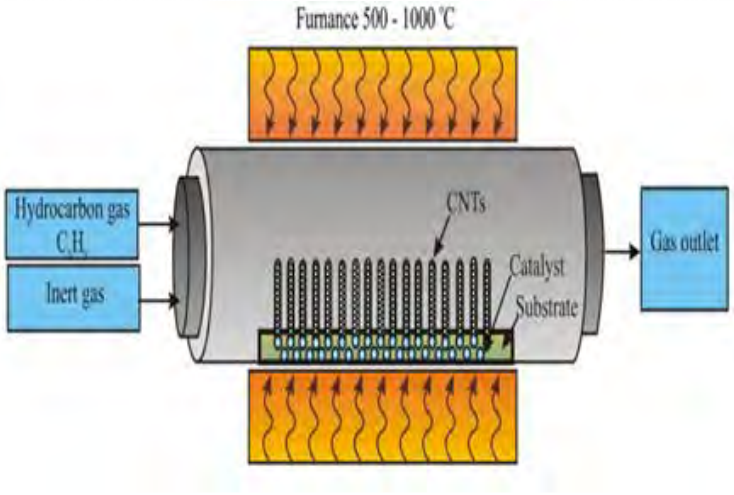


Figure 2.14. Schematic representation of CVD process (Zaytseva & Neumann, 2016)

05-4506832 pustaka.upsi.edu.my Perpustakaan Tuanku Bainun Kampus Sultan Abdul Jalil Shah PustakaTBainun ptbupsi

05-4506832 pustaka.upsi.edu.my Perpustakaan Tuanku Bainun Kampus Sultan Abdul Jalil Shah PustakaTBainun ptbupsi

2.10 Physical Properties Characterization

2.10.1 Density and Molar Volume

Density is an important physical property that provides information on the structural changes in glass materials. There are many factors that cause the density measurement including, change in coordination number, geometrical configuration, and degree of structural compactness within the chosen matrix (Deopa & Rao, 2017; Mawlud et al., 2017; Tiwari & Dhondiyal, 2021). Archimedes' principle has been used to obtain the molar volume by relying on the density of all the glass samples, as follows:

$$\rho_{\text{sample}} = \frac{W_{\text{air}}}{V} \tag{2.2}$$

05-4506832 pustaka.upsi.edu.my Perpustakaan Tuanku Bainun Kampus Sultan Abdul Jalil Shah PustakaTBainun ptbupsi

where ρ_{water} = 1 g/cm^3

W_{air} = weight of glass sample in air (g)

V = volume of glass sample (cm^3)

The molar volume of glass sample can be measured by the following expression:

$$V_m = \frac{M_w}{\rho} \tag{2.3}$$

where M_W = molecular weight of glass sample (g/mol)

ρ = density of glass sample (g/cm^3)

05-4506832 pustaka.upsi.edu.my Perpustakaan Tuanku Bainun Kampus Sultan Abdul Jalil Shah PustakaTBainun ptbupsi

05-4506832 pustaka.upsi.edu.my Perpustakaan Tuanku Bainun Kampus Sultan Abdul Jalil Shah PustakaTBainun ptbupsi

The study on physical parameters of the tellurite glass system has been investigated whereby, the density showed the increasing trend and the molar volume was found in the decreasing trend along with the increasing of ZnO contents (Elkhoshkhany et al., 2018). Due to this work, it was clearly stated that the density and molar volume characteristics can be correlated with each other with the presence of ZnO inside the glassy matrix. The addition of ZnO into tellurite-based host glass imposed the increment in density caused by the rearrangement of the internal structural network meanwhile, the decrement of molar volume may be associated with the following factors:

1. The decreasing in bond length or known as "inter-atomic spacing" between the atoms
2. The radius of Zn^{2+} (0.074 nm) is much smaller than Te^{2+} (0.097 nm) which attributes to more compactness and denser glass
3. The increasing of connectivity of glass (for example: increasing the number of bonds)

The physical characteristics had been investigated for ZnO doped tellurite-based glass whereby, the calculated density was found to increase along with the increase of ZnO concentrations in the glass network system (Gangwar et al., 2019). Meanwhile, it was revealed that the molar volume was found in the decreasing pattern which can be ascribed in terms of zinc inclusion into the base glass system thereby, cause the decrement of molar volume. Primarily, the ZnO itself incorporates a larger radius than the radius of tellurium oxide and can act as a network modifier creates weaker bonds in the glassy matrix system.

05-4506832 pustaka.upsi.edu.my Perpustakaan Tuanku Bainun Kampus Sultan Abdul Jalil Shah PustakaTBainun ptbupsi

05-4506832 pustaka.upsi.edu.my Perpustakaan Tuanku Bainun Kampus Sultan Abdul Jalil Shah PustakaTBainun ptbupsi

The interatomic spacing then becomes smaller caused by the weaker bond length in Zn-Te linkage comparable to the bond distance existing in Te-Te atoms. Thus far, the tellurite-based structure glass system is denser and promotes the higher compactness of the glass system.

The effect of Er^{3+} ions on the physical characteristics had been studied for phosphate glass whereby, the density values were observed in the increasing pattern from 4.0 to 5.6 g/cm^3 while the molar volume values showed the decreasing trend from 42.2 to 30.8 cm^3/mol, respectively (Ahmed et al., 2019). The increment of density is caused by the increasing content of dopant Er^{3+} ions which resulted in the creation of non-bridging oxygens (NBOs) in the glass structures. Furthermore, Er^{3+} ions possess a high coordination which attribute to decreasing the interatomic spacing between the atom nuclei's distance and thereby, causing the lattice constant to decrease in the glass structural network.

2.10.2 Rare-earth Ion Concentration, Inter-ionic Distance, and Polaron Radius

The ionic concentration of rare-earth, N and inter-ionic distance, R_i in glass sample can be computed by the relation (Chimalawong et al., 2012):

$$N = \frac{N_A * \rho * x}{M_W} \tag{2.4}$$

05-4506832 pustaka.upsi.edu.my Perpustakaan Tuanku Bainun Kampus Sultan Abdul Jalil Shah PustakaTBainun ptbupsi

05-4506832 pustaka.upsi.edu.my Perpustakaan Tuanku Bainun Kampus Sultan Abdul Jalil Shah PustakaTBainun ptbupsi

where N_A, ρ, x, and M_W are referred to as Avogadro's number, the mole fraction of rare-earth oxide, the density of glass, and average molecular weight of glass sample. The inter-ionic distance, R_i can be calculated according to the relation (Bhatia et al., 2015):

$$R_i = \left(\frac{1}{\sqrt{N}}\right)^{\frac{1}{3}} \tag{2.5}$$

It is a significant parameter in determining the inter-ionic forces which result in the compactness of the glass. Polaron is a quasiparticle which used to analyze the interactions between electrons and atoms in a solid material. A conduction polaron (or hole) existing with the polarization in a polar semiconductor or an ionic crystal forms a quasiparticle, which is known as a polaron (Devreese, 2003). Polaron radius, R_P can be expressed by using the following equation (Bhatia et al., 2015):

$$R_P = \left(\frac{1}{2}\right) \times \left(\frac{\pi}{6N}\right)^{\frac{1}{3}} \tag{2.6}$$

It should be noted that the value of R_P must be greater than the radius of an atom whereby, the electron is localized, but less than the distance separating them. Polarons are become the proper approach for identifying the electrons and holes within different conducting materials however, they are only important in highly polar or ionic solids.

05-4506832 pustaka.upsi.edu.my Perpustakaan Tuanku Bainun Kampus Sultan Abdul Jalil Shah PustakaTBainun ptbupsi

05-4506832 pustaka.upsi.edu.my Perpustakaan Tuanku Bainun Kampus Sultan Abdul Jalil Shah PustakaTBainun ptbupsi

2.10.3 Oxygen Packing Density and Field Strength

Oxygen packing density (OPD) is defined as the arrangement of oxygen atoms in the oxide glasses which can be related to the spatial oxygen dispersion and molar volume (Saraswati et al., 2021). The OPD can be estimated by the relation given (Bhatia et al., 2015):

$$OPD = \frac{1000 * n * \rho}{M_W} \tag{2.7}$$

where n, ρ, and M_W are denoted as the number of oxygen atoms in the composition, density of glass, and molecular weight of glass. The field strength, F around rare-earth ions can be computed by the expression:

05-4506832 pustaka.upsi.edu.my Perpustakaan Tuanku Bainun Kampus Sultan Abdul Jalil Shah PustakaTBainun ptbupsi

$$F = \frac{Z}{{R_P}^2} \tag{2.8}$$

where Z is the thickness of the glass sample and R_P is the polaron radius.

The study on physical characteristics including, the OPD parameter had been investigated for Er^{3+} ions doped zinc bismuth borate glasses (Mariyappan et al., 2019). It is clearly observed that the steady increment of OPD values along with the Er_2O_3 concentration which indicates the formation of bridging oxygens (BOs) ultimately assists to create the compactness in the glass structures.

05-4506832 pustaka.upsi.edu.my Perpustakaan Tuanku Bainun Kampus Sultan Abdul Jalil Shah PustakaTBainun ptbupsi

05-4506832 pustaka.upsi.edu.my Perpustakaan Tuanku Bainun Kampus Sultan Abdul Jalil Shah PustakaTBainun ptbupsi

2.11 Morphological Properties Characterization

Microstructure analysis can be referred to as the scientific investigation of the structure which involves three-dimensional shapes of a surface layer and thereby, may apply to sophisticated microscopes to form images of samples that cannot be seen with the naked eye. The microstructural analysis characterization including, SEM, EDX, and HR-TEM are significantly important for observing the surface morphology of the materials.

Firstly, SEM demonstrates the magnified micrographs of the size, shape, crystallography, and other physical or chemical properties of the prepared specimen (Ural, 2021). In the early 1950s, the commercial SEM investigation was continued along with extensive development studies by Charles Oatley and his co-workers at the University of Cambridge (Smith et al., 2008). Furthermore, it is well-known that SEM uses an electron beam to produce images with a resolution in the nanometer scale. The emitted electrons from a filament and moved into a beam in the electron source and thus, the beam is focused on the sample surfaces via a set of lenses located in an electron part. Commonly, the captured images ranging from approximately 1 cm to 5 microns and may be projected in a scanning mode with a magnification in the range of 20 X to 30 K X and spatial resolution from 50 – 100 nm. SEM is widely used to identify phases from the chemical analysis or crystalline structures. In addition, SEM is routinely used to produce high-resolution images of the materials, as well as to demonstrate the variations in chemical compositions by acquiring the elemental mapping images using EDX. Therefore, it was concluded that EDX

05-4506832 pustaka.upsi.edu.my Perpustakaan Tuanku Bainun Kampus Sultan Abdul Jalil Shah PustakaTBainun ptbupsi

05-4506832 pustaka.upsi.edu.my Perpustakaan Tuanku Bainun Kampus Sultan Abdul Jalil Shah PustakaTBainun ptbupsi

is simultaneously carried out with SEM for detecting the possible elemental and contaminants and spotting the chemical analyses typically, transition metal or RE elements.

Meanwhile, HR-TEM was the first technique used to identify the size distribution of nanoparticle samples (Woehrle et al., 2006). Briefly, HR-TEM is usually known as a microscopy method whereby, the beam of electrons is transmitted through an ultra-thin specimen and thus, interacts with the specimen as it passes through. Particularly, it comprises an electron gun that generates electrons and condensed them using a magnetic condenser lens which may use to modify the size of an electron. The specimen is positioned between the objective lens and condenser lens, as depicted in Figure 2.15.

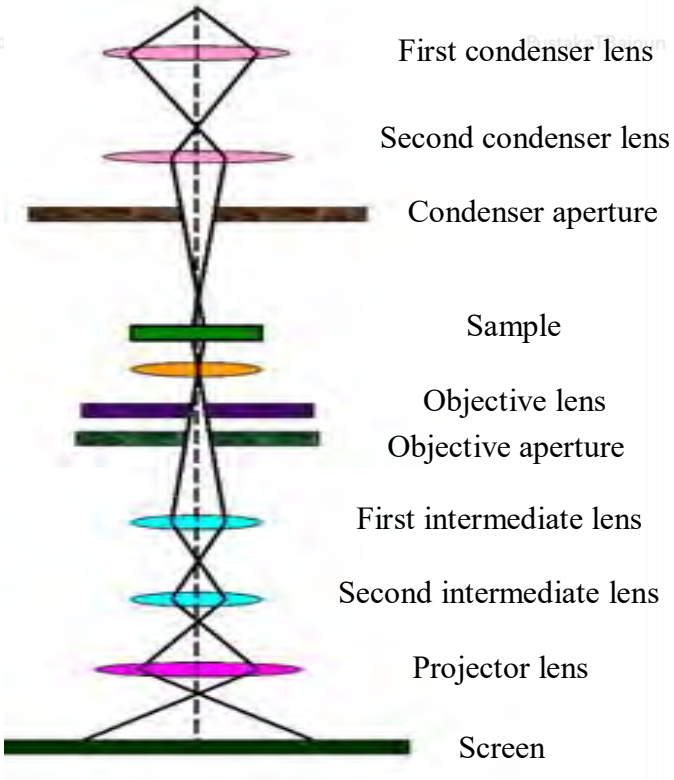


Figure 2.15. Schematic diagram of TEM instrument (Marturi, 2013)

05-4506832 pustaka.upsi.edu.my Perpustakaan Tuanku Bainun Kampus Sultan Abdul Jalil Shah PustakaTBainun ptbupsi

05-4506832 pustaka.upsi.edu.my Perpustakaan Tuanku Bainun Kampus Sultan Abdul Jalil Shah PustakaTBainun ptbupsi

Another important investigation is that the clustering of nanoparticles size in the glass network system detected by HR-TEM may be increased due to several factors that are stated as follows:

1. Coagulation process: The small particles will vanish via the collisions as the nanoparticles move around in the glass network and resulting in the formation of larger particles.
2. Ostwald ripening process: The growth of larger particles through the diffusion of smaller particles (Yao et al., 1993).
3. Coalescence of particles: The formation of larger particles due to the strong chemical and physical bonding.

05-4506832 pustaka.upsi.edu.my Perpustakaan Tuanku Bainun Kampus Sultan Abdul Jalil Shah PustakaTBainun ptbupsi

2.12 Structural Network Arrangement and Interatomic Bonding Characterization

The structural analysis characterization techniques including, XRD, FT-IR, and micro-Raman are considered important tools for characterizing the structural arrangement of amorphous glass matrix as well as, interatomic molecular of the carbon-based materials composition. Firstly, the identification of glasses known as an “amorphous solid” can be considered to possess a random arrangement of atoms, or non-equilibrium material whereby, the characteristics of atomic arrangement are more likely liquid and lack long-range periodicity in materials comparable to crystalline solids. Typically, the XRD characterization technique was employed to provide information on phases, crystal

05-4506832 pustaka.upsi.edu.my Perpustakaan Tuanku Bainun Kampus Sultan Abdul Jalil Shah PustakaTBainun ptbupsi

05-4506832 pustaka.upsi.edu.my Perpustakaan Tuanku Bainun Kampus Sultan Abdul Jalil Shah PustakaTBainun ptbupsi

orientation, structures, as well as other structural parameters including, defects, grain size, and crystallinity of the samples.

Importantly, XRD is analyzed based on the constructive interference of monochromatic X-rays whereby, the X-rays are produced by a cathode ray tube, filtered to generate monochromatic radiation, collimated to concentrate, and directed to the prepared samples (Bunaciu et al., 2015). The theoretical study of Bragg diffraction in XRD characterization is shown in Figure 2.16.

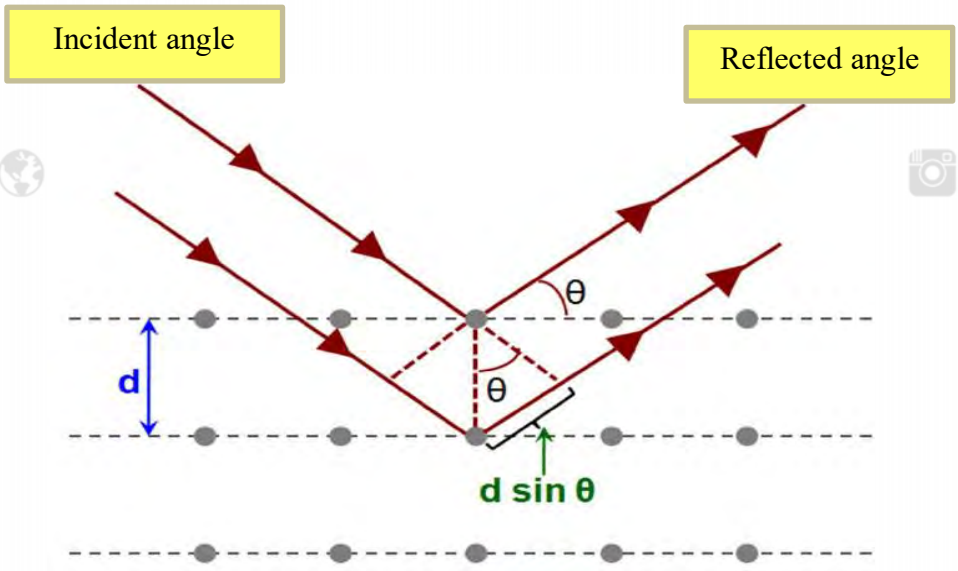


Figure 2.16. Schematic diagram of Bragg diffraction from the lattice plane when subjected to X-rays (Fitzpatrick et al., 2005)

The interaction of the incident rays with the prepared samples may produce constructive interference and a diffracted ray, as satisfied by Bragg's law:

05-4506832 pustaka.upsi.edu.my Perpustakaan Tuanku Bainun Kampus Sultan Abdul Jalil Shah PustakaTBainun ptbupsi

05-4506832 pustaka.upsi.edu.my Perpustakaan Tuanku Bainun Kampus Sultan Abdul Jalil Shah PustakaTBainun ptbupsi

$$n\lambda = 2d \sin \theta \quad (2.9)$$

where n is denoted as an integer, represents the order of reflection, λ is the wavelength of X-rays, d is the interplanar spacing that produces diffraction, and θ is the diffraction angle.

Essentially, the amorphous structure that exists in the glass materials network system was strongly proved with the presence of Er^{3+} rare-earth ions in tellurite-based glasses (Zhu et al., 2019). It was found that the absence of sharp peaks from XRD spectra completely corresponded to an amorphous state of glass materials. Additionally, this trend was observed with the occurrence of the long-range disorder in the glass structure.

Next, FT-IR is a well-known analytical characterization technique for obtaining information on the nature and the content of possible functional and structural groups in any materials. In particular, this technique may be used to trace and analyze the presence of oxides in the glass matrix system including, TeO_2 and B_2O_3 structural units. In FT-IR analysis, the optical and infrared photons from the light source move through the Michelson interferometer simultaneously. Moreover, a beam splitter, moving mirror, and fixed mirror are included in the Michelson interferometer. Before being recombined by the beam splitter, the light beam that was split into two by the team splitter is reflected from the moving mirror and fixed mirror. The intensity of interference light is recorded in an interferogram, with the optical path difference recorded along the horizontal axis.

05-4506832 pustaka.upsi.edu.my Perpustakaan Tuanku Bainun Kampus Sultan Abdul Jalil Shah PustakaTBainun ptbupsi

05-4506832 pustaka.upsi.edu.my Perpustakaan Tuanku Bainun Kampus Sultan Abdul Jalil Shah PustakaTBainun ptbupsi

Meanwhile, the Raman scattering technique plays a key role in measuring the vibrational energy modes of the sample by using scattered light. The principle working of Raman shows a monochromatic light is delivered to the materials while producing the scattering electrons in the different wavelengths. Additionally, Raman spectroscopy may significantly provide information on chemical and structural properties, as well as the characterization of substances via the characteristics of the Raman detector. When light is scattered by a molecule, the oscillating electromagnetic field of a photon causes the molecular electron cloud to become polarized and thus, affects a molecule to be in a higher state with the presence of photon energy that is transferred to the molecule.

2.13 Optical Properties Characterization

2.13.1 Optical Absorption Spectra

Optical absorption measurements are most commonly used for investigating the nature of glasses, primarily to determine the potential future applications in the fabrication of optical components and commercial filter glasses. UV-Vis spectrophotometers are usually used to analyze the optical bandgap and Urbach energy from the obtained optical absorption spectra. The standard approach in investigating the optically induced electronic transitions in glass materials is definitely to compute the optical absorption coefficient, which can be identified using different wavelengths.

05-4506832 pustaka.upsi.edu.my Perpustakaan Tuanku Bainun Kampus Sultan Abdul Jalil Shah PustakaTBainun ptbupsi

05-4506832 pustaka.upsi.edu.my Perpustakaan Tuanku Bainun Kampus Sultan Abdul Jalil Shah PustakaTBainun ptbupsi

Optical absorption occurred in glass materials, as indicated by two processes called emission and absorption that are taking place in an atom. The photons that were released as the atoms moved to lower energy levels are represented by the emission process. After being heated or stimulated to a high level and thus, the atoms have released the light. When the electrons are migrated to a lower energy level, they are actually releasing the excess energy, which can be resulted in light emission. Meanwhile, the absorption process occurs as the electrons absorb the photon energy, which causes the electrons to gain energy, and eventually move to the higher energy level. The electronic states consist of localized features and nature changes from localized to delocalized sections, which can be referred to as the "mobility edge". The separation of energy consists of valence and conduction bands between the mobility edges is known as the "mobility edge" (refer to Figure 2.17).

05-4506832 pustaka.upsi.edu.my Perpustakaan Tuanku Bainun Kampus Sultan Abdul Jalil Shah PustakaTBainun ptbupsi

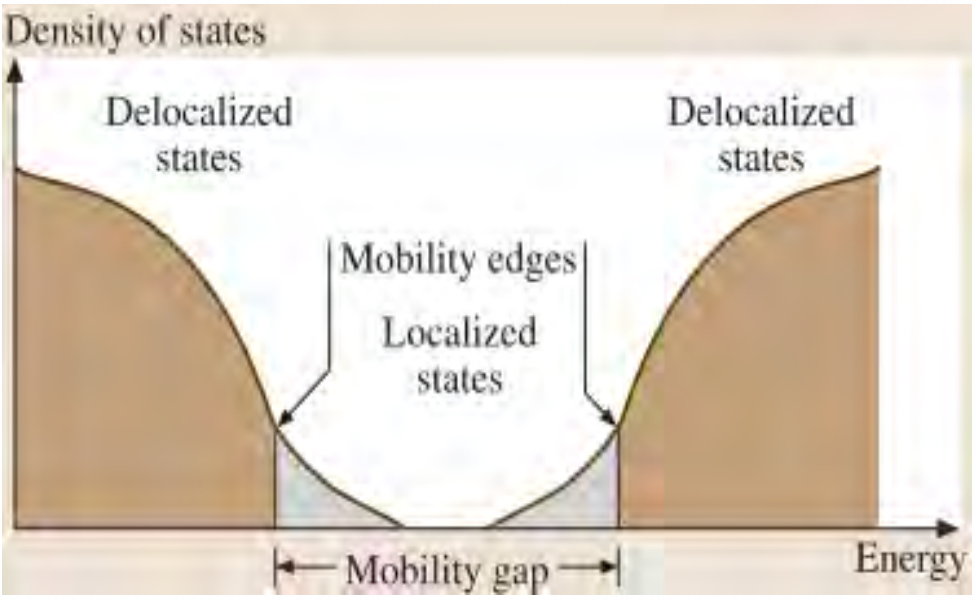


Figure 2.17. Schematic illustration in states of conduction and valence bands (Morigaki & Ogihara, 2006)

05-4506832 pustaka.upsi.edu.my Perpustakaan Tuanku Bainun Kampus Sultan Abdul Jalil Shah PustakaTBainun ptbupsi

05-4506832 pustaka.upsi.edu.my Perpustakaan Tuanku Bainun Kampus Sultan Abdul Jalil Shah PustakaTBainun ptbupsi

The investigation of linear optical absorption spectra of trivalent erbium ions doped tellurite glasses exhibited a rapid increment within the electronic absorption edge in the glassy matrix that indicates the absorption in the higher transition of Er^{3+} ions (Sajna et al., 2018). It was found that the peaks are recognized to the 4*f*-4*f* transition of the ground states, $^4I_{15/2}$ in erbium ions to the range of excited states which corresponding at 365 nm, 378 nm, 407 nm, 443 nm, 451 nm, 488 nm, 521 nm, 545 nm, 651 nm, 793 nm, 976 nm, and 1532 nm, respectively. Additionally, it was proposed that the extremely increasing in the absorption intensity is along with the concentration of erbium ions as doping in tellurite glasses. Thereby, some transitions which correlated with the lanthanide ions play the main major role in the environments and defined as hypersensitive transitions which select the important rules $|\Delta S| = 0$, $|\Delta L| \leq 2$. Moreover, it was attained that the erbium ions have the hypersensitive transitions of $^4I_{15/2} \rightarrow {}^4G_{11/2}$ and $^4I_{15/2} \rightarrow {}^2H_{11/2}$ where it is more intense compared to the rest of the transitions.

The effect of erbium ions doped tellurite glasses obtained from the absorption spectra whereby the glasses potentially attain the larger gain bandwidth for S-band amplifier and broadband optical amplifier in wavelength division multiplexing (WDM) at 1.53 μm, respectively (Pepe et al., 2019). The absorption bands of erbium ions doped glasses were indicated to the transition from the ground state level ($^4F_{15/2}$) to the level of the excited state which is as follows: ($^4I_{13/2}$, $^4I_{11/2}$, $^4I_{9/2}$, $^4F_{9/2}$, $^4S_{3/2}$, $^2H_{11/2}$, $^4F_{7/2}$, $^4F_{5/2}$, and $^4F_{3/2}$), respectively. As stated from the absorption spectra, the increase of erbium ions content may be attributed to the higher intensity of the absorption band peaks.

05-4506832 pustaka.upsi.edu.my Perpustakaan Tuanku Bainun Kampus Sultan Abdul Jalil Shah PustakaTBainun ptbupsi

05-4506832 pustaka.upsi.edu.my Perpustakaan Tuanku Bainun Kampus Sultan Abdul Jalil Shah PustakaTBainun ptbupsi

The spectroscopic characterization for optical absorption spectra had been investigated on erbium containing in the glass lattice system in which the optical absorption bands were characterized near $^4I_{13/2} \rightarrow {}^4I_{15/2}$ transition of the emission about the 1.53 μm of Er^{3+} ions at the wavelength of 400 nm in excitation condition (Jimenez et al., 2020). It was found that the erbium ions contained in the aluminophosphate glass consist of a high content of monovalent copper which can be attributed to the photonics technology system.

The recent research on the erbium ions doped into bismuth borotellurite glasses had been explored in investigating the optical absorption spectra in the wavelength range from 400 nm to 1750 nm which exist in the present glasses (Lakshmi et al., 2019). It was observed that the absorption bands centered from the ground state level of $^4I_{15/2}$ transition to the variation in the level of the excited state are given as follows: $^4F_{3/2}$, $^4F_{5/2}$, $^4F_{7/2}$, $^2H_{11/2}$, $^4S_{3/2}$, $^4F_{9/2}$, $^4I_{9/2}$, $^4I_{11/2}$, and $^4I_{13/2}$ transitions which respects to the stated wavelength regions at 442 nm, 451 nm, 488 nm, 522 nm, 544 nm, 653 nm, 797 nm, 976 nm, and 1531 nm, respectively. From the absorption bands obtained, the absorption intensities exhibited increasing order due to the existence of erbium ions content in the studied glasses. Therefore, it can be noticed from the absorption band, there was existing as the highest level of intensity originated at 522 nm which corresponds to the transition of $^4I_{15/2} \rightarrow {}^2H_{11/2}$ transition which is known as the “hypersensitive” level caused by the polarization in Er^{3+} ions and respects to the rule of selection indicated of $|\Delta S| = 0$, $|\Delta L| \leq 2$ and $|\Delta J| \leq 2$.

05-4506832 pustaka.upsi.edu.my Perpustakaan Tuanku Bainun Kampus Sultan Abdul Jalil Shah PustakaTBainun ptbupsi

05-4506832 pustaka.upsi.edu.my Perpustakaan Tuanku Bainun Kampus Sultan Abdul Jalil Shah PustakaTBainun ptbupsi

2.13.2 Optical Bandgap Energy

The fundamentals of the optical bandgap energy may be correlated to the differences between the valence and conduction bands. The electrons can flow freely from the valence to conduction bands in semiconductors due to the small bandgap value, thereby allowing for electrical conductivity in the material. Primarily, electrons existing in the conduction band are mostly free of the atom's nuclear charge and can flow freely in this band, which is referred to as a negative charge carrier. Therefore, when electrons leave the valence band and enter the conduction band, the state can be a positive charge carrier, known as a hole.

The semiconductors can be classified into two types, including the direct and indirect bandgap. In a direct bandgap semiconductor, the electrons at the conduction band's lowest state may emit an unoccupied state into the valence band via the photon emission with the energy mechanism. When an electron and a hole have the same momentum, a direct bandgap occurs. Meanwhile, the conduction band's minimal and valence band's maximum energy levels for the indirect bandgap semiconductor occurred at two different momentum values. Therefore, the indirect bandgap's electrons do not directly excite to the maximum of the valence band, which can be attributed to a change in momentum and energy, as well. Rather than emitting the photons, the energy can be transferred to the lattice, which is known as the phonons. The emission of photon energy that occurred in semiconductor materials for direct and indirect bandgap is presented in Figure 2.18.

05-4506832 pustaka.upsi.edu.my Perpustakaan Tuanku Bainun Kampus Sultan Abdul Jalil Shah PustakaTBainun ptbupsi

05-4506832 pustaka.upsi.edu.my Perpustakaan Tuanku Bainun Kampus Sultan Abdul Jalil Shah PustakaTBainun ptbupsi

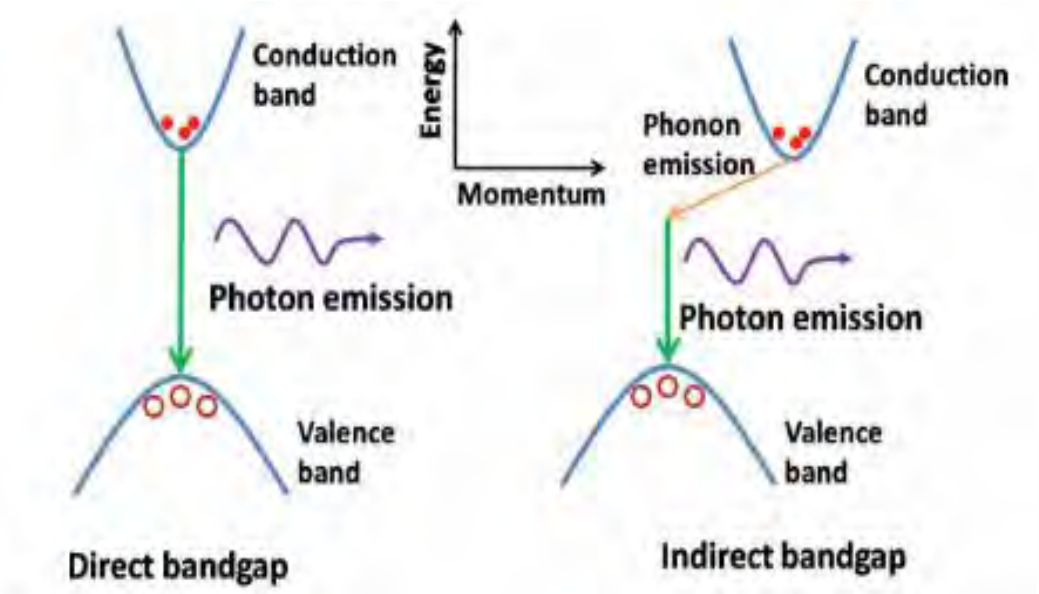


Figure 2.18. Schematic illustration of the photon emission processes (a) direct and (b) indirect bandgap semiconductors (Sun, 2010)

05-4506832 pustaka.upsi.edu.my Perpustakaan Tuanku Bainun Kampus Sultan Abdul Jalil Shah PustakaTBainun ptbupsi

According to Mott and Davis's theory (Mott et al., 1972), the relationship between the absorption coefficient, α(ω) and photon energy, ħω has been proposed to determine the indirect transition that occurred in the bandgap energy as expressed by the following equation:

$$\alpha(\omega) = \frac{\beta(\hbar\omega - E_{opt})^{n}}{\hbar\omega} \qquad (2.10)$$

where β is an energy-independent constant known as the band tailing parameter, E_{opt} is the optical bandgap energy, and n is a constant index that shows different values, $\frac{1}{2}$, 2, $\frac{3}{2}$, and 3 depending on the type of optical transitions. These values correspond to the direct allowed, indirect allowed, direct forbidden, and indirect forbidden transitions, respectively

05-4506832 pustaka.upsi.edu.my Perpustakaan Tuanku Bainun Kampus Sultan Abdul Jalil Shah PustakaTBainun ptbupsi

05-4506832 pustaka.upsi.edu.my Perpustakaan Tuanku Bainun Kampus Sultan Abdul Jalil Shah PustakaTBainun ptbupsi

(Stambouli et al., 2012). Apart from that, the absorption coefficient, α(ω) value can be identified from the absorbance of glass materials along with different wavelengths as represented via the relation:

$$\alpha(\omega)=2.303\left(\frac{A}{d}\right) \tag{2.11}$$

where A referred to the absorbance and d is the thickness of glass samples.

The investigation of optical characteristics of the erbium ions doped into zinc borotellurite glasses whereby, the optical bandgap energy values were indicated in the reduction trend from 3.40 eV to 2.34 eV for direct bandgap and from 3.32 eV to 2.79 eV for indirect bandgap energy (Chopra et al., 2018). It can be ascribed that the decrement in optical bandgap energy can be attributed typically to the altering of the network structures along with the addition of erbium oxide into the studied glasses. Other than that, the incorporation of rare-earth erbium ions into the tellurite glass may result in the interruption of Te-O-Te and B-O-B bridges existing in the glass formation. The bond linkages particularly can be attributed to the conversion to TeO_3 from TeO_4 structural units through the presence of TeO_{3+1} units and BO_3 units' group in the glass lattice system. Due to this conversion process, it can be summarized that the existence of non-bridging oxygens (NBOs) exhibits a more polarized comparable to bridging oxygens (BOs).

The improvement of optical bandgap energy via the inclusion of nanoparticles into the erbium-doped sodium-zinc-tellurite glass was investigated by Yusof et al., (2017). It

05-4506832 pustaka.upsi.edu.my Perpustakaan Tuanku Bainun Kampus Sultan Abdul Jalil Shah PustakaTBainun ptbupsi

05-4506832 pustaka.upsi.edu.my Perpustakaan Tuanku Bainun Kampus Sultan Abdul Jalil Shah PustakaTBainun ptbupsi

was found that the reduction of optical bandgap energy value along with the increase of dopant ions resulted from 3.08 to 3.03 eV. These findings may be correlated to the lowering of average bond energy which is caused by the formation of NBOs than BO ions in the glass host. Additionally, the reduction of optical bandgap energy was attributed to the higher number of NBOs than BOs with the presence of nanoparticle ions. The presence of a large number of NBOs implies the abundance of localized electrons which may act as donor centers in the glass network.

2.13.3 Urbach Energy

Urbach energy, ΔE is an optical parameter typically relates to the degree of structural disorder in amorphous material which convert the weak bonds into defects (Tiwari & Dhondiyal, 2021). The degree of disorderliness occurred in the amorphous glass due to the additional broadening and thus, could be attributed to the band tailing of energy states in the forbidden gap (Shakeri & Rezvani, 2011). As a result, the Urbach energy value can be determined by taking the reciprocals of the slopes of the linear potion in a lower photon energy region, which is the plot graph of the logarithm of absorption coefficient and function of photon energy curves. The Urbach energy value can be expressed as follows:

$$\alpha(\omega) = \beta \exp\left(\frac{\hbar\omega}{\Delta E}\right) \tag{2.12}$$

05-4506832 pustaka.upsi.edu.my Perpustakaan Tuanku Bainun Kampus Sultan Abdul Jalil Shah PustakaTBainun ptbupsi

05-4506832 pustaka.upsi.edu.my Perpustakaan Tuanku Bainun Kampus Sultan Abdul Jalil Shah PustakaTBainun ptbupsi

where β is a constant and ΔE is the energy of the band tail or known as Urbach energy. This exponential behavior can be ascribed to the band tails associated with the valence and conduction bands which extend into the bandgap.

The investigation of erbium, Er^{3+} ions doped strontium aluminate, $Sr_3Al_2O_6$ (SAO) had been investigated especially in exploring a new technology on the potential photonics whereby the Urbach energy value obtained from 0.68 ± 0.08 and 0.34 ± 0.03 eV, respectively (Singh et al., 2019). It was found that the Urbach energy corresponding to the localized band tail states includes the formation of a bandgap in which the atoms change from one energy state to another level of energy that occurred between the valence band and conduction band in the optical transitions. Usually, the Urbach energy presented the disorder of glass structure or can be said as the defects which were formed due to some of the changes in structural network in glass system.

The effect of erbium ions had been studied for lithium zinc fluoroborate glasses in which the Urbach energy showed the increment order from 0.176 to 0.219 eV along with the addition of Er^{3+} ions concentration (Prabhu et al., 2019). The Urbach energy presents the degree of disorderliness, especially in amorphous glass materials and values of Urbach energy were described from the band tail existing in the forbidden gap energy, respectively. In addition, it can be summarized that the value obtained for Urbach energy may be presented the number of defects or disorders in glass structure along with the increasing doping of Er^{3+} ions. However, the number of defects obtained in this research is quite smaller than the obtained lower value in Urbach energy presented in this glass system.

05-4506832 pustaka.upsi.edu.my Perpustakaan Tuanku Bainun Kampus Sultan Abdul Jalil Shah PustakaTBainun ptbupsi

05-4506832 pustaka.upsi.edu.my Perpustakaan Tuanku Bainun Kampus Sultan Abdul Jalil Shah PustakaTBainun ptbupsi

2.13.4 Refractive Index

The refractive index is an important measurement that may affect the candela distribution of the transmitted light and easy to change the intensity of light by improving the refractive index value of any material (Tiwari & Dhondiyal, 2021). In addition, the refractive index can be used as the optical parameter to facilitate the applications in photonic appliances, particularly in fiber optics and amplifiers, and is highly affected by the electron density or electronic polarizability of the glassy matrix system. Thereby, the refractive index value can be determined via the intercommunication of light with the electrons of the constituent atoms in the glass system. Theoretically, the fundamental of the refractive index can be calculated using the optical bandgap energy based on the relationship as stated by Dimitrov and Sakka (1996):

05-4506832 pustaka.upsi.edu.my Perpustakaan Tuanku Bainun Kampus Sultan Abdul Jalil Shah PustakaTBainun ptbupsi

$$\frac{n^2-1}{n^2+1} = 1-\sqrt{\frac{E_{opt}}{20}} \tag{2.13}$$

where n represents the refractive index and E_{opt} denotes as the optical bandgap energy.

Consequently, the value of the refractive index in the glass material depends on the following factors (Abdel-Baki & El-Diasty, 2007; Tiedje et al., 1992):

1. Polarizability of the first neighbor ions coordinated with anion

05-4506832 pustaka.upsi.edu.my Perpustakaan Tuanku Bainun Kampus Sultan Abdul Jalil Shah PustakaTBainun ptbupsi

05-4506832 pustaka.upsi.edu.my Perpustakaan Tuanku Bainun Kampus Sultan Abdul Jalil Shah PustakaTBainun ptbupsi

2. Field intensity Z/a^2 (i.e., polarization power), where Z is the valence of the ion (ionic charge) and a is the distance of separation (ionic radius)
3. Coordination number of the ion
4. Non-bridging oxygen bonds (NBOs)
5. Electronic polarizability of the oxide ion
6. Optical basicity of the glasses
7. Repulsion energy in the electrical excitation of rare-earth (RE) ions

The optical characterization of the refractive index had been studied for erbium-doped tellurite glasses embedded with nanoparticles into the host glass whereby, the refractive index value exhibited the increasing trend in the range of 2.381 to 2.425, respectively along with the increase of dopant ions concentration (Yusof et al., 2017). It was found that the increment of the refractive index was influenced by the embedment of nanoparticles in the glassy matrix system.

The optical spectroscopic for estimating the refractive index had been investigated on samarium ions doped borotellurite glass whereby, the refractive index showed a value in the range of 1.61 to 1.83, respectively along with the increase of TeO_2 concentration (Queiroz et al., 2019). As a result, it was discovered that the increase in refractive index is linked to an increasing trend in density and electronic polarizability, both of which are induced by the presence of TeO_2. Furthermore, the density increased from 3.05 to 4.31 g/cm^3, which may be explained by combining the modifier networks, include boron oxide, B_2O_3, and calcium oxide, CaO, into the tellurite glass matrix. In conclusion, it was reported

05-4506832 pustaka.upsi.edu.my Perpustakaan Tuanku Bainun Kampus Sultan Abdul Jalil Shah PustakaTBainun ptbupsi

05-4506832 pustaka.upsi.edu.my Perpustakaan Tuanku Bainun Kampus Sultan Abdul Jalil Shah PustakaTBainun ptbupsi

that the molecular weight of TeO_2 was 159.6 g/mol, which was higher than the molecular weights of B_2O_3 and CaO, which were 69.6182 g/mol and 56.0774 g/mol, respectively.

2.13.5 Reflection Loss, Transmission Coefficient, and Dielectric Constant

Additionally, the important optical parameters including, reflection loss, transmission coefficient, and dielectric constant can be deduced from the refractive index. Firstly, the reflection loss can be calculated by using Fresnel's formula as indicated as follows (Bhatia et al., 2015):

$$R_L = \left[\frac{(n-1)}{n+1}\right]^2 \quad (2.14)$$

05-4506832 pustaka.upsi.edu.my Perpustakaan Tuanku Bainun Kampus Sultan Abdul Jalil Shah PustakaTBainun ptbupsi

Meanwhile, the transmission coefficient is correlated to the linear refractive index based on the following simple expression (Linda et al., 2013):

$$\mathrm{T} = \frac{2n}{n^2+1} \quad (2.15)$$

The dielectric constant can be defined as the ability of a substance to generate electric energy in an electric field as indicated in the following equation (Bhatia et al., 2015):

$$\epsilon = n^2 \quad (2.16)$$

05-4506832 pustaka.upsi.edu.my Perpustakaan Tuanku Bainun Kampus Sultan Abdul Jalil Shah PustakaTBainun ptbupsi

05-4506832 pustaka.upsi.edu.my Perpustakaan Tuanku Bainun Kampus Sultan Abdul Jalil Shah PustakaTBainun ptbupsi

where *n* is referred to the refractive index.

2.13.6 Electronegativity

The electronegativity of an atom refers to its relative ability to attract the electrons in a bond toward itself (Thombre, 2016). The studies on electronegativity become the main concept in understanding the chemical bond and material properties that can be applied in any practical application. Furthermore, the atoms possessing large electronegativities, such as F and O, are able to attract the electrons in bonds more effectively than those with small electronegativities, such as Na and Mg. It is well known that Pauling initially proposed the methods for the early study concept of electronegativity by which to qualitatively characterize the transition from ionic to covalent bonds (Pauling, 1932). Afterward, the electronegativities of the main group elements, such as the concept of average electronegativity were introduced by Asokamani and Manjula (1989).

The defined average electronegativity parameter was intuitively correlated with the chemical potential when atoms interact to form a molecule and thereby, can be expressed in the following manner:

$$\chi_{1av} = \frac{\sum_i^n \chi_i n_i}{N} \tag{2.17}$$

05-4506832 pustaka.upsi.edu.my Perpustakaan Tuanku Bainun Kampus Sultan Abdul Jalil Shah PustakaTBainun ptbupsi

05-4506832 pustaka.upsi.edu.my Perpustakaan Tuanku Bainun Kampus Sultan Abdul Jalil Shah PustakaTBainun ptbupsi

where Σ over *i* presents values from 1 to *N*, χ_i is the Pauling electronegativity of an element, n_i is known as the number of atoms of the i_{th} element, and *N* is denoted as the number of elements present in the compound.

In connection with the concept of average electronegativity, Reddy et al., (2001) have derived the empirical relationship for average electronic oxide ion polarizability as follows:

$$\alpha_0{}^{2-} = 4.624 - 0.7569\chi_{1av} \tag{2.18}$$

where χ_{1av} is refer to the average electronegativity of the simple oxides. The obtained value of $\alpha_0{}^{2-}$ from Equation (2.18) was found to be in good agreement with previously obtained findings by other researchers. On the contrary, it should be noted that average electronegativity seems to exhibit a large value. Another approach was then explored by Reddy et al., (2001) in which the following empirical relation primarily for binary oxide glasses is as follows:

$$\alpha_0{}^{2-} = 3.319 - 0.3422\chi_{2av} \tag{2.19}$$

Another formula for all binary oxide glass compositions except TeO_2, GeO_2, and TiO_2 as a second oxide ion was demonstrated as follows:

$$\alpha_0{}^{2-} = \frac{(\chi_{3av} - 1.35)}{\chi_{3av} - 1.80} \tag{2.20}$$

05-4506832 pustaka.upsi.edu.my Perpustakaan Tuanku Bainun Kampus Sultan Abdul Jalil Shah PustakaTBainun ptbupsi

05-4506832 pustaka.upsi.edu.my Perpustakaan Tuanku Bainun Kampus Sultan Abdul Jalil Shah PustakaTBainun ptbupsi

where χ_{nav}, $n = 2$ and 3 can be referred to the average electronegativity of binary oxide glass.

Briefly, it can be noticed that a relation subjected to more approximation comparable to average electronegativity, Zhao et al., (2008) then introduced the concept of optical electronegativity, $\Delta\chi^*$and suggested the following empirical relation for binary oxide glass:

$$\alpha_0{}^{2-} = -0.9\Delta\chi^* + 3.5 \quad (2.21)$$

The optical electronegativity, $\Delta\chi^*$ can be calculated from optical bandgap energy or refractive index value based on the following empirical relations studied by Reddy and Nazeer Ahammed (1995):

$$\Delta\chi^* = 0.2688\, E_{opt} \quad (2.22)$$

$$\Delta\chi^* = 9.8e^{-n} \quad (2.23)$$

where E_{opt} is the optical bandgap energy and n is the refractive index of glass sample.

05-4506832 pustaka.upsi.edu.my Perpustakaan Tuanku Bainun Kampus Sultan Abdul Jalil Shah PustakaTBainun ptbupsi

05-4506832 pustaka.upsi.edu.my Perpustakaan Tuanku Bainun Kampus Sultan Abdul Jalil Shah PustakaTBainun ptbupsi

2.13.7 Judd-Ofelt's Theoretical Study

The numerical integration of optical absorption bands was performed to identify the experimental oscillator strength for transitions from the ground state $^4I_{15/2}$ to excited states (Marzouk et al., 2021). Judd-Ofelt's (J-O) theory was introduced as a fundamental stage for the characterization of absorption spectra that have been considered to determine the intensity of *f-f* transition in rare-earth (RE) ions (Judd, 1962; Ofelt, 1962).

The great approach of Judd-Ofelt's theory allows the estimation of oscillator strengths in absorption or luminescence, transition probabilities, branching ratios, and radiative lifetime using the empirical intensity parameters, (Ω_λ = 2, 4, 6) by fitting the experimental and theoretical oscillator forces of the stated absorption transitions. Based on the absorption spectra, the value of experimental oscillator strength for each observed transition state of excitation can be determined by measuring the area under the absorption bands using the following expression:

$$f_{exp} = \frac{2303\mathrm{mc}^2}{\pi e^2 \mathrm{N_A}} \int \varepsilon(v) dv \qquad (2.24)$$

where *m*, *c*, *e*, N_A, and ε are referred to as the electron mass, speed of light, electronic charge, Avogadro's number, and molar extinction coefficient obtained from the Beer-Lambert's law derivation, as given:

05-4506832 pustaka.upsi.edu.my Perpustakaan Tuanku Bainun Kampus Sultan Abdul Jalil Shah PustakaTBainun ptbupsi

05-4506832 pustaka.upsi.edu.my Perpustakaan Tuanku Bainun Kampus Sultan Abdul Jalil Shah PustakaTBainun ptbupsi

$$\varepsilon(v) = \frac{\log\left(\frac{I_0}{I_t}\right)}{NL} \tag{2.25}$$

where $\log\left(\frac{I_0}{I_t}\right)$ can be denoted as the measured absorbance with the specific frequency, N is known as the concentration of rare-earth ions (mol/1000 cm^3), and L can be represented as the thickness of the glass sample (cm). According to Judd-Ofelt's theory, the probability of theoretical dipole oscillator strength (f_{cal}) from the ground state (aJ) to the excited state (aJ') can be calculated based on the following expression:

$$f_{cal} = \left[\frac{8\pi^2 mcv}{3he^2(2J+1)}\right]\left[\frac{(n^2+1)^2}{9n}\right]S_{ed} \tag{2.26}$$

05-4506832 pustaka.upsi.edu.my Perpustakaan Tuanku Bainun Kampus Sultan Abdul Jalil Shah PustakaTBainun ptbupsi

$$S_{ed} = e^2 \sum_{\lambda=2,4,6} \Omega_\lambda |\langle aj|U\lambda|aj'\rangle|^2 \tag{2.27}$$

$$S_{md} = \frac{e^2}{4m^2c^2}|\langle ajIL + 2S|aj'\rangle|^2 \tag{2.28}$$

where v, n, and h are known as the transition wavenumber (cm^{-1}), refractive index, and Plank's constant, respectively; J is denoted as the total angular momentum of the ground state and the doubly reduced matrix elements of Judd-Ofelt's intensity parameters order, (Ω_λ = 2, 4, 6) between the manifold states of $|\langle aj|U\lambda|aj'\rangle|^2$ and $|\langle ajIL + 2S|aj'\rangle|^2$ of Er^{3+} ions in aquo solution (Carnall et al., 1968). Additionally, the quality of fitting for the theoretical

05-4506832 pustaka.upsi.edu.my Perpustakaan Tuanku Bainun Kampus Sultan Abdul Jalil Shah PustakaTBainun ptbupsi

05-4506832 pustaka.upsi.edu.my Perpustakaan Tuanku Bainun Kampus Sultan Abdul Jalil Shah PustakaTBainun ptbupsi

oscillator strengths value can be identified via the root-mean-square (δ_{rms}) as can be expressed as follows (Wen et al., 2019):

$$\delta_{rms} = \left[\frac{\Sigma(f_{cal}-f_{exp})^2}{\xi-3}\right]^2 \tag{2.29}$$

where ξ is the number of analyzed transitions. Meanwhile, as can be referred in the theoretical study proposed by Jacobs and Weber (1976), the intensity of erbium emission can be expressed by the ratio between Ω_4 and Ω_6 parameters. The spectroscopic quality factor, χ signify the emission strength of lasing properties in the glass matrix system (Amiar Rodin & Sahar, 2018). The spontaneous radiative transition probability *A(J-J')* for a particular transition located from the ground state to the excited state can be calculated as follows:

05-4506832 pustaka.upsi.edu.my Perpustakaan Tuanku Bainun Kampus Sultan Abdul Jalil Shah PustakaTBainun ptbupsi

$$\text{A(J-J')} = A_{ed}+A_{md} = \left[\frac{64\pi^4V^3}{3h(2J+1)}\right][\chi_{ed}S_{ed}+\chi_{md}S_{md}] \tag{2.30}$$

where A_{ed} and A_{md} can be referred to as average electric and magnetic dipole radiative transition probabilities, respectively meanwhile, χ_{ed} and χ_{md} are known as Lorentz local field correction for electric and magnetic dipole-dipole transition which can be expressed via the relation:

$$\chi_{ed} = \frac{n(n^2+2)^2}{9} \tag{2.31}$$

05-4506832 pustaka.upsi.edu.my Perpustakaan Tuanku Bainun Kampus Sultan Abdul Jalil Shah PustakaTBainun ptbupsi

05-4506832 pustaka.upsi.edu.my Perpustakaan Tuanku Bainun Kampus Sultan Abdul Jalil Shah PustakaTBainun ptbupsi

$$\chi_{md} = n^3 \tag{2.32}$$

Fluorescence branching ratio, β_R is defined as the fraction of total photon flux from the upper manifold to a lower manifold which determines the probability of achieving the stimulated emission under the suitable excitation (Jlassi et al., 2010; Walsh et al., 1998). The branching ratio for the upper state *J* can be evaluated to estimate the relative intensity of the emission lines from the excited states via the following expression:

$$\beta_R = \frac{A(J-J')}{\Sigma(A_{ed}+A_{md})|aJ,bJ'|} \tag{2.33}$$

The emitting state radiative lifetime, t_r can be referred to as the total spontaneous transition probabilities A(J-J') for all the transitions as calculated based on the expression (Hamza, Halimah, Muhammad, Chan, et al., 2019):

$$t_r = \frac{1}{\Sigma(A_{ed}+A_{md})|aJ,bJ'|} \tag{2.34}$$

The Judd-Ofelt's parameters can be implied to obtain the transition probabilities, $A_{J'J}$, branching ratio, β_R and radiative lifetime, τ_r for all the excited states levels. The flow diagram is presented as the summarization to obtain Judd-Ofelt's parameters calculation as follows, as illustrated in Figure 2.19.

05-4506832 pustaka.upsi.edu.my Perpustakaan Tuanku Bainun Kampus Sultan Abdul Jalil Shah PustakaTBainun ptbupsi

05-4506832 pustaka.upsi.edu.my Perpustakaan Tuanku Bainun Kampus Sultan Abdul Jalil Shah PustakaTBainun ptbupsi

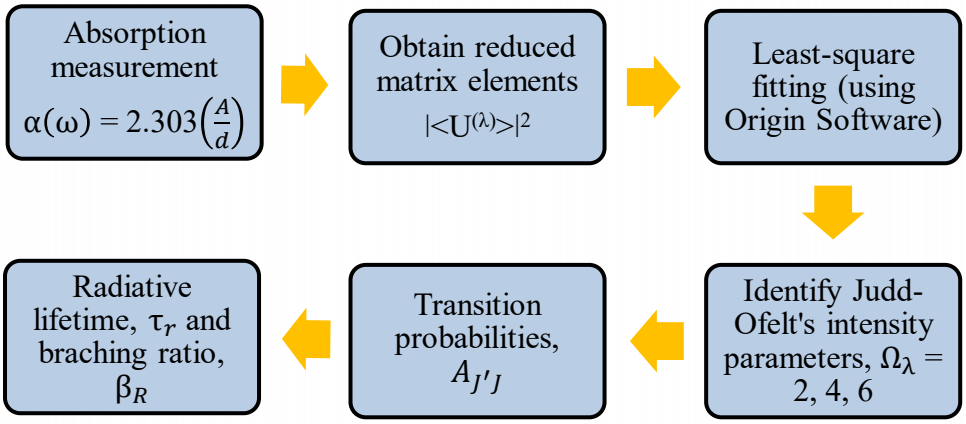


Figure 2.19. Flow diagram of Judd-Ofelt's intensity parameters calculation

The Judd-Ofelt's spectral intensity parameters, (Ω_λ = 2, 4, 6) of Er^{3+} ions doped oxycholoroborotellurite (OCBT) glass system were studied by Sailaja et al., (2021). It was found that the J-O intensity parameters showed the trend as $\Omega_6 > \Omega_2 > \Omega_4$ whereby, these parameters are useful to figure out the local network structure around the rare-earth (RE) ions. Apart from that, it was confirmed that these glasses possess the properties such as both structural symmetry and rigidity of the material. The Ω_2 intensity parameter is correlated to the structural symmetry and nature of metal-ligand bond around the Er^{3+} ions site meanwhile, the other Ω_4 and Ω_6 parameters are disclosed to the rigidity, viscosity, and basicity which demonstrates the bond between ligand atoms and Er^{3+} ions. Hence, it was noted that the Ω_6 parameter corresponds to the isomer shift (IS), which specifies the 6*s* electron density around Er^{3+} ions site.

05-4506832 pustaka.upsi.edu.my Perpustakaan Tuanku Bainun Kampus Sultan Abdul Jalil Shah PustakaTBainun ptbupsi

05-4506832 pustaka.upsi.edu.my Perpustakaan Tuanku Bainun Kampus Sultan Abdul Jalil Shah PustakaTBainun ptbupsi

The new broadband mid-infrared emission of Er^{3+}/Dy^{3+} co-doped tellurite glass system was investigated by Zhang et al., (2021). It was proposed that the prepared glasses possess the larger value of Ω_2 intensity parameter comparable with the Ω_4 and Ω_6 parameters, which indicates the excellent covalence nature and higher asymmetry. The three intensity parameters follow the $\Omega_2 > \Omega_4 > \Omega_6$ trend, indicating a moderate covalency of Er-O/ Dy-O bonds and local asymmetry around the Er^{3+}/Dy^{3+} ions. Besides, it was reported that the radiative properties such as, transition probabilities, branching ratio, and a radiative lifetime of Er^{3+}/Dy^{3+} co-doped tellurite glass were evaluated from the absorption spectra thereby, a higher value of radiative transition probability of Er^{3+}: $^4I_{11/2} \rightarrow {}^4I_{13/2}$ transition (47 s^{-1}) and Dy^{3+}: $^6H_{13/2} \rightarrow {}^6H_{15/2}$ transition (63 s^{-1}), respectively.

05-4506832 pustaka.upsi.edu.my Perpustakaan Tuanku Bainun Kampus Sultan Abdul Jalil Shah PustakaTBainun ptbupsi

2.13.8 Photoluminescence

A luminescent material, often known as a phosphor is defined as a solid that generates luminescence and transforms certain types of energy into electromagnetic radiation over thermal radiation. The phosphor materials typically contain one or more impurity ions or activators (A) whereby, the emission is produced by the activators (Ronda & Srivastava, 2006). Furthermore, a luminescent material can be easily excited according to the appropriate excitation and processes a high quantum efficiency. The activators are then compulsory to convert the absorbed energy into a suitable visible light frequency. Even though the electromagnetic radiation was released by the phosphors can be normally visible as well as, can be in the UV or infrared ranges.

05-4506832 pustaka.upsi.edu.my Perpustakaan Tuanku Bainun Kampus Sultan Abdul Jalil Shah PustakaTBainun ptbupsi

05-4506832 pustaka.upsi.edu.my Perpustakaan Tuanku Bainun Kampus Sultan Abdul Jalil Shah PustakaTBainun ptbupsi

Generally, the mechanism of luminescence is defined when the activator absorbs the exciting radiation in order to reach the excited state level in the absorption band. The excited state levels are able to emit the radiation energy in which the photon had been restored to the ground state level. This process takes place when the energy in the excited state excites the lattice vibration or called the phonon in order to heat the main lattice. Due to these different kinds of radiation of energy, the non-radiative process should be controlled to develop an efficient phosphor. The illustrated diagram of the photoluminescence band diagram mechanism is shown in Figure 2.20. The diagram demonstrates three energy level states whereby, E1 shows a low-level energy state (valence band) which consists of more electrons compared to E3, which exhibits a higher-level energy state. The electrons are then raised from the valence band to E3 via a UV stimulation in which they undergo a non-radiatively decay to the energy state level of E2.

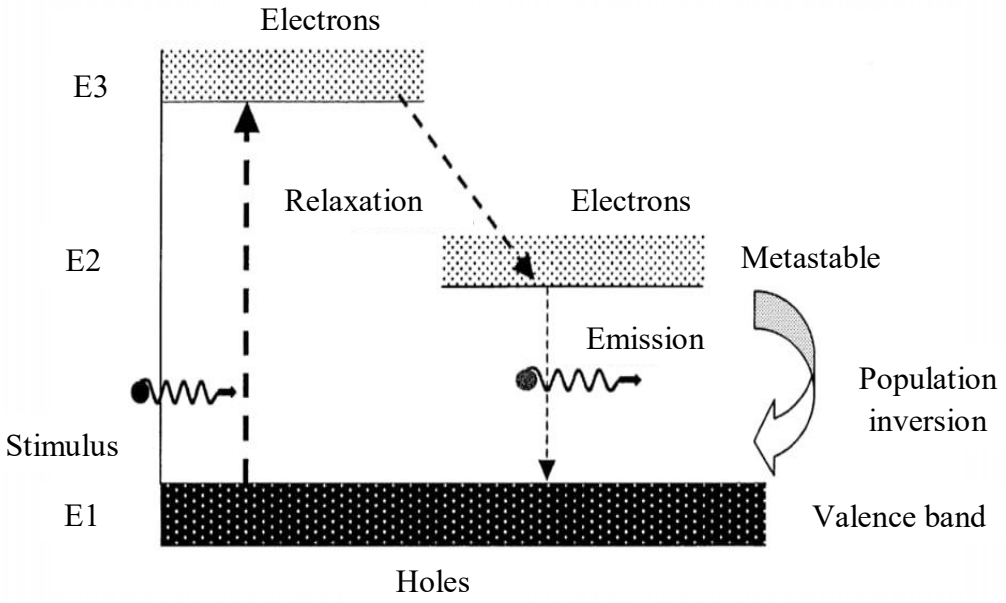


Figure 2.20. Schematic illustration of photoluminescence band diagram (McSherry et al., 2004)

05-4506832 pustaka.upsi.edu.my Perpustakaan Tuanku Bainun Kampus Sultan Abdul Jalil Shah PustakaTBainun ptbupsi

05-4506832 pustaka.upsi.edu.my Perpustakaan Tuanku Bainun Kampus Sultan Abdul Jalil Shah PustakaTBainun ptbupsi

As has been defined earlier, the luminescence process is commonly known as the emission of light from a material when it has been absorbed by external energy. Therefore, luminescence can be categorized into several kinds of energy whereby, the activators or sensitizers are used to excite high-energy photons based on the following:

i. Photoluminescence process in which involve the excitation via an electromagnetic radiation according to UV radiation.
ii. Electroluminescence process occurs when the excitation is generated directly via an electric field.
iii. Cathodoluminescence process occurs when the excitation from an intense electron bombardment beam.
iv. Chemiluminescence process occurs when the energy of a chemical reaction excites the material.
v. X-ray luminescence process takes place through the x-ray excitation.
vi. Triboluminescence process may be produced from the mechanical energy including, grinding process.

The absorption is referred to the luminescent materials which release the radiation as the excitation energy is absorbed. The excitation and absorption spectra are often highly correlated which indicates that the excitation energy can be absorbed by either the host lattice or activators. Additionally, as the high energy excitation is applied including, rapid electrons, gamma rays, or vacuum ultraviolet light thus, resulted in the host lattice

05-4506832 pustaka.upsi.edu.my Perpustakaan Tuanku Bainun Kampus Sultan Abdul Jalil Shah PustakaTBainun ptbupsi

05-4506832 pustaka.upsi.edu.my Perpustakaan Tuanku Bainun Kampus Sultan Abdul Jalil Shah PustakaTBainun ptbupsi

excitation process. The excitation spectra demonstrate that the incident radiation is absorbed by the host lattice or activator.

The optical properties of a luminescence center with the different host lattices are commonly not similar due to the center's immediate surroundings have been changed. The influence of host lattice on the optical properties of a required activator can be attributed into two major factors which are, the covalency and crystal field. Due to these factors, the host lattice interactions between electrons are reduced as the covalency increases through their spreading out over the wider orbitals. Hence, the electronic transition was shifted to lower energy between the different energy levels.

Emission is specifically defined as a radiative which returns to the ground state when the absorption and emission processes take place in a similar luminescence ion or center, and thereby, can occur as a result of the host lattice that may greatly influence the emission transitions. Typically, the emission does not exist during the relaxation process in which the transition may return to the ground state upon emission of radiation. In the absence of a radiation field, the emission occurs spontaneously whereas, the absorption can only take place in the presence of a radiation field. The emission process in the presence of the radiation field is known as the stimulated emission. The luminescence center reaches a high vibrational level of the ground state after the emission process and then relaxes to the lowest vibrational level of the ground state. Afterward, Stoke's shift is defined as the energy difference between the maximal level of excitation and emission bands. Hence, it

05-4506832 pustaka.upsi.edu.my Perpustakaan Tuanku Bainun Kampus Sultan Abdul Jalil Shah PustakaTBainun ptbupsi

05-4506832 pustaka.upsi.edu.my Perpustakaan Tuanku Bainun Kampus Sultan Abdul Jalil Shah PustakaTBainun ptbupsi

can be concluded that the larger the vibrational overlap then, the higher the Stoke's shift and thereby, may attribute to the larger optical bands.

The emission process takes place in several mechanisms including, radiative and non-radiative relaxation, cross-relaxation, as well as energy transfer (ET). As the definition of energy transfer (ET), the sensitizer and activator ions possess the physical interaction whereby, the ET may obtain its origin in electrostatic and exchange interaction. The ET process between the synthesizer (S) and activator (A) ions is given by the following chemical reaction:

$$S^* + A \rightarrow S + A^* \tag{2.35}$$

05-4506832 pustaka.upsi.edu.my Perpustakaan Tuanku Bainun Kampus Sultan Abdul Jalil Shah PustakaTBainun ptbupsi

The Coulomb interaction specifies the electrons that initially exist in the excited donor, as well as the electrons that were initially on the acceptor still remain there. It is sufficient that the excited sensitizer ions induce a dipole oscillation on the activator ion for the interaction to take place without any physical contact. Meanwhile, the energy transferred in the case of exchange interaction may be visualized by a double electron substitution reaction which is, the excited electron S* moves to A whereas, the one electron on A moves to S, respectively. Therefore, this type of interaction necessarily involves the electronic charge distribution overlap including, the physical contact between the sensitizer (S) and activator (A) ions. The illustration of the energy transfer (ET) process is depicted in Figure 2.21.

05-4506832 pustaka.upsi.edu.my Perpustakaan Tuanku Bainun Kampus Sultan Abdul Jalil Shah PustakaTBainun ptbupsi

05-4506832 pustaka.upsi.edu.my Perpustakaan Tuanku Bainun Kampus Sultan Abdul Jalil Shah PustakaTBainun ptbupsi

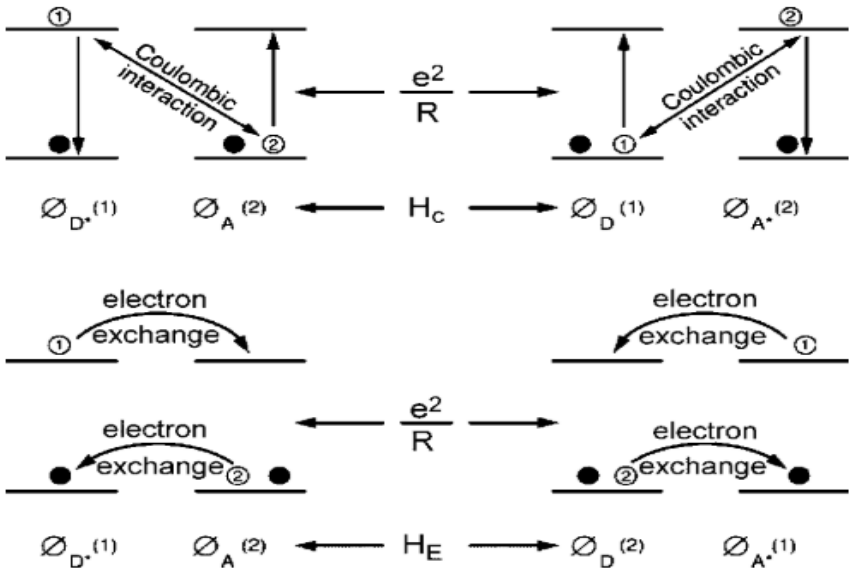


Figure 2.21. Schematic diagram of energy transfer and exchange interaction between two ions via Coulomb interaction (Ronda, 2007)

05-4506832 pustaka.upsi.edu.my Perpustakaan Tuanku Bainun Kampus Sultan Abdul Jalil Shah PustakaTBainun ptbupsi

In a further cross-relaxation phenomenon, the excited electrons are partially transferred their energy to other ions which involve the quenched emission band at a very high concentration of synthesizer ions. For instance, the illustration of the schematic diagram for the two terbium (Tb^{3+}) ions process, is depicted in Figure 2.22. In this case, the energy difference between the excited state level of $^5D_3$ and $^5D_4$ corresponds to the energy difference between the ground state of $^7F_6$ and higher ^7F_J states. The cross-relaxation takes place when the emission from both $^5D_3$ and $^5D_4$ excited states is observed in the host lattices at low Tb concentrations unless the gap between these two states requires relatively high-energy phonons.

05-4506832 pustaka.upsi.edu.my Perpustakaan Tuanku Bainun Kampus Sultan Abdul Jalil Shah PustakaTBainun ptbupsi

05-4506832 pustaka.upsi.edu.my Perpustakaan Tuanku Bainun Kampus Sultan Abdul Jalil Shah PustakaTBainun ptbupsi

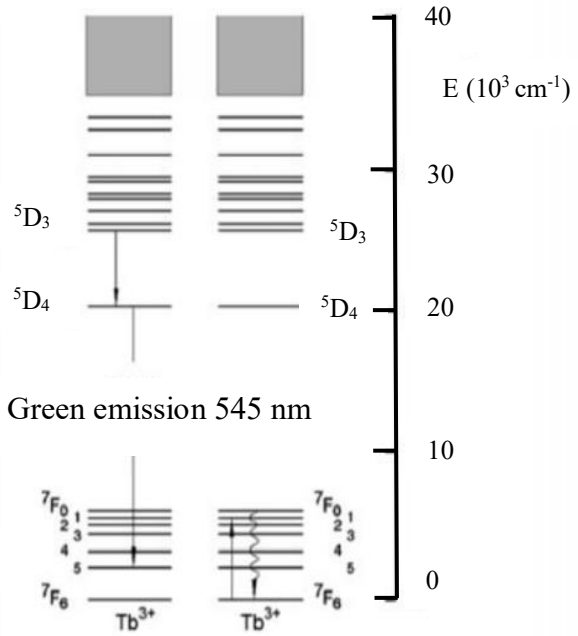


Figure 2.22. Schematic diagram of cross-relaxation between two Tb^{3+} ions (Ronda, 2007)

05-4506832 pustaka.upsi.edu.my Perpustakaan Tuanku Bainun Kampus Sultan Abdul Jalil Shah PustakaTBainun ptbupsi

To date, the photoluminescence studies of Eu^{3+} ions doped zinc-fluorophosphate glasses were investigated by Sreedhar et al., (2019). It was found that the photoluminescence (PL) excitation spectrum resulted in the red emission at 610 nm. In addition, the more intense absorption bands were obtained from the excitation spectrum located at 394 nm and 465 nm which corresponds to the $^7F_0 \rightarrow ^5L_6$ and $^7F_0 \rightarrow ^5D_2$ transitions, respectively. The excitation bands in the wavelength range of 380 to 480 nm are noticeably stronger for using these glasses in various device applications.

05-4506832 pustaka.upsi.edu.my Perpustakaan Tuanku Bainun Kampus Sultan Abdul Jalil Shah PustakaTBainun ptbupsi

05-4506832 pustaka.upsi.edu.my Perpustakaan Tuanku Bainun Kampus Sultan Abdul Jalil Shah PustakaTBainun ptbupsi

2.14 Applications on Glass Fiber/ GO/ rGO/ CNTs-coated Glass

Up to now, the continuous research on new advanced glass coatings with carbon-based nanomaterials (CBNs) has received a dramatic increase to overcome the limitations of current glass materials which in turn has the possibility to enhance the optical properties of glass composites. The combination of extraordinary intrinsic properties of graphene derivatives, as well as their nanoscale size, have been denoted as a potential candidate and incorporated into many kinds of glass coatings.

Generally, owing to graphene's negatively charged surface and large aspect ratio nanosheet structure which found to enhance the luminescence properties in glass applications. Therefore, Wang et al., (2020) fabricated the graphene coating of $Ln^{3+}(Yb^{3+}/Er^{3+})$-doped germanium tellurite glasses for the solid-state material luminescence. By the addition of graphene layer onto the glass surfaces, the luminescence emission property was improved as more energy of propagation direction is parallel to an interface is excited high surface-plasmon mode at an incidence angle is less than 15° and the surface-plasmon mode then efficiently excites the $Ln^{3+}(Yb^{3+}/Er^{3+})$-doped glasses. This result led to an enhancement luminescence of graphene-coated glass, showing comparable performance to the uncoated glass.

The incorporation of GO/rGO into the glass fibers has led to profound improvements in the mechanical properties of the resultant composites. Mahmood et al., (2018) combined the GO-coated glass fibers by electrophoretic deposition meanwhile,

05-4506832 pustaka.upsi.edu.my Perpustakaan Tuanku Bainun Kampus Sultan Abdul Jalil Shah PustakaTBainun ptbupsi

05-4506832 pustaka.upsi.edu.my Perpustakaan Tuanku Bainun Kampus Sultan Abdul Jalil Shah PustakaTBainun ptbupsi

rGO-coated glass fibers by a subsequent chemical reduction approach. The enhancement of both coated-glass fibers was believed via the fiber-matrix interfacial shear strength which was analyzed by the single-fiber fragmentation test. Another important factor to be improved is the piezoresistive response which is contrary to the uncoated fibers, confirming that these graphene-coated fibers have the possibility as the strain sensors in the load-bearing devices.

Notably, Yan et al., (2021) proposed that the introduction of GO coating on the single-mode fiber structure increased the refractive index (RI) sensitivity which in turn reduced the magnetic field sensitivity of the sensor due to its thicker GO coating surface on the core components. Moreover, the proposed GO-coated sensing structure improved the performance of the sensor by incorporating only GO nanosheets which have broad applications in the liquid environment prospects.

In a typical example, Silva et al., (2021) were successfully able to produce titania/ rGO composite coatings which showed great improvements in the photosensitive properties. The GO was produced by Hummer's method and subsequently, reduced to rGO with the irradiated UVA light whereby, the light increased both the electrical conductivity and hydrophilicity of the composite material. This finding is attributable to a hydrophilic behavior that can be induced in the prepared samples using a direct current (DC) voltage and these results provide a smart material application.

05-4506832 pustaka.upsi.edu.my Perpustakaan Tuanku Bainun Kampus Sultan Abdul Jalil Shah PustakaTBainun ptbupsi

05-4506832 pustaka.upsi.edu.my Perpustakaan Tuanku Bainun Kampus Sultan Abdul Jalil Shah PustakaTBainun ptbupsi

Likewise, Yilbas et al., (2018) demonstrated a combination of graphene and GO films onto the functionalized silica particle's glass surface which showed the improvement of optical transmittance. When combining with graphene-based nanomaterials (GBNs), the hydrophobic characteristics of the surface were slightly changed whereby, the contact angle was found to improve from 157° to 160° over the entire glass surfaces. Other than that, the results present the enhancement of optical transmittance and decrease the scattering of the incident UV-visible radiation from the glass surfaces. It can be concluded that this is a significant and potential improvement to the optical properties which allows the inclusion of graphene films on the hydrophobic surfaces which in turn these findings are introduced into many kinds of usable applications.

Recently, the CNTs-coated glass fibers were found to significantly increase the conductive interfacial strength of the glass fiber which strongly affects the electrical properties of composite material (Tzounis et al., 2019). Similarly, Chan et al., (2021) proposed the functionalities of CNTs nanostructures which reasonable to improve the optical characteristics of coated glass, as well as potentially tuning the optical bandgap and thus, changing the semiconductor properties state of the glass-ceramic composites. In another work, considerable attention is focused on the CNTs-coated glass fibers in which the oxygen functional groups that existed on the CNTs enhanced the interfacial bonding strength studied by Zhao et al., (2021). Due to the strong advantages in which the covalent functionalization of CNTs enables the tuning of optical properties of glass matrix system through the hybridization of sp^2 groups and thus, the bond character existed on the

05-4506832 pustaka.upsi.edu.my Perpustakaan Tuanku Bainun Kampus Sultan Abdul Jalil Shah PustakaTBainun ptbupsi

05-4506832 pustaka.upsi.edu.my Perpustakaan Tuanku Bainun Kampus Sultan Abdul Jalil Shah PustakaTBainun ptbupsi

functionalized between the two carbon atoms affects the optical absorption (Gifford et al., 2019).

Differently, CNTs are widely considered promising materials for glass fibers due to their high performance to the significant results. To this aim, Rodríguez-González et al., (2021) developed an effective strategy to coat MWCNTs onto the glass fiber surfaces by applying an ultrasound standing wave. By the addition of CNTs coating material, it was found that the ultrasonic deposition of CNTs on the glass fiber decreases the electrical resistance, suggesting a potential standing wave field to coat MWCNTs onto the glass fibers. As a result, the CNTs-coated glass fibers showed a great of multiscale composites with the desired multifunctional properties. A summary of the previous studies on uncoated and coated glasses is summarized in Table 2.2.

05-4506832 pustaka.upsi.edu.my Perpustakaan Tuanku Bainun Kampus Sultan Abdul Jalil Shah PustakaTBainun ptbupsi

Table 2.2

Summarization of the previous studies on tellurite-based (uncoated) glass and glass fiber/GO/rGO/CNTs-coated-glass

Research title	Findings
Enhanced 1.5 μm emission from Yb^{3+}/ Er^{3+} codoped tungsten tellurite glasses for broadband near-infrared optical fiber amplifiers and tunable fiber lasers	The inclusion of dopant material into host glass caused a strong 1.5 μm emission with full width at high maximum (FWHM) and thus, attribute to a highly efficient resonance energy transfer process (Yuan et al., 2021)

05-4506832 pustaka.upsi.edu.my Perpustakaan Tuanku Bainun Kampus Sultan Abdul Jalil Shah PustakaTBainun ptbupsi

05-4506832 pustaka.upsi.edu.my Perpustakaan Tuanku Bainun Kampus Sultan Abdul Jalil Shah PustakaTBainun ptbupsi

Broadband mid-infrared emission in Dy^{3+}/ Er^{3+} co-doped tellurite glass	The Judd-Ofelt's parameters follow the $\Omega_2 > \Omega_4 > \Omega_6$ trend whereby, the studied glass shows a moderate covalency of Er-O/ Dy-O bonds and local symmetry around Er^{3+}/ Dy^{3+} ions (Zhang et al., 2021)
Enhancing near-infrared luminescence of Ln^{3+}(Yb^{3+}/ Er^{3+})-doped germanium tellurite glasses by coating with graphene	The luminescence emission property was improved by the addition of graphene layer onto the glass surfaces (Wang et al., 2020)
Hydrophobic and optical characteristics of graphene and graphene oxide films transferred onto functionalized silica particles deposited glass surfaces	The present study showed the improvement of optical characteristics and reduce the scattering of UV-visible radiation on the glass surfaces (Yilbas et al., 2018)
Mechanical properties and strain monitoring of glass-epoxy composites with graphene-coated fibers	The enhancement of both GO-coated glass fibers and rGO-coated glass fibers was believed due to the fiber-matrix interfacial shear strength (Mahmood et al., 2018)

05-4506832 pustaka.upsi.edu.my Perpustakaan Tuanku Bainun Kampus Sultan Abdul Jalil Shah PustakaTBainun ptbupsi

05-4506832 pustaka.upsi.edu.my Perpustakaan Tuanku Bainun Kampus Sultan Abdul Jalil Shah PustakaTBainun ptbupsi

Optical effects of divalent functionalization of carbon nanotubes	The covalent functionalization of CNTs allows for tuning the optical properties of glass matrix via a hybridization of sp^2 groups. As a result, the optical absorption was strongly influenced by the functionalized bond between two carbon atoms (Gifford et al., 2019)

2.15 Summary

05-4506832 pustaka.upsi.edu.my Perpustakaan Tuanku Bainun Kampus Sultan Abdul Jalil Shah PustakaTBainun ptbupsi

In summary, the theoretical study related to this research work was presented. The calculation, expression formulas, and recent literature on optical properties including, optical absorption spectra, optical bandgap energy, Urbach energy, refractive index, electronegativity, other optical parameters, and photoluminescence were discussed in this work. Referring to the previous findings, it can be concluded that the optical properties such as refractive index, optical bandgap energy, and Judd-Ofelt's intensity parameters were important parameters to achieve excellent optical properties of the rGO- and CNTs-coated glasses.

05-4506832 pustaka.upsi.edu.my Perpustakaan Tuanku Bainun Kampus Sultan Abdul Jalil Shah PustakaTBainun ptbupsi

05-4506832 pustaka.upsi.edu.my Perpustakaan Tuanku Bainun Kampus Sultan Abdul Jalil Shah PustakaTBainun ptbupsi

CHAPTER 3

RESEARCH METHODOLOGY

05-4506832 pustaka.upsi.edu.my Perpustakaan Tuanku Bainun Kampus Sultan Abdul Jalil Shah PustakaTBainun ptbupsi

3.1 Introduction

This chapter presents the methodology of glass fabrication and characterization techniques to investigate the optical and structural properties of tellurite glass coated with reduced graphene oxide (rGO) and carbon nanotubes (CNTs). The optical properties cover the UV-Vis spectroscopy and photoluminescence; meanwhile, the structural properties cover Field Emission Scanning Electron Microscopy (FESEM), Transmission Electron Microscopy (TEM), X-ray Diffraction (XRD), Fourier Transform Infrared (FT-IR), X-ray Fluorescence, and Raman analyses. The synthesis method of GO, rGO, and CNTs were clearly presented and thus, this chapter ends with a brief experimental work in this research.

05-4506832 pustaka.upsi.edu.my Perpustakaan Tuanku Bainun Kampus Sultan Abdul Jalil Shah PustakaTBainun ptbupsi

05-4506832 pustaka.upsi.edu.my Perpustakaan Tuanku Bainun Kampus Sultan Abdul Jalil Shah PustakaTBainun ptbupsi

3.2 Glass Fabrication

3.2.1 Melt-quenching Technique

The two sets of glass series of zinc borotellurite doped with erbium oxide nanoparticles with the chemical composition of {(0.47(1-y)) TeO_2 + (0.2 (1-y)) B_2O_3 + (0.29 (1-y)) ZnO + (y) Er_2O_3 (nanoparticles)} -rGO/-CNTs (coated) whereby, y = 0.005, 0.01, 0.02, 0.03, 0.04, and 0.05 mol% were synthesized via a conventional melt-quenching technique. The high purity of raw materials consisted of Tellurium (IV) Oxide, TeO_2 (Sigma Aldrich, 99.99%), Boron Oxide, B_2O_3 (Sigma Aldrich, 98.50%), Zinc Oxide, ZnO (Sigma Aldrich, 99.99%), and Erbium (III) Oxide Nanoparticles, Er_2O_3 NPs (Sigma Aldrich, 99.99%), as listed in Table 3.1. All the chemical powders were weighed using an electrical balance in accordance of calculated compositions with an accuracy of ±0.0001 g to obtain 13 g of mixed powder.

The weighed chemical powder was then placed into a platinum crucible and stirred using a glass rod for 30 minutes in order to obtain a completely homogeneous mixture. The mixture was transferred to the first electric furnace at 400 °C for an hour to undergo the pre-heating process probably to remove the water content or moisture contained in the mixture. Next, the mixture was melted at a high temperature of an electrical furnace at 900 °C for 2 hours certainly to obtain a good performance of transparent glass and having a low tendency of fragility in glass materials.

05-4506832 pustaka.upsi.edu.my Perpustakaan Tuanku Bainun Kampus Sultan Abdul Jalil Shah PustakaTBainun ptbupsi

05-4506832 pustaka.upsi.edu.my Perpustakaan Tuanku Bainun Kampus Sultan Abdul Jalil Shah PustakaTBainun ptbupsi

The molten chemical powder was poured instantly into a cylindrical stainless-steel mold that had been pre-heated at 400 °C about an hour earlier to avoid the glass cracking which could result from the thermal shock and to prevent the solidification from taking place during the quenching process. The melt was then immediately annealed at 400 °C for an hour to release the thermal stress or strain and get rid of the air bubbles which might exist in glass materials. The fabricated glasses were allowed to cool down at room temperature for 5 hours before being polished on both sides using the different types of sandpaper to attain the highly flat, shiny, and smooth glass surfaces. The glass samples were then ready to be deposited with rGO and CNTs solution via a simple and low-cost spray coating technique for further optical and structural characterization in the glass materials, as illustrated in Figure 3.1 meanwhile, the flow diagram of the fabrication and deposition process of the ZBTEr (NPs)-rGO, ZBTEr (NPs)-CNTs, and ZBTEr (NPs)-uncoated glass samples is presented in Figure 3.2.

Table 3.1

The details of high purity raw chemical powders

Chemical powders	Supplier company	Purity level	Particle size
Tellurium (IV) oxide, TeO_2	Sigma Aldrich	≥99.99%	Microns size
Boron oxide, B_2O_3	Sigma Aldrich	≥98.50%	Microns size
Zinc oxide, ZnO	Sigma Aldrich	≥99.99%	Microns size
Erbium (III) oxide nanoparticles, Er_2O_3 NPs	Sigma Aldrich	≥99.99%	20 – 30 nm

05-4506832 pustaka.upsi.edu.my Perpustakaan Tuanku Bainun Kampus Sultan Abdul Jalil Shah PustakaTBainun ptbupsi

05-4506832 pustaka.upsi.edu.my Perpustakaan Tuanku Bainun Kampus Sultan Abdul Jalil Shah PustakaTBainun ptbupsi



Figure 3.1. Schematic representation for synthesis and deposition of rGO and CNTs onto tellurite-based glass surfaces

05-4506832 pustaka.upsi.edu.my Perpustakaan Tuanku Bainun Kampus Sultan Abdul Jalil Shah PustakaTBainun ptbupsi

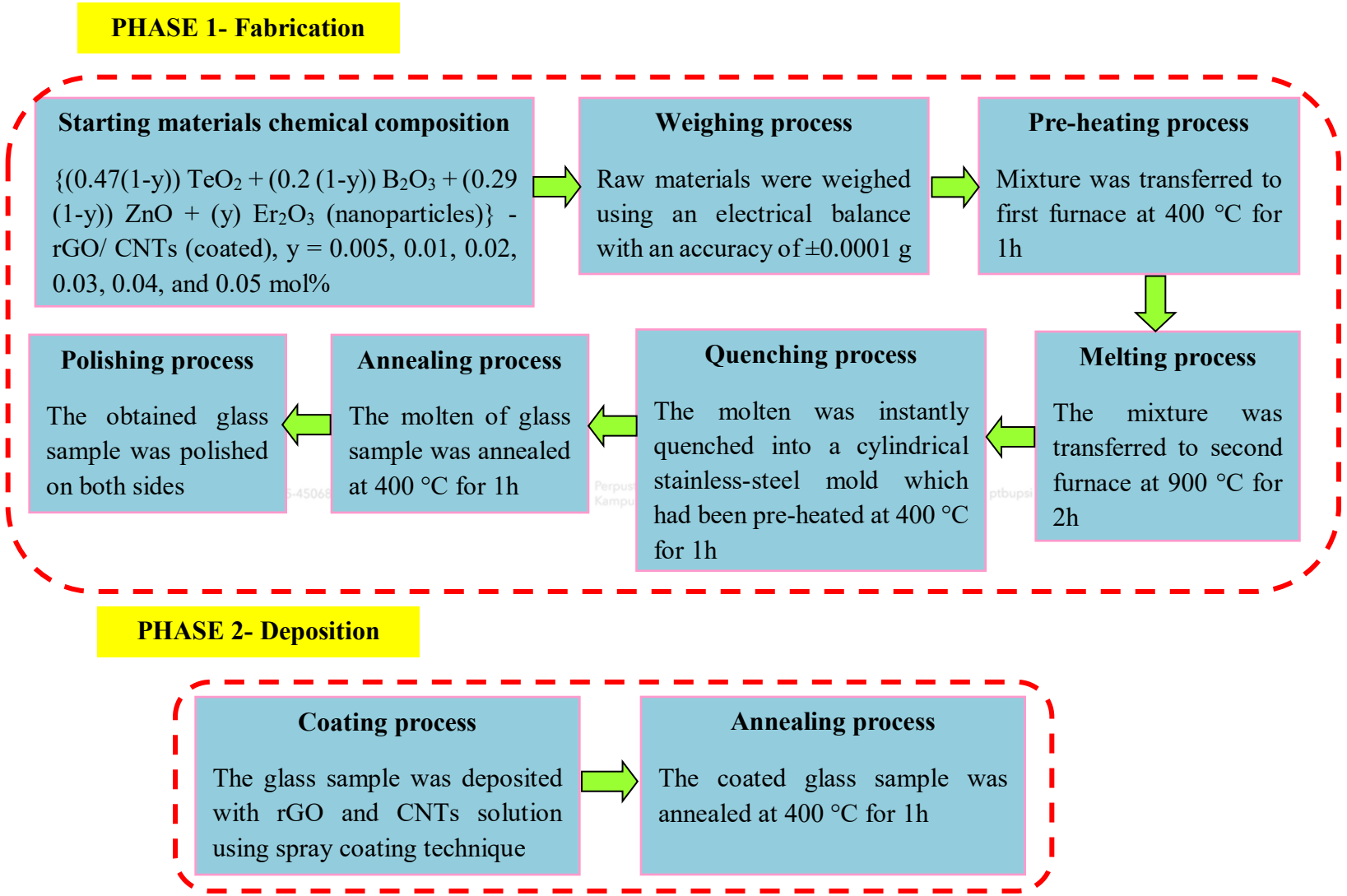


Figure 3.2. Flow diagram of glass fabrication and deposition process for ZBTEr (NPs)-rGO and ZBTEr (NPs)-CNTs glasses

05-4506832 pustaka.upsi.edu.my Perpustakaan Tuanku Bainun Kampus Sultan Abdul Jalil Shah PustakaTBainun ptbupsi

3.3 Synthesis of Graphene Oxide and Reduced Graphene Oxide

3.3.1 Electrochemical Exfoliation Method

The GO can be derived from graphite electrodes via an electrochemical exfoliation method. The graphite rods were attached to a direct current (DC) voltage power supply as the function of an anode and cathode electrodes. The electrodes were then instantly immersed in the dissolved electrolyte solution and immediately allowed for exfoliation of bulk graphite transformed into GO flakes about 24 hours, as shown in Figure 3.3. A commercially anionic surfactant known as sodium dodecyl sulphate (SDS) was added to the de-ionized (DI) water to prepare the electrolyte solution due to that surfactant can assist to promote the stabilization of graphene sheets that occurred during the exfoliation process (Narayan & Kim, 2015). In addition, the presence of a surfactant might inhibit the formation of aggregation and agglomerated structures.

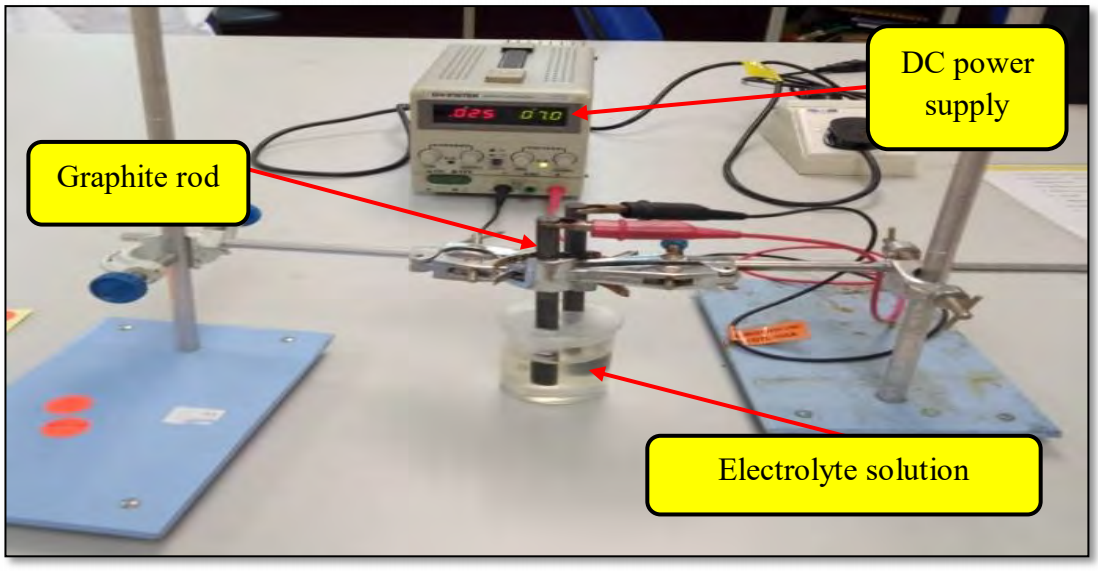


Figure 3.3. Experimental set up to synthesize GO via electrochemical exfoliation technique

05-4506832 pustaka.upsi.edu.my Perpustakaan Tuanku Bainun Kampus Sultan Abdul Jalil Shah PustakaTBainun ptbupsi

05-4506832 pustaka.upsi.edu.my Perpustakaan Tuanku Bainun Kampus Sultan Abdul Jalil Shah PustakaTBainun ptbupsi

3.3.2 Reduction of GO to rGO

The graphene oxide solution was reduced by using hydrazine hydrate as a reducing agent. Immediately after the process of GO synthesis, 0.5 ml of hydrazine hydrate was subsequently added into the 50 ml GO solution in a triple neck, round bottom flask and ready for immersion in a hot water. The mixture was then followed by additional stirring for 24 hours using a magnetic stirrer held at a temperature ~95 °C, as depicted in Figure 3.4.

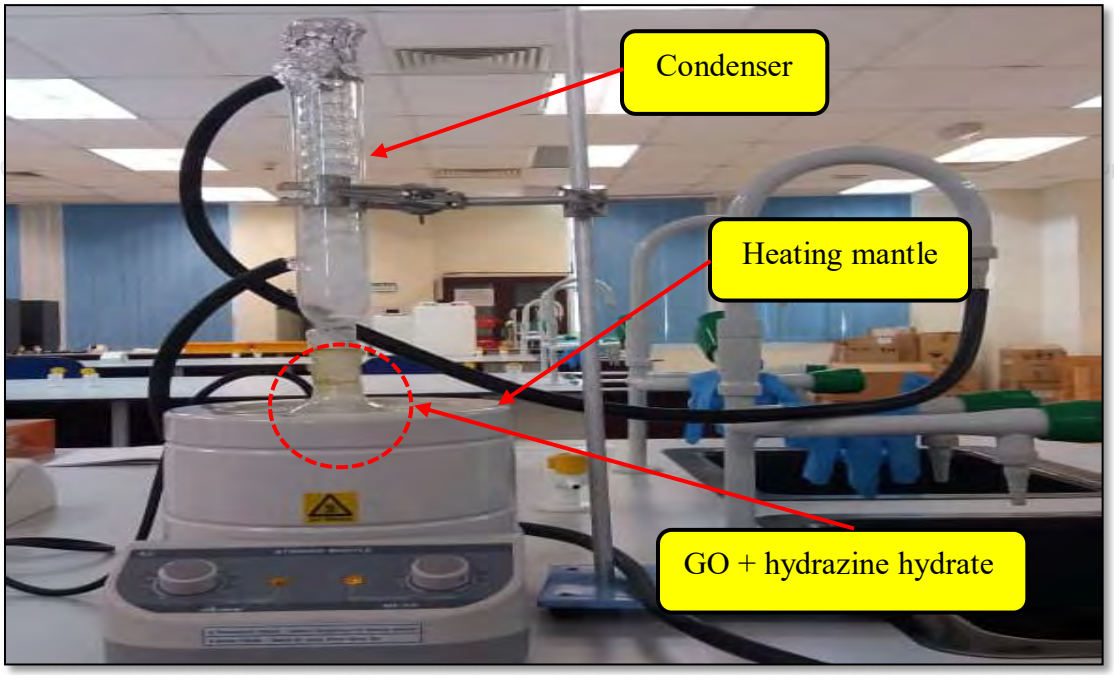


Figure 3.4. Experimental set up for reduction process of GO to rGO

05-4506832 pustaka.upsi.edu.my Perpustakaan Tuanku Bainun Kampus Sultan Abdul Jalil Shah PustakaTBainun ptbupsi

05-4506832 pustaka.upsi.edu.my Perpustakaan Tuanku Bainun Kampus Sultan Abdul Jalil Shah PustakaTBainun ptbupsi

3.4 Dispersion of Carbon Nanotubes

The dispersion of CNTs can essentially involve 0.5 g of multi-walled carbon nanotubes (MWCNTs) powder (ChemAR, 95%) was first placed in a beaker that assisted with the commercially anionic sodium dodecyl sulphate (SDS) surfactant in the electrolyte solution, as shown in Figure 3.5. The mixture was then allowed to dilute the CNTs under the moderate magnetic stirring process for 3 hours at room temperature, resulting from the optimum effect between the addition of surfactant structures and CNTs interaction (Fatemi & Foroutan, 2015). Subsequently, the obtained CNTs solution was ready to proceed as a coating material on top of the tellurite-based glass surfaces by utilizing a spray coating technique.

05-4506832 pustaka.upsi.edu.my Perpustakaan Tuanku Bainun Kampus Sultan Abdul Jalil Shah PustakaTBainun ptbupsi

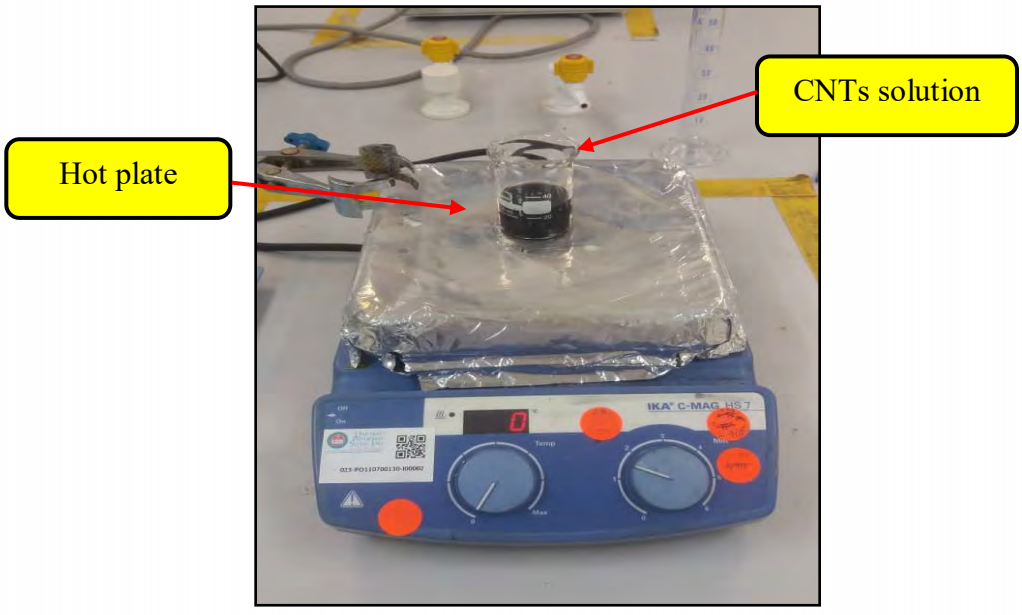


Figure 3.5. Experimental set up to disperse the MWCNTs

05-4506832 pustaka.upsi.edu.my Perpustakaan Tuanku Bainun Kampus Sultan Abdul Jalil Shah PustakaTBainun ptbupsi

05-4506832 pustaka.upsi.edu.my Perpustakaan Tuanku Bainun Kampus Sultan Abdul Jalil Shah PustakaTBainun ptbupsi

3.5 Glass Deposition Process

3.5.1 Spray Coating Technique

The as-prepared tellurite-based glass samples are ready to be deposited with rGO and CNTs using the spray coating technique. The nozzle of an airbrush system with a diameter size of about 0.25 mm was used for the coating process at approximately ~10 cm constant distance from the nozzle to the glass surfaces, as shown in Figure 3.6 (experimental procedure) and Figure 3.7 (schematic diagram), respectively. The rGO- and CNTs-coated glass samples were then annealed at a temperature of about 400 °C for an hour in an argon (Ar) ambient state, as shown in Figure 3.8.

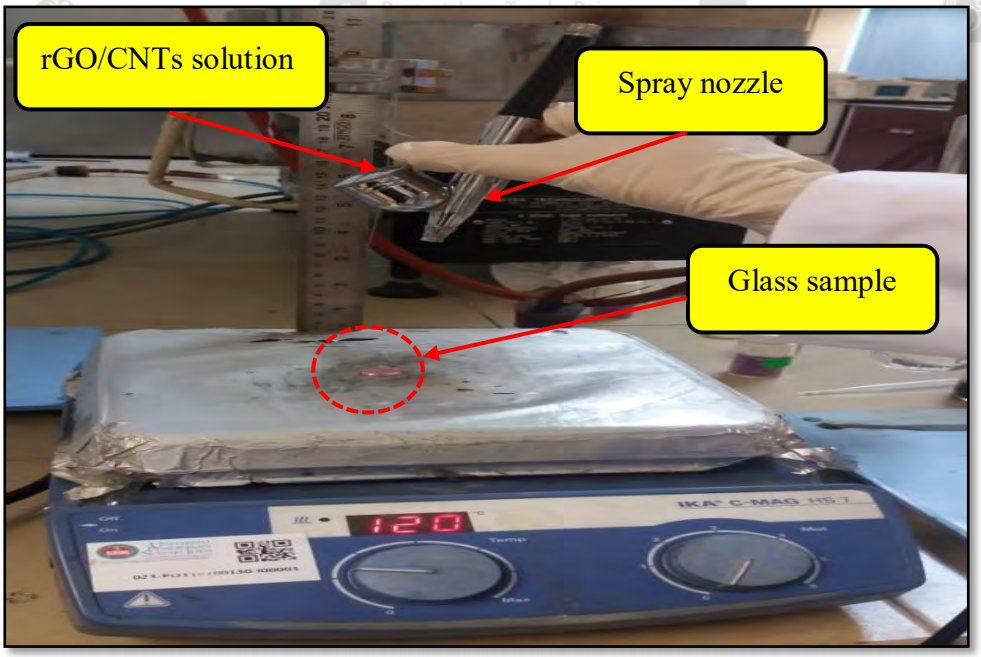


Figure 3.6. Experimental procedure of rGO-coated and CNTs-coated glass samples via spray coating technique

05-4506832 pustaka.upsi.edu.my Perpustakaan Tuanku Bainun Kampus Sultan Abdul Jalil Shah PustakaTBainun ptbupsi

05-4506832 pustaka.upsi.edu.my Perpustakaan Tuanku Bainun Kampus Sultan Abdul Jalil Shah PustakaTBainun ptbupsi

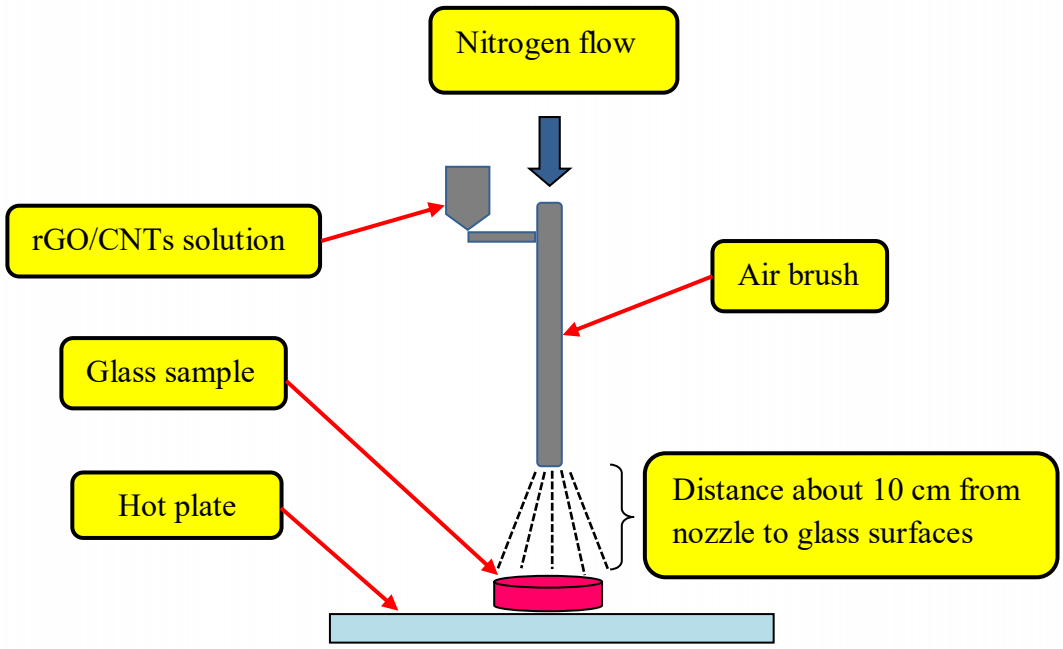


Figure 3.7. Schematic diagram of rGO- coated and CNTs-coated glass via spray coating technique

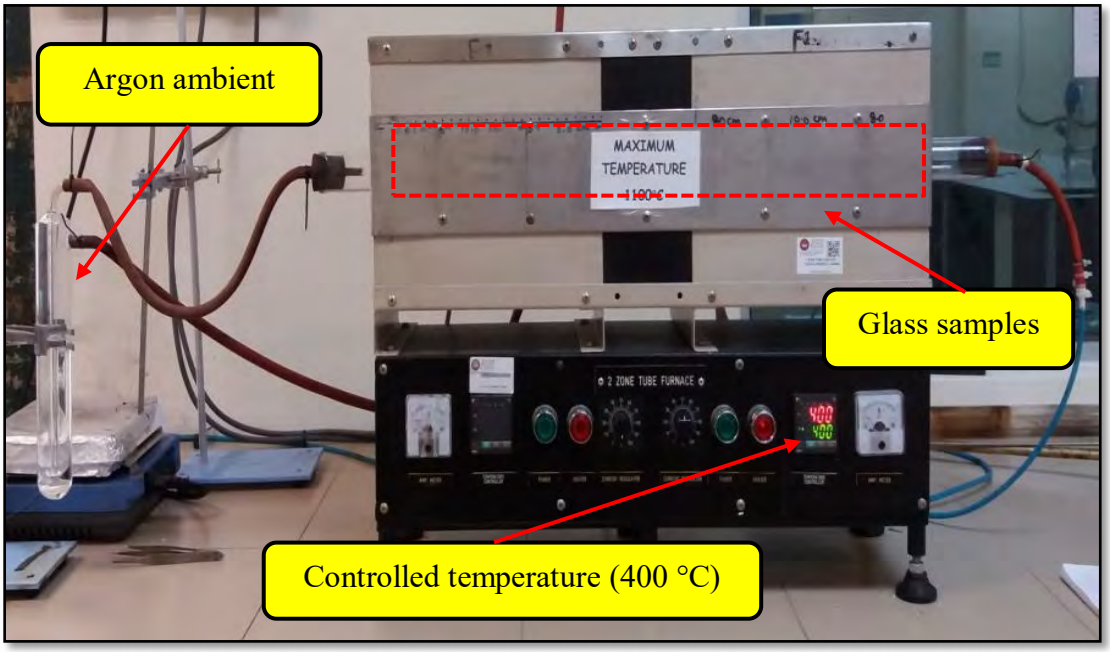


Figure 3.8. Experimental set up of the annealing process for rGO-coated and CNTs-coated glass samples via 2-zone tube furnace

05-4506832 pustaka.upsi.edu.my Perpustakaan Tuanku Bainun Kampus Sultan Abdul Jalil Shah PustakaTBainun ptbupsi

05-4506832 pustaka.upsi.edu.my Perpustakaan Tuanku Bainun Kampus Sultan Abdul Jalil Shah PustakaTBainun ptbupsi

3.6 Physical Properties Characterization

3.6.1 Density and Molar Volume Measurement

The density of all the glass samples was measured at room temperature (21 °C) by using the densimeter with a standard error of around ±0.0001 g/cm^3 and with acetone (with the density of 791 kg/m^3) as the immersion liquid. Acetone is suitable to be used as an immersion liquid because of its low surface tension in order to avoid air bubbles and is compatible with the glass samples. The densimeter applied the basic principle of Archimedes to obtain the density of all the glass samples. Then, the data of the glass samples was calculated by using that instrument.

05-4506832 pustaka.upsi.edu.my Perpustakaan Tuanku Bainun Kampus Sultan Abdul Jalil Shah PustakaTBainun ptbupsi

3.7 Structural Properties Characterization

3.7.1 Field Emission Scanning Electron Microscopy and Energy Dispersive X-ray

SEM is an essential analysis for the identification of the surface morphology of non-material, the diameter, thickness, length, and orientation. In order to analyze the image clearly on the surface, a focused electron has been used in the SEM analysis. Besides, SEM is known as high-resolution imaging, which offers increased magnification and the ability to observe very fine surface structures at lower accelerating voltage.

In addition, SEM is used for observing and imaging the surface morphology and structure of the as-prepared glass samples. The observation of the surface morphology of

05-4506832 pustaka.upsi.edu.my Perpustakaan Tuanku Bainun Kampus Sultan Abdul Jalil Shah PustakaTBainun ptbupsi

05-4506832 pustaka.upsi.edu.my Perpustakaan Tuanku Bainun Kampus Sultan Abdul Jalil Shah PustakaTBainun ptbupsi

tellurite-based glasses coated with rGO and CNTs was investigated using a FESEM instrument (Brand: ZEISS, Model: MERLIN) at i-CRIM Centralized Laboratory, Centre for Research and Instrumentation Management (CRIM), Research Complex, Universiti Kebangsaan Malaysia and by using FESEM (Brand: Hitachi, Model: SU8020) at the Chemistry Department Central Facility (CenFac), Universiti Malaya. During the observation, SEM was operated at an accelerating voltage of 2 – 30 kV and the images were captured using the upper detector at a working distance of 4 mm under the magnification range from 1 to 200 K X. The glass sample materials were coated with platinum using Quorum Q150P S Cooled Sputter Coater before identifying the structure of the glass materials. In addition, the SEM instrument was equipped with an EDX for analyzing the elemental composition in the rGO and CNTs samples. Then, the SEM and EDX instruments were significantly used for observing the morphological structure on the glass surfaces and detecting the possible elements in the solutions, as presented in Figure 3.9.

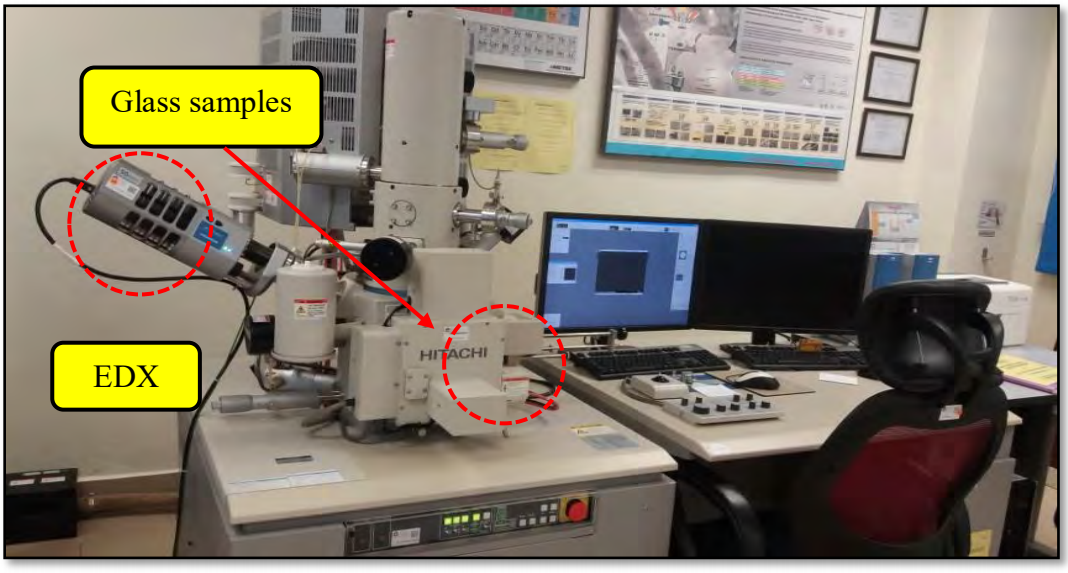


Figure 3.9. FESEM was used to investigate the microstructure surfaces onto the rGO-coated and CNTs-coated glasses

05-4506832 pustaka.upsi.edu.my Perpustakaan Tuanku Bainun Kampus Sultan Abdul Jalil Shah PustakaTBainun ptbupsi

05-4506832 pustaka.upsi.edu.my Perpustakaan Tuanku Bainun Kampus Sultan Abdul Jalil Shah PustakaTBainun ptbupsi

3.7.2 High Resolution Transmission Electron Microscopy

HR-TEM is an important tool to identify the nano-size particles and analyze their size based on the high resolution and quality using the TEM (LEO 912AB) at the Faculty of Science, Universiti Putra Malaysia. In this study, the nanoparticles form of glass samples was initially prepared by dispersing uniformly in an acetone solution before being proceeded to place the solution contains the glass samples on the instrument sample holder. Then, the glass samples were penetrated via focusing electrons emitted under the scanning process which was controlled by using the computer connected to the instrument. The image of nano-size particles appeared to possess an accuracy of about ±0.01. The basic principle of an electron microscope shows a good resolution with a wavelength lower than light in order to obtain a better-quality image of nano-size particles.

3.7.3 X-ray Diffraction

XRD is an analytical technique used for phase recognition of crystalline materials, which are either crystalline or amorphous structures. Crystalline structure can be determined with the formation of atoms in a regular pattern while amorphous structure exhibits atoms randomly in liquid. The XRD can be functioned to identify the crystal structure arrangement of materials, single crystal or particle orientation, size, shape, internal stress of low crystalline parts, and lattice parameters from the peak. In addition, XRD can be performed to obtain information from the local structures in glasses, including the nearest

05-4506832 pustaka.upsi.edu.my Perpustakaan Tuanku Bainun Kampus Sultan Abdul Jalil Shah PustakaTBainun ptbupsi

05-4506832 pustaka.upsi.edu.my Perpustakaan Tuanku Bainun Kampus Sultan Abdul Jalil Shah PustakaTBainun ptbupsi

neighbor distances and coordination numbers. The scattering of X-ray gives a diffused pattern in glasses in which the presence of long-range periodicity instead of sharp lines on crystalline substances show the absence of long-range periodicity in the glass system.

XRD is an essential analysis to examine the characterization of glass materials and to identify the structural arrangement in the glass system. Then, the crystallinity or amorphous structure of the as-prepared tellurite glasses was investigated using an XRD instrument (Bruker, D2 Phaser with the scan range, θ of (10° – 60°) at the Faculty of Bioengineering Technology, Universiti Malaysia Kelantan. During the measurement, the tellurite glass samples were put in the sample holder and an X-rays beam from CuKα emission in the wavelength, λ = 0.154 nm hit to glass samples at room temperature. Then, the obtained XRD pattern was matched with the references or standard data, as demonstrated in Figure 3.10.

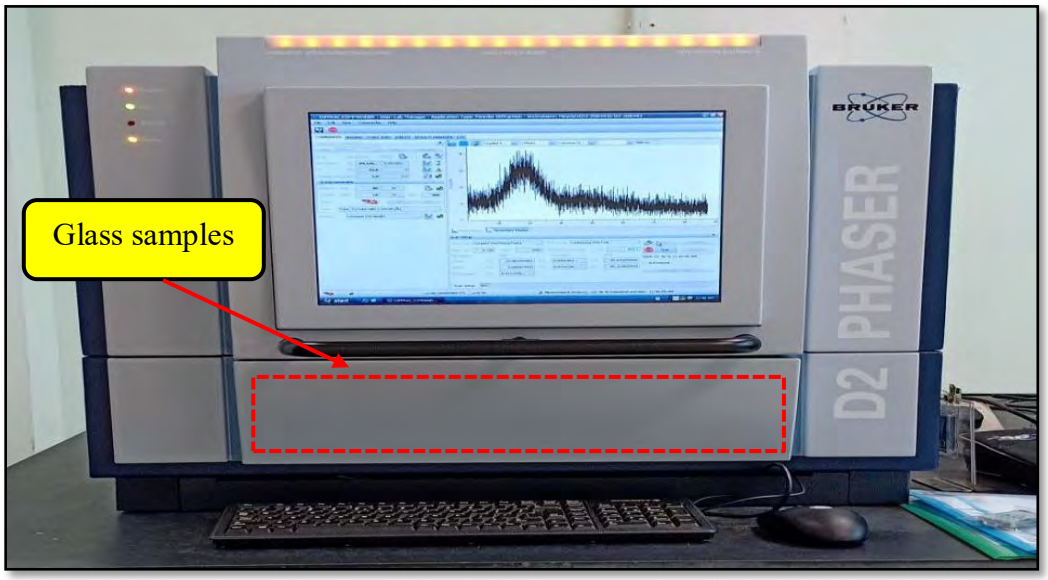


Figure 3.10. XRD measurement (Bruker, D2 Phaser) used for investigation of the amorphous nature of rGO- and CNTs-coated glass samples

05-4506832 pustaka.upsi.edu.my Perpustakaan Tuanku Bainun Kampus Sultan Abdul Jalil Shah PustakaTBainun ptbupsi

05-4506832 pustaka.upsi.edu.my Perpustakaan Tuanku Bainun Kampus Sultan Abdul Jalil Shah PustakaTBainun ptbupsi

3.7.4 Fourier Transform Infrared Spectroscopy

FT-IR spectroscopy is an analysis process which can be used to analyze the structural bonding of glass network forming. One of the important advantages of FTIR spectroscopy is that it can provide useful guidance on the structure of molecules rapidly without any estimation technique and explains many facts about the structural arrangement and properties of glasses. The fundamental necessity of this analysis is that there must be a net change in dipole moment during the vibration of the molecule or functional group in this study.

The investigation of the bonding parameter and structural units in the glass network matrix of all the glass samples was performed by using the KBr pallet technique at the Faculty of Science, Universiti Putra Malaysia. The sample was grounded into powder form through the grinding process and weighed with an accuracy of ~0.005 g. The obtained powder was then mixed thoroughly with the high purity of KBr powder of 0.2 g and pressed at 0.1 until 0.2 kbar pressure by using an evacuator die. Later, the transparent pallet was mounted in the spectrometer in order to undergo for the scanning process. The transmission spectra were measured within the region of 400 – 4000 cm^{-1} at room temperature. The obtained final infrared spectrum was computed and shown on the computer screen. The error of this instrument is approximately ±10 µm.

05-4506832 pustaka.upsi.edu.my Perpustakaan Tuanku Bainun Kampus Sultan Abdul Jalil Shah PustakaTBainun ptbupsi

05-4506832 pustaka.upsi.edu.my Perpustakaan Tuanku Bainun Kampus Sultan Abdul Jalil Shah PustakaTBainun ptbupsi

3.7.5 Micro-Raman Spectroscopy

Raman scattering technique is a molecular vibration or rotation in which the vibration structural units and phonon energy of host material may be inferred. In particular, Raman spectroscopy is able to probe the nature of defects in graphitic materials due to the G and 2D (known as the G', being symmetry allowed) peaks that always satisfy the Raman selection rule, the Raman-forbidden D and D' bands appear in the Raman spectrum which reflected in the defect-activated Raman intensities. This technique is used for investigating the graphene from graphite and its sensitivity towards the defects, excess charge (doping), strain, and atomic arrangement of the edges. In the Raman scattering process, the peaks are activated by a single-phonon inter-valley and intra-valley scattering process, respectively where the defect distributes the missing momentum for satisfying the momentum conservation.

The structural properties of as-prepared GO, rGO and CNTs samples are studied using micro-Raman spectroscopy located at i-CRIM Centralized Laboratory, Centre for Research, and Instrumentation Management (CRIM), Research Complex, Universiti Kebangsaan Malaysia. Furthermore, the Raman spectra were operated from 100 – 4000 cm^{-1} about 5 minutes in each running process, as depicted in Figure 3.11.

05-4506832 pustaka.upsi.edu.my Perpustakaan Tuanku Bainun Kampus Sultan Abdul Jalil Shah PustakaTBainun ptbupsi

05-4506832 pustaka.upsi.edu.my Perpustakaan Tuanku Bainun Kampus Sultan Abdul Jalil Shah PustakaTBainun ptbupsi



Figure 3.11 Micro-Raman spectroscopy was used to identify the nature of defects in GO, rGO, and CNTs samples

05-4506832 pustaka.upsi.edu.my Perpustakaan Tuanku Bainun Kampus Sultan Abdul Jalil Shah PustakaTBainun ptbupsi

3.8 Optical Properties Characterization

3.8.1 Ultraviolet-Visible Spectroscopy

UV-Vis spectroscopy is a powerful tool for identifying the optical absorption spectra of glass samples. The analysis of optical properties such as optical absorption spectra, optical bandgap energy, and Urbach energy can be further analyzed via the obtained optical absorption spectrum. The instrument which is a UV-Vis spectrophotometer (The Cary 5000) from NANO-SciTech Laboratory, Centre for Nanoscience and Nanotechnology, Institute of Science, Universiti Teknologi MARA (UiTM) and also conducted at i-CRIM Centralized Laboratory, Centre for Research, and Instrumentation Management (CRIM), Research Complex, Universiti Kebangsaan Malaysia were applied for optical properties in the range of wavelength about 200 – 800 nm that was carried out at room temperature. The

05-4506832 pustaka.upsi.edu.my Perpustakaan Tuanku Bainun Kampus Sultan Abdul Jalil Shah PustakaTBainun ptbupsi

05-4506832 pustaka.upsi.edu.my Perpustakaan Tuanku Bainun Kampus Sultan Abdul Jalil Shah PustakaTBainun ptbupsi

prepared rGO-coated and CNTs-coated glass samples with a thickness of ~2 mm was then placed in the sample holder in order to analyze the characterization process. Lastly, the obtained optical absorption spectra were recorded by the computer system which is connected to the instrument, as shown in Figure 3.12.



Figure 3.12 UV-Vis spectrophotometer (The Cary 5000) was applied to analyze the optical absorption spectra of rGO-coated and CNTs-coated tellurite glass samples

3.8.2 Photoluminescence

Photoluminescence is a light emitting analysis applied to any substance and used to determine the optical emission via a photon-excitation. It was followed by the light that is directed onto the sample, where it is absorbed or imparted the excess energy. In fact, photo-excitation causes the electrons to move into the excited states of the glass materials. The

05-4506832 pustaka.upsi.edu.my Perpustakaan Tuanku Bainun Kampus Sultan Abdul Jalil Shah PustakaTBainun ptbupsi

05-4506832 pustaka.upsi.edu.my Perpustakaan Tuanku Bainun Kampus Sultan Abdul Jalil Shah PustakaTBainun ptbupsi

photoluminescence spectrometer (Edinburgh Instrument, Model FLS920) was used to analyze the emission spectra of glass sample at i-CRIM Centralized Laboratory, Centre for Research and Instrumentation Management (CRIM), Research Complex, Universiti Kebangsaan Malaysia. The photoluminescence instrument used in this study is presented in Figure 3.13.



Figure 3.13 Photoluminescence (PL) spectrometer was used to determine the optical emission characterization of rGO- and CNTs-coated tellurite glass samples

3.9 Brief Description of Experimental Work

The overall experimental work was summarized which can be described as follows (refer Figure 3.14):

05-4506832 pustaka.upsi.edu.my Perpustakaan Tuanku Bainun Kampus Sultan Abdul Jalil Shah PustakaTBainun ptbupsi

05-4506832 pustaka.upsi.edu.my Perpustakaan Tuanku Bainun Kampus Sultan Abdul Jalil Shah PustakaTBainun ptbupsi

i. Stage 1: Fabrication of the ZBTEr (NPs) glasses by utilizing a conventional melt-quenching technique.

ii. Stage 2: Physical characterization of the ZBTEr (NPs) glasses.

iii. Stage 3: Synthesis of GO and rGO by using electrochemical exfoliation and reduction process, respectively as well as the synthesis of CNTs with assisted surfactant.

iv. Stage 4: Glass coating of the ZBTEr (NPs) glass samples with coating materials (rGO and CNTs) by using a spray coating technique.

05-4506832 pustaka.upsi.edu.my Perpustakaan Tuanku Bainun Kampus Sultan Abdul Jalil Shah PustakaTBainun ptbupsi

v. Stage 5: Optical and structural characterization of the ZBTEr (NPs)-rGO and ZBTEr (NPs)-CNTs glasses.

05-4506832 pustaka.upsi.edu.my Perpustakaan Tuanku Bainun Kampus Sultan Abdul Jalil Shah PustakaTBainun ptbupsi

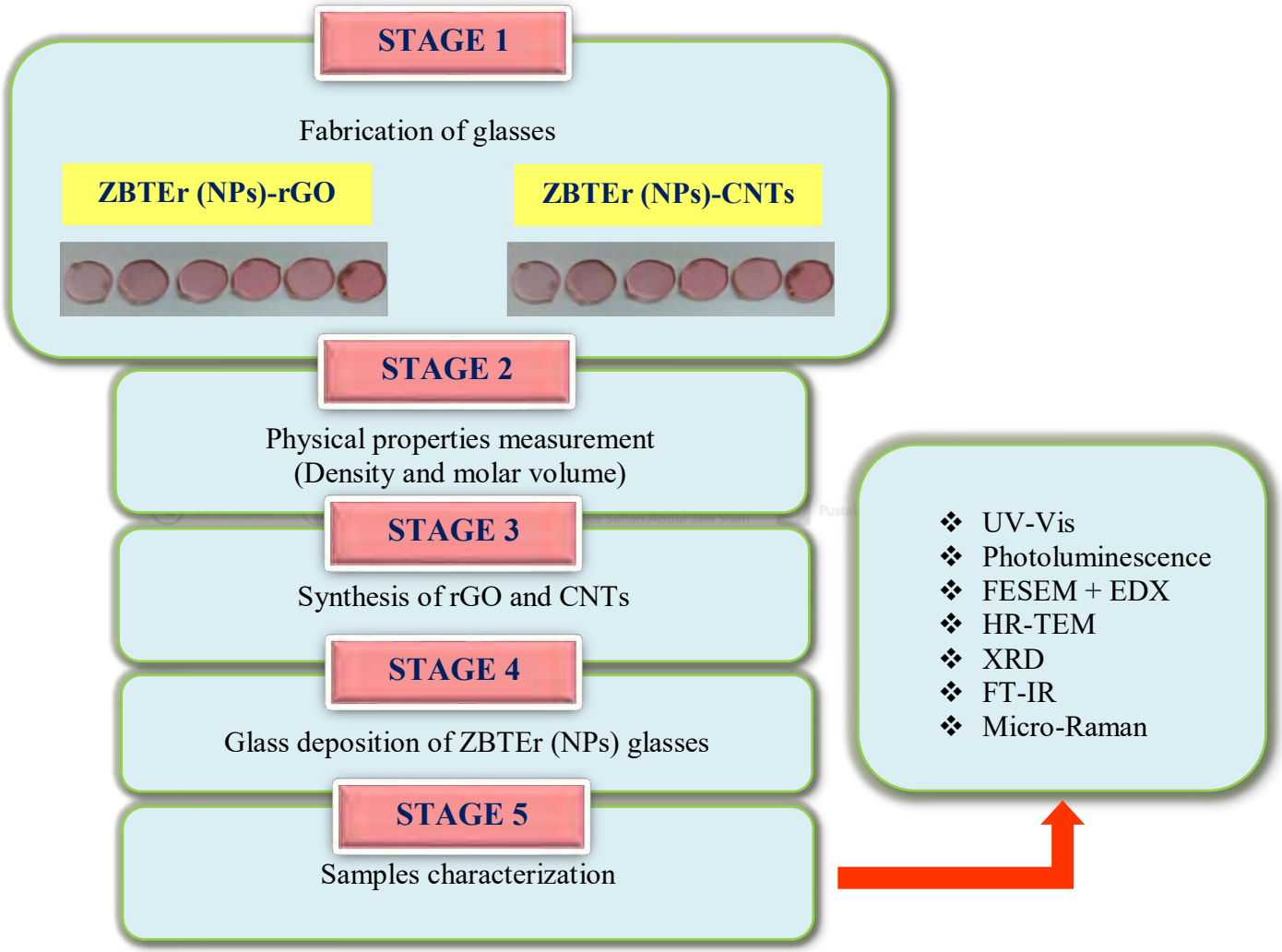


Figure 3.14 Research flow chart of overall experimental study

05-4506832 pustaka.upsi.edu.my Perpustakaan Tuanku Bainun Kampus Sultan Abdul Jalil Shah PustakaTBainun ptbupsi

3.10 Summary

In summary, it was concluded that the detailed procedure to fabricate the tellurite glasses doped with erbium nanoparticles via a melt-quenched technique was presented. The spray coating technique had been used to proceed with the deposition process onto glass samples with rGO and CNTs solution separately. The characterization of the coated tellurite-based glasses were characterized to investigate the optical, structural, and physical properties of the glass matrix system, were briefly explained in this work.

05-4506832 pustaka.upsi.edu.my Perpustakaan Tuanku Bainun Kampus Sultan Abdul Jalil Shah PustakaTBainun ptbupsi
05-4506832 pustaka.upsi.edu.my Perpustakaan Tuanku Bainun Kampus Sultan Abdul Jalil Shah PustakaTBainun ptbupsi

05-4506832 pustaka.upsi.edu.my Perpustakaan Tuanku Bainun Kampus Sultan Abdul Jalil Shah PustakaTBainun ptbupsi

CHAPTER 4

RESULTS AND DISCUSSION

05-4506832 pustaka.upsi.edu.my Perpustakaan Tuanku Bainun Kampus Sultan Abdul Jalil Shah PustakaTBainun ptbupsi

4.1 Introduction

In this chapter, the results of physical, structural, and optical properties of the studied glasses were discussed. This chapter can be divided into four main subsections. The first subsection discusses on the characterization of ZBTEr (NPs)-uncoated glass. The second subsection describes the characterization of ZBTEr (NPs)-rGO glasses. Meanwhile, the third subsection explains the characterization of ZBTEr (NPs)-CNTs glasses. This chapter is ended with the last subsection which discusses the comparative analysis between ZBTEr (NPs)-uncoated, ZBTEr (NPs)-rGO, ZBTEr (NPs)-CNTs glasses and previous studies.

05-4506832 pustaka.upsi.edu.my Perpustakaan Tuanku Bainun Kampus Sultan Abdul Jalil Shah PustakaTBainun ptbupsi

05-4506832 pustaka.upsi.edu.my Perpustakaan Tuanku Bainun Kampus Sultan Abdul Jalil Shah PustakaTBainun ptbupsi

4.2 Physical and Structural Properties of Tellurite Glass Doped with Erbium Nanoparticles (ZBTEr (NPs)-uncoated)

4.2.1 Density and Molar Volume

The density data for a glass series denoted as the ZBTEr (NPs)-uncoated glasses were tabulated in Table 4.1. According to Figure 4.1, the density data of ZBTEr (NPs)-uncoated glasses show the increment trend along with an increase of Er^{3+} nanoparticles (Er-NPs) concentration. This effect may be ascribed to the existence of the excess amount of oxygen in the amorphous system (Nazrin et al., 2018). Moreover, the obtained results correspond to the presence of TeO_4 functional groups with the supported FT-IR spectra, as demonstrated in Figure 4.5. Additionally, the excess of oxygen takes place at high density particularly, via the substitution of ZnO by TeO_2 structural units in the glassy matrix.

The density data of ZBTEr (NPs)-uncoated glasses show an increasing trend which can be correlated with the addition of Er-NPs ions nanoparticles and lead to the degradation of the crosslinked network in the glass system. Furthermore, Er-NPs ions comprise trivalent electrons which increase the tendency to release three electrons and may capture one electron from the oxygen to immediately break the glass network chain. Afterward, it is observed that the breaking of the continuous linking network attributes to the formation of non-bridging oxygens (NBOs) and thereby, leads the molecules to become denser.

The trend of density in the studied glasses may be influenced from the incorporation of heavy metal ions into the glassy matrix system. The increasing trend of density can be

05-4506832 pustaka.upsi.edu.my Perpustakaan Tuanku Bainun Kampus Sultan Abdul Jalil Shah PustakaTBainun ptbupsi

05-4506832 pustaka.upsi.edu.my Perpustakaan Tuanku Bainun Kampus Sultan Abdul Jalil Shah PustakaTBainun ptbupsi

explained in terms of atomic mass in which the atomic mass of erbium oxide, Er_2O_3 nanoparticles (Z_{Er} = 167.259 $gmol^{-1}$) is heavier than the atomic mass of tellurium oxide, TeO_2 (Z_{Te} = 127.600 $gmol^{-1}$), zinc oxide, ZnO (Z_{Zn} = 65.409 $gmol^{-1}$) and boron oxide, B_2O_3 (Z_B = 69.618 $gmol^{-1}$). The factor of a large number in atomic mass of erbium leads to the increasing of compactness and thus, attribute to the increment in densities for the ZBTEr (NPs)-uncoated glasses.

Meanwhile, the molar volume of the ZBTEr (NPs)-uncoated glasses was found increased as the density increases along with erbium, Er-NPs concentration. The formation of NBOs existing in the glassy matrix may break the bonds of tellurite host glass and thus, increase the free space in the glass network system (Nazrin et al., 2018).

05-4506832 pustaka.upsi.edu.my Perpustakaan Tuanku Bainun Kampus Sultan Abdul Jalil Shah PustakaTBainun ptbupsi

Particularly, the theoretical relationship between the density and molar volume is inversely proportional to each other. However, the obtained trend shows that the molar volume value is directly proportional with the density. The occurrence of this trend can be related to the atomic radius differences between tellurite and erbium oxides. It is noted that the atomic radius of erbium oxide, Er_2O_3 nanoparticles (r = 175 pm) is greater than the atomic radius of tellurite oxide, TeO_2 (r = 140 pm). Therefore, it can be noticed that the higher atomic radius in erbium oxide than tellurite oxide will produce an excess free volume as the Er-NPs concentration increases. Nevertheless, the molar volume decreased slightly at 0.01 mol% Er_2O_3 nanoparticles concentration, as shown in Figure 4.1. This behavior can be correlated to the trend of density and the incorporation of ZnO which is known to possess the dual nature properties to a certain concentration of dopants in the

05-4506832 pustaka.upsi.edu.my Perpustakaan Tuanku Bainun Kampus Sultan Abdul Jalil Shah PustakaTBainun ptbupsi

05-4506832 pustaka.upsi.edu.my Perpustakaan Tuanku Bainun Kampus Sultan Abdul Jalil Shah PustakaTBainun ptbupsi

glass network. Other than that, the addition of Er-NPs content into the glass interstices causes an increase in the interatomic spacing between the atoms and bond length of Er-O and Te-O thereby, leads to the increment in molar volume of the glasses.

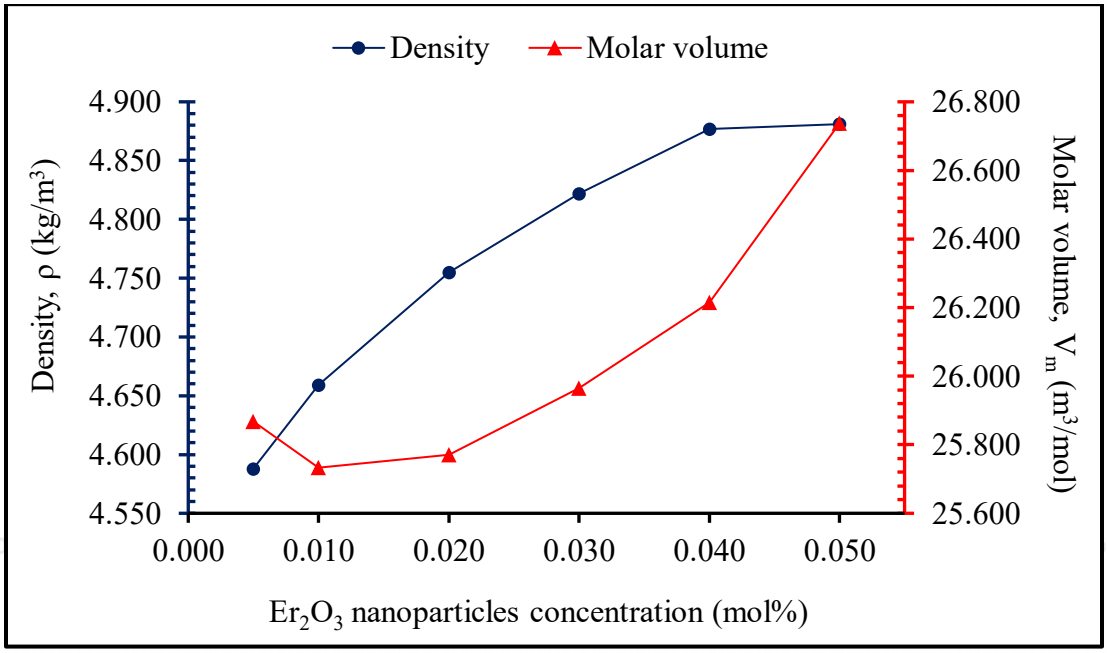


Figure 4.1. Variation of density and molar volume as a function of Er_2O_3 nanoparticles concentration of the ZBTEr (NPs)-uncoated glasses

05-4506832 pustaka.upsi.edu.my Perpustakaan Tuanku Bainun Kampus Sultan Abdul Jalil Shah PustakaTBainun ptbupsi

05-4506832 pustaka.upsi.edu.my Perpustakaan Tuanku Bainun Kampus Sultan Abdul Jalil Shah PustakaTBainun ptbupsi

Table 4.1

Density and molar volume with the different Er_2O_3 nanoparticles concentration for ZBTEr (NPs)-uncoated glasses

Er_2O_3 nanoparticles concentration (mol%)	Density, ρ (kg/m^3) (±0.0001)	Molar volume, V_m (m^3/mol) (±0.0001)
0.005	4.588	25.868
0.010	4.659	25.733
0.020	4.755	25.771
0.030	4.822	25.964
0.040	4.877	26.215
0.050	4.881	26.737

05-4506832 pustaka.upsi.edu.my Perpustakaan Tuanku Bainun Kampus Sultan Abdul Jalil Shah PustakaTBainun ptbupsi

4.2.2 Erbium Inter-ionic Distance, Polaron Radius, Field Strength, and Oxygen Packing Density

Further studies of the structural changes caused by Er-NPs in the tellurite glass system, some related physical properties such as Er^{3+} ion concentration (N), erbium inter-ionic distance (R_i), polaron radius (R_P), erbium field strength (F), and oxygen packing density (OPD) were determined using the equations which have been stated in subsections 2.10.2 and 2.10.3 and the calculated data are presented in Table 4.2.

Figure 4.2 shows that the erbium ion concentration (N) increases with the increase of Er-NPs concentration. This data is important to identify the erbium inter-ionic distance

05-4506832 pustaka.upsi.edu.my Perpustakaan Tuanku Bainun Kampus Sultan Abdul Jalil Shah PustakaTBainun ptbupsi

05-4506832 pustaka.upsi.edu.my Perpustakaan Tuanku Bainun Kampus Sultan Abdul Jalil Shah PustakaTBainun ptbupsi

(R_i) and polaron radius (R_p). The observed decrease of R_p with the increase of Er-NPs content can be correlated to the increased value of erbium ion concentration (N). Additionally, it was believed that the shorter distance between Er and O atoms may attribute to the increasing of Er-O bond strength in the glassy matrix and hence, generating a stronger field strength around the Er^{3+} ions sites.

The increment of density values depends on the multi-composition of the ZBTEr (NPs)-uncoated glass matrix which causes the oxygen packing density (OPD) to increase from 74.047 – 74.960 g.atom/L along with the increase of Er-NPs concentration from 0.005 – 0.02 mol%, as depicted in Figure 4.3. The observed increase of the OPD value in the glass matrix may be ascribed to the decrease in the interstitial space of the glass network which resulted from the introduction of erbium atoms containing large atomic, as well as ionic radii. Furthermore, these results were affected due to a higher number of atoms per unit composition and the increasing number of NBOs which indicates more inter-atomic spacing and disordered structures in the glass network.

Meanwhile, the OPD value decreased in the range of 74.823 – 73.475 g.atom/L along with the increase of Er-NPs concentration from 0.03 – 0.05 mol% which ascribed to the existence of NBOs and broken B-O and Te-O bonds along with the increase of molar volume from 25.773 – 26.737 m^3/mol. The covalent nature of the glass network structure was increased which in turn reduced the ionic nature along with the increased molar volume and thereby, indicating the emergence of loose packing that exists in the glass

05-4506832 pustaka.upsi.edu.my Perpustakaan Tuanku Bainun Kampus Sultan Abdul Jalil Shah PustakaTBainun ptbupsi

05-4506832 pustaka.upsi.edu.my Perpustakaan Tuanku Bainun Kampus Sultan Abdul Jalil Shah PustakaTBainun ptbupsi

matrix. Other than that, the obtained field strength value indicates the high solubility of rare-earth oxides in the tellurite glass system.

With regards to this, it was concluded that the physical properties of the tellurite-based amorphous glass matrix were not influenced by the rGO and CNTs coating materials. It is worth noting that the rGO and CNTs layers on the glass surface does not affects the density and molar volume of the tellurite glass system. Apart from that, rGO and CNTs give significant effects on the optical properties of tellurite glass. Hence, the rGO and CNTs coating materials are excellent candidates which offer enormous potential to improve the optical properties of the tellurite glass system which will be discussed in sections 4.4 and 4.6.

05-4506832 pustaka.upsi.edu.my Perpustakaan Tuanku Bainun Kampus Sultan Abdul Jalil Shah PustakaTBainun ptbupsi
05-4506832 pustaka.upsi.edu.my Perpustakaan Tuanku Bainun Kampus Sultan Abdul Jalil Shah PustakaTBainun ptbupsi

05-4506832 pustaka.upsi.edu.my Perpustakaan Tuanku Bainun Kampus Sultan Abdul Jalil Shah PustakaTBainun ptbupsi

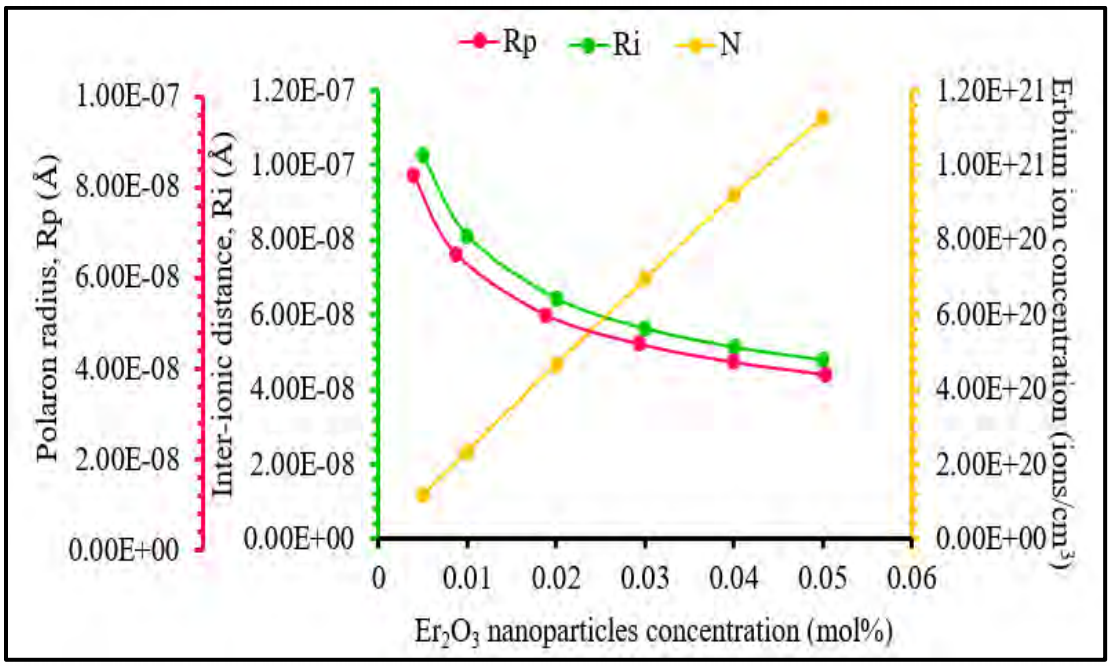


Figure 4.2. Variation of erbium ion concentration (N), erbium inter-ionic distance (R_i), and polaron radius (R_p) as a function of Er_2O_3 nanoparticles concentration for ZBTEr (NPs)-uncoated glasses

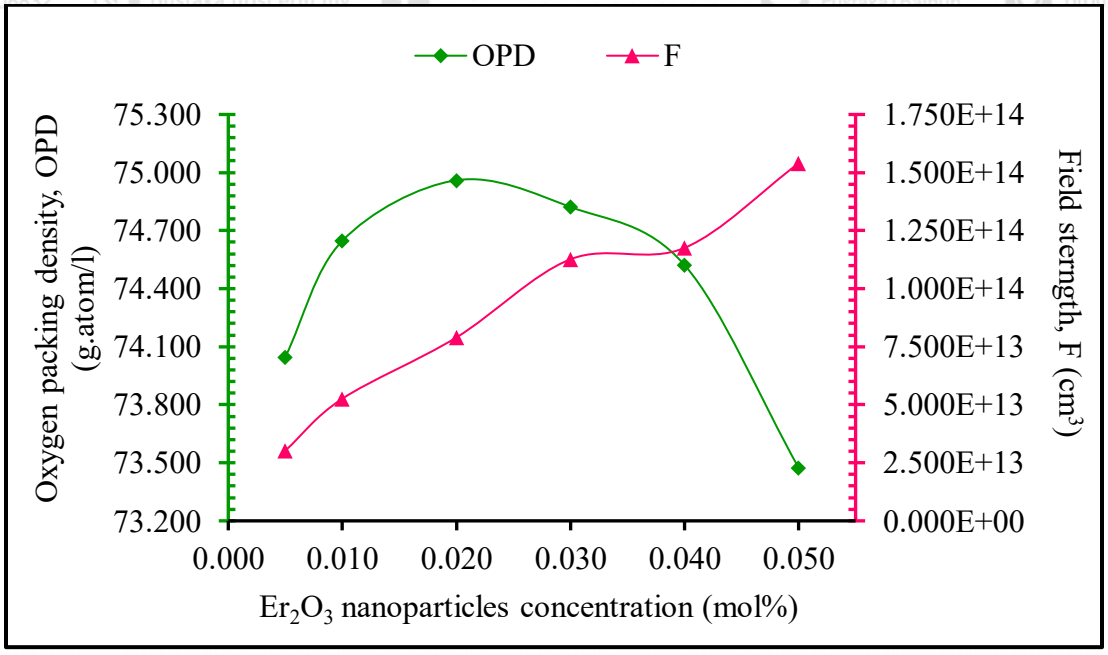


Figure 4.3. Variation of oxygen packing density (OPD) and field strength (F) as a function of Er_2O_3 nanoparticles concentration for ZBTEr (NPs)-uncoated glasses

05-4506832 pustaka.upsi.edu.my Perpustakaan Tuanku Bainun Kampus Sultan Abdul Jalil Shah PustakaTBainun ptbupsi

05-4506832 pustaka.upsi.edu.my Perpustakaan Tuanku Bainun Kampus Sultan Abdul Jalil Shah PustakaTBainun ptbupsi

Table 4.2

Erbium ion concentration (N), erbium inter-ionic distance (R_i), polaron radius (R_P), erbium field strength (F), and oxygen packing density (OPD) with the different Er_2O_3 nanoparticles concentration for ZBTEr (NPs)-uncoated glasses

Er_2O_3 nanoparticles concentration (mol%)	N (ions/cm^3) ($\times10^{20}$) (±1.495)	R_i (Å) ($\times10^{-7}$) (±0.188)	R_P (Å) ($\times10^{-8}$) (±0.756)	F (cm^3) ($\times10^{13}$) (±1.575)	OPD (g.atom/L) (±0.398)
0.005	1.164	1.024	8.254	3.024	74.047
0.010	2.340	0.811	6.540	5.261	74.647
0.020	4.674	0.644	5.193	7.898	74.960
0.030	6.958	0.564	4.548	11.265	74.823
0.040	9.189	0.514	4.145	11.755	74.522
0.050	11.262	0.481	3.874	15.395	73.475

05-4506832 pustaka.upsi.edu.my Perpustakaan Tuanku Bainun Kampus Sultan Abdul Jalil Shah PustakaTBainun ptbupsi

05-4506832 pustaka.upsi.edu.my Perpustakaan Tuanku Bainun Kampus Sultan Abdul Jalil Shah PustakaTBainun ptbupsi

4.2.3 X-ray Diffraction of ZBTEr (NPs)-uncoated Glass

The structural investigation was studied by XRD spectroscopy to confirm the amorphous nature of the studied tellurite-based glass. Based on the XRD spectra shown in Figure 4.4, the presence of a broad diffusion or hump pattern was observed within the range of 20° – 40° in the 2θ diffraction scale which indeed validates the amorphous structural arrangement of all the prepared glass samples. These results are in accordance to the study by Bulus et al., (2019). Apparently, the ZBTEr (NPs)-uncoated glass samples show the absence of sharp diffraction peaks in the XRD spectra which confirms the existence of long-range structural disorder characteristics or lack of atomic orderliness takes place in the glass network system (Amiar Rodin & Sahar, 2018).

05-4506832 pustaka.upsi.edu.my Perpustakaan Tuanku Bainun Kampus Sultan Abdul Jalil Shah PustakaTBainun ptbupsi

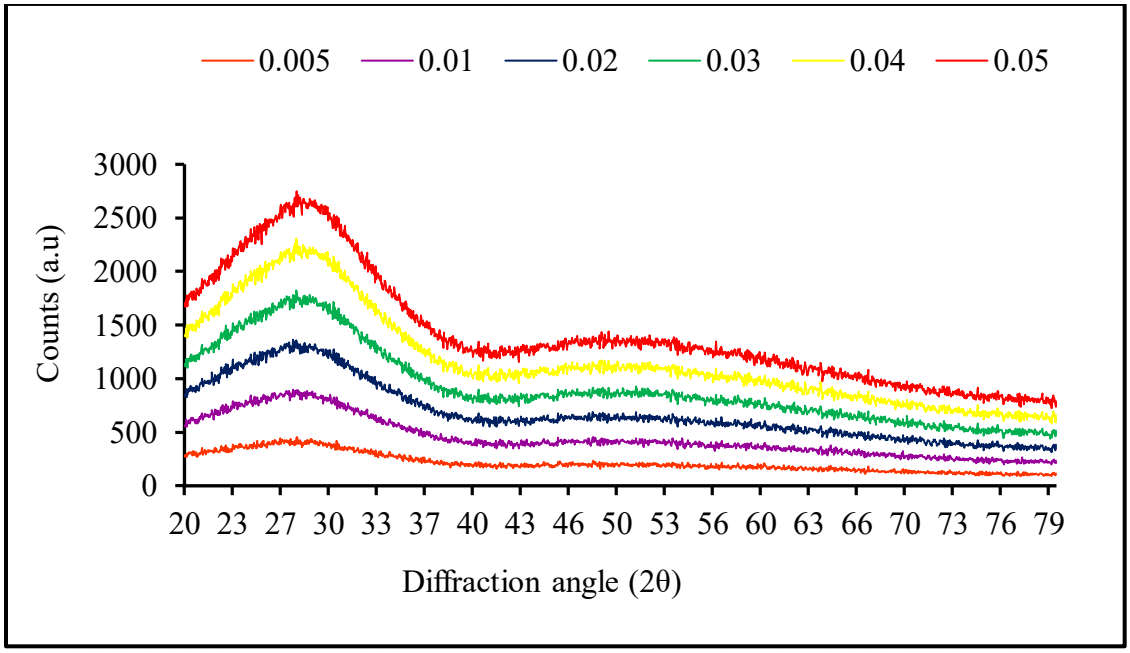


Figure 4.4. XRD spectra of ZBTEr (NPs)-uncoated glasses

05-4506832 pustaka.upsi.edu.my Perpustakaan Tuanku Bainun Kampus Sultan Abdul Jalil Shah PustakaTBainun ptbupsi

05-4506832 pustaka.upsi.edu.my Perpustakaan Tuanku Bainun Kampus Sultan Abdul Jalil Shah PustakaTBainun ptbupsi

4.2.4 Fourier Transform Infrared Analysis of ZBTEr (NPs)-uncoated Glass

The structural parameters were determined by FT-IR spectroscopy and the obtained data illustrates the structural bonding with functional groups of the glass network system. The transmission spectra of ZBTEr (NPs)-uncoated glass samples are recorded in Figure 4.5 and summarized in Table 4.3. It is noted that there are several peaks shown in the transmission spectra for all samples which indicate the local structure in the glass matrix. Generally, the transmission spectra of the ZBTEr (NPs)-uncoated glasses correspond to three transmission bands with different concentrations of Er_2O_3 nanoparticles in the range of 656 – 664 cm^{-1}, 1233 – 1252 cm^{-1}, and 1327 – 1343 cm^{-1} (as indicated by the vertical dotted line) meanwhile, some shoulders are presented in the range of 414 – 421 cm^{-1}.

05-4506832 pustaka.upsi.edu.my Perpustakaan Tuanku Bainun Kampus Sultan Abdul Jalil Shah PustakaTBainun ptbupsi

The transmission band of pure TeO_3 is generally located at 640 cm^{-1}. The characteristics of tellurite oxide composed of two different kinds of structural configuration units including, TeO_4 trigonal bipyramid units (tbp) and TeO_3 trigonal pyramid units (tp) (Marczewska & Środa, 2018). The existence of transmission band located in the range of 656 – 664 cm^{-1} demonstrate to the stretching vibrational modes of Te-O bands that exists in Te-bridging oxygen and Te-nonbridging oxygen, respectively. The formation of Te-bridging oxygen is associated to the TeO_4 trigonal bipyramid structural units (tbp) meanwhile, the Te-nonbridging oxygen correlates to the TeO_3 trigonal pyramid structural units (tp) (Leśniak et al., 2019). Specifically, the first transmission band is dominated by the bands in the range of 600 – 650 cm^{-1}, corresponds to the high content of TeO_4 structural group meanwhile, the second transmission band is located in the range of 650 – 700 cm^{-1},

05-4506832 pustaka.upsi.edu.my Perpustakaan Tuanku Bainun Kampus Sultan Abdul Jalil Shah PustakaTBainun ptbupsi

05-4506832 pustaka.upsi.edu.my Perpustakaan Tuanku Bainun Kampus Sultan Abdul Jalil Shah PustakaTBainun ptbupsi

which correlates to the TeO_3 structural groups exists in the glass system. Furthermore, the transmission band in the range of 656 – 664 cm^{-1} indicates the presence of the Te-nonbridging oxygen, TeO_3 functional groups. These broadened bands may be related to the structural properties of TeO_2 including, bond lengths, bond angles and coordination numbers in the disordered amorphous glass materials (Gupta et al., 2020).

Concerning the addition of modifier oxide into the glassy matrix system, the transmission band characteristics of pure borate oxide, BO_3 is centered at 806 cm^{-1}. Primarily, the transmission bands of BO_4 and BO_3 are proposed to form a stable glass formation via the introduction of boroxyl ring. According to the work by Krogh-Moe, he suggested that the vibrational modes of borate glass are active based on three spectral regions (Julien et al., 1989). From the obtained transmission spectra, the first group of the band is observed around 600 – 800 cm^{-1} which can be related to the bending vibrations of various borate arrangements B-O-B. Meanwhile, the second group of the band is located around 800 – 1200 cm^{-1} which corresponds to the B-O stretching vibrations of tetrahedral BO_4- structural units. Lastly, the third group of the band is obtained around 1200 – 1800 cm^{-1} which corresponds to the B-O stretching of trigonal BO_3 structural units.

Additionally, the transmission spectra are observed around 1233 – 1253 cm^{-1} which caused by the B-O-B stretching vibrations of polymerized BO_3 groups (Nazrin et al., 2018; Pach-Zawada et al., 2021). The transmission band is presented around 1327 – 1343 cm^{-1} can be ascribed with the trigonal B-O bond stretching vibrations that existed in the isolated trigonal BO_3 structural units. Finally, the transmission band is observed around 1388 –

05-4506832 pustaka.upsi.edu.my Perpustakaan Tuanku Bainun Kampus Sultan Abdul Jalil Shah PustakaTBainun ptbupsi

05-4506832 pustaka.upsi.edu.my Perpustakaan Tuanku Bainun Kampus Sultan Abdul Jalil Shah PustakaTBainun ptbupsi

1410 cm^{-1} can be associated with the trigonal B-O bond stretching vibrations of BO_3 structural units from various kinds of borate groups.

The inexistence of ZnO in the transmission band proved that the zinc lattice is completely broken down after the glass formation. Moreover, the inclusion of small proportion of ZnO modifier into the glassy matrix system, may break the Te-O-Te and Te-O-B bonds and thereby, introduces the coordination effects known as dangling bonds (Te-O^{-}…Zn^{2+}…O-Te), which attributes to formation of TeO_4 structural units and the decrease of TeO_3 structural units (Kaur et al., 2021). Nevertheless, the absence of Er-NPs in the transmission spectra signifies a low concentration of dopant ions which is unable to detect by the device.

05-4506832 pustaka.upsi.edu.my Perpustakaan Tuanku Bainun Kampus Sultan Abdul Jalil Shah PustakaTBainun ptbupsi

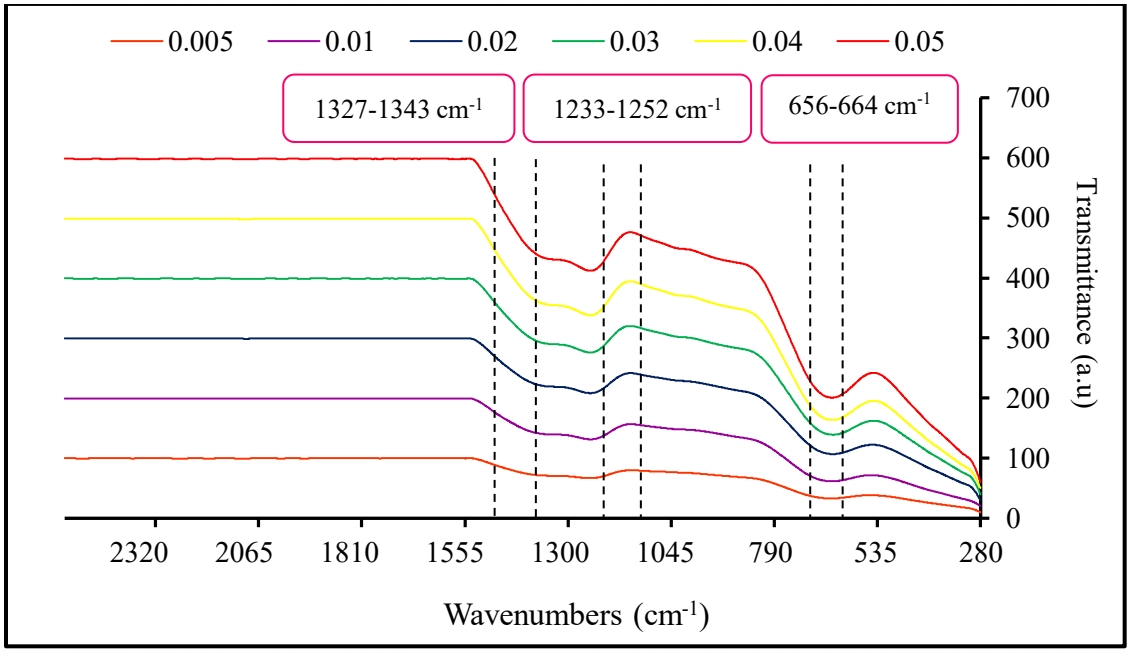


Figure 4.5. FT-IR spectra of ZBTEr (NPs)-uncoated glasses

05-4506832 pustaka.upsi.edu.my Perpustakaan Tuanku Bainun Kampus Sultan Abdul Jalil Shah PustakaTBainun ptbupsi

05-4506832 pustaka.upsi.edu.my Perpustakaan Tuanku Bainun Kampus Sultan Abdul Jalil Shah PustakaTBainun ptbupsi

Table 4.3

Assignments of transmission bands of ZBTEr (NPs)-uncoated glasses

No.	Band positions (cm^{-1})						Assignments
1	642	637	633	637	645	645	TeO_3 functional groups with the existing of TeO and TeO^- bonds (Kaur et al., 2021)
2	1226	1223	1225	1227	1226	1223	Stretching vibrations of trigonal B-O bond in BO_3 tetrahedra including, the linkage of oxygen between various groups (Leśniak et al., 2019)
3	1348	1345	1334	1341	1338	1331	Stretching vibrations of trigonal B-O bond in isolated $(BO_3)^{3-}$ structural units from borate groups (metaborates, pyroborates, and orthoborates) (Lesniak et al., 2020)

05-4506832 pustaka.upsi.edu.my Perpustakaan Tuanku Bainun Kampus Sultan Abdul Jalil Shah PustakaTBainun ptbupsi

05-4506832 pustaka.upsi.edu.my Perpustakaan Tuanku Bainun Kampus Sultan Abdul Jalil Shah PustakaTBainun ptbupsi

05-4506832 pustaka.upsi.edu.my Perpustakaan Tuanku Bainun Kampus Sultan Abdul Jalil Shah PustakaTBainun ptbupsi

4.2.5 High Resolution Transmission Electron Microscopy Analysis of ZBTEr (NPs)-uncoated Glass

The particle size analysis was utilized by the HR-TEM technique to determine the particles size and the growth of nano-size particles after the glass formation process, as presented in Figure 4.6. The HR-TEM image clearly shows the appearance of different sizes of Er-NPs after the glass formation with an average diameter ranging from ~25 nm and ~30 nm. The particle size was found to increase in size compared to the size of Er-NPs before the glass formation in approximately ~15 nm. Apart from that, the nanoparticles exist in three-dimensional spherical shape structures which confirmed a good distribution of erbium particle size in the tellurite glass system.

The growth of particles size in the glass materials can be correlated to the effect of high temperature during the glass melting process. Therefore, it was proposed that the melting temperature may reduce the nanoparticles agglomeration. The introduction of thermal energy to the smaller particles via the surface diffusion leads to the assembly of free energy minimization (Yao et al., 1993). Consequently, the appearance of different nanoparticles size was influenced by several factors including, high thermal energy, growth mechanism, and nucleation (Liu et al., 2022).

05-4506832 pustaka.upsi.edu.my Perpustakaan Tuanku Bainun Kampus Sultan Abdul Jalil Shah PustakaTBainun ptbupsi

05-4506832 pustaka.upsi.edu.my Perpustakaan Tuanku Bainun Kampus Sultan Abdul Jalil Shah PustakaTBainun ptbupsi

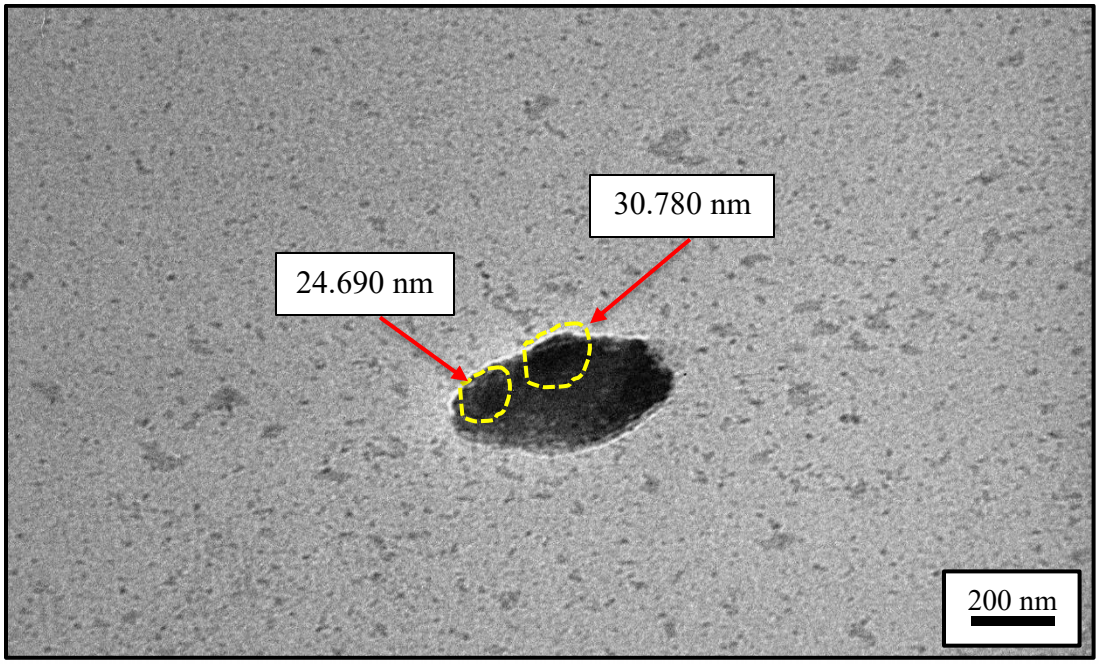


Figure 4.6. TEM images of the ZBTEr (NPs)-uncoated glass matrix displaying Er (NPs) distribution at 0.05 mol% Er_2O_3 NPs concentration with the magnification of 150 K X

05-4506832 pustaka.upsi.edu.my Perpustakaan Tuanku Bainun Kampus Sultan Abdul Jalil Shah PustakaTBainun ptbupsi

Meanwhile, the characteristics of nanoparticles image after the glass formation may be associated with the grain growth by the high temperature of the heat energy during the melt-quenched process and thereby, promoting the tendency of smaller particles to dissolve and transform into bigger particles (Greenwood, 1956). Additionally, Figure 4.7 illustrates the increasing size of nanoparticles which relates to Ostwald's ripening effect whereby, the small particles are dissolved and transformed to be larger particles during the glass formation (Yusof, Ghoshal, & Azlan, 2017).

05-4506832 pustaka.upsi.edu.my Perpustakaan Tuanku Bainun Kampus Sultan Abdul Jalil Shah PustakaTBainun ptbupsi

05-4506832 pustaka.upsi.edu.my Perpustakaan Tuanku Bainun Kampus Sultan Abdul Jalil Shah PustakaTBainun ptbupsi

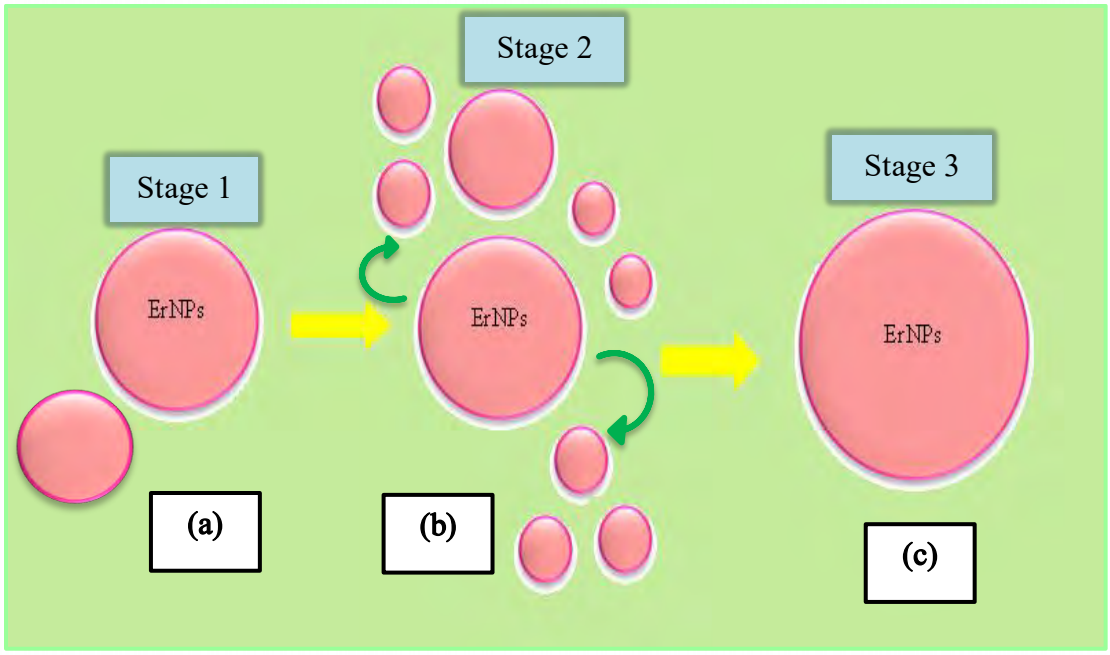


Figure 4.7. The possible mechanism of growth of nanoparticles in the ZBTEr (NPs)-uncoated glass matrix system whereby, (a) stage 1 indicates the assembly of differently sized particles, (b) stage 2 shows the particles exchange into atoms to form the bigger particles, and (c) stage 3 presents the formation of a bigger particle through Oswald's ripening effect

4.3 Structural Properties of Reduced Graphene Oxide-coated Tellurite Glass Doped with Erbium Nanoparticles (ZBTEr (NPs)-rGO)

4.3.1 Field Emission Scanning Electron Microscopy and Energy Dispersive X-ray Analyses of ZBTEr (NPs)-rGO Glass

Morphological and microstructure properties of the prepared ZBTEr (NPs)-rGO glasses were studied by scanning electron microscopy (SEM), as depicted in Figure 4.8 (a) – (d), respectively. The observations were successfully obtained for the rGO coating layers on the tellurite-based glass surfaces. It can be seen from the Figure 4.8 (a) that there are formation of wrinkles, folded regimes, and agglomerated layers surrounded by the thin

05-4506832 pustaka.upsi.edu.my Perpustakaan Tuanku Bainun Kampus Sultan Abdul Jalil Shah PustakaTBainun ptbupsi

05-4506832 pustaka.upsi.edu.my Perpustakaan Tuanku Bainun Kampus Sultan Abdul Jalil Shah PustakaTBainun ptbupsi

rGO nanosheets. Additionally, these results proved that the reduced graphene sheets are relatively large in structure despite the nanosheets, promoting the rippled and entangled existing in each rGO layer (Sharma et al., 2020). Moreover, the rGO flakes are unevenly distributed over the glass surfaces which indicates a high content of rGO accumulated in a specific region due to the uncontrolled spray coating technique and thereby, resulting in highly dense agglomerated nanostructures.

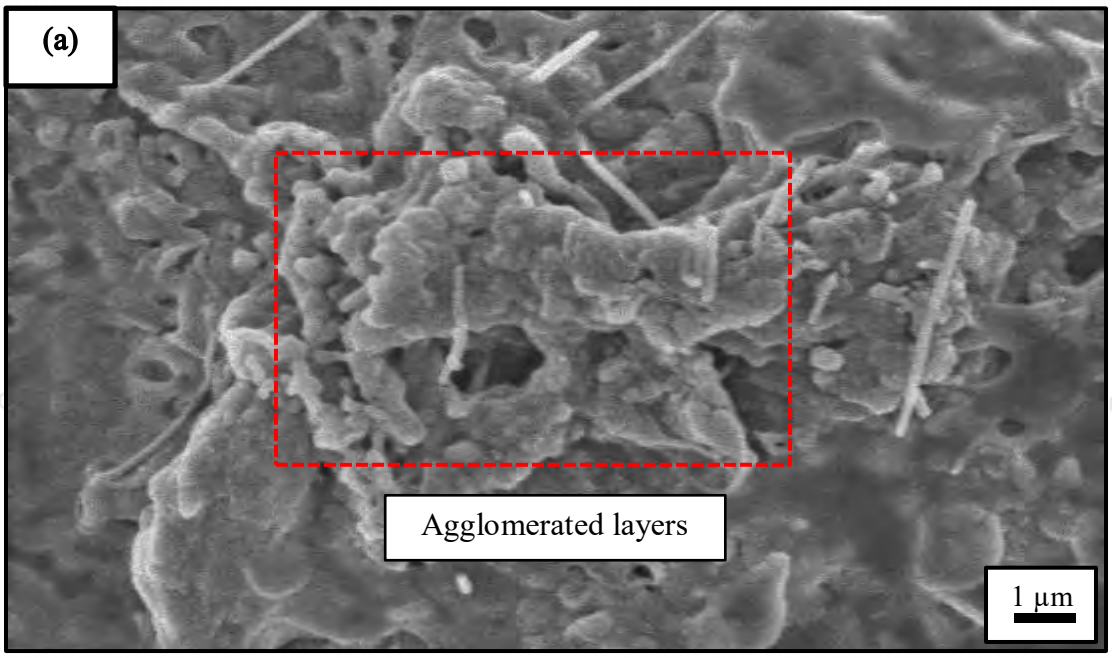
Other than that, it can be observed that the GO nanosheets are well intercalated in the electrolyte solution to form a stable dispersion in the initial oxidation process which greatly affects the high-quality rGO, as previously described in subsection 3.3. These observations could be accounted with the addition of hydrazine hydrate as a role of reducing agent which removed some amount of oxygen-containing functional groups located on the basal plane of sp^2 carbon due to the weakest van der Waal's forces and interactions with other nanosheets (Al-Gaashani et al., 2019). Consequently, the lamellas structures of rGO nanosheets are found to be highly aggregated together with the existing small crumpled features and wavy-like structures which represent the separated graphitic rGO nanosheets during the successful reduction process, as demonstrated in Figure 4.8 (c).

Meanwhile, Figures 4.8 (b) and (d) reveal the individual sheets whereby, the smooth surfaces resemble flower petals-like structures. These results clearly proved that the rGO nanosheets are grown randomly onto the tellurite-based glass surfaces which depends on the spreading rate of irregular rGO distribution via a simple spray coating technique. Additionally, Figure 4.8 (d) shows the appearance of very thin and bright layers

05-4506832 pustaka.upsi.edu.my Perpustakaan Tuanku Bainun Kampus Sultan Abdul Jalil Shah PustakaTBainun ptbupsi

05-4506832 pustaka.upsi.edu.my Perpustakaan Tuanku Bainun Kampus Sultan Abdul Jalil Shah PustakaTBainun ptbupsi

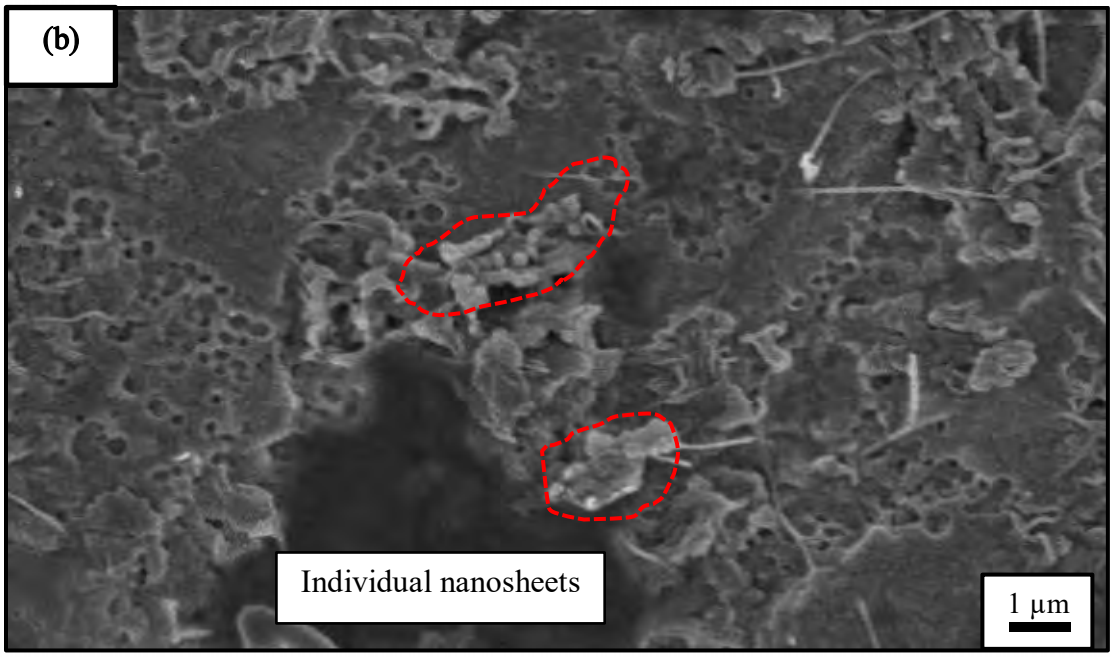
on the glass surfaces as these characteristics were believed due to the well-dispersed of rGO throughout the electrochemical reduction process and thus, rGO nanolayers were obviously seen to be visible and transparent. Therefore, the morphological analysis briefly displays that the ZBTEr (NPs)-rGO glasses are completely fulfilled with layers of rGO structures.

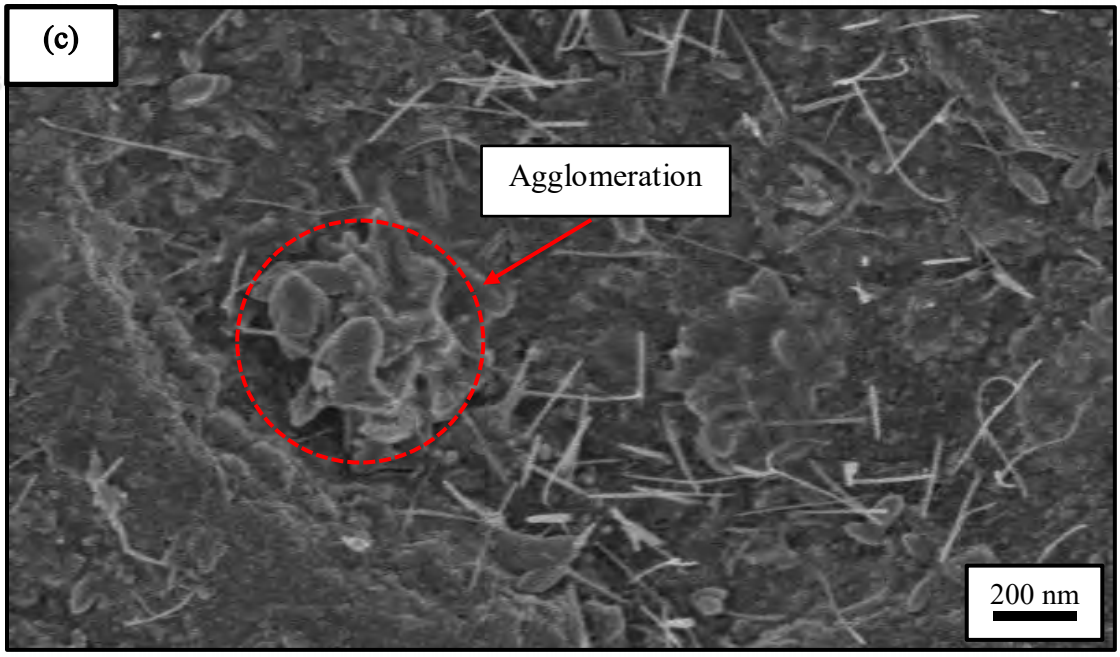


(Continue)

05-4506832 pustaka.upsi.edu.my Perpustakaan Tuanku Bainun Kampus Sultan Abdul Jalil Shah PustakaTBainun ptbupsi

05-4506832 pustaka.upsi.edu.my Perpustakaan Tuanku Bainun Kampus Sultan Abdul Jalil Shah PustakaTBainun ptbupsi





(Continue)

05-4506832 pustaka.upsi.edu.my Perpustakaan Tuanku Bainun Kampus Sultan Abdul Jalil Shah PustakaTBainun ptbupsi

05-4506832 pustaka.upsi.edu.my Perpustakaan Tuanku Bainun Kampus Sultan Abdul Jalil Shah PustakaTBainun ptbupsi

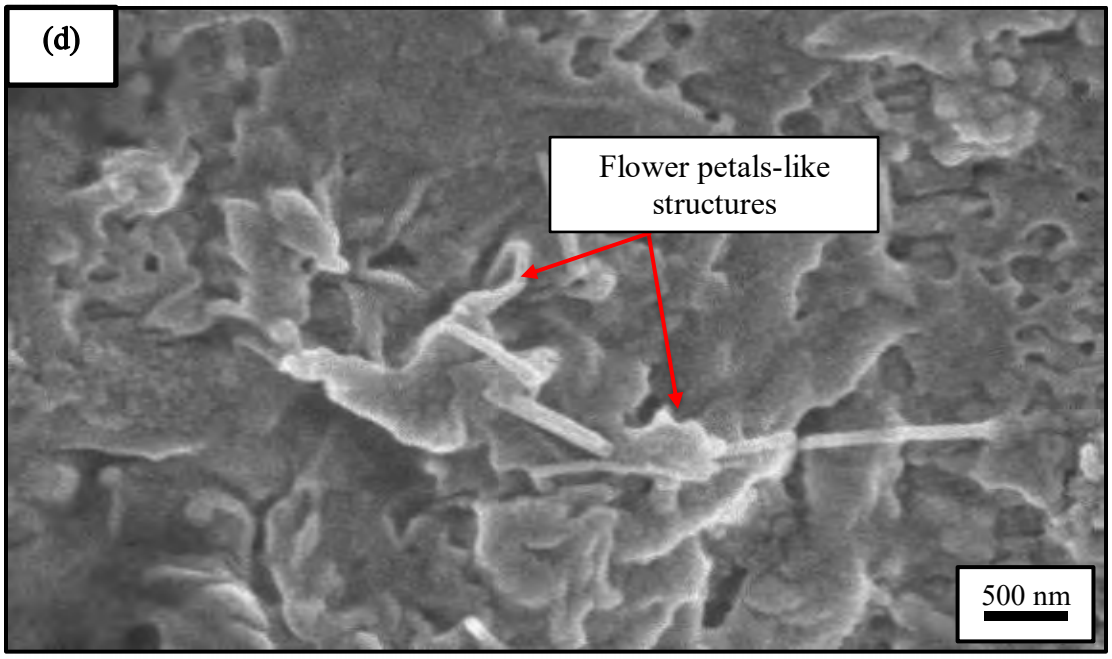


Figure 4.8. SEM micrographs of the ZBTEr (NPs)-rGO glass showing the different of rGO structures at 0.03 mol% Er_2O_3 nanoparticles concentration with the magnification of (a) 50 K X, (b) - (c) 30 K X, and (d) 70 K X

05-4506832 pustaka.upsi.edu.my Perpustakaan Tuanku Bainun Kampus Sultan Abdul Jalil Shah PustakaTBainun ptbupsi

Figure 4.9 shows the schematic illustration of the rGO coating layer attached to the ZBTEr (NPs) glass surfaces which can be associated with a high distribution of rGO that is totally covered on the glass surfaces. Furthermore, it can be clearly visualized from SEM images that the rGO nanolayers are strongly bonded on the glass surfaces, suggesting that the influence of rGO coating on the glass matrix system may correlate to the availability of oxygen-based functional groups and hence, promote a stronger interaction bonding between rGO and tellurite-based glass surfaces.

05-4506832 pustaka.upsi.edu.my Perpustakaan Tuanku Bainun Kampus Sultan Abdul Jalil Shah PustakaTBainun ptbupsi

05-4506832 pustaka.upsi.edu.my Perpustakaan Tuanku Bainun Kampus Sultan Abdul Jalil Shah PustakaTBainun ptbupsi

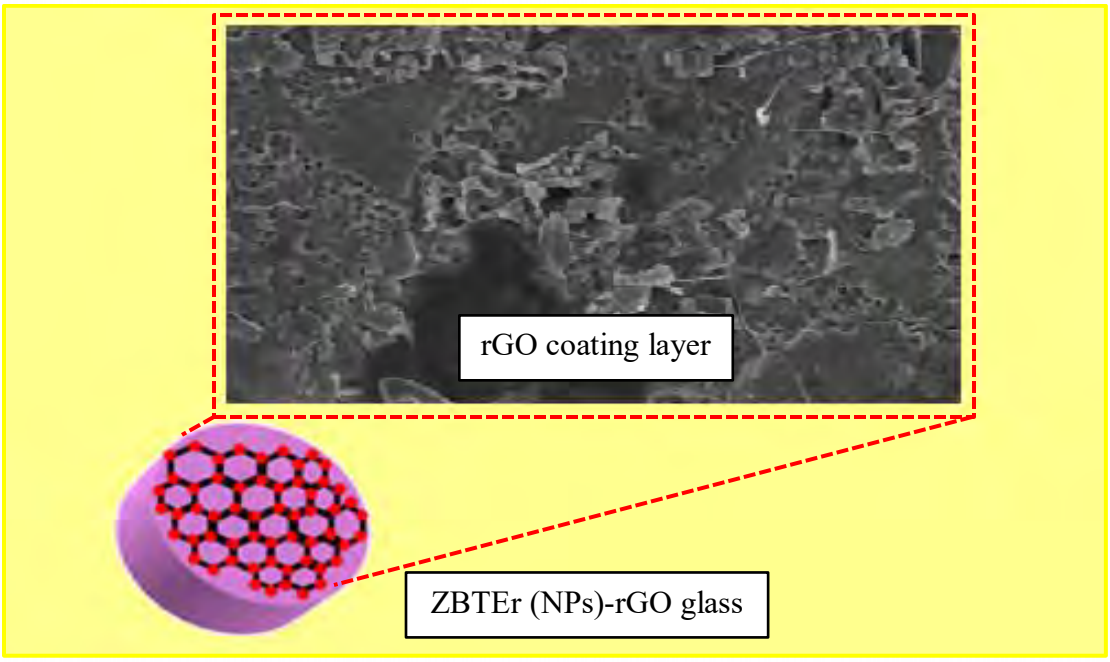


Figure 4.9. Schematic illustration of rGO layer-coated onto the ZBTEr (NPs) glass surfaces

05-4506832 pustaka.upsi.edu.my Perpustakaan Tuanku Bainun Kampus Sultan Abdul Jalil Shah PustakaTBainun ptbupsi

Regarding the morphological properties of the ZBTEr (NPs)-rGO glasses, it is important to further prove the existence of rGO layers attached to the glass surfaces and thus, these findings were supported by the EDX analysis in order to investigate the possible elemental composition of the synthesized rGO sample. Therefore, the respective weight and atomic percentages of the existing elements are summarized in Table 4.4 through the EDX scan which was carried out randomly on any region area of the rGO sample, as indicated by spectrum 1 and 2, respectively.

Figure 4.10 (a) – (b) depicts the obtained EDX spectra which clearly confirmed that the rGO sample was composed of several possible elements including, carbon (C), nitrogen (N), oxygen (O), sodium (Na), and sulphur (S) with respect of different SEM

05-4506832 pustaka.upsi.edu.my Perpustakaan Tuanku Bainun Kampus Sultan Abdul Jalil Shah PustakaTBainun ptbupsi

05-4506832 pustaka.upsi.edu.my Perpustakaan Tuanku Bainun Kampus Sultan Abdul Jalil Shah PustakaTBainun ptbupsi

microstructures. These results demonstrated that the presence amount of C element exhibited the highest weight percentage estimated at approximately ~2.530 to 5.400 wt % with 0.100 M SDS-rGO concentration of the synthesized rGO sample. Afterward, the weight percentage of the O element was achieved around ~1.190 wt % at spectrum 2 which was found higher than spectrum 1 in which the O element content was around ~0.220 wt %, respectively. Consequently, the amount of O element decreased which was due to the fact that a reduction process takes place from GO into rGO solution.

Furthermore, it can be noticed that the amount of Na element was found higher about ~0.210 wt % at spectrum 2 compared to spectrum 1 about 0.030 wt % meanwhile, the presence of S element containing the weight percentage of 0.330 wt % at spectrum 2 which found higher than the weight percentage of 0.100 wt % at spectrum 1, respectively. The presence of the N element shows the weight percentage around ~0.590 to 0.910 wt % existing in the rGO sample can be correlated to the electrochemical reduction of GO which was obtained using the reductant agent of hydrazine hydrate which acts as a key element.

Prior to the results of EDX elemental composition as presented in Figure 4.10, the observations of EDX maps for all the possible elements such as C, N, O, Na, and S were required in order to further confirm the existence of these elements that exist in the rGO solution, as depicted in Figure 4.11 (a) – (e). As a result, these findings relatively prove a good agreement with the weight percentages of element's content. Therefore, it can be concluded that the incorporation of rGO by the presence of all elements in this work.

05-4506832 pustaka.upsi.edu.my Perpustakaan Tuanku Bainun Kampus Sultan Abdul Jalil Shah PustakaTBainun ptbupsi

05-4506832 pustaka.upsi.edu.my Perpustakaan Tuanku Bainun Kampus Sultan Abdul Jalil Shah PustakaTBainun ptbupsi

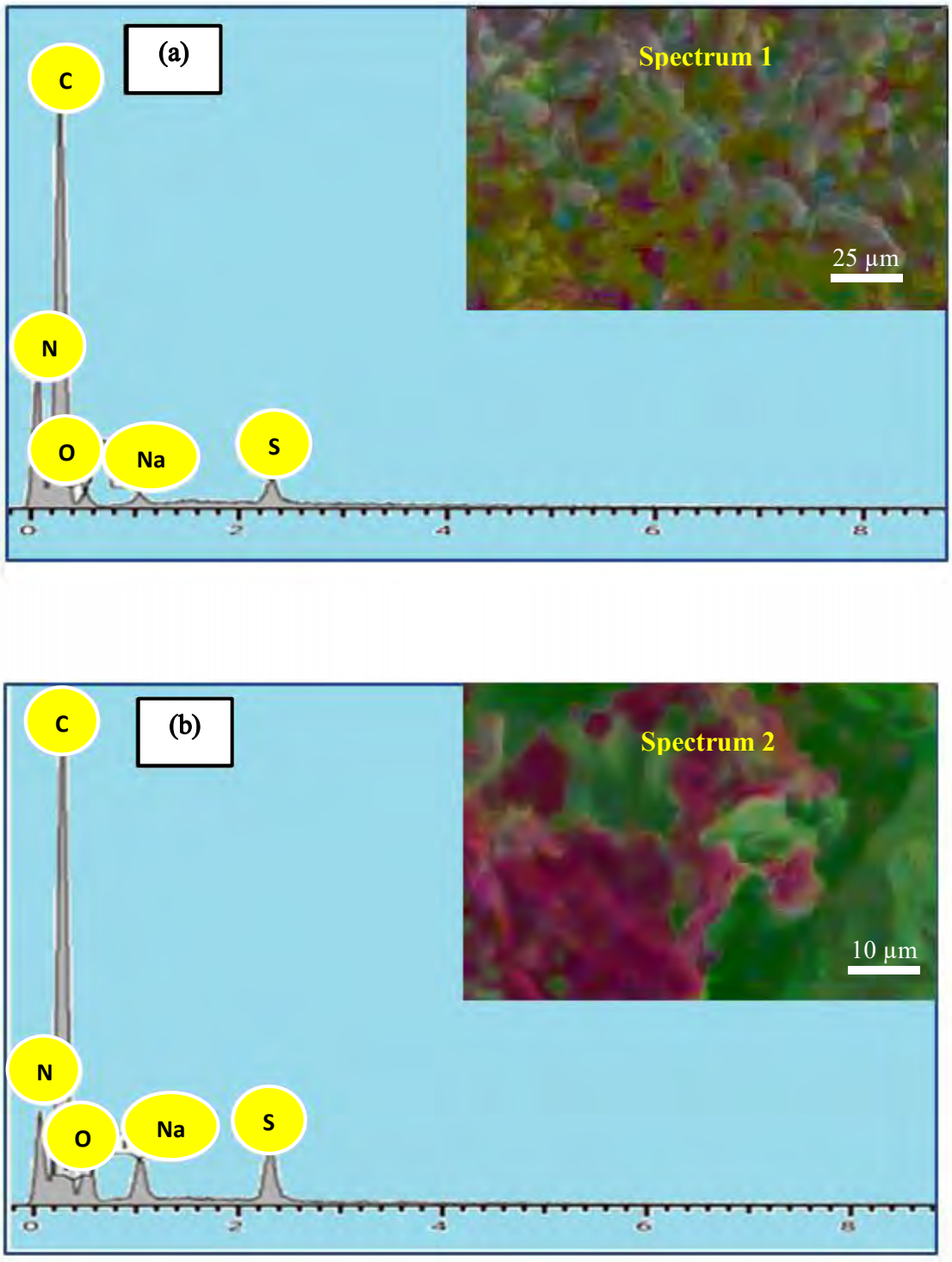
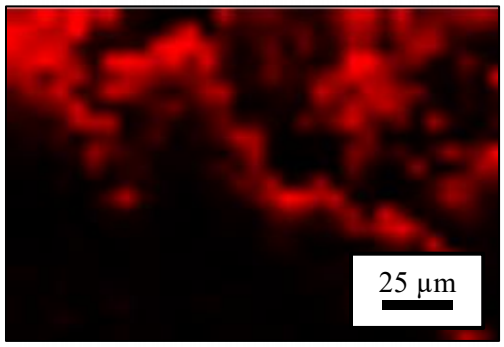


Figure 4.10. The EDX spectra with supported microstructure images of the ZBTEr (NPs)-rGO glass surfaces followed by two different regions at (a) 25 µm and (b) 10 µm

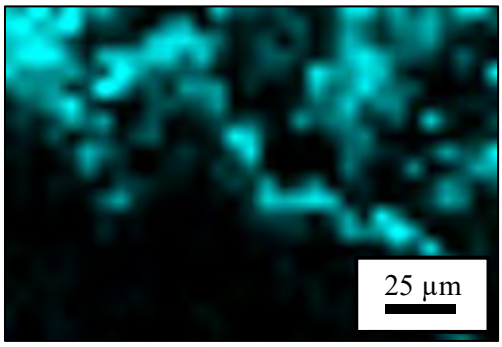
05-4506832 pustaka.upsi.edu.my Perpustakaan Tuanku Bainun Kampus Sultan Abdul Jalil Shah PustakaTBainun ptbupsi

05-4506832 pustaka.upsi.edu.my Perpustakaan Tuanku Bainun Kampus Sultan Abdul Jalil Shah PustakaTBainun ptbupsi

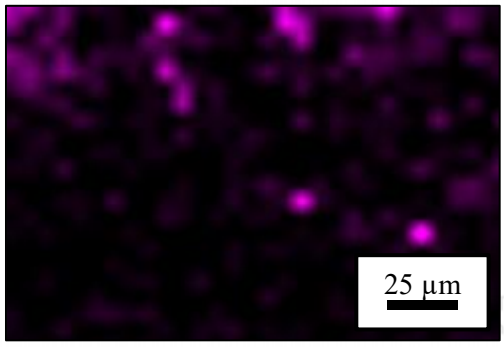
(a) C Kα1_2



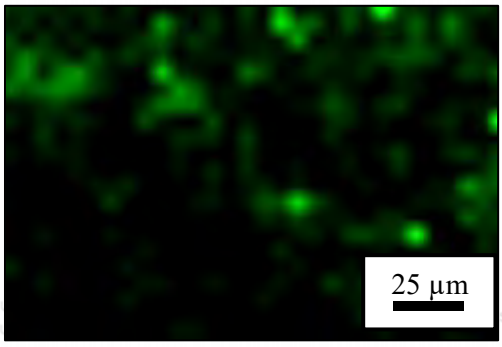
(b) N Kα1_2



(c) O Kα1_2



(d) Na Kα1_2



(e) S Kα1_2

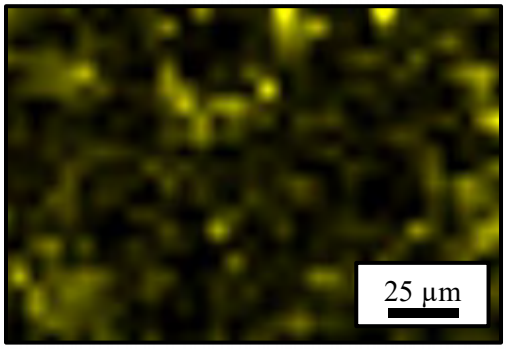


Figure 4.11. The EDX elemental mappings of (a) carbon (C), (b) nitrogen (N), (c) oxygen (O), (d) sodium (Na), and (e) sulphur (S) with the magnification of 20 K X

05-4506832 pustaka.upsi.edu.my Perpustakaan Tuanku Bainun Kampus Sultan Abdul Jalil Shah PustakaTBainun ptbupsi

05-4506832 pustaka.upsi.edu.my Perpustakaan Tuanku Bainun Kampus Sultan Abdul Jalil Shah PustakaTBainun ptbupsi

Table 4.4

The weight and atomic percentages, % of elements content with the different spectrum of rGO solution sample

Regions	Elements	Weight %	Atomic %
Spectrum 1	C K	2.530	77.770
	N K	0.590	15.430
	O K	0.220	5.160
	Na K	0.030	0.520
	S K	0.100	1.120
Spectrum 2	C K	5.400	73.960
	N K	0.910	10.640
	O K	1.190	12.230
	Na K	0.210	1.490
	S K	0.330	1.690

05-4506832 pustaka.upsi.edu.my Perpustakaan Tuanku Bainun Kampus Sultan Abdul Jalil Shah PustakaTBainun ptbupsi

05-4506832 pustaka.upsi.edu.my Perpustakaan Tuanku Bainun Kampus Sultan Abdul Jalil Shah PustakaTBainun ptbupsi

4.3.2 Micro-Raman Analysis of rGO

Further structural investigation, micro-Raman spectroscopy was employed to investigate the materials by virtue of characteristics vibrational modes and particularly, the removal of functional groups of the materials substantially change the vibration mode of the materials (Sharma et al., 2019). According to Figure 4.12 and summarized data in Table 4.5, it can be seen that the presence of two prominent characteristics peaks of GO and rGO sample, namely, the defective mode (D-peak) and graphitic mode (G-peak), which was located in the range of 1353 – 1346 cm^{-1} and 1600 – 1603 cm^{-1}, respectively. The appearance of the D-peak can be correlated to the structural defects including, band-length disorder, band-angle disorder, edge defects, and dangling bond meanwhile, the G-peak can be associated with the vibration of sp^2 carbon atoms that exist in the plane (Wang et al., 2020).

In addition to the obtained Raman spectra, it can be clearly seen that the G-peak of GO approximately ~1600 cm^{-1} and D-peak about ~1353 cm^{-1} meanwhile, the G-peak of rGO was appeared at around ~1603 cm^{-1} and D-peak around ~1346 cm^{-1}, respectively. Generally, the reduction process of GO into rGO had caused the change in shift of G-peak which was observed from 1600 cm^{-1} to 1603 cm^{-1}. This change may be correlated with the removal of functional groups of graphene hexagonal sheets from sp^3 to sp^2 hybridization. Besides that, there is a shift observed for D-peak from 1353 cm^{-1} to 1346 cm^{-1} which correlates to the attachment of functional groups that create the imperfection in the nanosheet structure. The process of removal the oxygen functional groups which alter the graphene shape from hexagonal to pentagonal nanostructures was attributed to the shift in

05-4506832 pustaka.upsi.edu.my Perpustakaan Tuanku Bainun Kampus Sultan Abdul Jalil Shah PustakaTBainun ptbupsi

05-4506832 pustaka.upsi.edu.my Perpustakaan Tuanku Bainun Kampus Sultan Abdul Jalil Shah PustakaTBainun ptbupsi

the D-peak of rGO during the reduction process and thereby, suggesting a low quantity of oxygen atoms in the rGO sample (Liu & Speranza, 2021).

Furthermore, the intensity ratio of D and G peaks (I_D/I_G) can be determined to reveal the degree of disorders and defects in the carbon-based materials (Wang et al., 2020). As can be seen from the micro-Raman spectra, it can be clearly observed that the calculated value of the I_D/I_G ratio of pristine GO is 0.87 meanwhile, the I_D/I_G ratio of rGO produced after the reduction process was found to decrease at approximately 0.82. In the case of the GO sample, the low intensity of GO production via an electrochemical exfoliation technique indicates the low amount of GO which resulted from the high agglomerated layers diffused during the intercalation process. Additionally, the increment in the I_D/I_G ratio of GO was attributed to the GO-functionalization assisted with the sodium dodecyl sulphate (SDS) surfactant which in turn restores the sp^3 domain of GO nanostructures during the oxidation process (Nurhafizah et al., 2020). Consequently, these results confirmed that the GO production is well-stabilized assisted by a commercially SDS surfactant during the electrochemical exfoliation process and thus, leads to the higher content of functionalized groups that existed in GO nanosheets.

Meanwhile, the decrement in the I_D/I_G ratio of rGO ascribes to the lower number of defects in the rGO nanostructures through the breaking up of GO nanostructures that distorted the sp^2 graphitic domains during the chemical reduction process. Additionally, it was believed that the addition of hydrazine hydrate into the GO solution may remove several oxygen-containing functional groups that existed in GO structures when the

05-4506832 pustaka.upsi.edu.my Perpustakaan Tuanku Bainun Kampus Sultan Abdul Jalil Shah PustakaTBainun ptbupsi

05-4506832 pustaka.upsi.edu.my Perpustakaan Tuanku Bainun Kampus Sultan Abdul Jalil Shah PustakaTBainun ptbupsi

reduction process takes place. Furthermore, it can be observed that the rGO exhibits is relatively lower intensity of D-peak, as compared to GO which implies more disordered carbon nanostructures. Due to these, the obtained intensity is attributed to the formation of decreased size of in-plane sp^2 domains which acts as the disordered carbon during the GO reduction process (Fang et al., 2019).

Moreover, the graphitic changes in rGO nanostructures cause more agglomeration and aggregation formation, which is confirmed by SEM analysis, as has been stated in subsection 4.3.1. Other than that, the low number of defects in the rGO sample assisted with the high stabilization role of the reducing agent may be correlated to the distance between two neighbour defects of graphitic nanostructures. As a result, several ionic bonds are broken due to the removal of oxygen-containing functional groups during the reduction approach which in turn introduces structural defects (Wang et al., 2020).

Usually, the I_D/I_G ratio was observed to be less than 1 for GO and rGO which relates to the formation of partially ordered structures in the GO reduction. These findings were in good agreement with the previous studies (Ikram et al., 2020; Mandal et al., 2019; Sharma et al., 2020) whereby, the I_D/I_G ratio of rGO is found to decrease compared to the I_D/I_G ratio of GO and thereby, indicating to the introduction of lesser defects on the rGO surfaces.

05-4506832 pustaka.upsi.edu.my Perpustakaan Tuanku Bainun Kampus Sultan Abdul Jalil Shah PustakaTBainun ptbupsi

05-4506832 pustaka.upsi.edu.my Perpustakaan Tuanku Bainun Kampus Sultan Abdul Jalil Shah PustakaTBainun ptbupsi

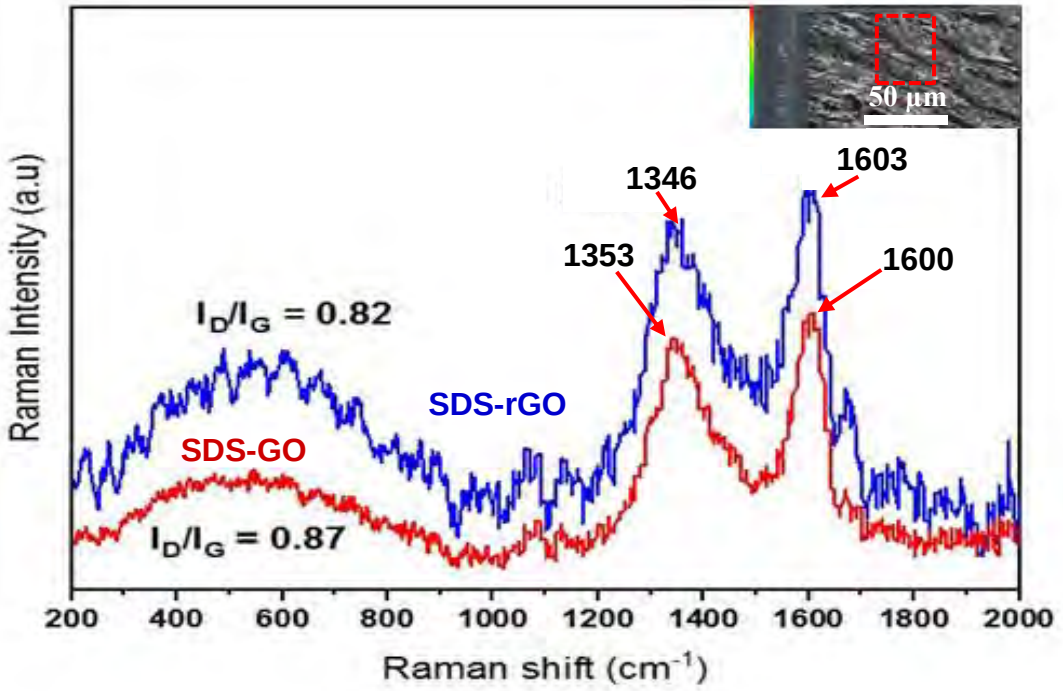


Figure 4.12. Micro-Raman spectra of GO and rGO with supported microstructure image of the ZBTEr (NPs)-rGO glass surfaces at 50 µm

Table 4.5

Micro-Raman peaks position and I_D/I_G ratio of GO and rGO solution samples

Samples	D-peak (cm^{-1})	G-peak (cm^{-1})	I_D/I_G ratio
GO	1353	1600	0.87
rGO	1346	1603	0.82

05-4506832 pustaka.upsi.edu.my Perpustakaan Tuanku Bainun Kampus Sultan Abdul Jalil Shah PustakaTBainun ptbupsi

05-4506832 pustaka.upsi.edu.my Perpustakaan Tuanku Bainun Kampus Sultan Abdul Jalil Shah PustakaTBainun ptbupsi

4.4 Optical Properties of Reduced Graphene Oxide-coated Tellurite Glass Doped with Erbium Nanoparticles (ZBTEr (NPs)-rGO)

4.4.1 Optical Absorption Spectra

UV-Vis spectroscopy was conducted to investigate the characteristics of glasses by identifying the optical properties of the ZBTEr (NPs)-rGO glasses system. The optical absorption occurred in glass materials which are categorized into two-processes known as emission and absorption that are taking place in an atom (Morigaki & Ogihara, 2006; Zimmermann, 2010). The emission process indicates the photons which have been released as the atom move to a lower energy level and the atom emits the light after being heated or excited at the high state level. Meanwhile, the absorption occurs when the electron absorbs the photon energy that may cause the electrons to gain their energy and thus, those electrons may be able to jump into a higher state of energy level.

Figures 4.13 and 4.14 depict the typical optical absorption spectra of ZBTEr (NPs)-rGO and ZBTEr (NPs)-uncoated glasses obtained in the range of 400 – 1200 nm at different concentrations of Er^{3+} nanoparticles with the existed absorption bands in various wavelengths. Generally, it can be clearly observed from both figures that the peaks are recognized to the existence of 4*f*–4*f* transition in the ground state level, $^4G_{11/2}$ respected to the characteristics of Er^{3+} ions to the range of various excited states level ($^2H_{9/2}$, $^4F_{5/2}$, $^4F_{7/2}$, $^2H_{11/2}$, $^4S_{3/2}$, $^4F_{9/2}$, $^4I_{11/2}$, and $^4I_{9/2}$) which correspond to the absorption positions of 487, 522, 550, 652, and 980 nm, respectively. The strong edge localization in graphene nanostructures could be attributed to the strong electron-phonon coupling which ascribes

05-4506832 pustaka.upsi.edu.my Perpustakaan Tuanku Bainun Kampus Sultan Abdul Jalil Shah PustakaTBainun ptbupsi

05-4506832 pustaka.upsi.edu.my Perpustakaan Tuanku Bainun Kampus Sultan Abdul Jalil Shah PustakaTBainun ptbupsi

to the level of oxygen reduction in the rGO nanosheets (Lundie et al., 2015). Other than that, it can be noticed that both absorption spectra have the similar characteristics in which the optical absorption edges are not clearly clarified from these absorption bands which was subjected to the existence of the structural disorder and amorphous in nature of glasses. These results were proved by the XRD pattern in subsection 4.2.3.

The shift in the optical absorption peaks of ZBTEr (NPs)-rGO glasses system occurs due to the decreasing amount of oxygen functional groups which weakens the interlayer coupling between the rGO nanolayers and thus, causes the electrons to easily excite at the lower energy (Muruganandi et al., 2018). The deoxygenation upon the GO reduction is caused via the decrement of disorder-induced states within π-π* gaps. Consequently, these results could be attributed to the improvement of optical absorption spectra in the ZBTEr (NPs)-rGO glasses system and hence, leading to the strong bonding between the rGO coating layer and tellurite glass surfaces.

As can be referred from Figures 4.13 and 4.14, the absorption bands of the ZBTEr (NPs)-rGO glasses are more intense than ZBTEr (NPs)-uncoated glasses. The red shift of the absorption band can be clearly seen in the ZBTEr (NPs)-rGO glasses compared to the ZBTEr (NPs)-uncoated glasses. These trends can be correlated to the existence of sp^2 carbon content and the reduction of oxygen groups, which agrees well with the micro-Raman analysis (refer to subsection 4.3.2). In addition, the absorbance peak of the ZBTEr (NPs)-rGO glass was found to be lower compared to the ZBTEr (NPs)-uncoated glass which corresponds to the higher absorption peaks due to the existing π-π* transition of

05-4506832 pustaka.upsi.edu.my Perpustakaan Tuanku Bainun Kampus Sultan Abdul Jalil Shah PustakaTBainun ptbupsi

05-4506832 pustaka.upsi.edu.my Perpustakaan Tuanku Bainun Kampus Sultan Abdul Jalil Shah PustakaTBainun ptbupsi

aromatic C=C bond (Abid et al., 2018; Khan et al., 2016). Furthermore, the improvement in the optical absorption was correlated to the functionalization of rGO whereby, the atoms considerably show the tendency to absorb the photon energy under the UV light absorption. In particular, the photon energy can be considered to successfully attribute to enhance the optical properties of the glass materials. In fact, it can be noted that the rGO coating on the ZBTEr (NPs) glass surfaces causes the alteration of electronic states which was due to the restoration of electronic conjugation within the rGO nanosheets during the reduction process.

The improvement in optical absorption reduces the optical absorbance of the ZBTEr (NPs)-rGO glasses which was due to the synergic effects of rGO nanostructures through the formation of sp^2 clusters carbon domains resulting from the removal of oxygen contents in rGO and due to the exciton peak, n-π^* transition of C=O bond, and π-π^* transition of C-C bond that exists in the rGO graphitic material (Jia et al., 2018; Labhane et al., 2016). Specifically, the increased amount of sp^2 hybridized carbon atoms remarkably promotes the tuning of optoelectronics properties of the glass material such as optical bandgap energy (Sreeja & Anila, 2019), which will be discussed in the subsection 4.4.2.

In summary, it can be summarized that the optical absorption band was increased for the ZBTEr (NPs)-rGO glasses which clearly revealed the strong interaction between the rGO coating layer and tellurite-based glass surfaces. The influence of rGO coating on the ZBTEr (NPs) glasses system demonstrates the increased optical properties which beneficial for photonic applications such as optical switching devices.

05-4506832 pustaka.upsi.edu.my Perpustakaan Tuanku Bainun Kampus Sultan Abdul Jalil Shah PustakaTBainun ptbupsi

05-4506832 pustaka.upsi.edu.my Perpustakaan Tuanku Bainun Kampus Sultan Abdul Jalil Shah PustakaTBainun ptbupsi

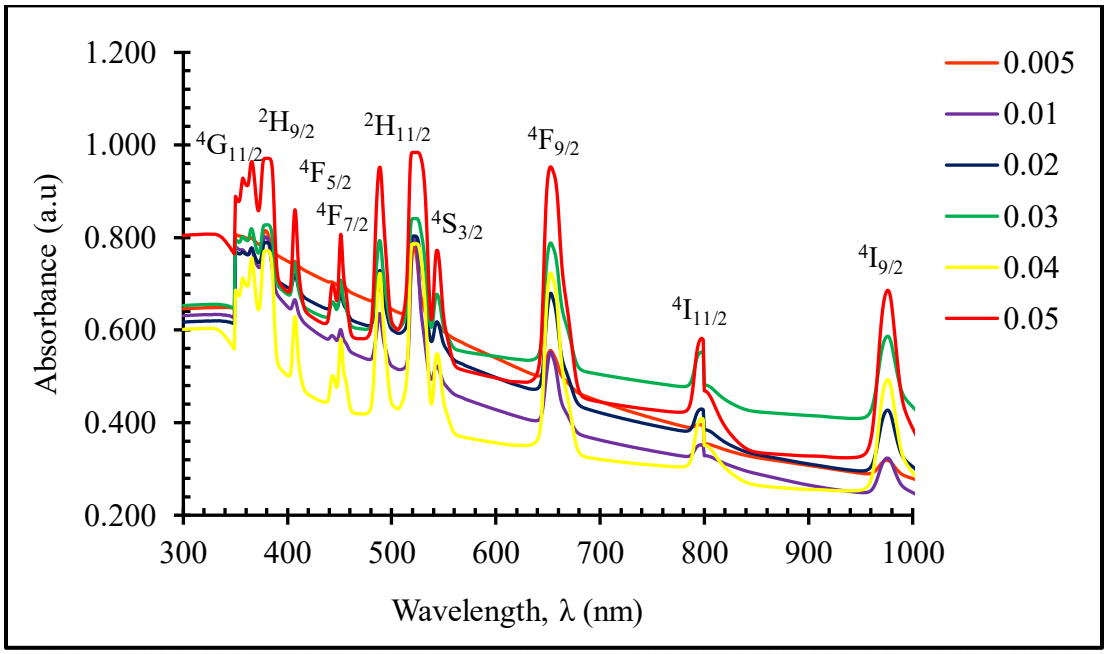


Figure 4.13. Optical absorption spectra of ZBTEr (NPs)-rGO glasses

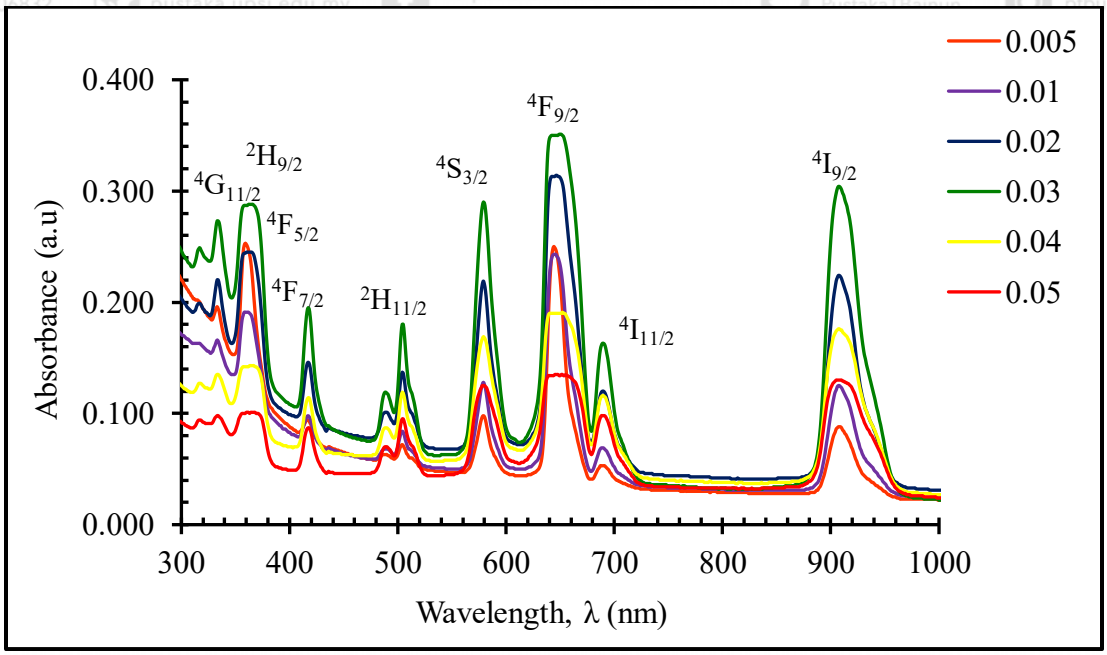


Figure 4.14. Optical absorption spectra of ZBTEr (NPs)-uncoated glasses (Azlan, Halimah, Shafinas, et al., 2015)

05-4506832 pustaka.upsi.edu.my Perpustakaan Tuanku Bainun Kampus Sultan Abdul Jalil Shah PustakaTBainun ptbupsi

05-4506832 pustaka.upsi.edu.my Perpustakaan Tuanku Bainun Kampus Sultan Abdul Jalil Shah PustakaTBainun ptbupsi

4.4.2 Optical Bandgap Energy

Further optical properties of the ZBTEr (NPs)-rGO glasses were investigated to identify the optical bandgap energy based on the Tauc's plot, known as a plotted graph of photon energy, $\hbar\omega$ against optical bandgap energy, $\alpha\hbar\omega$, as shown in Figure 4.15. The optical bandgap energy of the ZBTEr (NPs)-rGO glasses can be estimated from the absorbance spectra, which firstly extrapolates the linear portion of the curves to the intercept of $\hbar\omega$ located on the *x*-axis and gives the value of optical bandgap energy, E_{opt} by using the given Equations 2.10 and 2.11, as has been stated in subsection 2.13.2.

According to Figure 4.16 and summarized data in Table 4.6, it can be clearly observed that the calculated optical bandgap energy value of ZBTEr (NPs)-rGO glasses was found to decrease in the range of 1.913 – 2.980 eV compared to the ZBTEr (NPs)-uncoated glasses. Consequently, it was noticed that the deposition of rGO nanostructures onto the glass surfaces alters the bandgap energy of ZBTEr (NPs)-rGO glasses which due to the photon absorption transitions in C=O (n-π) and C=C (π-π^*) states that exists in the rGO graphitic materials, respectively (Sreeja et al., 2017). These results can be ascribed to a shift of absorption band which relatively demonstrated the influence of the rGO coating layer on the tellurite glass surfaces, as proved in the previous subsection 4.4.1.

05-4506832 pustaka.upsi.edu.my Perpustakaan Tuanku Bainun Kampus Sultan Abdul Jalil Shah PustakaTBainun ptbupsi

05-4506832 pustaka.upsi.edu.my Perpustakaan Tuanku Bainun Kampus Sultan Abdul Jalil Shah PustakaTBainun ptbupsi

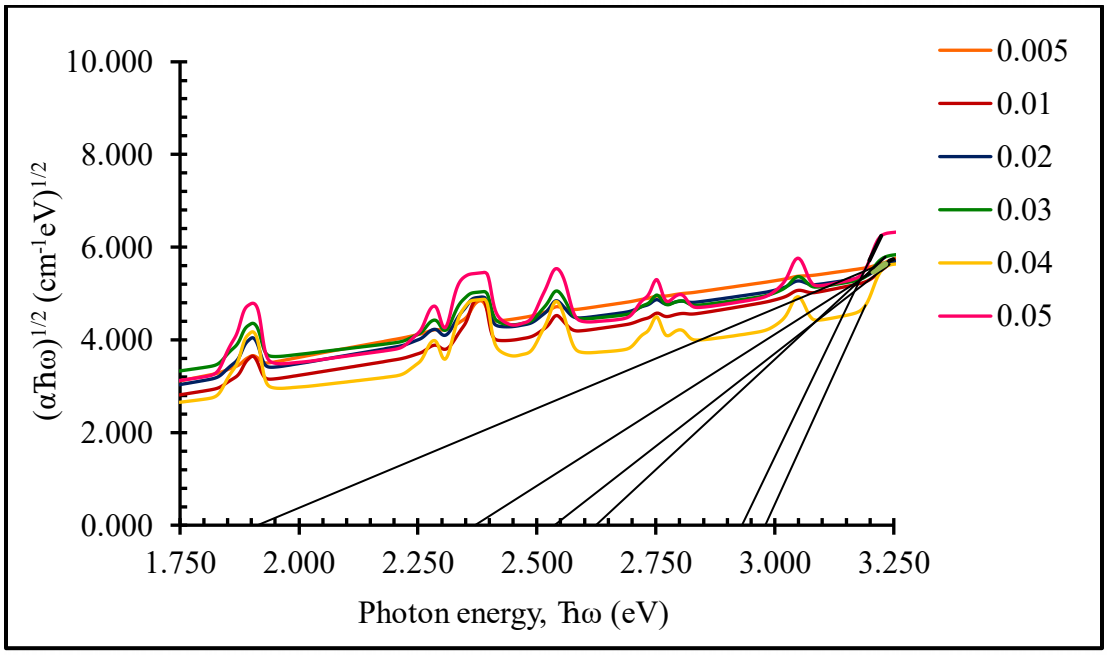


Figure 4.15. Tauc's plot of $(\alpha\hbar\omega)^{1/2}$ against photon energy, $\hbar\omega$ of ZBTEr (NPs)-rGO glasses

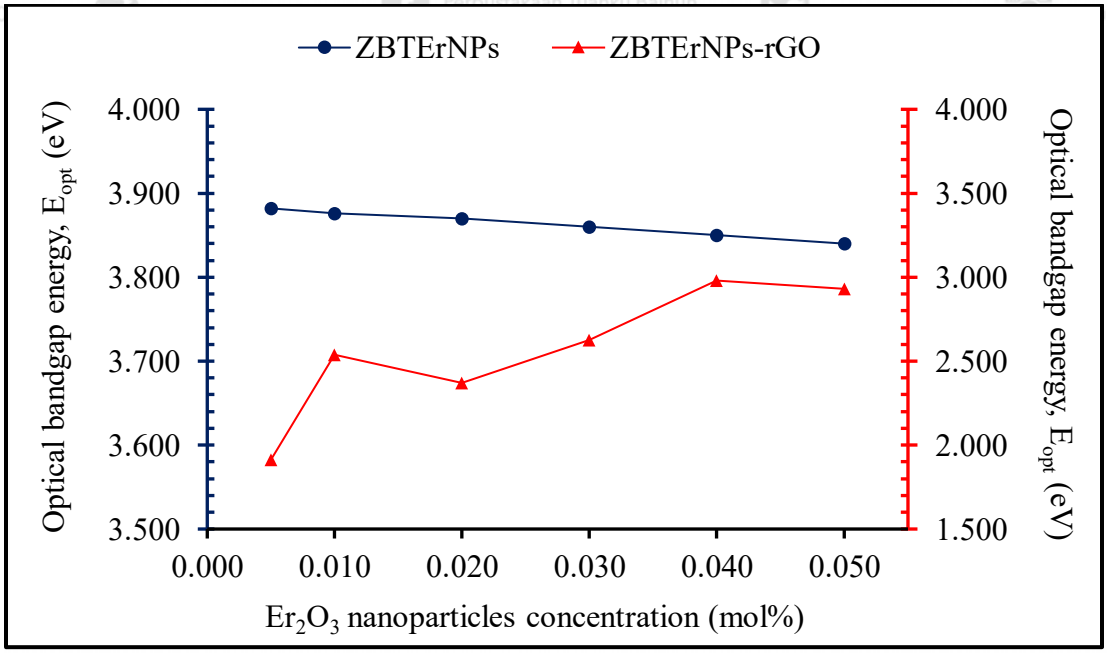


Figure 4.16. Variation of optical bandgap energy as a function of Er_2O_3 nanoparticles concentration for ZBTEr (NPs)-uncoated and ZBTEr (NPs)-rGO glasses

05-4506832 pustaka.upsi.edu.my Perpustakaan Tuanku Bainun Kampus Sultan Abdul Jalil Shah PustakaTBainun ptbupsi

05-4506832 pustaka.upsi.edu.my Perpustakaan Tuanku Bainun Kampus Sultan Abdul Jalil Shah PustakaTBainun ptbupsi

Table 4.6

Comparison of optical bandgap energy (E_{opt}) value between ZBTEr (NPs)-uncoated and ZBTEr (NPs)-rGO glasses

Er_2O_3 nanoparticles concentration (mol%)	Optical bandgap energy, $\boldsymbol{E_{opt}}$ (eV) (±0.100)
ZBTEr (NPs)-uncoated	
0.005	3.882
0.010	3.876
0.020	3.870
0.030	3.860
0.040	3.850
0.050	3.840
ZBTEr (NPs)-rGO	
0.005	1.913
0.010	2.537
0.020	2.370
0.030	2.624
0.040	2.980
0.050	2.931

05-4506832 pustaka.upsi.edu.my Perpustakaan Tuanku Bainun Kampus Sultan Abdul Jalil Shah PustakaTBainun ptbupsi

05-4506832 pustaka.upsi.edu.my Perpustakaan Tuanku Bainun Kampus Sultan Abdul Jalil Shah PustakaTBainun ptbupsi

Generally, the optical bandgap energy of the ZBTEr (NPs)-rGO glasses was lower than the ZBTEr (NPs)-uncoated glasses, indicating the introduction of a high amount of sp^2 hybridized carbon atoms in the rGO nanostructures resulting from reduction process (Aradhana et al., 2018). As the incorporation of rGO onto the tellurite-based glass surfaces, the optical absorption spectra are shifted which indicates the strong bonding interaction between the rGO coating layer and glass material and thereby, may attribute to the decreasing trend in optical bandgap energy value of ZBTEr (NPs)-rGO glasses, as comparable to the ZBTEr (NPs)-uncoated glasses.

Additionally, it can be noticed that the deposition of rGO on the ZBTEr (NPs) glass surfaces exhibited a strong interaction for the improvement of optoelectronics and photonics applications since it has a tunable bandgap which in turn decreases the optical properties. As a result, the improved value of optical bandgap energy of the glass system can be undoubtedly assigned to the π-π^* allowed transitions between the valence and conduction bands with the assisted of functionalized rGO and thus, resulting in the wide bandgap energy semiconductor glass material (Arranz-Mascarós et al., 2020; Sreeja & Anila, 2019). The primary mechanism of the excitation principle takes place in the presence of photons with the bandgap energy as well as, electrons generated in the valence band, as shown in Figure 4.17.

05-4506832 pustaka.upsi.edu.my Perpustakaan Tuanku Bainun Kampus Sultan Abdul Jalil Shah PustakaTBainun ptbupsi

05-4506832 pustaka.upsi.edu.my Perpustakaan Tuanku Bainun Kampus Sultan Abdul Jalil Shah PustakaTBainun ptbupsi

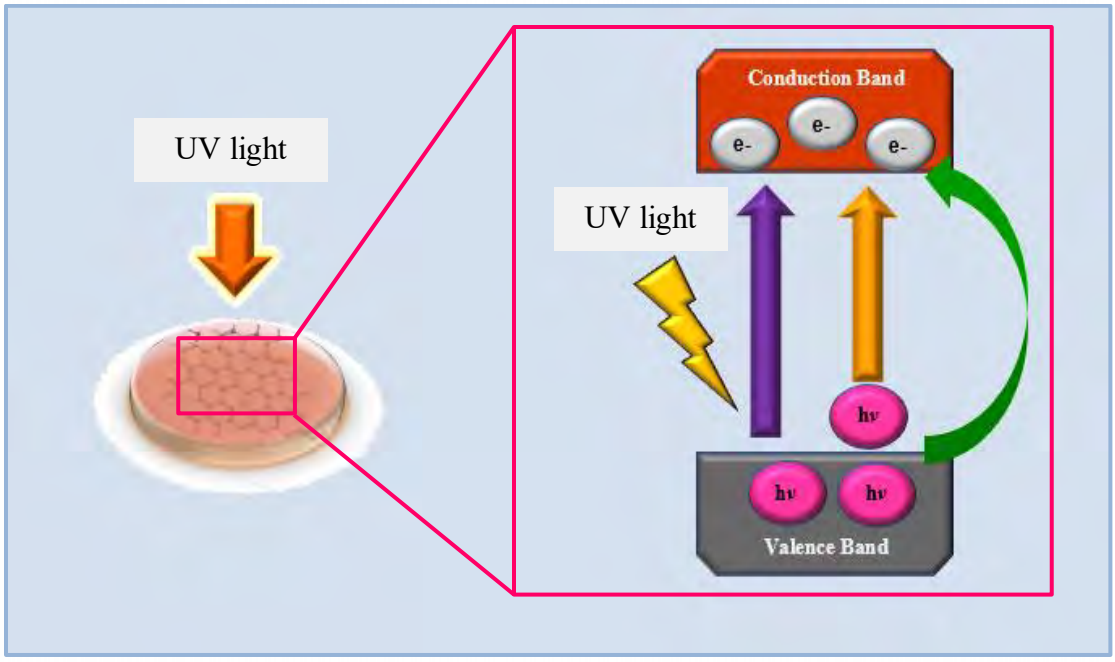


Figure 4.17. The possible mechanism of photon excitation on the ZBTEr (NPs)-rGO glass system with the presence of UV light leading to the excitation of electrons from valence band (VB) to conduction band (CB)

05-4506832 pustaka.upsi.edu.my Perpustakaan Tuanku Bainun Kampus Sultan Abdul Jalil Shah PustakaTBainun ptbupsi

Apart from that, the functionalization of rGO surfaces has great potential for improving the bandgap energy structures of the ZBTEr (NPs) glass system. Particularly, the combination between the rGO and tellurite-based glass led to achieve the desirable properties especially, for semiconductor devices. Therefore, it was believed that the effects of oxygen-containing functional groups including, hydroxyl, epoxide, carbonyl, and carboxyl that are attached to the precise location of rGO surfaces extremely may involve in tuning the bandgap energy of the glass material. Remarkably, it can be noticed that the epoxide functional groups are highly effective in tuning the bandgap energy of the glass material, as comparable to the hydroxyl groups whereby, these groups are only stable as an isolated hydroxyl which then preferable to convert into an epoxide group, as previously

05-4506832 pustaka.upsi.edu.my Perpustakaan Tuanku Bainun Kampus Sultan Abdul Jalil Shah PustakaTBainun ptbupsi

05-4506832 pustaka.upsi.edu.my Perpustakaan Tuanku Bainun Kampus Sultan Abdul Jalil Shah PustakaTBainun ptbupsi

reported by Jin et al., (2020). In contrast, the carbonyl and carboxyl groups were not significantly attributed to the bandgap opening due to these groups generate more surface defects which in turn make them less effective in adjusting the bandgap energy. Unlike hydroxyl groups, the carbonyl and carboxyl structures are predicted to be metastable and stabilized however, their effects on the bandgap energy are relatively minimal. Consequently, more breaking of aromatic hexagonal carbon-ring structures is required for the formation of the carboxyl and carbonyl groups which may produce more holes in the rGO layers and thus, resulting in the wide bandgap opening of materials.

Furthermore, graphene-based materials like rGO have received considerable attention primarily for potential optical limiting applications due to the behavior of rGO structures by manipulating the sp^2 and sp^3 carbon fractions via a controlled removal of oxygen groups during GO reduction, which has been proved by micro-Raman spectra in subsection 4.3.2. Due to these, it can be concluded that the π-conjugation was restored with a new formation of sp^2-bonded aromatic regions which indicates that an electronically insulating GO was successfully converted to be a semiconducting material and thus, transforms into a graphene-like semi-metal which is called the rGO (Aradhana et al., 2018). Importantly, the potential of rGO is proving itself to be a highly versatile material as the rGO has a strong influence when combined with the ZBTEr (NPs) glass system. Therefore, it can be remarked that the rGO has a significant impact in order to improve the optical bandgap energy of the glass material by deposition of rGO onto the tellurite-based glass surfaces.

05-4506832 pustaka.upsi.edu.my Perpustakaan Tuanku Bainun Kampus Sultan Abdul Jalil Shah PustakaTBainun ptbupsi

05-4506832 pustaka.upsi.edu.my Perpustakaan Tuanku Bainun Kampus Sultan Abdul Jalil Shah PustakaTBainun ptbupsi

By knowing the rGO properties, it can be noticed that the rGO should be predominantly attributed to a wide range of semiconductor applications that enhanced the optical-related properties as well as, can be used for photonic material including, fiber optics technology. Nevertheless, the photonic bandgap fiber optics are often exhibiting a difficulty to produce due to a relatively high energy loss which substantially limits the uses of fiber optics. Therefore, it is worth noting that the effects of rGO on the tellurite-based glass surfaces have a possibility to achieve an excellent improvement in the bandgap energy of the ZBTEr (NPs)-rGO glasses system.

Typically, it can be concluded that the ZBTEr (NPs)-rGO glass with 0.04 mol% of Er_2O_3 nanoparticles concentration sample possesses a larger bandgap energy value of 2.980 eV than the other rGO-coated glass samples, which in turn allows in reducing the high loss of energy. Besides the optical bandgap energy, the considerable properties of the refractive index particularly have a correlation with its bandgap energy that strongly influences the optical properties of glass material, that will be discussed in next subsection 4.4.4. As a result, this present work particularly anticipated for fabrication of efficient fiber optics as the ZBTEr (NPs)-rGO glasses improved their optical performance.

05-4506832 pustaka.upsi.edu.my Perpustakaan Tuanku Bainun Kampus Sultan Abdul Jalil Shah PustakaTBainun ptbupsi

05-4506832 pustaka.upsi.edu.my Perpustakaan Tuanku Bainun Kampus Sultan Abdul Jalil Shah PustakaTBainun ptbupsi

4.4.3 Urbach Energy

The Urbach energy was analyzed as a parameter that relates to the degree of structural disorder in an amorphous material from the conversion of weak bonds into defects. The Urbach energy values can be determined by taking the reciprocals of the slopes of the linear portion based on the plotted graph between log (α) and photon energy, ħω curves (refer to Figure 4.18) by using the given Equation 2.12, as has been stated in subsection 2.13.3.

Figure 4.19 shows the variation of Urbach energy values of ZBTEr (NPs)-rGO glasses which exhibited in the range of 0.118 – 0.408 eV in which the trend of Urbach energy was found to increase from 0.005 to 0.02 mol% compared to the ZBTEr (NPs)-uncoated glasses. Therefore, these results were considered due to the higher number of defects in the ZBTEr (NPs)-rGO glasses matrix which attributes to an increased content of non-bridging oxygens (NBOs) (Amjad et al., 2013).

Meanwhile, the Urbach energy values of the ZBTEr (NPs)-rGO glasses were seen to gradually decrease with the increasing Er_2O_3 nanoparticles concentration specifically, at 0.04 – 0.05 mol% which indicates the decrease in broadening of static disorder-related parts (El-diasty et al., 2006). Additionally, the trend of Urbach energy was correlated with the low level of oxygen atoms and formation of agglomerated nanostructures attached to the glass surfaces, as has been mentioned in Figures 4.8 (a) and (c), respectively and thereby, resulting in the lower defects content compared to the ZBTEr (NPs)-uncoated

05-4506832 pustaka.upsi.edu.my Perpustakaan Tuanku Bainun Kampus Sultan Abdul Jalil Shah PustakaTBainun ptbupsi

05-4506832 pustaka.upsi.edu.my Perpustakaan Tuanku Bainun Kampus Sultan Abdul Jalil Shah PustakaTBainun ptbupsi

glasses. The comparison of Urbach energy value between the ZBTEr (NPs)-rGO and ZBTEr (NPs)-uncoated glasses is summarized in Table 4.7.

Furthermore, it can be noticed that the Urbach energy value of the ZBTEr (NP)-rGO glasses was ascribed to the higher tendency of the glass material for the conversion of the weak bonds into structural defects, which is similar to the ZBTEr (NPs)-uncoated glasses. Interestingly, the Urbach energy was associated with the phonon-assisted indirect electronic transition whereby, these phonons assist the existing electrons located in the indirect transition to move into the conduction band (CB) (Jlassi et al., 2011).

Moreover, the improved value of Urbach energy was suggested to be caused by several factors, including the strong bonding of rGO bonding interactions between the rGO coating layer and tellurite-based glass surfaces as well as, inhomogeneity of rGO structures on the glass surfaces. As a result, it can be summarized that the improvement of Urbach energy was considered responsible for better bonding interaction between the rGO coating layer and tellurite-based glass surfaces. Therefore, these findings are confirmed via the morphological analysis, as has been stated in subsection 4.3.1.

05-4506832 pustaka.upsi.edu.my Perpustakaan Tuanku Bainun Kampus Sultan Abdul Jalil Shah PustakaTBainun ptbupsi

05-4506832 pustaka.upsi.edu.my Perpustakaan Tuanku Bainun Kampus Sultan Abdul Jalil Shah PustakaTBainun ptbupsi

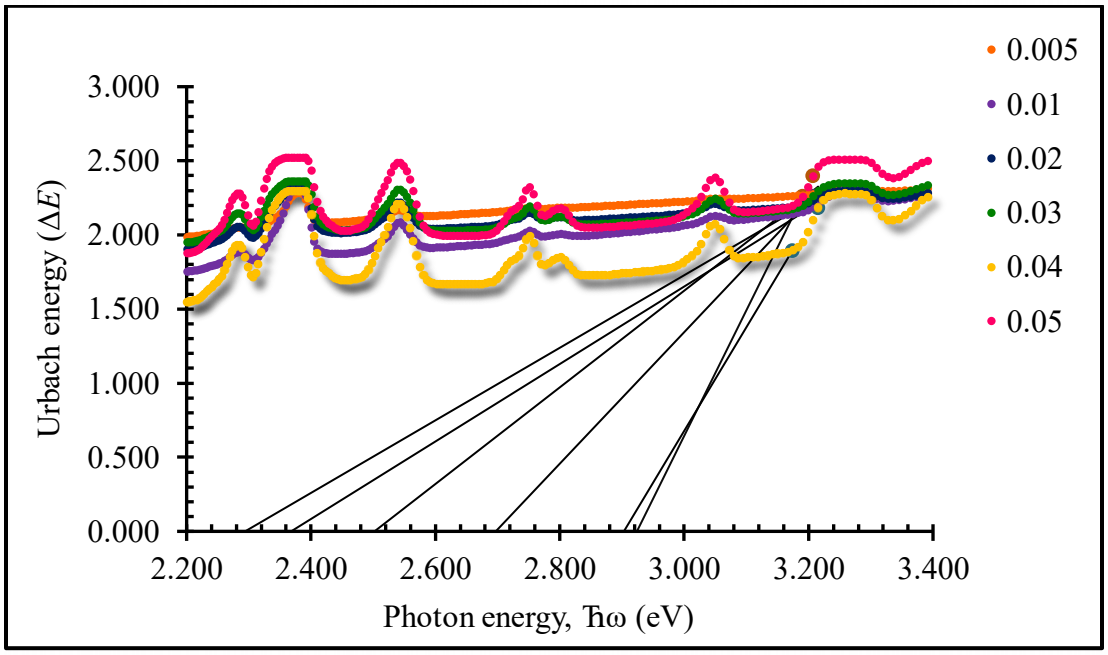


Figure 4.18. Plotted graph of log (α) against photon energy, ħω of ZBTEr (NPs)-rGO glasses

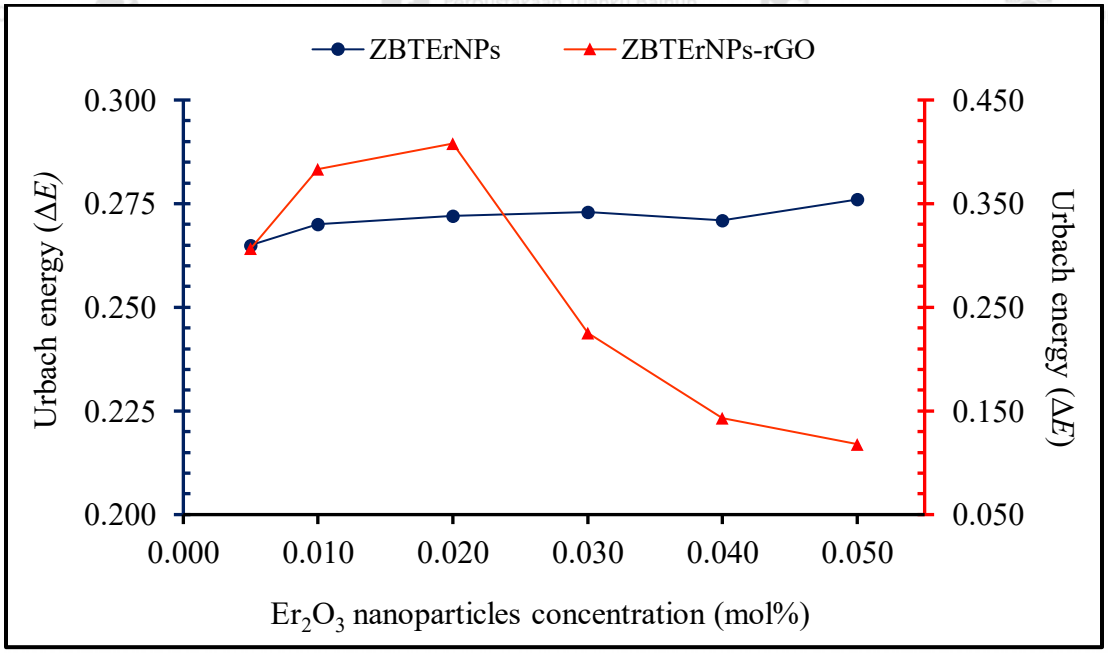


Figure 4.19. Variation of Urbach energy as a function of Er_2O_3 nanoparticles concentration for ZBTEr (NPs)-uncoated and ZBTEr (NPs)-rGO glasses

05-4506832 pustaka.upsi.edu.my Perpustakaan Tuanku Bainun Kampus Sultan Abdul Jalil Shah PustakaTBainun ptbupsi

05-4506832 pustaka.upsi.edu.my Perpustakaan Tuanku Bainun Kampus Sultan Abdul Jalil Shah PustakaTBainun ptbupsi

Table 4.7

Comparison of Urbach energy (ΔE) value between ZBTEr (NPs)-uncoated and ZBTEr (NPs)-rGO glasses

Er_2O_3 nanoparticles concentration (mol%)	Urbach energy, ΔE (eV) (±0.100)
ZBTEr (NPs)-uncoated	
0.005	0.265
0.010	0.270
0.020	0.272
0.030	0.273
0.040	0.271
0.050	0.276
ZBTEr (NPs)-rGO	
0.005	0.307
0.010	0.383
0.020	0.408
0.030	0.225
0.040	0.143
0.050	0.118

05-4506832 pustaka.upsi.edu.my Perpustakaan Tuanku Bainun Kampus Sultan Abdul Jalil Shah PustakaTBainun ptbupsi

05-4506832 pustaka.upsi.edu.my Perpustakaan Tuanku Bainun Kampus Sultan Abdul Jalil Shah PustakaTBainun ptbupsi

4.4.4 Refractive Index

The refractive index is a vital measurement that may affect the candela distribution of the transmitted light and easy to change the intensity of light by improving the refractive index value of the material. Additionally, the refractive index value was influenced by the interaction of light with the electrons of constituent atoms of the glass materials (Halimah et al., 2017) which can be calculated by using the given Equation 2.13, as has been stated in subsection 2.13.4.

Figure 4.20 shows a plotted graph of the refractive index of the ZBTEr (NPs)-rGO and ZBTEr (NPs)-uncoated glasses along with the Er_2O_3 nanoparticles concentration. It can be clearly observed that the refractive index, *n* values of the ZBTEr (NPs)-rGO glasses exhibit an increasing pattern ranging from 2.402 – 2.775, which was found higher than ZBTEr (NPs)-uncoated glasses. As a result, this trend can be ascribed to the presence of the rGO layers on the tellurite-based glass surfaces which can be understood in terms of the rearrangement of oxygen and carbon atoms on the rGO surfaces as well as, the effects of decreasing of reduction numbers (Antidormi et al., 2020; Minitha et al., 2018). As a consequence, the restoration of new structures and properties in the rGO material was obviously caused by the GO reduction process and thus, promoting the less oxygen-containing functional groups that existed in the rGO surfaces. Hence, these functional groups attribute to the outstanding properties of rGO, which in turn affects the increasing value of the refractive index in the glass materials.

05-4506832 pustaka.upsi.edu.my Perpustakaan Tuanku Bainun Kampus Sultan Abdul Jalil Shah PustakaTBainun ptbupsi

05-4506832 pustaka.upsi.edu.my Perpustakaan Tuanku Bainun Kampus Sultan Abdul Jalil Shah PustakaTBainun ptbupsi

As can be referred in Table 4.8, it can be noted that the rGO coating layers may increase the refractive index value of the ZBTEr (NPs) glass system which was associated with the higher number of defects that occurred in the rGO layers. Additionally, these results corresponded to the high amount of sp^2 carbon atoms and population redistribution of delocalized π-electrons resulting from the removal of the oxygen functional groups in rGO nanosheets which has been proved by Raman spectra (refer to Figure 4.12) and thus, attribute to the main component of optical non-linearity in the glassy amorphous system (Omidvar et al., 2018). Notably, the improved value of the refractive index of the ZBTEr (NPs)-rGO glasses was mainly due to the free carriers belonging to the sp^2 domain clusters which are considered responsible for the increase in the optical non-linearity materials (Jiménez-pérez et al., 2018).

05-4506832 pustaka.upsi.edu.my Perpustakaan Tuanku Bainun Kampus Sultan Abdul Jalil Shah PustakaTBainun ptbupsi

Additionally, the enhanced values of the refractive index for ZBTEr (NPs)-rGO glasses confirm the formation of localized energy levels between the conduction and valence bands which may create the free barriers belonging to the sp^2 electron domain that exists in rGO nanostructures (Jiménez-pérez et al., 2018). These results were relatively correlated with the optical bandgap energy value, which has been stated in subsection 4.4.2.

On top of that, the improvement of the refractive index indicates that the rGO layers attribute in increment the optical properties of glass materials which are useful for fiber optics technology. In fact, it is crucial that a higher refractive index is beneficial for manufacturing the fiber core in the optical fiber, and thus, it should be acknowledged that the addition of rGO as the coating material offers a reasonable performance to be used in

05-4506832 pustaka.upsi.edu.my Perpustakaan Tuanku Bainun Kampus Sultan Abdul Jalil Shah PustakaTBainun ptbupsi

05-4506832 pustaka.upsi.edu.my Perpustakaan Tuanku Bainun Kampus Sultan Abdul Jalil Shah PustakaTBainun ptbupsi

the fiber core. In the present work, it can be noticed that the ZBTEr (NPs)-rGO glass sample with 0.005 mol% Er_2O_3 nanoparticles concentration possesses a value of 2.775 which clearly shows the highest refractive index value and thereby, shows great potential for high-performance fiber optics applications. By taking the improvement effects between the rGO coating layer and tellurite glass surfaces, it is evidence that the ZBTEr (NPs)-rGO glasses with tunable bandgap energy and refractive index may be highly utilized in the optimization of fiber optics.

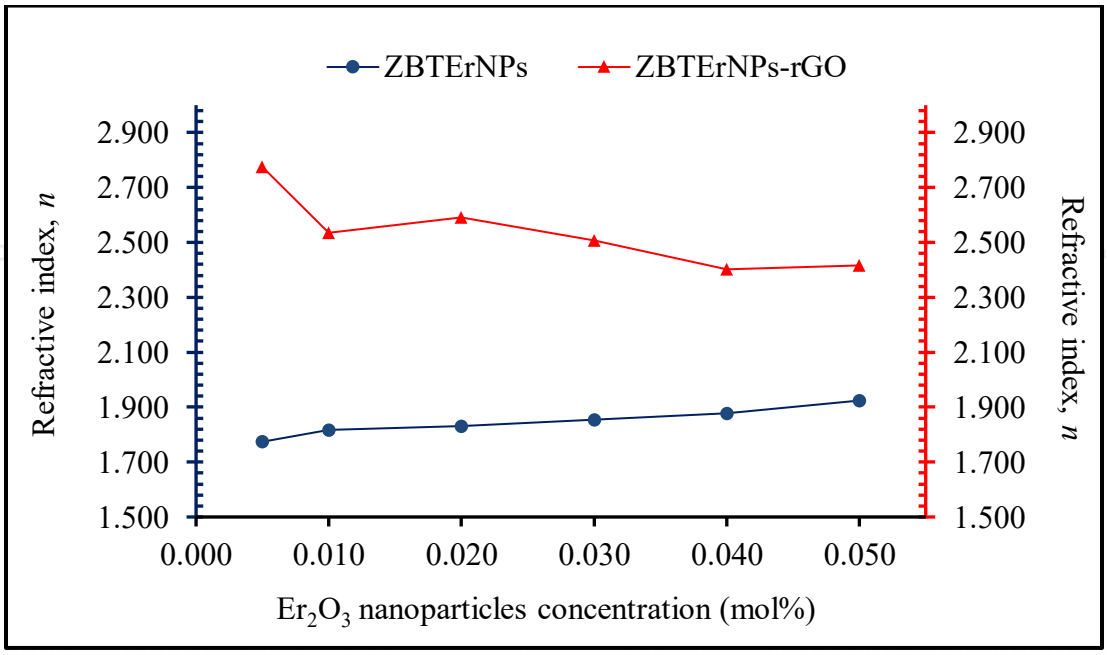


Figure 4.20. Variation of refractive index as a function of Er_2O_3 nanoparticles concentration for ZBTEr (NPs)-uncoated and ZBTEr (NPs)-rGO glasses

05-4506832 pustaka.upsi.edu.my Perpustakaan Tuanku Bainun Kampus Sultan Abdul Jalil Shah PustakaTBainun ptbupsi

05-4506832 pustaka.upsi.edu.my Perpustakaan Tuanku Bainun Kampus Sultan Abdul Jalil Shah PustakaTBainun ptbupsi

Table 4.8

Comparison of refractive index (n) values between ZBTEr (NPs)-uncoated and ZBTEr (NPs)-rGO glasses

Er_2O_3 nanoparticles concentration (mol%)	Refractive index (*n*) (±0.100)
ZBTEr (NPs)-uncoated	
0.005	1.774
0.010	1.818
0.020	1.830
0.030	1.855
0.040	1.878
0.050	1.924
ZBTEr (NPs)-rGO	
0.005	2.775
0.010	2.534
0.020	2.591
0.030	2.506
0.040	2.402
0.050	2.416

05-4506832 pustaka.upsi.edu.my Perpustakaan Tuanku Bainun Kampus Sultan Abdul Jalil Shah PustakaTBainun ptbupsi

05-4506832 pustaka.upsi.edu.my Perpustakaan Tuanku Bainun Kampus Sultan Abdul Jalil Shah PustakaTBainun ptbupsi

4.4.5 Reflection Loss, Transmission Coefficient, and Dielectric Constant

For further studies of the optical properties of the ZBTEr (NPs)-rGO glassy matrix, some related optical parameters such as; reflection loss (R_L), transmission coefficient (T), and dielectric constant (ϵ) were calculated by using the given Equations 2.14, 2.15, and 2.16, respectively, as has been stated in subsection 2.13.5. Additionally, these optical parameters can be deduced from the refractive index value in which these parameters are significant in the fiber optics field.

Figure 4.21 shows the plotted graph of reflection loss, transmission coefficient, and dielectric constant of the ZBTEr (NPs)-rGO glasses along with the concentration of Er_2O_3 nanoparticles. It can be noticed that these optical parameter values were exhibited in a non-linear trend in which the reflection loss, transmission coefficient, and dielectric constant value lies in the range of (0.169 – 0.221), (0.638 – 0.709), and (5.769 – 7.701), respectively, as summarized in Table 4.9.

The observed variation of both reflection loss and dielectric constant along with the concentration of Er_2O_3 nanoparticles exhibited a decreasing trend which was caused by the changes in optical absorption of the ZBTEr (NPs)-rGO glasses. Additionally, the decreasing value of the dielectric constant may be correlated to an increasing value of the transmission coefficient.

05-4506832 pustaka.upsi.edu.my Perpustakaan Tuanku Bainun Kampus Sultan Abdul Jalil Shah PustakaTBainun ptbupsi

05-4506832 pustaka.upsi.edu.my Perpustakaan Tuanku Bainun Kampus Sultan Abdul Jalil Shah PustakaTBainun ptbupsi

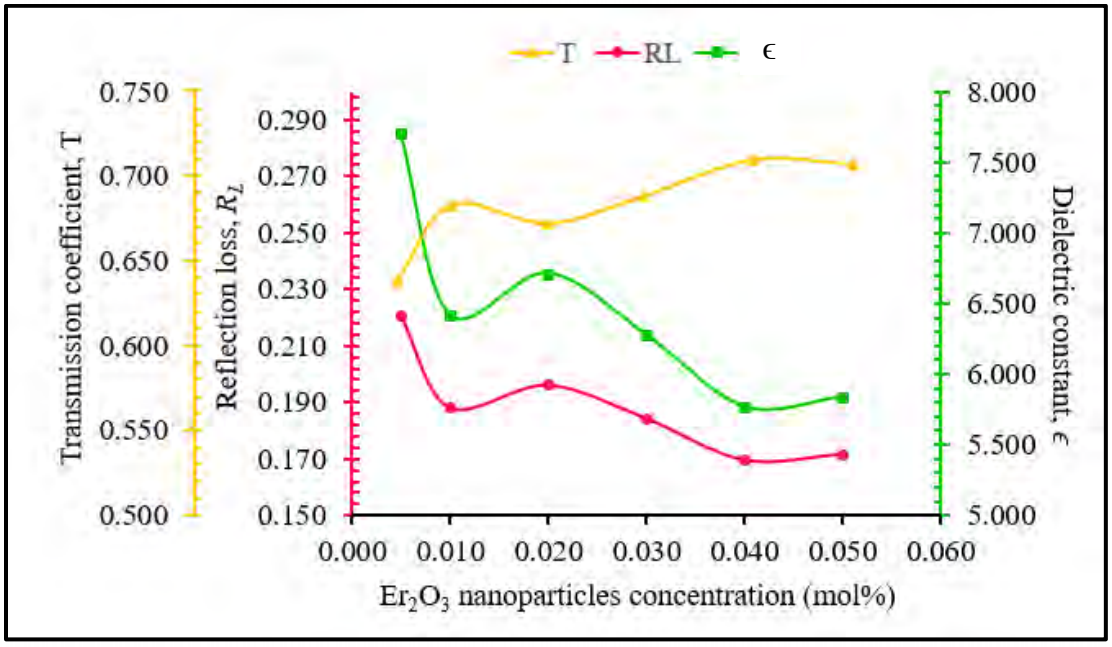


Figure 4.21. Variation of reflection loss, transmission coefficient, and dielectric constant as a function of Er_2O_3 nanoparticles concentration for ZBTEr (NPs)-rGO glasses

05-4506832 pustaka.upsi.edu.my Perpustakaan Tuanku Bainun Kampus Sultan Abdul Jalil Shah PustakaTBainun ptbupsi

Table 4.9

Variation of reflection loss (R_L), transmission coefficient (T), and dielectric constant (ϵ) for ZBTEr (NPs)-rGO glasses

Er_2O_3 nanoparticles concentration (mol%)	R_L (±0.004)	T (±0.005)	ϵ (±0.129)
0.005	0.221	0.638	7.701
0.010	0.188	0.683	6.421
0.020	0.196	0.672	6.713
0.030	0.185	0.688	6.280
0.040	0.169	0.709	5.769
0.050	0.172	0.707	5.837

05-4506832 pustaka.upsi.edu.my Perpustakaan Tuanku Bainun Kampus Sultan Abdul Jalil Shah PustakaTBainun ptbupsi

05-4506832 pustaka.upsi.edu.my Perpustakaan Tuanku Bainun Kampus Sultan Abdul Jalil Shah PustakaTBainun ptbupsi

4.4.6 Electronegativity

Further studies of optical properties involve electronegativity which is defined as a vital concept that relates the chemical bonding and implies valuable applications in estimating the properties of materials and innovating new materials (Zhao et al., 2008).

The Pauling electronegativity, average electronegativity, and average electronegativity-based oxide ion polarizability of the TeO_2, B_2O_3, ZnO, and Er_2O_3 oxides which constitute the ZBTEr (NPs)-rGO glass system were calculated by using the Equations 2.17, 2.18, 2.19, and 2.20, respectively which has been stated in subsection 2.13.6 and summarized in Table 4.10. Therefore, these results simultaneously verify a good agreement with the previously reported studies (Al-Harbi et al., 2021).

05-4506832 pustaka.upsi.edu.my Perpustakaan Tuanku Bainun Kampus Sultan Abdul Jalil Shah PustakaTBainun ptbupsi

Table 4.10

Pauling electronegativity (χ_i), average electronegativity (χ_{av}), and average electronegativity-based oxide ion polarizability $\alpha_0^{2-}(\chi_{nav})$*, n = 1, 2, 3 of the ZBTEr (NPs)-rGO glasses*

Oxides	$\boldsymbol{\chi_i}$	$\boldsymbol{\chi_{av}}$	$\boldsymbol{\alpha_0^{2-}(\chi_{1av})}$	$\boldsymbol{\alpha_0^{2-}(\chi_{2av})}$	$\boldsymbol{\alpha_0^{2-}(\chi_{3av})}$
TeO_2	Te = 2.100	2.993	2.358	2.295	1.377
B_2O_3	B = 2.040	2.880	2.444	2.334	1.417
ZnO	Zn = 1.650	2.545	2.698	2.448	1.604
Er_2O_3	Er = 1.240	2.536	2.705	2.451	1.611
	O = 3.440				

05-4506832 pustaka.upsi.edu.my Perpustakaan Tuanku Bainun Kampus Sultan Abdul Jalil Shah PustakaTBainun ptbupsi

05-4506832 pustaka.upsi.edu.my Perpustakaan Tuanku Bainun Kampus Sultan Abdul Jalil Shah PustakaTBainun ptbupsi

A similar approach was applied to ZBTEr (NPs)-rGO glass system in which the average electronegativity-based oxide ion polarizability, α_0^{2-} (χ_{av}) values were presented along with the increase of Er^{3+} nanoparticles concentration, as shown in Table 4.11. It can be clearly observed that the average electronegativity-based oxide ion polarizability values exhibited the increasing trend along with the increase of Er_2O_3 nanoparticles concentration meanwhile, the obtained values of refractive index-based oxide ion polarizability in the range of 3.254 – 3.669 which was ascribed from the higher refractive index values, as stated in previously Table 4.8. The increment of refractive index values may be correlated to the role of the residual amount of oxygenated functional groups that exist in the rGO nanosheet layers and thereby, may shift the refractive index-based oxide ion polarizability values in the glassy matrix.

05-4506832 pustaka.upsi.edu.my Perpustakaan Tuanku Bainun Kampus Sultan Abdul Jalil Shah PustakaTBainun ptbupsi
05-4506832 pustaka.upsi.edu.my Perpustakaan Tuanku Bainun Kampus Sultan Abdul Jalil Shah PustakaTBainun ptbupsi

05-4506832 pustaka.upsi.edu.my Perpustakaan Tuanku Bainun Kampus Sultan Abdul Jalil Shah PustakaTBainun ptbupsi

Table 4.11

Average electronegativity (χ_{av}), average electronegativity-based oxide ion polarizability, α_0^{2-} (χ_{nav}), n = 1, 2, 3, and refractive index-based oxide ion polarizability, $\alpha_0^{2-}(n)$ of ZBTEr (NPs)-rGO glasses

Er_2O_3 nanoparticles concentration (mol%)	$\boldsymbol{\chi_{av}}$	$\boldsymbol{\alpha_0^{2-}(\chi_{1av})}$	$\boldsymbol{\alpha_0^{2-}(\chi_{2av})}$	$\boldsymbol{\alpha_0^{2-}(\chi_{3av})}$	$\boldsymbol{\alpha_0^{2-}(n)}$
0.005	2.834	2.479	2.349	1.435	3.669
0.010	2.832	2.480	2.349	1.436	3.419
0.020	2.829	2.483	2.350	1.437	3.447
0.030	2.826	2.485	2.352	1.439	3.361
0.040	2.823	2.487	2.353	1.439	3.254
0.050	2.820	2.489	2.354	1.441	3.314

05-4506832 pustaka.upsi.edu.my Perpustakaan Tuanku Bainun Kampus Sultan Abdul Jalil Shah PustakaTBainun ptbupsi

05-4506832 pustaka.upsi.edu.my Perpustakaan Tuanku Bainun Kampus Sultan Abdul Jalil Shah PustakaTBainun ptbupsi

Figure 4.22 shows a least-square plot graph that presents the correlation between the average electronegativity-based oxide ion polarizability, α_0^{2-} (χ_{1av}) and refractive index-based oxide ion polarizability, $\alpha_0^{2-}(n)$ in the ZBTEr (NPs)-rGO glass system. Herein, the plotted graph from the average electronegativity values was not demonstrated reliable results. Due to these findings, the correlation between these two variables was improved as the optical electronegativity is introduced, as summarized in Table 4.12. The obtained results are more reliable as compared to the average electronegativity values. Hence, these findings may be considered satisfactory for ZBTEr (NPs)-rGO glasses.

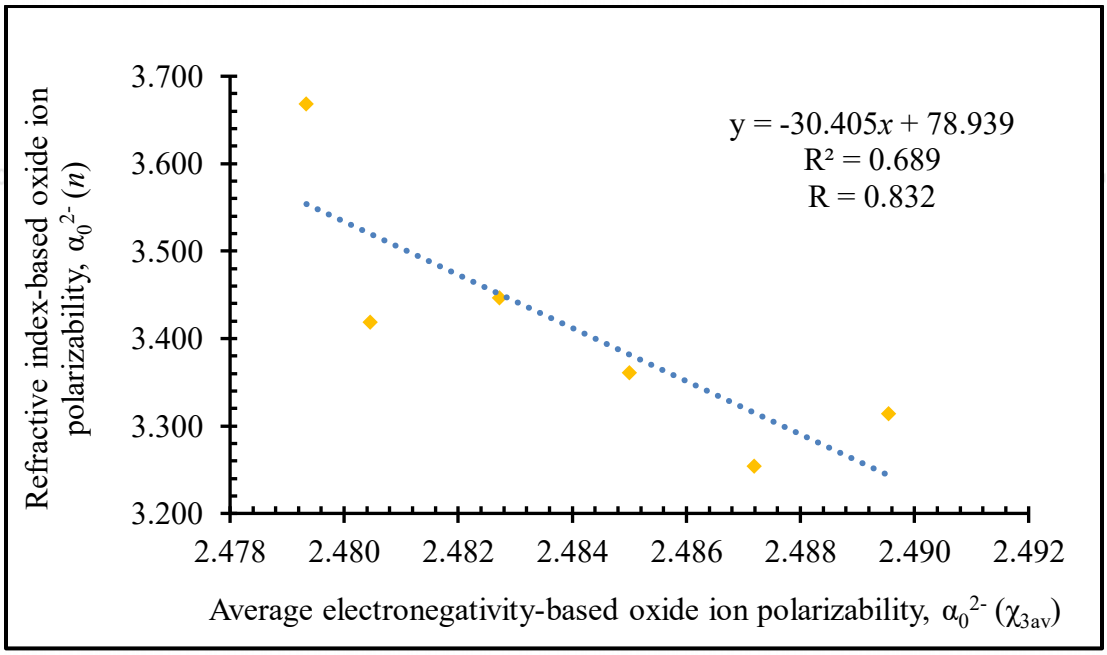


Figure 4.22. Least square plot of refractive index-based oxide ion polarizability, $\alpha_0^{2-}(n)$ against average electronegativity-based oxide ion polarizability, α_0^{2-} (χ_{3av}) of ZBTEr (NPs)-rGO glasses

05-4506832 pustaka.upsi.edu.my Perpustakaan Tuanku Bainun Kampus Sultan Abdul Jalil Shah PustakaTBainun ptbupsi

05-4506832 pustaka.upsi.edu.my Perpustakaan Tuanku Bainun Kampus Sultan Abdul Jalil Shah PustakaTBainun ptbupsi

Table 4.12

Optical energy bandgap-based optical electronegativity $\Delta\chi^*(E_{opt})$, refractive index-based optical electronegativity $\Delta\chi^*$ (n), energy bandgap optical electronegativity-based oxide ion polarizability α_0^{2-} ($\Delta\chi^*(E_{opt})$), and refractive index optical electronegativity-based oxide ion polarizability $\alpha_0^{2-}(\Delta\chi^*(n))$ of ZBTEr (NPs)-rGO glasses

Er_2O_3 nanoparticles concentration (mol%)	$\Delta\chi^*(\boldsymbol{E_{opt}})$	$\Delta\chi^*$ (n)	$\boldsymbol{\alpha_0^{2-}}(\Delta\chi^*(\boldsymbol{E_{opt}}))$	$\boldsymbol{\alpha_0^{2-}}(\Delta\chi^*(n))$
0.005	0.514	0.611	3.037	2.950
0.010	0.682	0.778	2.886	2.800
0.020	0.637	0.735	2.927	2.839
0.030	0.705	0.799	2.865	2.780
0.040	0.801	0.887	2.779	2.702
0.050	0.788	0.875	2.791	2.713

05-4506832 pustaka.upsi.edu.my Perpustakaan Tuanku Bainun Kampus Sultan Abdul Jalil Shah PustakaTBainun ptbupsi

05-4506832 pustaka.upsi.edu.my Perpustakaan Tuanku Bainun Kampus Sultan Abdul Jalil Shah PustakaTBainun ptbupsi

Other than that, the energy bandgap optical electronegativity-based oxide ion polarizability, $\alpha_0^{2-}(\Delta\chi^*(E_{opt}))$ and energy bandgap-oxide ion polarizability of the ZBTEr (NPs)-rGO glass system were calculated and illustrated in Figure 4.23. Meanwhile, the obtained least square plot of $\alpha_0^{2-}(\Delta\chi^*(n))$ in Figure 4.24 shows the high accuracy with the refractive index data. Therefore, $\alpha_0^{2-}(\Delta\chi^*(n))$ demonstrates reliable results for oxide ion polarizability as compared to the obtained results of $\alpha_0^{2-}(\Delta\chi^*(E_{opt}))$ which has less accuracy of fitting in the ZBTEr (NPs)-rGO glasses. The difference between $\alpha_0^{2-}(\Delta\chi^*(n))$ and $\alpha_0^{2-}(\Delta\chi^*(E_{opt}))$ could be attributed due to the existence of localized density of states in the energy bandgap according to Davis-Mott's theory for the conduction band that exists in the non-crystalline system (Mott et al., 1972).

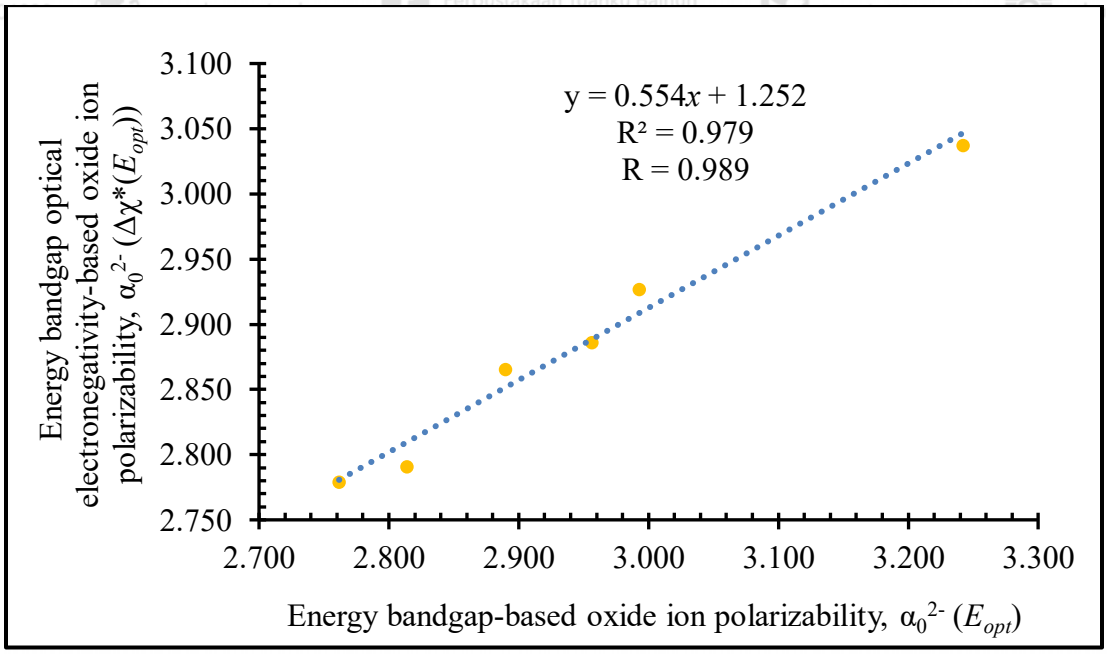


Figure 4.23. Least square plot of energy bandgap optical electronegativity-based oxide ion polarizability, $\alpha_0^{2-}(\Delta\chi^*(E_{opt}))$ with energy bandgap-based oxide ion polarizability, $\alpha_0^{2-}(E_{opt})$ of ZBTEr (NPs)-rGO glasses

05-4506832 pustaka.upsi.edu.my Perpustakaan Tuanku Bainun Kampus Sultan Abdul Jalil Shah PustakaTBainun ptbupsi

05-4506832 pustaka.upsi.edu.my Perpustakaan Tuanku Bainun Kampus Sultan Abdul Jalil Shah PustakaTBainun ptbupsi

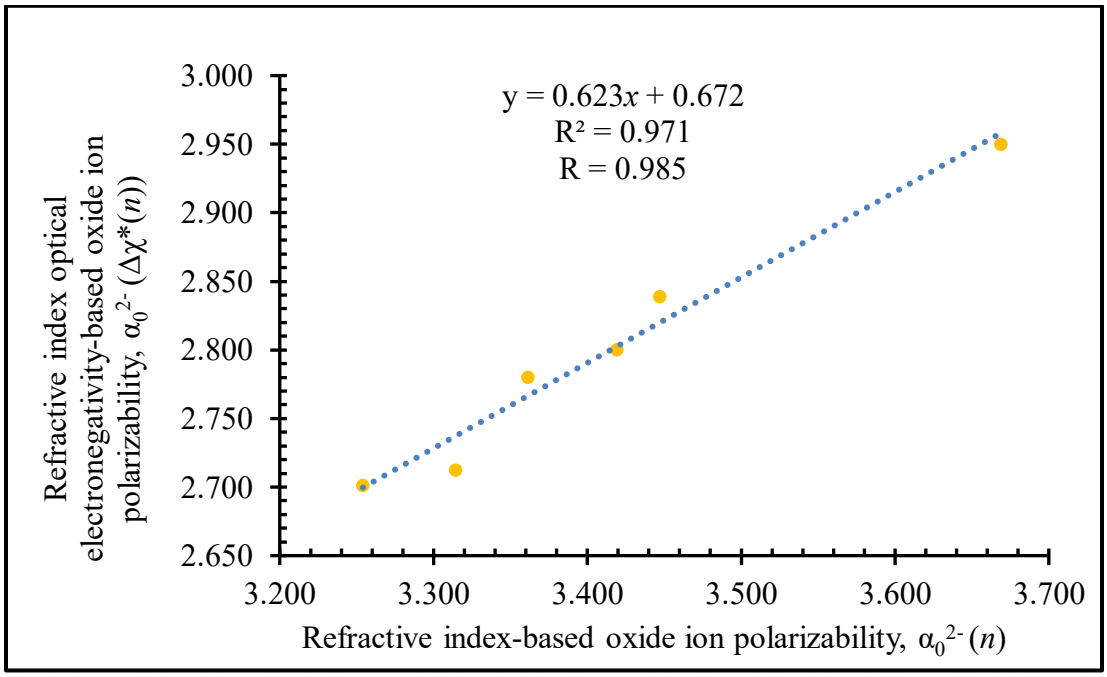


Figure 4.24. Least square plot of refractive index optical electronegativity-based oxide ion polarizability, $\alpha_0^{2-}(\Delta\chi^*(n))$ with refractive index-based oxide ion polarizability, $\alpha_0^{2-}(n)$ of ZBTEr (NPs)-rGO glasses

05-4506832 pustaka.upsi.edu.my Perpustakaan Tuanku Bainun Kampus Sultan Abdul Jalil Shah PustakaTBainun ptbupsi

Apart from that, it can be noticed that the obtained results indicate the stronger covalency of the ligand bonds which caused by the differences of electronegativity values. Due to these, the tendency of bonding electrons is attracted towards more electronegativities between the two atoms of different electronegativities in a covalent bond.

05-4506832 pustaka.upsi.edu.my Perpustakaan Tuanku Bainun Kampus Sultan Abdul Jalil Shah PustakaTBainun ptbupsi

05-4506832 pustaka.upsi.edu.my Perpustakaan Tuanku Bainun Kampus Sultan Abdul Jalil Shah PustakaTBainun ptbupsi

4.4.7 Judd-Ofelt's Analysis

Judd-Ofelt's intensity parameters known as a numerical integration of corresponding absorption bands which was employed to determine experimental oscillator strength for transitions from the ground state $^4I_{15/2}$ to different excited states level (Marzouk et al., 2021) by using the given Equations 2.24, 2.25, 2.26, 2.27, and 2.28, respectively which has been described in subsection 2.13.7. Judd-Ofelt's theoretical study was introduced as a fundamental stage for the characterization of absorption spectra that has been considered to identify the intensity of *f-f* transition in REIs (Judd, 1962; Ofelt, 1962). The great approach of Judd-Ofelt's theory allows the estimation of oscillator strengths in absorption or luminescence, transition probabilities, branching ratios, and radiative lifetime using the empirical intensity parameters, (Ω_λ = 2, 4, 6) by fitting the experimental and theoretical oscillator forces of the stated absorption transitions. According to the obtained absorption spectra of the ZBTEr (NPs)-rGO glasses (refer to Figure 4.13), the value of experimental oscillator strength for each observed transition state of excitation can be determined by analyzing from the area under the absorption bands.

The oscillator strength data provide indirect information on the symmetry and bonding nature of REIs in the glassy matrix in which the increasing value of oscillator strength indicates the lower symmetry and thus, attribute to strong covalent nature between ligand (Awang et al., 2015; Said Mahraz et al., 2015). The calculated and experimental oscillator strength along with the root mean square deviation values of the ZBTEr (NPs)-rGO glasses are summarized in Table 4.13. It is clearly stated that the oscillator strength

05-4506832 pustaka.upsi.edu.my Perpustakaan Tuanku Bainun Kampus Sultan Abdul Jalil Shah PustakaTBainun ptbupsi

05-4506832 pustaka.upsi.edu.my Perpustakaan Tuanku Bainun Kampus Sultan Abdul Jalil Shah PustakaTBainun ptbupsi

showed the highest value for transition band at $^4I_{15/2} \rightarrow {}^4F_{5/2}$ which was correlated to the most intense than other transitions and obey the hyper sensitive transitions (HST) (Jørgensen & Judd, 1964). This HST means the band transitions correlating to the Er^{3+} ions nanoparticles which express the sensitivity of oscillator strengths to the environment on the lanthanide ions and obey the selection rule of $|\Delta J| \leq 2$, $|\Delta L| \leq 2$ and $\Delta S = 0$ (Yusof, Ghoshal, & Azlan, 2017). The value of oscillator strength of these HST exhibits the decreasing trend which indicates the presence of higher symmetry along with the decreasing in covalency between Er^{3+} ions and the surrounding ligand with the increment of Er^{3+} ions concentration (Amiar Rodin & Sahar, 2018).

Additionally, the trend of oscillator strength value was due to the intermolecular interactions of orbitals and reactivity between the rGO sheets (Maslov et al., 2016). The accuracy of fit between the experimental and calculated oscillator strengths was derived via root mean square deviation, δ_{rms} (Marzouk et al., 2021). Thus, the obtained very small δ_{rms} value approximately in the range of $(0.084 - 0.567) \times 10^{-20}$ verifies the good agreement between the experimental and calculated oscillator strengths.

05-4506832 pustaka.upsi.edu.my Perpustakaan Tuanku Bainun Kampus Sultan Abdul Jalil Shah PustakaTBainun ptbupsi

05-4506832 pustaka.upsi.edu.my Perpustakaan Tuanku Bainun Kampus Sultan Abdul Jalil Shah PustakaTBainun ptbupsi

Table 4.13

The experimental (f_{exp} ×10^{-6}) and calculated oscillator strength (f_{cal} ×10^{-6}) along with the root mean square deviation (δ_{rms} ×10^{-6}) of ZBTEr (NPs)-rGO glasses

Absorption transition	ZBTEr (NPs)-rGO glasses											
	0.005 Er NPs		0.010 Er NPs		0.020 Er NPs		0.030 Er NPs		0.040 Er NPs		0.050 Er NPs	
Ground state ($^4I_{15/2}$)	f_{exp}	f_{cal}	f_{exp}	f_{cal}	f_{exp}	f_{cal}	f_{exp}	f_{cal}	f_{exp}	f_{cal}	f_{exp}	f_{cal}
$^4I_{15/2} \rightarrow {}^4F_{5/2}$	0.383	2.777	0.967	0.977	1.106	1.120	0.943	1.063	1.259	1.555	1.338	1.841
$^4I_{15/2} \rightarrow {}^4F_{7/2}$	0.309	0.214	0.210	0.231	0.383	0.400	0.383	0.678	0.700	1.159	1.081	1.746
$^4I_{15/2} \rightarrow {}^4H_{11/2}$	0.381	1.568	0.561	0.553	0.648	0.635	0.703	0.604	1.138	0.882	1.491	1.048
$^4I_{15/2} \rightarrow {}^4S_{3/2}$	0.136	0.173	0.221	0.216	0.324	0.319	0.648	0.581	0.903	0.798	1.255	1.103
$^4I_{15/2} \rightarrow {}^4F_{9/2}$	0.037	0.091	0.081	0.069	0.133	0.122	0.373	0.189	0.639	0.355	0.957	0.545
RMS deviation δ_{rms} (×10^{-20})	0.410		0.343		0.567		0.084		0.150		0.224	

05-4506832 pustaka.upsi.edu.my Perpustakaan Tuanku Bainun Kampus Sultan Abdul Jalil Shah PustakaTBainun ptbupsi

05-4506832 pustaka.upsi.edu.my Perpustakaan Tuanku Bainun Kampus Sultan Abdul Jalil Shah PustakaTBainun ptbupsi

Based on the optical absorption bands as stated in Figure 4.13, it is observed that, for $^4I_{15/2}\rightarrow{}^4I_{13/2}$, $^4I_{15/2}\rightarrow{}^4I_{11/2}$, $^4I_{15/2}\rightarrow{}^4I_{9/2}$, $^4I_{15/2}\rightarrow{}^4F_{9/2}$, $^4I_{15/2}\rightarrow{}^4S_{3/2}$, $^4I_{15/2}\rightarrow{}^2H_{11/2}$, $^4I_{15/2}\rightarrow{}^4F_{7/2}$, and $^4I_{15/2}\rightarrow{}^2G_{9/2}$ transitions, the obtained experimental oscillator values are in good agreement with the calculated values, demonstrating the validity of values of Ω_2, Ω_4 and Ω_6 parameters which are estimated from the experimental UV intensities based on the least-square fitting method, as proposed by Judd-Ofelt's theory (Marzouk et al., 2021). The intensity parameters with the spectroscopic quality factor indicate as the fundamental key in determining the coordination of trivalent Er^{3+} ions for ZBTEr (NPs)-rGO glasses, as shown in Table 4.14. In particular, the Ω_2 intensity parameter can be associated with the chemical bonding nature, the polarizability of ligand ions or molecule, symmetry around the REIs, and covalency of Er-O in the Er^{3+} ions nanoparticles region sites (Bhardwaj et al., 2014; Tanabe et al., 1992) whereby, it strongly depends on the hyper sensitive transitions oscillator strength. Meanwhile, the Ω_4 and Ω_6 intensity parameters are correlated to the long-range order of glasses, which may be referred as the viscosity and rigidity of glass composition and affect the bonds between ligand atom and Er^{3+} ions (Ahmadi et al., 2016; Krupke, 1966). The Ω_2 intensity parameter is sensitive to the local structure around the REIs site (Jørgensen & Reisfeld, 1983).

In the present work, it can be seen from Figure 4.25 that the Ω_2 parameter possess the higher value between 0.005 to 0.02 mol% of ZBTEr (NPs)-rGO glasses thus, the Judd-Ofelt's intensity parameters indicate the $\Omega_2 > \Omega_6 > \Omega_4$ trend uniformly, as reported by previous reports (Ahmadi et al., 2016; Amiar Rodin & Sahar, 2018; Azlan, Halimah, Suriani, Azlina, Umar, et al., 2019). It should be noticed the strong π-localized states that

05-4506832 pustaka.upsi.edu.my Perpustakaan Tuanku Bainun Kampus Sultan Abdul Jalil Shah PustakaTBainun ptbupsi

05-4506832 pustaka.upsi.edu.my Perpustakaan Tuanku Bainun Kampus Sultan Abdul Jalil Shah PustakaTBainun ptbupsi

existed in rGO structures disrupted the network of sp^2 hybridized bonds which influenced the strong covalency and asymmetry of surrounding ligand bonds around Er^{3+} ions sites. Furthermore, the Ω_2 values are found to decrease with increasing of Er^{3+} ions concentration from 0.03 to 0.05 mol% of the ZBTEr (NPs)-rGO glasses, as a means of the weaker covalent bonding of Er^{3+} ions ligand bonds. This trend corresponds to the addition of graphene-based nanomaterials containing several oxidized groups deposited onto glass surfaces that might attribute to the long-range structural disorder effects.

In addition, the decrement of Ω_2 values can be ascribed that the covalency decreases and reduction of asymmetry of the local environment around the Er^{3+} ions site. The decreasing trend of Ω_2 value with the inclusion of Er^{3+} ions nanoparticles content can be observed as reported in the Er^{3+}-doped borozincate (Marzouk et al., 2021), Dy^{3+}-doped tellurite oxyfluoride (Wan et al., 2021), and Er^{3+}-doped halageno-antimonate (Iezid et al., 2021) glasses. Meanwhile, the increasing trend of Ω_6 parameter can be assigned to relatively strong long-range effects, high ionicity, and vibrational amplitude of Er-O bonds (Azlan, Halimah, Suriani, Azlina, Umar, et al., 2019).

Referring to the theoretical study (Jacobs & Weber, 1976), the intensity of erbium emission can be expressed by the ratio between Ω_4 and Ω_6 parameters. The spectroscopic quality factor, χ signify the emission strength of lasing properties in the glass matrix system (Amiar Rodin & Sahar, 2018). As can be referred in Table 4.14, the χ value lies in the range between 0.163 to 0.923 whereby, 0.01 mol% Er^{3+} nanoparticles concentration of the ZBTEr (NPs)-rGO glass exhibit a maximum value of 0.923, indicating that coated-glass

05-4506832 pustaka.upsi.edu.my Perpustakaan Tuanku Bainun Kampus Sultan Abdul Jalil Shah PustakaTBainun ptbupsi

05-4506832 pustaka.upsi.edu.my Perpustakaan Tuanku Bainun Kampus Sultan Abdul Jalil Shah PustakaTBainun ptbupsi

can be more promising laser material. However, the lower χ value obtained at 0.05 mol% Er^{3+} nanoparticles concentration of the ZBTEr (NPs)-rGO glass is correlated to the quenching factor of stimulated transitions intensities (Awang et al., 2015).

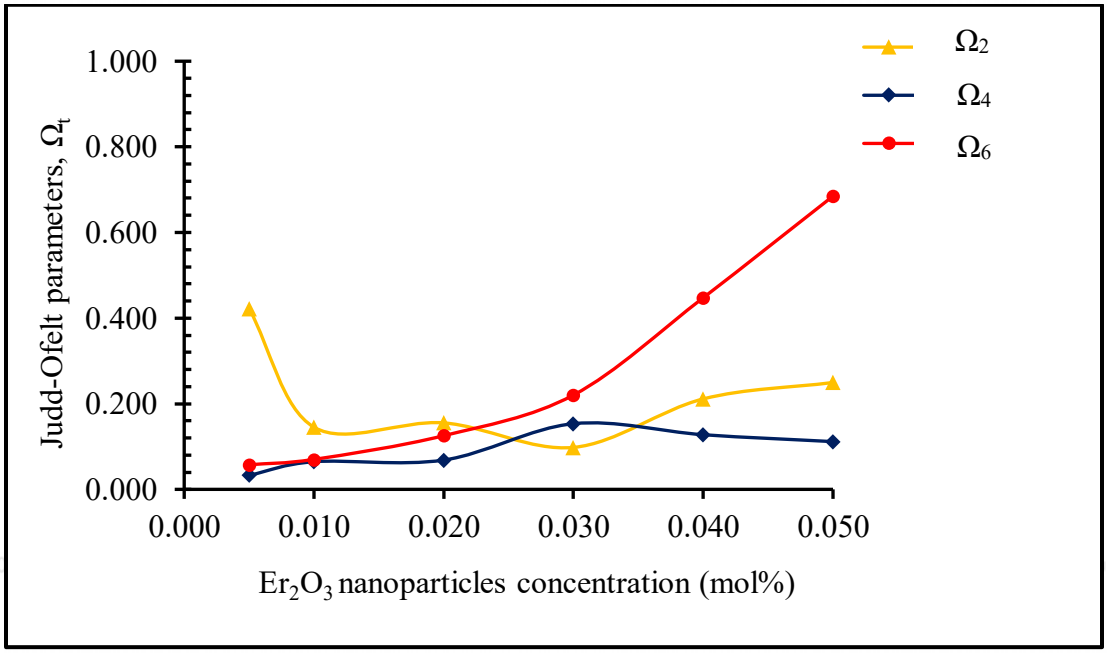


Figure 4.25. Variation of the Judd-Ofelt's intensity parameters, Ω_t ($t = 2, 4, 6$) as a function of Er_2O_3 nanoparticles concentration for ZBTEr (NPs)-rGO glasses

05-4506832 pustaka.upsi.edu.my Perpustakaan Tuanku Bainun Kampus Sultan Abdul Jalil Shah PustakaTBainun ptbupsi

05-4506832 pustaka.upsi.edu.my Perpustakaan Tuanku Bainun Kampus Sultan Abdul Jalil Shah PustakaTBainun ptbupsi

Table 4.14

Judd-Ofelt's intensity parameters ($\Omega_\lambda \times 10^{-20}$ cm^2) and spectroscopic quality factor, $\chi = \frac{\Omega_4}{\Omega_6}$ of ZBTEr (NPs)-rGO glasses

Er_2O_3 nanoparticles concentration (mol%)	Ω_2	Ω_4	Ω_6	$\chi = \frac{\Omega_4}{\Omega_6}$	Ω_i Trends
0.005	0.422	0.032	0.058	0.570	$\Omega_2 > \Omega_6 > \Omega_4$
0.010	0.145	0.065	0.070	0.923	$\Omega_2 > \Omega_6 > \Omega_4$
0.020	0.155	0.068	0.125	0.546	$\Omega_2 > \Omega_6 > \Omega_4$
0.030	0.098	0.153	0.220	0.696	$\Omega_6 > \Omega_4 > \Omega_2$
0.040	0.211	0.128	0.448	0.285	$\Omega_6 > \Omega_2 > \Omega_4$
0.050	0.250	0.112	0.685	0.163	$\Omega_6 > \Omega_2 > \Omega_4$

05-4506832 pustaka.upsi.edu.my Perpustakaan Tuanku Bainun Kampus Sultan Abdul Jalil Shah PustakaTBainun ptbupsi

05-4506832 pustaka.upsi.edu.my Perpustakaan Tuanku Bainun Kampus Sultan Abdul Jalil Shah PustakaTBainun ptbupsi

The integrated absorption bands of each transition can be used as an input data to study the Judd Ofelt's analysis of ZBTEr (NPs)-rGO glasses, which is necessary to obtain the radiative transition probability (A), branching ratio (β_R), and radiative lifetime (t_r) for all the Er^{3+} ions nanoparticles concentration varies from 0.005, 0.01, 0.02, 0.03, 0.04, and 0.05 mol% by using the given Equations 2.30, 2.31, 2.32, 2.33, and 2.34, respectively, as has been stated in subsection 2.13.7 and the obtained data are summarized in the following Table 4.15 – 4.20, respectively. Furthermore, the phonon energy of the host glass matrix determines the radiative properties of the Er^{3+} ions whereby, the higher radiative probabilities of transitions depend on the lower phonon energy of the tellurite host system (Lalla et al., 2020).

Branching ratio is defined as the fraction of total photon flux from the upper manifold to a lower manifold which determines the probability of achieving the stimulated emission under the suitable excitation (Jlassi et al., 2010; Walsh et al., 1998). The obtained value of branching ratio relevant for the $^2H_{11/2} \rightarrow {}^4I_{15/2}$ transition was determined in the range of 0.900 – 0.970 for all the ZBTEr (NPs)-rGO (coated) glasses: Er^{3+} ions nanoparticles concentration, indicates the possibility in obtaining the strong green emission which is frequently used for laser applications under the stated excitation. On the other hand, these result was supported in previous studies such as Er^{3+} ions nanoparticles doped zinc borotellurite (Azlan et al., 2019; Azlan et al., 2015), Er^{3+}-doped sodium borotellurite (Amiar Rodin & Sahar, 2018), and Er^{3+}-doped oxyfluorogermanotellurite (Zanane et al., 2020) glasses.

05-4506832 pustaka.upsi.edu.my Perpustakaan Tuanku Bainun Kampus Sultan Abdul Jalil Shah PustakaTBainun ptbupsi

05-4506832 pustaka.upsi.edu.my Perpustakaan Tuanku Bainun Kampus Sultan Abdul Jalil Shah PustakaTBainun ptbupsi

Meanwhile, the radiative lifetime of the emission bands for the $^2H_{11/2} \rightarrow {}^4I_{15/2}$ transition of the ZBTEr (NPs)-rGO glass exhibit the range from 0.245 – 0.819 ms which is lower than other emitting levels. The incorporation of graphene-based nanomaterials deposited onto tellurite glass surface gives the significant radiative lifetime value which is strongly linked with the lower amount of oxygen contents that existed in rGO nanosheets. Moreover, the effect of reduction degree and arrangement of oxygen groups create difference on the coated-glass performance by a factor of sp^2/sp^3 hybrid ratio. The shorter radiative lifetime value corresponds to the non-radiative decay process whereby, the radiative lifetime is ascribed to be proportional to the radiative decay rate (Aarts et al., 2011). Conversely, the longer the radiative lifetime is observed at $^4I_{9/2} \rightarrow {}^4I_{15/2}$ transition which is strongly associated with the radiation trapping effect that occurred in the glassy matrix (Hamza et al., 2019).

05-4506832 pustaka.upsi.edu.my Perpustakaan Tuanku Bainun Kampus Sultan Abdul Jalil Shah PustakaTBainun ptbupsi

05-4506832 pustaka.upsi.edu.my Perpustakaan Tuanku Bainun Kampus Sultan Abdul Jalil Shah PustakaTBainun ptbupsi

Table 4.15

The magnetic dipole and electric dipole radiative transition probabilities (A_{MD}, A_{ED}), emission branching ratio (β_R), and radiative lifetime (t_r) of 0.005 mol% ZBTEr (NPs)-rGO glass

Er_2O_3 nanoparticles concentration (mol%)	Transition	λ (nm)	A_{MD} (s^{-1})	A_{ED} (s^{-1})	β_R	t_r (ms)
0.005	$^4I_{13/2} \rightarrow {}^4I_{15/2}$	1530	196.120	39.510	1.000	4.244
	$^4I_{11/2} \rightarrow {}^4I_{13/2}$	2804	38.390	6.510	0.418	
	$^4I_{15/2}$	990		62.480	0.582	9.313
	$^4I_{9/2} \rightarrow {}^4I_{11/2}$	4168	7.980	0.310	0.158	
	$^4I_{13/2}$	1676		18.580	0.354	
	$^4I_{15/2}$	800		25.630	0.488	19.047
	$^4F_{9/2} \rightarrow {}^4I_{9/2}$	3771	12.890	2.180	0.036	
	$^4I_{11/2}$	1980	35.580	28.110	0.152	
	$^4I_{13/2}$	1161		18.000	0.043	
	$^4I_{15/2}$	660		322.200	0.769	2.387
	$^4S_{3/2} \rightarrow {}^4I_{9/2}$	1710		18.060	0.029	
	$^4I_{11/2}$	1212		12.920	0.021	
	$^4I_{13/2}$	846		172.270	0.280	
	$^4I_{15/2}$	545		412.220	0.670	1.625
	$^2H_{11/2} \rightarrow {}^4F_{9/2}$	2497		17.330	0.004	
	$^4I_{9/2}$	1502		54.880	0.013	
	$^4I_{11/2}$	1104		28.250	0.007	
	$^4I_{13/2}$	792		51.880	0.013	
	$^4I_{15/2}$	522		3932.880	0.963	0.245
	$^4F_{7/2} \rightarrow {}^4F_{9/2}$	1942		2.540	0.002	
	$^4I_{9/2}$	1282		43.100	0.040	
	$^4I_{11/2}$	980		52.550	0.049	
	$^4I_{13/2}$	726		75.720	0.071	
	$^4I_{15/2}$	493		896.710	0.838	0.934
	$^2G_{9/2} \rightarrow {}^4F_{7/2}$	2439		6.900	0.005	
	$^2H_{11/2}$	1907		6.920	0.005	
	$^4F_{9/2}$	1081		9.090	0.021	
	$^4I_{9/2}$	840		23.560	0.018	
	$^4I_{11/2}$	699		167.340	0.126	
	$^4I_{13/2}$	560		684.520	0.514	
	$^4I_{15/2}$	410		414.470	0.311	0.751

05-4506832 pustaka.upsi.edu.my Perpustakaan Tuanku Bainun Kampus Sultan Abdul Jalil Shah PustakaTBainun ptbupsi

05-4506832 pustaka.upsi.edu.my Perpustakaan Tuanku Bainun Kampus Sultan Abdul Jalil Shah PustakaTBainun ptbupsi

Table 4.16

The magnetic dipole and electric dipole radiative transition probabilities (A_{MD}, A_{ED}), emission branching ratio (β_R), and radiative lifetime (t_r) of 0.01 mol% ZBTEr (NPs)-rGO glass

Er_2O_3 nanoparticles concentration (mol%)	Transition	λ (nm)	A_{MD} (s^{-1})	A_{ED} (s^{-1})	β_R	t_r (ms)
0.01	$^4I_{13/2} \rightarrow {}^4I_{15/2}$	1530	149.330	31.860	1.000	5.519
	$^4I_{11/2} \rightarrow {}^4I_{13/2}$	2804	29.230	5.020	0.465	
	$^4I_{15/2}$	990		39.440	0.535	13.570
	$^4I_{9/2} \rightarrow {}^4I_{11/2}$	4168	6.070	0.270	0.114	
	$^4I_{13/2}$	1676		15.600	0.281	
	$^4I_{15/2}$	800		33.530	0.604	18.026
	$^4F_{9/2} \rightarrow {}^4I_{9/2}$	3771	9.810	0.560	0.025	
	$^4I_{11/2}$	1980	27.090	18.770	0.112	
	$^4I_{13/2}$	1161		15.130	0.037	
	$^4I_{15/2}$	660		336.300	0.825	2.453
	$^4S_{3/2} \rightarrow {}^4I_{9/2}$	1710		16.540	0.032	
	$^4I_{11/2}$	1212		11.030	0.021	
	$^4I_{13/2}$	846		144.320	0.279	
	$^4I_{15/2}$	545		345.340	0.668	1.933
	$^2H_{11/2} \rightarrow {}^4F_{9/2}$	2497		4.200	0.003	
	$^4I_{9/2}$	1502		19.340	0.016	
	$^4I_{11/2}$	1104		14.940	0.012	
	$^4I_{13/2}$	792		26.570	0.022	
	$^4I_{15/2}$	522		1155.980	0.947	0.819
	$^4F_{7/2} \rightarrow {}^4F_{9/2}$	1942		1.240	0.001	
	$^4I_{9/2}$	1282		32.970	0.033	
	$^4I_{11/2}$	980		54.070	0.054	
	$^4I_{13/2}$	726		102.610	0.103	
	$^4I_{15/2}$	493		805.940	0.809	1.003
	$^2G_{9/2} \rightarrow {}^4F_{7/2}$	2439		2.010	0.002	
	$^2H_{11/2}$	1907		4.370	0.005	
	$^4F_{9/2}$	1081		6.180	0.034	
	$^4I_{9/2}$	840		6.900	0.008	
	$^4I_{11/2}$	699		82.090	0.098	
	$^4I_{13/2}$	560		360.690	0.429	
	$^4I_{15/2}$	410		357.060	0.424	1.188

05-4506832 pustaka.upsi.edu.my Perpustakaan Tuanku Bainun Kampus Sultan Abdul Jalil Shah PustakaTBainun ptbupsi

05-4506832 pustaka.upsi.edu.my Perpustakaan Tuanku Bainun Kampus Sultan Abdul Jalil Shah PustakaTBainun ptbupsi

Table 4.17

The magnetic dipole and electric dipole radiative transition probabilities (A_{MD}, A_{ED}), emission branching ratio (β_R), and radiative lifetime (t_r) of 0.02 mol% ZBTEr (NPs)-rGO glass

Er_2O_3 nanoparticles concentration (mol%)	Transition	λ (nm)	A_{MD} (s^{-1})	A_{ED} (s^{-1})	β_R	t_r (ms)
0.02	$^4I_{13/2} \rightarrow {}^4I_{15/2}$	1530	159.630	60.080	1.000	4.551
	$^4I_{11/2} \rightarrow {}^4I_{13/2}$	2804	31.250	9.150	0.355	
	$^4I_{15/2}$	990		73.310	0.645	8.795
	$^4I_{9/2} \rightarrow {}^4I_{11/2}$	4168	6.490	0.460	0.089	
	$^4I_{13/2}$	1676		30.410	0.391	
	$^4I_{15/2}$	800		40.430	0.520	12.855
	$^4F_{9/2} \rightarrow {}^4I_{9/2}$	3771	10.490	0.700	0.018	
	$^4I_{11/2}$	1980	28.960	35.190	0.104	
	$^4I_{13/2}$	1161		21.260	0.034	
	$^4I_{15/2}$	660		520.100	0.843	1.622
	$^4S_{3/2} \rightarrow {}^4I_{9/2}$	1710		29.480	0.029	
	$^4I_{11/2}$	1212		21.190	0.021	
	$^4I_{13/2}$	846		283.010	0.280	
	$^4I_{15/2}$	545		677.210	0.670	0.989
	$^2H_{11/2} \rightarrow {}^4F_{9/2}$	2497		4.930	0.003	
	$^4I_{9/2}$	1502		28.240	0.019	
	$^4I_{11/2}$	1104		19.230	0.013	
	$^4I_{13/2}$	792		38.060	0.026	
	$^4I_{15/2}$	522		1394.090	0.939	0.674
	$^4F_{7/2} \rightarrow {}^4F_{9/2}$	1942		1.650	0.001	
	$^4I_{9/2}$	1282		58.810	0.034	
	$^4I_{11/2}$	980		78.970	0.046	
	$^4I_{13/2}$	726		118.950	0.069	
	$^4I_{15/2}$	493		1465.550	0.850	0.580
	$^2G_{9/2} \rightarrow {}^4F_{7/2}$	2439		2.480	0.002	
	$^2H_{11/2}$	1907		5.860	0.004	
	$^4F_{9/2}$	1081		9.550	0.020	
	$^4I_{9/2}$	840		8.650	0.006	
	$^4I_{11/2}$	699		122.200	0.085	
	$^4I_{13/2}$	560		582.630	0.407	
	$^4I_{15/2}$	410		679.540	0.475	0.699

05-4506832 pustaka.upsi.edu.my Perpustakaan Tuanku Bainun Kampus Sultan Abdul Jalil Shah PustakaTBainun ptbupsi

05-4506832 pustaka.upsi.edu.my Perpustakaan Tuanku Bainun Kampus Sultan Abdul Jalil Shah PustakaTBainun ptbupsi

Table 4.18

The magnetic dipole and electric dipole radiative transition probabilities (A_{MD}, A_{ED}), emission branching ratio (β_R), and radiative lifetime (t_r) of 0.03 mol% ZBTEr (NPs)-rGO glass

Er_2O_3 nanoparticles concentration (mol%)	Transition	λ (nm)	A_{MD} (s^{-1})	A_{ED} (s^{-1})	β_R	t_r (ms)
0.03	$^4I_{13/2} \rightarrow {}^4I_{15/2}$	1530	144.430	92.330	1.000	4.224
	$^4I_{11/2} \rightarrow {}^4I_{13/2}$	2804	28.270	14.030	0.284	
	$^4I_{15/2}$	990		106.650	0.716	6.714
	$^4I_{9/2} \rightarrow {}^4I_{11/2}$	4168	5.880	0.740	0.051	
	$^4I_{13/2}$	1676		46.750	0.357	
	$^4I_{15/2}$	800		77.570	0.592	7.638
	$^4F_{9/2} \rightarrow {}^4I_{9/2}$	3771	9.490	0.510	0.010	
	$^4I_{11/2}$	1980	26.200	51.870	0.078	
	$^4I_{13/2}$	1161		35.560	0.035	
	$^4I_{15/2}$	660		883.530	0.877	0.993
	$^4S_{3/2} \rightarrow {}^4I_{9/2}$	1710		47.040	0.030	
	$^4I_{11/2}$	1212		32.790	0.021	
	$^4I_{13/2}$	846		434.240	0.280	
	$^4I_{15/2}$	545		1039.100	0.669	0.644
	$^2H_{11/2} \rightarrow {}^4F_{9/2}$	2497		2.920	0.002	
	$^4I_{9/2}$	1502		31.740	0.023	
	$^4I_{11/2}$	1104		28.100	0.021	
	$^4I_{13/2}$	792		53.790	0.040	
	$^4I_{15/2}$	522		1241.870	0.914	0.736
	$^4F_{7/2} \rightarrow {}^4F_{9/2}$	1942		2.300	0.001	
	$^4I_{9/2}$	1282		90.510	0.033	
	$^4I_{11/2}$	980		136.180	0.049	
	$^4I_{13/2}$	726		232.970	0.084	
	$^4I_{15/2}$	493		2319.180	0.834	0.360
	$^2G_{9/2} \rightarrow {}^4F_{7/2}$	2439		2.200	0.001	
	$^2H_{11/2}$	1907		9.130	0.004	
	$^4F_{9/2}$	1081		14.740	0.014	
	$^4I_{9/2}$	840		7.770	0.004	
	$^4I_{11/2}$	699		168.340	0.081	
	$^4I_{13/2}$	560		817.820	0.391	
	$^4I_{15/2}$	410		1055.340	0.505	0.479

05-4506832 pustaka.upsi.edu.my Perpustakaan Tuanku Bainun Kampus Sultan Abdul Jalil Shah PustakaTBainun ptbupsi

05-4506832 pustaka.upsi.edu.my Perpustakaan Tuanku Bainun Kampus Sultan Abdul Jalil Shah PustakaTBainun ptbupsi

Table 4.19

The magnetic dipole and electric dipole radiative transition probabilities (A_{MD}, A_{ED}), emission branching ratio (β_R), and radiative lifetime (t_r) of 0.04 mol% ZBTEr (NPs)-rGO glass

Er_2O_3 nanoparticles concentration (mol%)	Transition	λ (nm)	A_{MD} (s^{-1})	A_{ED} (s^{-1})	β_R	t_r (ms)
0.04	$^4I_{13/2} \rightarrow {}^4I_{15/2}$	1530	127.190	153.350	1.000	3.565
	$^4I_{11/2} \rightarrow {}^4I_{13/2}$	2804	24.900	22.690	0.206	
	$^4I_{15/2}$	990		183.160	0.794	4.334
	$^4I_{9/2} \rightarrow {}^4I_{11/2}$	4168	5.170	1.06	0.043	
	$^4I_{13/2}$	1676		79.68	0.545	
	$^4I_{15/2}$	800		60.41	0.413	6.834
	$^4F_{9/2} \rightarrow {}^4I_{9/2}$	3771	8.360	0.880	0.007	
	$^4I_{11/2}$	1980	23.080	88.760	0.088	
	$^4I_{13/2}$	1161		40.010	0.031	
	$^4I_{15/2}$	660		1115.390	0.874	0.783
	$^4S_{3/2} \rightarrow {}^4I_{9/2}$	1710		72.210	0.027	
	$^4I_{11/2}$	1212		54.960	0.021	
	$^4I_{13/2}$	846		744.620	0.281	
	$^4I_{15/2}$	545		1781.790	0.671	0.377
	$^2H_{11/2} \rightarrow {}^4F_{9/2}$	2497		5.030	0.003	
	$^4I_{9/2}$	1502		51.660	0.028	
	$^4I_{11/2}$	1104		30.150	0.016	
	$^4I_{13/2}$	792		70.810	0.039	
	$^4I_{15/2}$	522		1670.420	0.914	0.547
	$^4F_{7/2} \rightarrow {}^4F_{9/2}$	1942		2.720	0.001	
	$^4I_{9/2}$	1282		143.190	0.035	
	$^4I_{11/2}$	980		158.220	0.038	
	$^4I_{13/2}$	726		163.650	0.040	
	$^4I_{15/2}$	493		3647.400	0.886	0.243
	$^2G_{9/2} \rightarrow {}^4F_{7/2}$	2439		3.160	0.001	
	$^2H_{11/2}$	1907		10.060	0.003	
	$^4F_{9/2}$	1081		20.000	0.009	
	$^4I_{9/2}$	840		11.440	0.003	
	$^4I_{11/2}$	699		238.740	0.072	
	$^4I_{13/2}$	560		1262.580	0.382	
	$^4I_{15/2}$	410		1750.420	0.530	0.303

05-4506832 pustaka.upsi.edu.my Perpustakaan Tuanku Bainun Kampus Sultan Abdul Jalil Shah PustakaTBainun ptbupsi

05-4506832 pustaka.upsi.edu.my Perpustakaan Tuanku Bainun Kampus Sultan Abdul Jalil Shah PustakaTBainun ptbupsi

Table 4.20

The magnetic dipole and electric dipole radiative transition probabilities (A_{MD}, A_{ED}), emission branching ratio (β_R), and radiative lifetime (t_r) of 0.05 mol% ZBTEr (NPs)-rGO glass

Er_2O_3 nanoparticles concentration (mol%)	Transition	λ (nm)	A_{MD} (s^{-1})	A_{ED} (s^{-1})	β_R	t_r (ms)
0.05	$^4I_{13/2} \rightarrow {}^4I_{15/2}$	1530	129.420	237.460	1.000	2.726
	$^4I_{11/2} \rightarrow {}^4I_{13/2}$	2804	25.340	34.780	0.174	
	$^4I_{15/2}$	990		284.660	0.826	2.900
	$^4I_{9/2} \rightarrow {}^4I_{11/2}$	4168	5.260	1.570	0.036	
	$^4I_{13/2}$	1676		124.530	0.648	
	$^4I_{15/2}$	800		60.800	0.316	5.204
	$^4F_{9/2} \rightarrow {}^4I_{9/2}$	3771	8.510	1.150	0.005	
	$^4I_{11/2}$	1980	23.480	138.040	0.091	
	$^4I_{13/2}$	1161		52.290	0.029	
	$^4I_{15/2}$	660		1560.540	0.875	0.561
	$^4S_{3/2} \rightarrow {}^4I_{9/2}$	1710		109.130	0.026	
	$^4I_{11/2}$	1212		85.480	0.021	
	$^4I_{13/2}$	846		1166.010	0.281	
	$^4I_{15/2}$	545		2790.140	0.672	0.241
	$^2H_{11/2} \rightarrow {}^4F_{9/2}$	2497		6.040	0.003	
	$^4I_{9/2}$	1502		74.790	0.034	
	$^4I_{11/2}$	1104		36.720	0.017	
	$^4I_{13/2}$	792		97.260	0.044	
	$^4I_{15/2}$	522		2007.230	0.903	0.450
	$^4F_{7/2} \rightarrow {}^4F_{9/2}$	1942		3.500	0.001	
	$^4I_{9/2}$	1282		217.720	0.035	
	$^4I_{11/2}$	980		212.260	0.035	
	$^4I_{13/2}$	726		146.460	0.024	
	$^4I_{15/2}$	493		5558.150	0.906	0.163
	$^2G_{9/2} \rightarrow {}^4F_{7/2}$	2439		3.970	0.001	
	$^2H_{11/2}$	1907		12.730	0.003	
	$^4F_{9/2}$	1081		28.450	0.006	
	$^4I_{9/2}$	840		14.690	0.003	
	$^4I_{11/2}$	699		338.780	0.068	
	$^4I_{13/2}$	560		1869.960	0.375	
	$^4I_{15/2}$	410		2713.430	0.545	0.201

05-4506832 pustaka.upsi.edu.my Perpustakaan Tuanku Bainun Kampus Sultan Abdul Jalil Shah PustakaTBainun ptbupsi

05-4506832 pustaka.upsi.edu.my Perpustakaan Tuanku Bainun Kampus Sultan Abdul Jalil Shah PustakaTBainun ptbupsi

4.4.8 Luminescence Analysis

Figures 4.26 and 4.27 depict the luminescence spectra of Er^{3+} nanoparticles for ZBTEr (NPs)-rGO and ZBTEr (NPs)-uncoated glasses which were measured at 375 nm and used as an excitation wavelength within the range of 500 – 600 nm for the determination of visible luminescence. It can be seen from Figure 4.26 that there are two prominent emission peaks are observed at 539 nm and 558 nm which are assigned to $^2H_{11/2} \rightarrow {}^4I_{15/2}$ and $^4S_{3/2} \rightarrow {}^4I_{15/2}$ transitions, respectively meanwhile, Figure 4.27 shows only one prominent peak in the range of 550 – 560 nm. Furthermore, Figure 4.26 presents the strongest emission peak at 558 nm exhibits the highest luminescence intensity in ZBTEr (NPs)-rGO glasses and hence, it is appropriate for green laser applications (Maheshvaran et al., 2013). Particularly, the obtained bands are associated with the stark splitting effects which correlate to the low symmetry of the local environment around the Er^{3+} ions nanoparticles site (Hamza, Halimah, Muhammad, & Chan, 2019; Iezid et al., 2021; Zhang et al., 2018).

As can be referred to Figure 4.26, it can be noticed that the ZBTEr (NPs)-rGO glass sample with 0.04 and 0.05 mol% of Er_2O_3 nanoparticles concentration shows a higher peak intensity than the other concentration of glasses. These results clearly proved by Judd-Ofelt's calculation whereby, the observed data of Ω_i intensity parameters and spectroscopic quality reveal the enhancement for the ZBTEr (NPs)-rGO glasses than ZBTEr (NPs)-uncoated glasses.

05-4506832 pustaka.upsi.edu.my Perpustakaan Tuanku Bainun Kampus Sultan Abdul Jalil Shah PustakaTBainun ptbupsi

05-4506832 pustaka.upsi.edu.my Perpustakaan Tuanku Bainun Kampus Sultan Abdul Jalil Shah PustakaTBainun ptbupsi

In addition, it is found that the inclusion of Er^{3+} affects the emission intensity of the rGO-coated tellurite glasses meanwhile, the shape of emission spectra remains unchanged. Therefore, it can be noticed that the ZBTEr (NPs)-rGO is more intense than ZBTEr (NPs)-uncoated glasses. The obtained luminescence intensity is found at the higher concentration of Er^{3+} ions which relates to the luminescence concentration quenching (LCQ) that caused by the energy transfer (ET) mechanism through the interactions of Er^{3+} ions nanoparticles and OH^- groups in the glassy matrix (Câmara et al., 2021). The observed luminescent green emission peaks of Er^{3+} nanoparticles can be attributed to the visible light emission by transitions of excited optical centers existing in the deep levels.

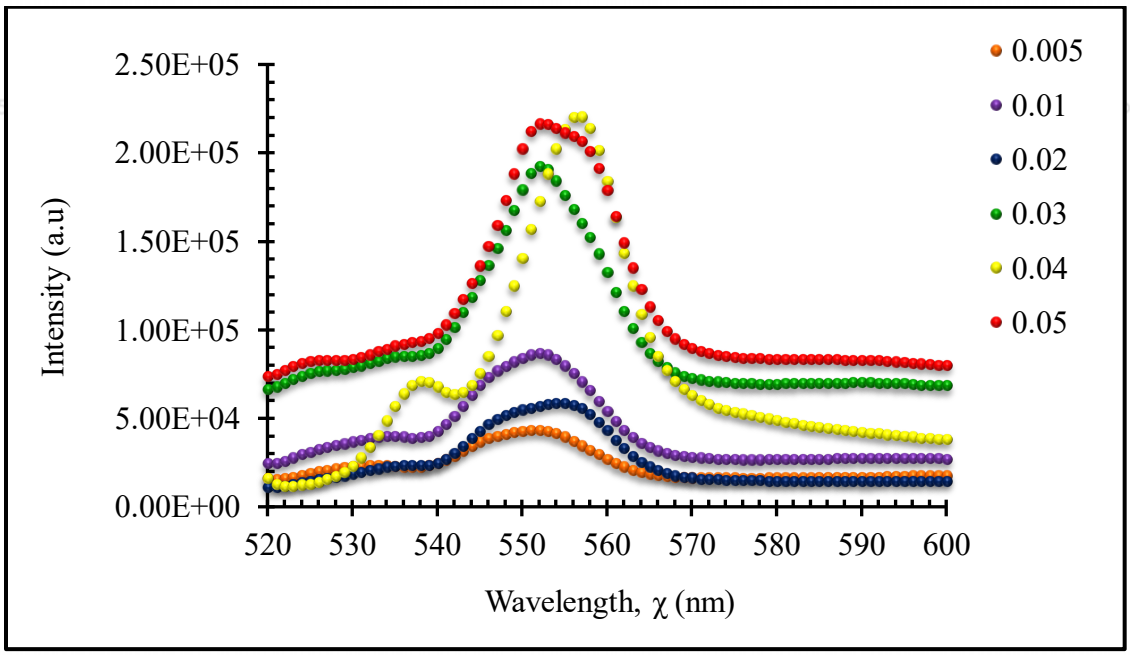


Figure 4.26. Luminescence spectra of ZBTEr (NPs)-rGO glasses

05-4506832 pustaka.upsi.edu.my Perpustakaan Tuanku Bainun Kampus Sultan Abdul Jalil Shah PustakaTBainun ptbupsi

05-4506832 pustaka.upsi.edu.my Perpustakaan Tuanku Bainun Kampus Sultan Abdul Jalil Shah PustakaTBainun ptbupsi

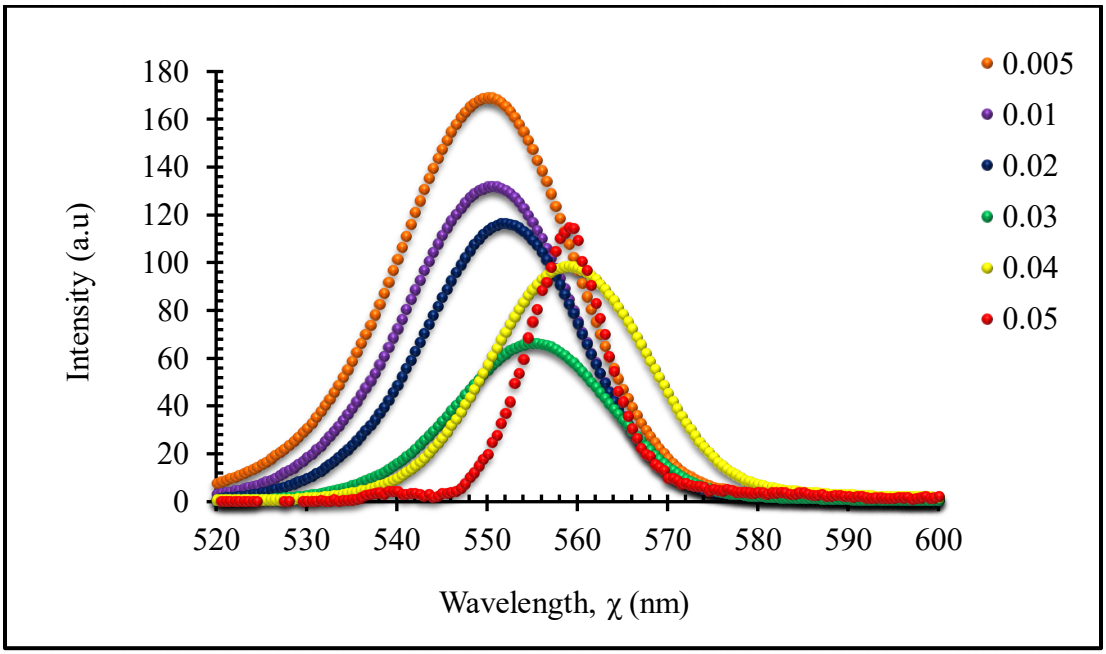


Figure 4.27. Luminescence spectra of ZBTEr (NPs)-uncoated glasses (Azlan, Halimah, Suriani, Azlina, Umar, et al., 2019)

05-4506832 pustaka.upsi.edu.my Perpustakaan Tuanku Bainun Kampus Sultan Abdul Jalil Shah PustakaTBainun ptbupsi

The proposed mechanism of luminescence enhancement observed at the 375 nm excitation is demonstrated by using the schematic energy levels diagram of Er^{3+} ions nanoparticles, as shown in Figure 4.28. Afterward, the excitation occurs when Er^{3+} ions are promoted to excite from the ground state $^4I_{15/2}$ to the excited state $^4G_{11/2}$ level by a process called the ground state absorption (GSA). The excited Er^{3+} ions nanoparticles then decay non-radiatively (NR) whereby, the electrons stored in the $^4G_{11/2}$ level are populated to the transition $^2H_{9/2}$, $^4F_{5/2}$, and $^4F_{7/2}$ levels via multi-phonon relaxation (MPR) process. The electrons occupied at the $^4F_{7/2}$ level are then relaxed non-radiatively and populate to the next lower $^2H_{11/2}$ level whereby, the present state is related to the thermal equilibrated population with the excited state $^4S_{3/2}$ level (Balda et al., 2016; Guo et al., 2020). Thereafter, it was followed by the electrons at the excited state of $^2H_{11/2}$ + $^4S_{3/2}$ levels are eventually decayed radiatively (R) to the ground state $^4I_{15/2}$, resulting in the intense green emissions

05-4506832 pustaka.upsi.edu.my Perpustakaan Tuanku Bainun Kampus Sultan Abdul Jalil Shah PustakaTBainun ptbupsi

05-4506832 pustaka.upsi.edu.my Perpustakaan Tuanku Bainun Kampus Sultan Abdul Jalil Shah PustakaTBainun ptbupsi

at 539 nm and 558 nm, respectively. However, it is observed from Figure 4.26 that there is absence of a red emission peak in the present ZBTEr (NPs)-rGO glasses along with the increase of Er^{3+} ions nanoparticles. This may be due to the effect of the low concentration of Er_2O_3 nanoparticles in the glassy matrix system. A similar report to the ZBTEr (NPs)-rGO glasses relates the 385 nm excitation wavelength and emission range for Er^{3+}-doped tellurite-based glasses (Azlan et al., 2015).

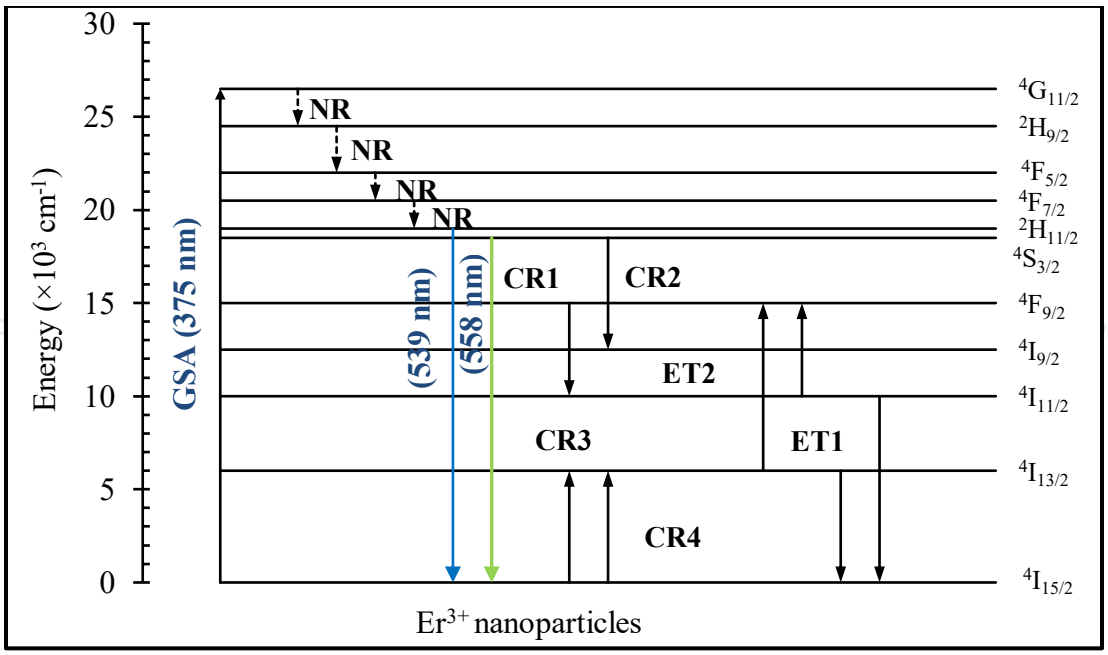


Figure 4.28. Schematic energy levels diagram of Er^{3+} nanoparticles of ZBTEr (NPs)-rGO and ZBTEr (NPs)-uncoated glasses

05-4506832 pustaka.upsi.edu.my Perpustakaan Tuanku Bainun Kampus Sultan Abdul Jalil Shah PustakaTBainun ptbupsi

05-4506832 pustaka.upsi.edu.my Perpustakaan Tuanku Bainun Kampus Sultan Abdul Jalil Shah PustakaTBainun ptbupsi

4.5 Structural Properties of Carbon Nanotubes-coated Tellurite Glass Doped with Erbium Nanoparticles (ZBTEr (NPs)-CNTs)

4.5.1 Field Emission Scanning Electron Microscopy and Energy Dispersive X-ray Analyses of ZBTEr (NPs)-CNTs Glasses

The microstructural and morphological properties of the prepared ZBTEr (NPs)-CNTs glasses were investigated via scanning electron microscopy (SEM), as shown in Figure 4.29 (a) – (d), respectively. It was clearly observed that the CNTs layer was evenly distributed on the glass surfaces which was due to the relatively high homogeneity of CNTs dispersion over the whole region on the glass surfaces. Besides, it can be noted that the interaction between the CNTs coating layer and tellurite-based glass surfaces was probably stronger than that of ZBTEr (NPs)-uncoated glasses due to the CNTs were successfully employed the good distribution for all the ZBTEr (NPs)-CNTs glass samples.

Figure 4.29 (a) reveals the microstructure image of highly twisted CNTs deposited on the ZBTEr (NPs) glass surfaces. From top view observation, it can be seen clearly that the average diameter of the nanotube was determined to be approximately in the range of 8.6 – 8.8 mm, respectively. Meanwhile, Figure 4.29 (b) shows relatively dense agglomerated structures of CNTs on the glass surfaces (refer to dotted line rectangle for clarity). When the CNTs solution was deposited on the glass surfaces, it can be ascribed that the sodium dodecyl sulphate (SDS) surfactant assists the CNTs to disperse well during the dispersion process which is caused by the strong repulsion to inhibit the formation of high CNTs agglomeration (Yanmaz et al., 2021). In addition to this, the inclusion of SDS into the CNTs solution may considerably reduce the strength of van der Waals attraction

05-4506832 pustaka.upsi.edu.my Perpustakaan Tuanku Bainun Kampus Sultan Abdul Jalil Shah PustakaTBainun ptbupsi

05-4506832 pustaka.upsi.edu.my Perpustakaan Tuanku Bainun Kampus Sultan Abdul Jalil Shah PustakaTBainun ptbupsi

forces and thereby, demonstrate a stronger bonding interaction between the CNTs coating layer and tellurite-based glass surfaces.

According to Figure 4.29 (c), it can be noticed that the CNTs deposition onto glass surfaces was inhomogeneous due to the high chemical stability and strong van der Waals forces between the nanotubes (Watt & Gerhardt, 2020). The inhomogeneous distribution of CNTs implied the aggregated nanostructures onto the glass surfaces (refer to dotted line ellipse). When the aggregation structures were formed onto the ZBTEr (NPs)-CNTs glass surfaces thus, it was attributed to a low homogenous deformation, and the obtained individual CNTs that attached on the glass surfaces seemingly to form the folded, unwind or buckle layers.

05-4506832 pustaka.upsi.edu.my Perpustakaan Tuanku Bainun Kampus Sultan Abdul Jalil Shah PustakaTBainun ptbupsi

Besides, the aggregation structures can be explained by the strength of the van der Waals interaction forces which are tightly bound together on the glass surfaces (Bodelot et al., 2019). Nevertheless, the observations mostly accommodate through the aggregation structures which are noticeable as the homogeneity of CNTs coating layer on the ZBTEr (NPs)-CNTs glass surfaces, resulting in a strong possibility for potential applications of glass coatings.

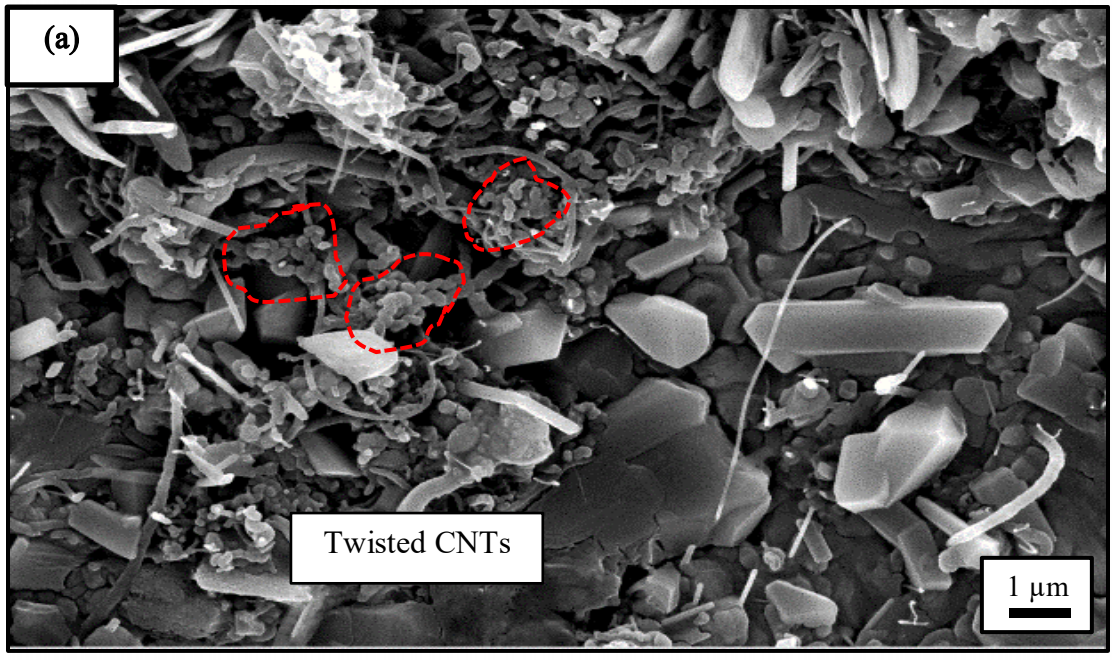
Based on the visual inspection of CNTs layers which tend to attach on the glass surfaces, the SEM image shows a rougher appearance and randomly oriented CNTs rather than forming of a uniform surface, as clearly seen in Figure 4.29 (d). As compared to Figure 4.29 (a) – (c), the surface morphology indicates the uneven surface of CNTs with the

05-4506832 pustaka.upsi.edu.my Perpustakaan Tuanku Bainun Kampus Sultan Abdul Jalil Shah PustakaTBainun ptbupsi

05-4506832 pustaka.upsi.edu.my Perpustakaan Tuanku Bainun Kampus Sultan Abdul Jalil Shah PustakaTBainun ptbupsi

observed several protruded nanotubes that exist on the glass surfaces which can be associated with the successfully stability and adsorption between SDS and CNTs layers and hence, encouraging the thickened layers of CNTs structures. Furthermore, the SDS was the most effective surfactant among other surfactants whereby, the SDS itself may easily adsorb towards CNTs with the existing polar group protruding network and thus, resulting to reduce the surface tension between hydrophobic CNTs and water surface during the dispersion process (Goh et al., 2021). Therefore, it may be concluded that the effects of SDS influenced the CNTs structures on the coated glass surfaces. Overall, these results support that the presence of SDS undoubtedly assists the CNTs in improving the dispersion efficiency which potentially possible to further enhance the new glass coating performance.

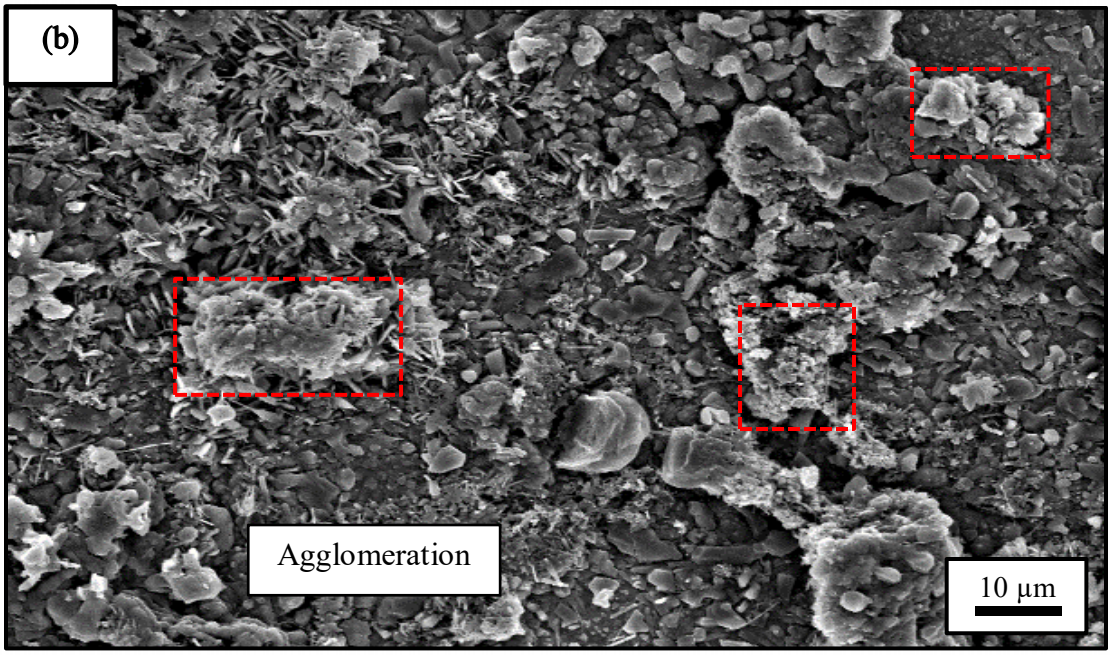
05-4506832 pustaka.upsi.edu.my Perpustakaan Tuanku Bainun Kampus Sultan Abdul Jalil Shah PustakaTBainun ptbupsi

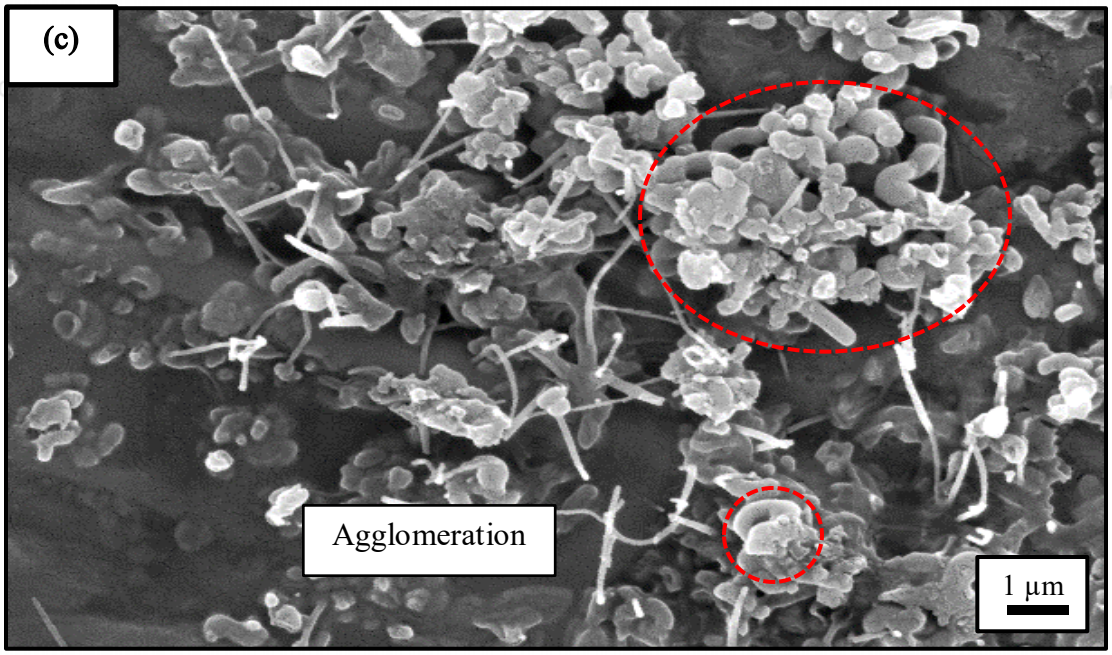


(Continue)

05-4506832 pustaka.upsi.edu.my Perpustakaan Tuanku Bainun Kampus Sultan Abdul Jalil Shah PustakaTBainun ptbupsi

05-4506832 pustaka.upsi.edu.my Perpustakaan Tuanku Bainun Kampus Sultan Abdul Jalil Shah PustakaTBainun ptbupsi





(Continue)

05-4506832 pustaka.upsi.edu.my Perpustakaan Tuanku Bainun Kampus Sultan Abdul Jalil Shah PustakaTBainun ptbupsi

05-4506832 pustaka.upsi.edu.my Perpustakaan Tuanku Bainun Kampus Sultan Abdul Jalil Shah PustakaTBainun ptbupsi

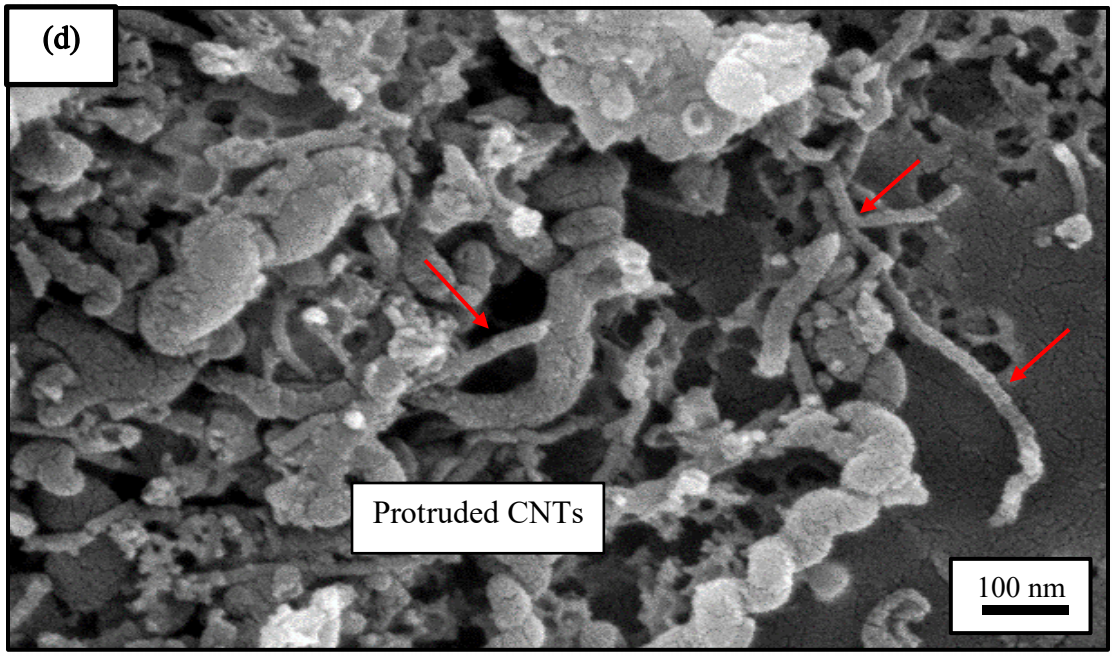


Figure 4.29. SEM micrographs of the ZBTEr (NPs)-CNTs glass showing the different of CNTs nanostructures at 0.04 mol% Er_2O_3 nanoparticles concentration with the magnification of (a), (c) 20 K X, (b) 2 K X, and (d) 50 K X

05-4506832 pustaka.upsi.edu.my Perpustakaan Tuanku Bainun Kampus Sultan Abdul Jalil Shah PustakaTBainun ptbupsi

Figure 4.30 presents the schematic illustration of the CNTs coating layer attached to the ZBTEr (NPs) glass surfaces which were correlated due to a strong electrostatic attraction between the SDS-CNTs and tellurite-based glass surfaces. Other than that, it was believed that the spray coating method helps to attain the close packing of nanotube structures that are fully occupied on the glass surfaces.

05-4506832 pustaka.upsi.edu.my Perpustakaan Tuanku Bainun Kampus Sultan Abdul Jalil Shah PustakaTBainun ptbupsi

05-4506832 pustaka.upsi.edu.my Perpustakaan Tuanku Bainun Kampus Sultan Abdul Jalil Shah PustakaTBainun ptbupsi

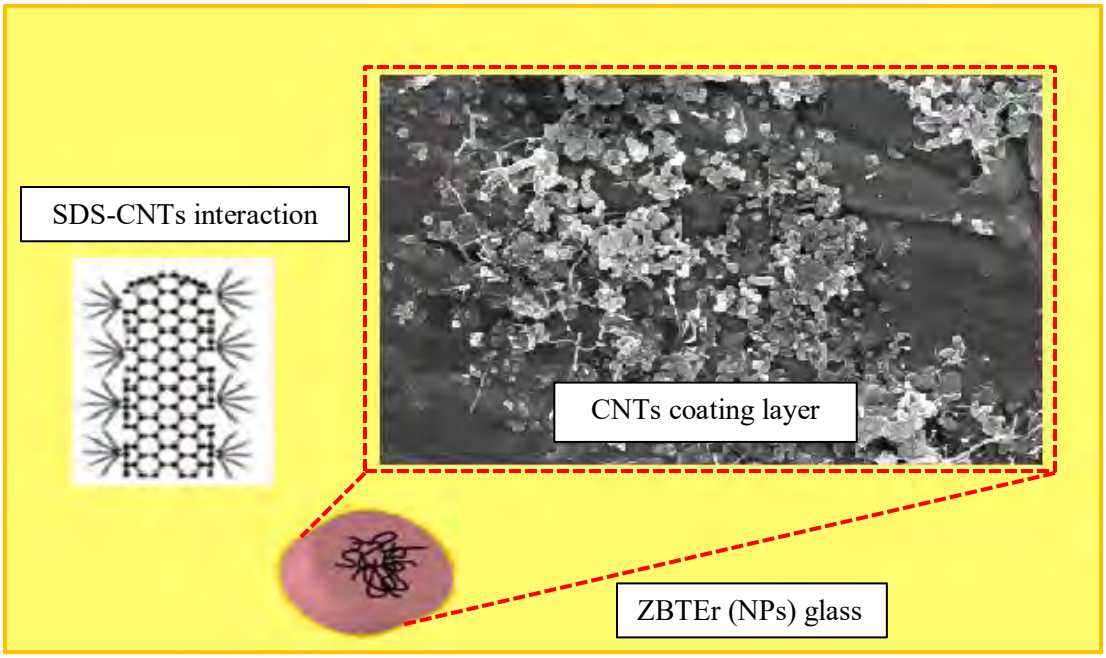


Figure 4.30. Schematic illustration of CNTs layer-coated on the ZBTEr (NPs) glass surfaces

05-4506832 pustaka.upsi.edu.my Perpustakaan Tuanku Bainun Kampus Sultan Abdul Jalil Shah PustakaTBainun ptbupsi

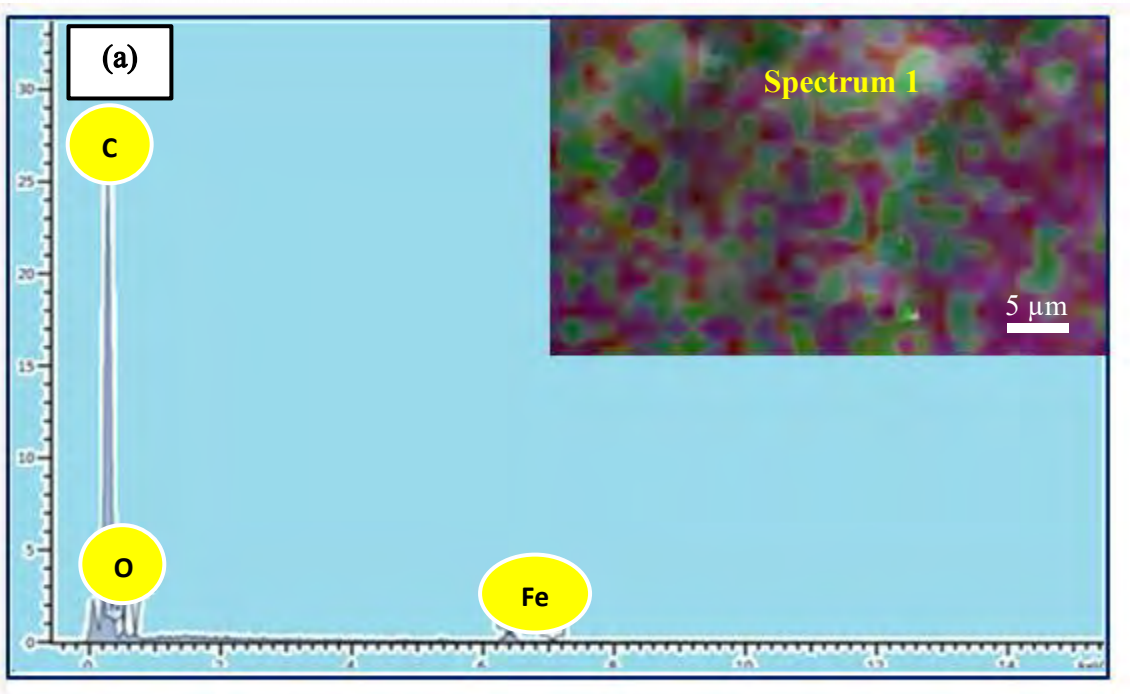
Referring to the morphological analysis of the ZBTEr (NPs)-CNTs glasses, it is important to further confirm the existence of the CNTs layer that is strongly attached on the glass surfaces and thus, these findings were supported by the EDX analysis for detection of any possible elements of the prepared CNTs sample. Furthermore, the respective weight and atomic percentages of the existing elements are presented in Table 4.21 via the EDX scan which was performed randomly on any region area of the CNTs sample, as shown in spectrums 1 and 2, respectively.

From the EDX spectra in Figure 4.31 (a) – (b), it can be clearly seen that the CNTs sample exhibited several possible elements including, carbon (C), oxygen (O), and iron (Fe) with respect to the SEM microstructures. Additionally, it can be noticed that the strong

05-4506832 pustaka.upsi.edu.my Perpustakaan Tuanku Bainun Kampus Sultan Abdul Jalil Shah PustakaTBainun ptbupsi

05-4506832 pustaka.upsi.edu.my Perpustakaan Tuanku Bainun Kampus Sultan Abdul Jalil Shah PustakaTBainun ptbupsi

peak was attributed to the C element comparable to other elements for both EDX spectra. The presence of a trace amount of C has the highest weight percentage estimated in the range of ~18.460 to 21.450 % and subsequently followed by the O element from ~1.740 to 1.830 %, respectively. Meanwhile, the Fe distribution was found higher about ~1.460 % located at spectrum 1 than spectrum 2, whereby the Fe content was about ~1.020 %, respectively.



(Continue)

05-4506832 pustaka.upsi.edu.my Perpustakaan Tuanku Bainun Kampus Sultan Abdul Jalil Shah PustakaTBainun ptbupsi

05-4506832 pustaka.upsi.edu.my Perpustakaan Tuanku Bainun Kampus Sultan Abdul Jalil Shah PustakaTBainun ptbupsi

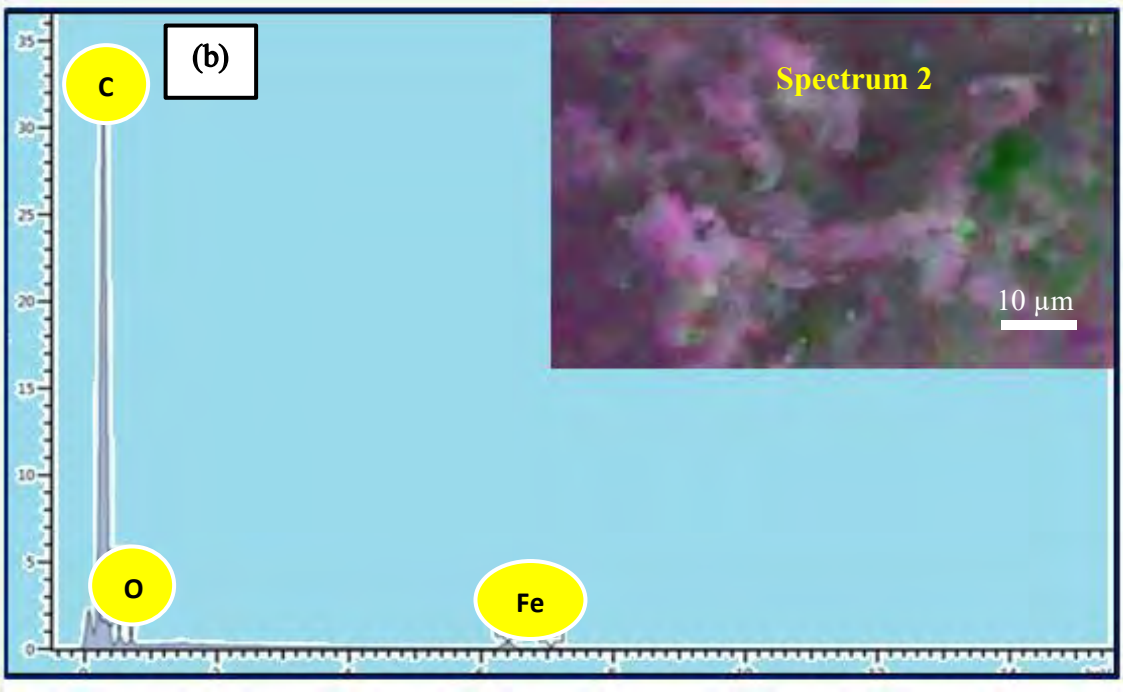


Figure 4.31. The EDX spectra with supported microstructure images of the ZBTEr (NPs)-CNTs glass surfaces followed by two different regions at (a) 5 µm and (b) 10 µm

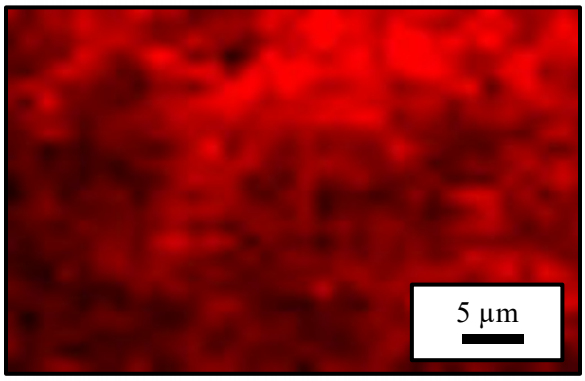
05-4506832 pustaka.upsi.edu.my Perpustakaan Tuanku Bainun Kampus Sultan Abdul Jalil Shah PustakaTBainun ptbupsi

According to the results of EDX elemental composition as outlined above, the observation of EDX maps for all the existing elements such as C, O, and Fe was consistent with the weight percentages, as illustrated in Figure 4.32 (a) – (c). Consequently, it can be confirmed that the existence of CNTs by the presence of all elements in this work.

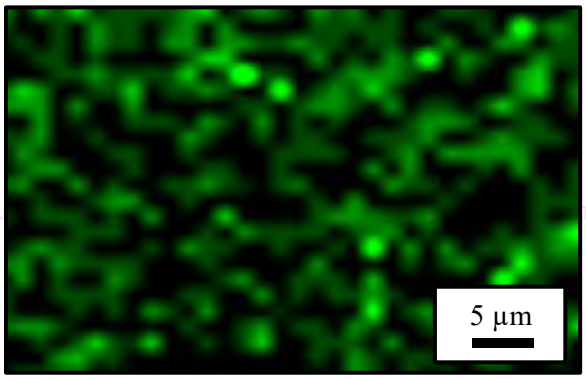
05-4506832 pustaka.upsi.edu.my Perpustakaan Tuanku Bainun Kampus Sultan Abdul Jalil Shah PustakaTBainun ptbupsi

05-4506832 pustaka.upsi.edu.my Perpustakaan Tuanku Bainun Kampus Sultan Abdul Jalil Shah PustakaTBainun ptbupsi

(a) C Kα1_2



(b) Fe Kα1_2



(c) O Kα1_2

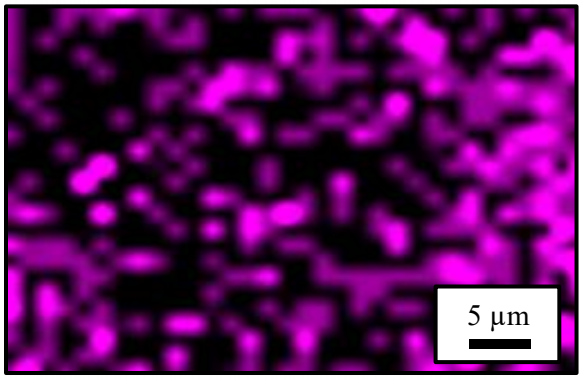


Figure 4.32. The EDX elemental mappings of (a) carbon (C), (b) iron (Fe), and (c) oxygen (O) with the magnification of 20 K X

05-4506832 pustaka.upsi.edu.my Perpustakaan Tuanku Bainun Kampus Sultan Abdul Jalil Shah PustakaTBainun ptbupsi

05-4506832 pustaka.upsi.edu.my Perpustakaan Tuanku Bainun Kampus Sultan Abdul Jalil Shah PustakaTBainun ptbupsi

Table 4.21

The weight and atomic percentages, % of elements content with the different spectrum of CNTs solution sample

Regions	Elements	Weight %	Atomic %
Spectrum 1	C K	18.460	76.770
	O K	1.740	5.440
	Fe K	1.460	1.300
Spectrum 2	C K	21.450	81.080
	O K	1.830	5.200
	Fe K	1.020	0.830

05-4506832 pustaka.upsi.edu.my Perpustakaan Tuanku Bainun Kampus Sultan Abdul Jalil Shah PustakaTBainun ptbupsi

4.5.2 Micro-Raman Analysis of CNTs

The micro-Raman spectrum of the pristine CNTs presents three prominent characteristic peaks namely, the D-, G-, and G'-peaks which clearly presented, as depicted in Figure 4.33. The D-peak is located approximately at 1346 cm^{-1}, which was attributed to the disorder caused by the defects. Meanwhile, the G-peak is located approximately at 1579 cm^{-1}, was due to the in-plane vibration that exists in the graphite lattice (Piao et al., 2021). In addition, the pristine CNTs exhibit the G'-peak located around 2696 cm^{-1}, which is the lower peak comparable with the D- and G-peaks indicating the higher defects in the sample.

05-4506832 pustaka.upsi.edu.my Perpustakaan Tuanku Bainun Kampus Sultan Abdul Jalil Shah PustakaTBainun ptbupsi

05-4506832 pustaka.upsi.edu.my Perpustakaan Tuanku Bainun Kampus Sultan Abdul Jalil Shah PustakaTBainun ptbupsi

Based on these results, the intensity was found higher in the D- and G-peaks region than in the G' region whereby, the G' intensity was utilized in order to indicate the existence of CNTs. Noticeably, the intensities of D-, G-, and G'- peaks are gradually decreased along with the increase of wavelength in the CNTs sample. Furthermore, the calculated I_D/I_G ratio of pristine CNTs shows a higher value of 1.10 which is, conversely to the previous studies. It was noted that the higher value of the I_D/I_G ratio demonstrates the low crystallinity of the sample thereby, may attribute to the presence of the large amount of amorphous carbon and defects that exist in the CNTs sample. This result indicates that the poor crystallinity of CNTs resulted from the large agglomeration produced in the CNTs sample. The micro-Raman peaks position of the as-prepared CNTs sample is summarized in Table 4.22.

05-4506832 pustaka.upsi.edu.my Perpustakaan Tuanku Bainun Kampus Sultan Abdul Jalil Shah PustakaTBainun ptbupsi

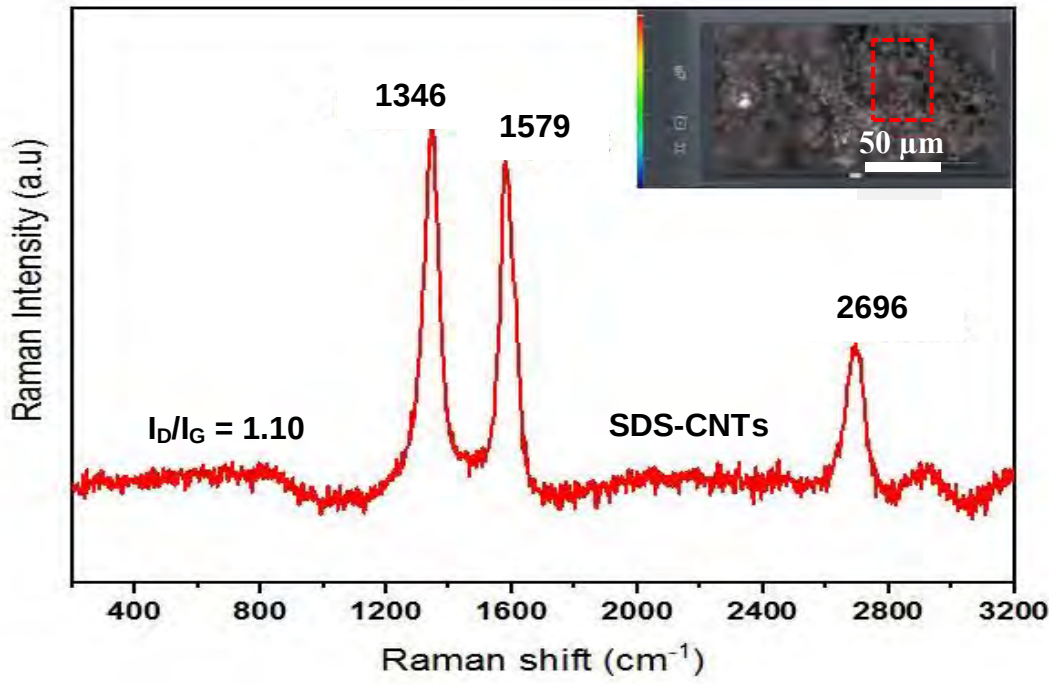


Figure 4.33. Micro-Raman spectra of CNTs with supported microstructure image of the ZBTEr (NPs)-CNTs glass surfaces at 50 µm

05-4506832 pustaka.upsi.edu.my Perpustakaan Tuanku Bainun Kampus Sultan Abdul Jalil Shah PustakaTBainun ptbupsi

05-4506832 pustaka.upsi.edu.my Perpustakaan Tuanku Bainun Kampus Sultan Abdul Jalil Shah PustakaTBainun ptbupsi

Table 4.22

Micro-Raman peaks position and I_D/I_G ratio of CNTs sample

Sample	D-peak (cm^{-1})	G-peak (cm^{-1})	G'-peak (cm^{-1})	I_D/I_G ratio
CNTs	1346	1579	2696	1.10

4.6 Optical Properties of Carbon Nanotubes-coated Tellurite Glass Doped with Erbium Nanoparticles (ZBTEr (NPs)-CNTs)

4.6.1 Optical Absorption Spectra

05-4506832 pustaka.upsi.edu.my Perpustakaan Tuanku Bainun Kampus Sultan Abdul Jalil Shah PustakaTBainun ptbupsi

The optical characterization via UV-Vis spectroscopy was carried out to investigate the optical properties of the ZBTEr (NPs)-CNTs glass matrix. Figure 4.34 shows the typical optical absorption spectra of ZBTEr (NPs)-CNTs glasses in the range of 300 – 800 nm with the existing absorption bands in various wavelengths. It can be seen the absorption bands demonstrated the characteristics of Er^{3+} nanoparticles arise from the ground state level to the level of the excited states. The obtained optical absorption edge is not sharply defined in the glass matrix system due to the characteristics of the amorphous structural network, as presented by the XRD pattern (refer to Figure 4.4) which has been described in subsection 4.2.3.

05-4506832 pustaka.upsi.edu.my Perpustakaan Tuanku Bainun Kampus Sultan Abdul Jalil Shah PustakaTBainun ptbupsi

05-4506832 pustaka.upsi.edu.my Perpustakaan Tuanku Bainun Kampus Sultan Abdul Jalil Shah PustakaTBainun ptbupsi

The optical absorption spectra of ZBTEr (NPs)-CNTs glasses consist of several absorption bands which are indicated relatively from the ground state level, $^4G_{11/2}$ to the several levels of the excited states which are as follows: ($^2H_{9/2}$ + $^4F_{5/2}$ + $^4F_{7/2}$ + $^2H_{11/2}$ + $^4S_{3/2}$ + $^4F_{9/2}$ + $^4I_{11/2}$ + $^4I_{9/2}$) with the absorption positions of various wavelengths located at 87, 522, 550, and 652 nm, respectively. These results clearly indicated the 4*f* shell electrons that are fortified with the outer 5*s* and 5*p* bonding electrons and lead to sharp absorption and emission bands. Furthermore, the characteristics of absorption edge that exists in the ZBTEr (NPs)-CNTs glass were shifted to the longer wavelength along with the increase of Er^{3+} nanoparticles concentration and thereby, may lead to less rigidity of the amorphous glass matrix.

In comparison, the shifted optical absorption spectra of the ZBTEr (NPs)-CNTs glasses can be ascribed to the effect of the electronic transitions between the two energy levels whereby, the nanotube functionalization may alter the optical absorption of the ZBTEr (NPs)-CNTs glasses than ZBTEr (NPs)-uncoated glasses, as shown in Figure 4.35. In particular, the presence of functionalization via π-π interactions caused by the π-π stacking that exists on the CNTs and non-polar molecules containing the aromatic rings or known as C=C bonds may attribute to control the optical absorption characteristics in the ZBTEr (NPs)-CNTs glasses. Moreover, the strong of π-π electrostatic interactions assisted with the functionalized CNTs demonstrate the highly favorable as compared to other interactions which in turn, may attribute to the enhancement of optical absorption in the amorphous matrix system. The increased interaction energy which was due to the easy

05-4506832 pustaka.upsi.edu.my Perpustakaan Tuanku Bainun Kampus Sultan Abdul Jalil Shah PustakaTBainun ptbupsi

05-4506832 pustaka.upsi.edu.my Perpustakaan Tuanku Bainun Kampus Sultan Abdul Jalil Shah PustakaTBainun ptbupsi

formation of offset π-π stacking may be considered to achieve the highly covalent bonding that was composed entirely of sp^2 bonds that existed on the tubular CNTs.

The association between the CNTs nanostructures and tellurite-based glasses demonstrates the more π-π stacking and thus, creating a better coating effect on the ZBTEr (NPs) glass surfaces. Additionally, the photon absorbance of ZBTEr (NPs)-CNTs glasses was greatly affected by the strong interaction between the graphitic CNTs and tellurite-based glass surfaces. These results attribute to more photons scattered during the coating process and thus, loss of more energy was attributed to a shift of absorption spectra of the ZBTEr (NPs)-CNTs glasses.

Additionally, the performance of ZBTEr (NPs)-CNTs glasses possessed a high absorbance value which was reasonable due to the influence of intra-band and inter-band processes that exist in the CNTs nanostructures. Therefore, CNTs are among the promising materials with their ability especially, to generate high performance of glass coatings production.

Additionally, the CNTs functionalization was another important factor for the shift in the optical absorption of the ZBTEr (NPs)-CNTs glasses. These results were indicated by the van der Waals force which occurs in the electrostatic interaction, the individual nanotubes are reduced via the functionalization on the surface and thus, these modified nanostructures of CNTs may attribute to the changes of optical absorption shift in the ZBTEr (NPs)-CNTs glasses. It was noted that the π-tight bonds attached on the CNTs

05-4506832 pustaka.upsi.edu.my Perpustakaan Tuanku Bainun Kampus Sultan Abdul Jalil Shah PustakaTBainun ptbupsi

05-4506832 pustaka.upsi.edu.my Perpustakaan Tuanku Bainun Kampus Sultan Abdul Jalil Shah PustakaTBainun ptbupsi

surface can be correlated to improve the optical absorption in the ZBTEr (NPs)-CNTs glass system.

In summary, it can be noticed that these findings show the improvement in the optical absorption spectra of the ZBTEr (NPs)-CNTs glasses compared to the ZBTEr (NPs)-uncoated glasses. Hence, this work demonstrates a good bonding interaction between the CNTs layer and tellurite-based glass surfaces to further improve the optical characteristics of the glass materials.

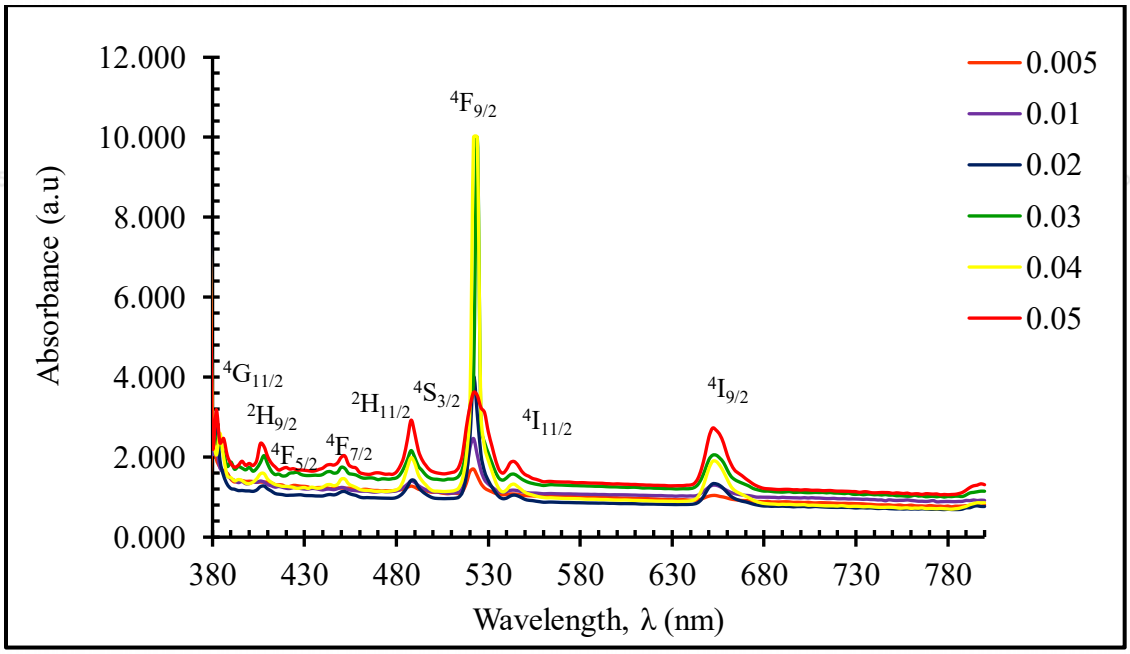


Figure 4.34. Optical absorption spectra of ZBTEr (NPs)-CNTs glasses

05-4506832 pustaka.upsi.edu.my Perpustakaan Tuanku Bainun Kampus Sultan Abdul Jalil Shah PustakaTBainun ptbupsi

05-4506832 pustaka.upsi.edu.my Perpustakaan Tuanku Bainun Kampus Sultan Abdul Jalil Shah PustakaTBainun ptbupsi

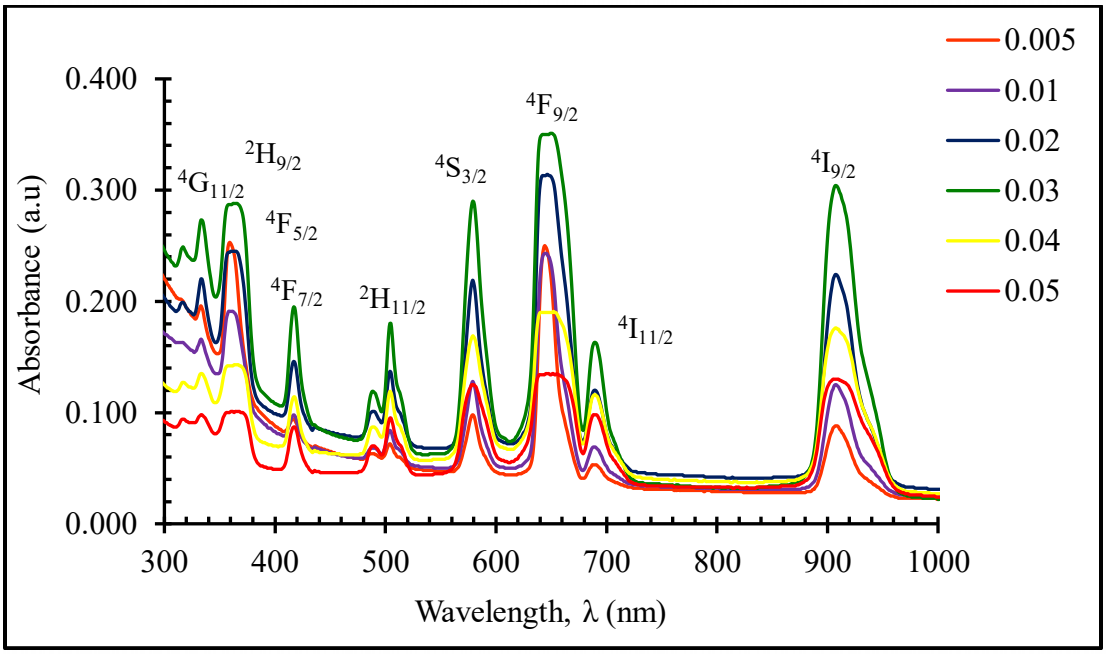


Figure 4.35. Optical absorption spectra of ZBTEr (NPs)-uncoated glasses (Azlan, Halimah, Shafinas, et al., 2015)

05-4506832 pustaka.upsi.edu.my Perpustakaan Tuanku Bainun Kampus Sultan Abdul Jalil Shah PustakaTBainun ptbupsi

4.6.2 Optical Bandgap Energy

Further optical properties of the ZBTEr (NPs)-CNTs glasses were studied to determine the optical bandgap energy via a Tauc's plot graph consisting of the photon energy, $\hbar\omega$ against optical bandgap energy, $\alpha\hbar\omega$ as depicted in Figure 4.36. Importantly, the optical bandgap energy value can be calculated based on the absorbance spectra and thus, extrapolating the linear part of the curves to obtain the optical bandgap energy value by applying the given Equations 2.10 and 2.11, respectively which have been described in subsection 2.13.2.

According to Figure 4.37, it was clearly observed that the optical bandgap energy displayed a non-linear trend along with Er_2O_3 nanoparticles concentration in the range of

05-4506832 pustaka.upsi.edu.my Perpustakaan Tuanku Bainun Kampus Sultan Abdul Jalil Shah PustakaTBainun ptbupsi

05-4506832 pustaka.upsi.edu.my Perpustakaan Tuanku Bainun Kampus Sultan Abdul Jalil Shah PustakaTBainun ptbupsi

2.513 – 2.875 eV. This presented trend can be associated with the shift in optical absorption by the effects of CNTs nanolayers on top of the ZBTEr (NPs) glass surfaces, as clearly proved in Figure 4.34. The characteristics of relatively broad absorption of highly quality CNTs were allowed to investigate the optical bandgap energy in the ZBTEr (NPs)-CNTs glasses.

In similar work to previous ZBTEr (NPs)-rGO glass system, it can be noticed that the CNTs nanostructures may efficiently improve the optical bandgap energy value that exists in the ZBTEr (NPs)-CNTs glasses as compared to the ZBTEr (NPs)-uncoated glasses. As can be referred to Table 4.23, the improved value of optical bandgap energy was clearly presented along with the increase of Er_2O_3 nanoparticles concentration in the ZBTEr (NPs)-CNTs glass system which can be understood in terms of the structural rearrangement that takes place as the CNTs layer attached on the glass surfaces. Nevertheless, the trend of ZBTEr (NPs)-CNTs glass system exhibited a higher optical bandgap energy value at 0.05 mol% which attributes to a higher content of homogeneity of CNTs distribution during the spray coating technique. This effect is eventually caused due to the change of electronic transitions between the valence and conduction band's edges from each other and leads to the increment of bandgap energy.

05-4506832 pustaka.upsi.edu.my Perpustakaan Tuanku Bainun Kampus Sultan Abdul Jalil Shah PustakaTBainun ptbupsi

05-4506832 pustaka.upsi.edu.my Perpustakaan Tuanku Bainun Kampus Sultan Abdul Jalil Shah PustakaTBainun ptbupsi

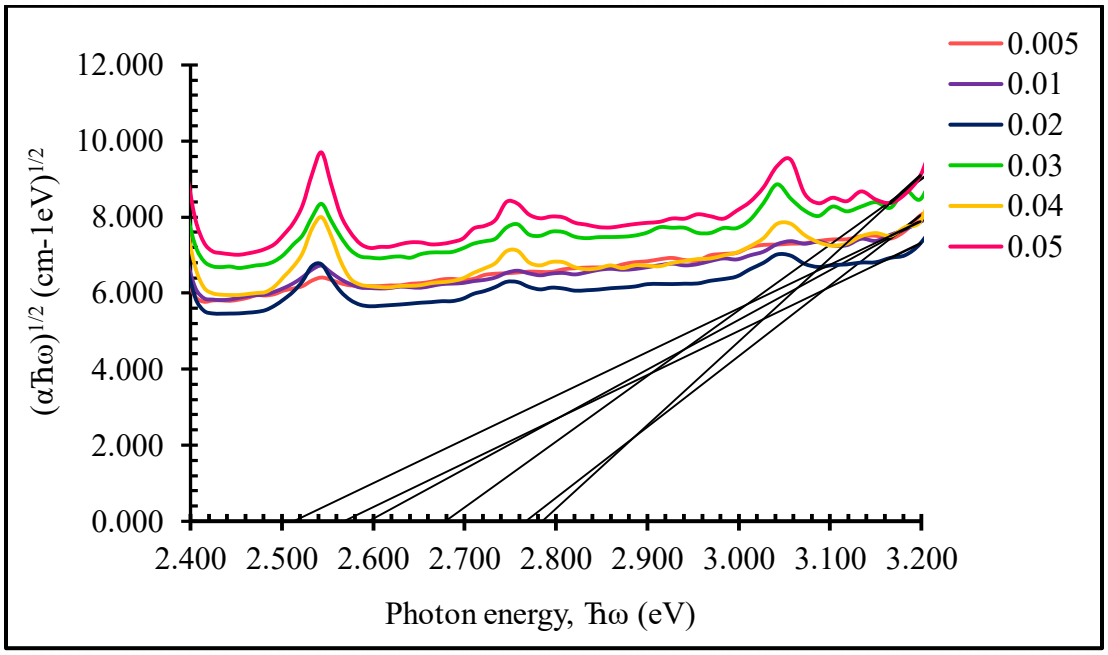


Figure 4.36. Tauc's plot of $(\alpha\hbar\omega)^{1/2}$ against photon energy, ħω of ZBTEr (NPs)-CNTs glasses

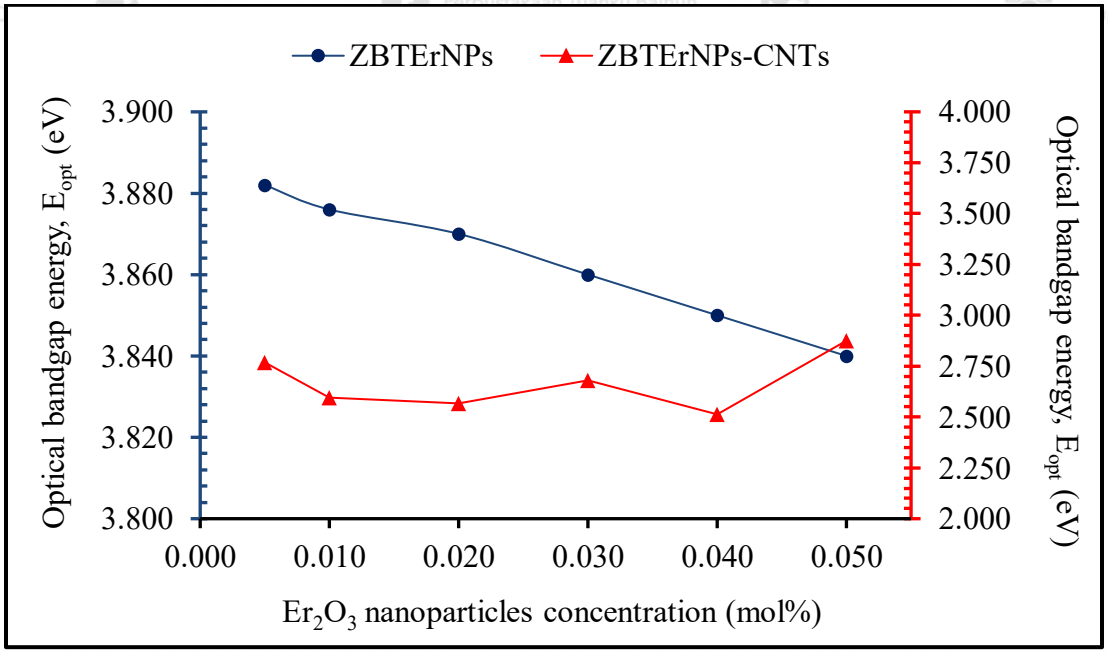


Figure 4.37. Variation of optical bandgap energy as a function of Er_2O_3 nanoparticles concentration for ZBTEr (NPs)-uncoated and ZBTEr (NPs)-CNTs glasses

05-4506832 pustaka.upsi.edu.my Perpustakaan Tuanku Bainun Kampus Sultan Abdul Jalil Shah PustakaTBainun ptbupsi

05-4506832 pustaka.upsi.edu.my Perpustakaan Tuanku Bainun Kampus Sultan Abdul Jalil Shah PustakaTBainun ptbupsi

Table 4.23

Comparison of optical bandgap energy (E_{opt}) value between ZBTEr (NPs)-uncoated and ZBTEr (NPs)-CNTs glasses

Er_2O_3 nanoparticles concentration (mol%)	Optical bandgap energy, $\boldsymbol{E_{opt}}$ (eV) (±0.100)
ZBTEr (NPs)-uncoated	
0.005	3.882
0.010	3.876
0.020	3.870
0.030	3.860
0.040	3.850
0.050	3.840
ZBTEr (NPs)-CNTs	
0.005	2.767
0.010	2.595
0.020	2.568
0.030	2.679
0.040	2.513
0.050	2.875

05-4506832 pustaka.upsi.edu.my Perpustakaan Tuanku Bainun Kampus Sultan Abdul Jalil Shah PustakaTBainun ptbupsi

05-4506832 pustaka.upsi.edu.my Perpustakaan Tuanku Bainun Kampus Sultan Abdul Jalil Shah PustakaTBainun ptbupsi

Generally, the optical bandgap energy of the ZBTEr (NPs)-CNTs glasses relatively possessed low bandgap energy values at 0.02 and 0.04 mol% Er_2O_3 nanoparticles concentration due to the lowest absorbance value, as indicated from the previous optical absorbance spectra (refer to Figure 4.34). Other than that, the high degree amount of CNTs composition was affected the coated-glass samples which caused by the electronic interactions between the CNTs and tellurite-based glass surfaces via physical contact. The previous work showed that the ZBTEr (NPs)-uncoated glasses exhibited a higher optical bandgap energy ranging from 3.840 – 3.882 eV (Azlan, Halimah, Shafinas, et al., 2015).

In contrast, the reduction of optical bandgap energy in the ZBTEr (NPs)-CNTs glasses was believed due to the tunable band structures of CNTs which offer the potential candidates for use in optoelectronic devices (Qian et al., 2020). The calculated optical bandgap energy values of ZBTEr (NPs)-CNTs glasses can be correlated to the electron-photon assisted transition with the existing excitons state of nanotubes. These localized excitons generated with high binding energy acted as electron traps which possibly reduce the bandgap energy between the conduction and valence bands of the ZBTEr (NPs)-CNTs glasses, as illustrated in Figure 4.38.

The deposition of CNTs on the ZBTEr (NPs) glass surfaces exhibits the strong electron-phonon coupling (C-C stretching mode) that contributes high binding energies to the localized excitons (Perebeinos et al., 2005). This can be ascribed to the electron traps that filled the conduction band (CB)-valence band (VB) gap with the occupied electrons and thereby, leading to the closing of the gap, and electrons require less energy to move

05-4506832 pustaka.upsi.edu.my Perpustakaan Tuanku Bainun Kampus Sultan Abdul Jalil Shah PustakaTBainun ptbupsi

05-4506832 pustaka.upsi.edu.my Perpustakaan Tuanku Bainun Kampus Sultan Abdul Jalil Shah PustakaTBainun ptbupsi

from valence to conduction band. Last but not least, all the ZBTEr (NPs)-CNTs glass samples induced great optical bandgap energy which attributes to the highly semiconductor properties of the material.

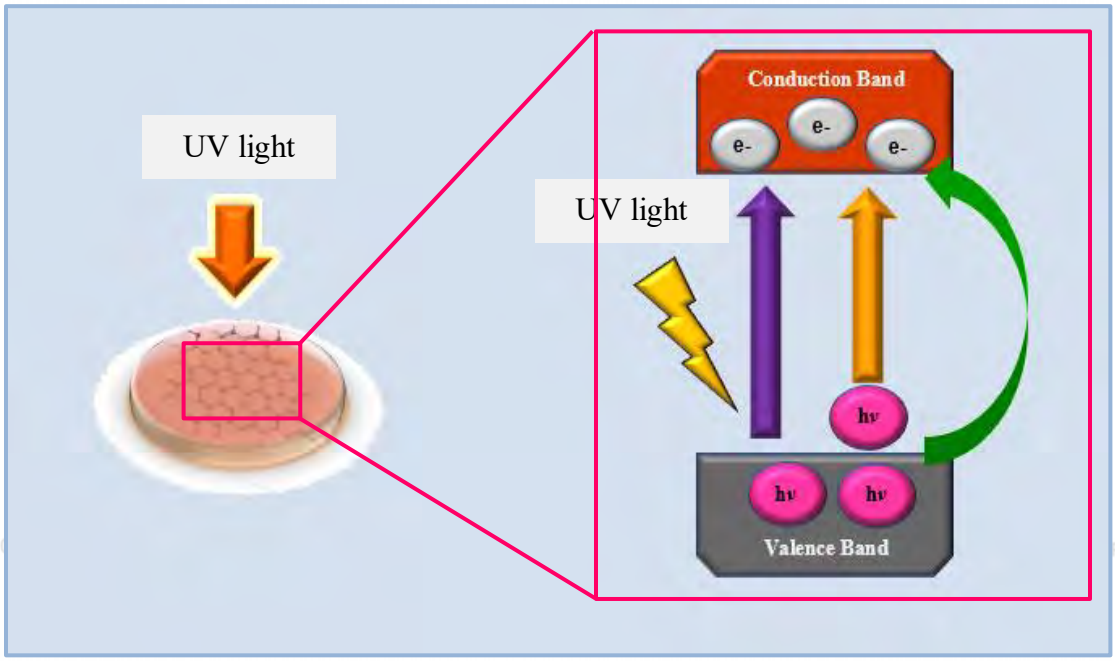


Figure 4.38. The possible mechanism of photon excitation on the ZBTEr (NPs)-CNTs glass system with the presence of UV light leading to the excitation of electrons from valence band (VB) to conduction band (CB)

Based on the aforementioned as stated earlier, the chirality and diameter of CNTs critically influence the optical characteristics in the ZBTEr (NPs)-CNTs glasses whereby, the specific electronic band structure located at the Brillouin zone (BZ) can be directly improved the optical bandgap energy through the crossed valence and conduction bands, resulting to the semiconducting properties (Khosravi et al., 2021). In addition, it can be

05-4506832 pustaka.upsi.edu.my Perpustakaan Tuanku Bainun Kampus Sultan Abdul Jalil Shah PustakaTBainun ptbupsi

05-4506832 pustaka.upsi.edu.my Perpustakaan Tuanku Bainun Kampus Sultan Abdul Jalil Shah PustakaTBainun ptbupsi

observed that intense optical absorption occurred when the incident photon energy corresponds to the energy differences between the valence and conduction bands.

The reduction of optical bandgap energy value in the ZBTEr (NPs)-CNTs glasses can be related to the chemical functionalization of CNTs whereby, the absorbance intensity of the ZBTEr (NPs)-CNTs glasses improved owing to the strong interaction ability between the CNTs coating layer and glass surfaces, particularly demonstrating the excellent stability of the ZBTEr (NPs)-CNTs glass coating.

In conclusion, it can be summarized that the ZBTEr (NPs)-CNTs glass with 0.05 mol% of Er_2O_3 nanoparticles concentration sample shows a higher bandgap energy value of 2.875 eV than the other CNTs-coated glass samples. Consequently, the wide-band gap in the material allows for the reduction of the loss of energy and thus, making it the optimal material for fiber optics.

4.6.3 Urbach Energy

The Urbach energy, ΔE can be characterized as a degree of disorderliness in an amorphous or crystalline solid material (Divina et al., 2019). Particularly, glass materials mostly possess high Urbach energy values and have the tendency to convert weak bonds into defects. Therefore, the Urbach energy can be obtained by taking the reciprocal slope of the linear portion in the lower photon energy based on the plotted graph between the logarithm

05-4506832 pustaka.upsi.edu.my Perpustakaan Tuanku Bainun Kampus Sultan Abdul Jalil Shah PustakaTBainun ptbupsi

05-4506832 pustaka.upsi.edu.my Perpustakaan Tuanku Bainun Kampus Sultan Abdul Jalil Shah PustakaTBainun ptbupsi

of absorption coefficient, log (α) and function of photon energy, ħω curves (refer to Figure 4.39) by using the given Equation 2.12 which has been described in subsection 2.13.3.

Figure 4.40 shows the variation of Urbach energy value of the ZBTEr (NPs)-CNTs glasses which demonstrated a non-linear trend ranging from 0.158 – 0.375 eV, which is higher than the ZBTEr (NPs)-uncoated glasses. As can be seen in Table 4.24, the ZBTEr (NPs)-CNTs glass at 0.005 mol% of Er_2O_3 nanoparticles concentration (0.375 eV) exhibited a higher value of Urbach energy among the other samples which reflects the growing number of defects and thus, enabling the higher tendency of the glass materials to change the weak bonds into the structural defects in the ZBTEr (NPs)-CNTs glass system. Additionally, it can be noted that the high amount of CNTs layers consisting of a large agglomeration structure on the glass surfaces were possibly affected by the high defects in the glass matrix, as clearly proved by FESEM analysis (refer to Figures 4.29 (b) and (c)), respectively as has been stated in subsection 4.5.1.

Other than that, it was revealed that a non-linear trend of the Urbach energy values along with the increase of Er^{3+} nanoparticles of the ZBTEr (NPs)-CNTs glasses can be correlated to the change in the optical absorption characteristics, which has been presented in Figure 4.34. Referring to Figure 4.40, it can be clearly seen that the variation of Urbach energy values can be ascribed to the different number of defects in CNTs layers for the ZBTEr (NPs)-CNTs glasses surface. As a result, these CNTs layers that are attached to the glass surfaces consist with a large number of twisted nanotubes and agglomerated structures which strongly attribute to the high defects in the ZBTEr (NPs)-CNTs glasses.

05-4506832 pustaka.upsi.edu.my Perpustakaan Tuanku Bainun Kampus Sultan Abdul Jalil Shah PustakaTBainun ptbupsi

05-4506832 pustaka.upsi.edu.my Perpustakaan Tuanku Bainun Kampus Sultan Abdul Jalil Shah PustakaTBainun ptbupsi

Apart from that, the deposition of CNTs onto the ZBTEr (NPs) glass surfaces was found to enhance the Urbach energy in the amorphous materials which correspond to the localized band tail states. The existence of forbidden bandgap energy occurred when the atoms move from one energy state to another energy level between the valence and conduction bands existing in the optical transitions (Singh et al., 2019). Consequently, it was found that the increment of Urbach energy value was influenced by the higher degree of defects of structural bonding and contributed more to the existence of non-bridging oxygens (NBOs). Thus, it was summarized that the CNTs improve the Urbach energy in the amorphous materials, resulting in the interaction between the CNTs coating layer and tellurite-based glass surfaces.

05-4506832 pustaka.upsi.edu.my Perpustakaan Tuanku Bainun Kampus Sultan Abdul Jalil Shah PustakaTBainun ptbupsi
05-4506832 pustaka.upsi.edu.my Perpustakaan Tuanku Bainun Kampus Sultan Abdul Jalil Shah PustakaTBainun ptbupsi

05-4506832 pustaka.upsi.edu.my Perpustakaan Tuanku Bainun Kampus Sultan Abdul Jalil Shah PustakaTBainun ptbupsi

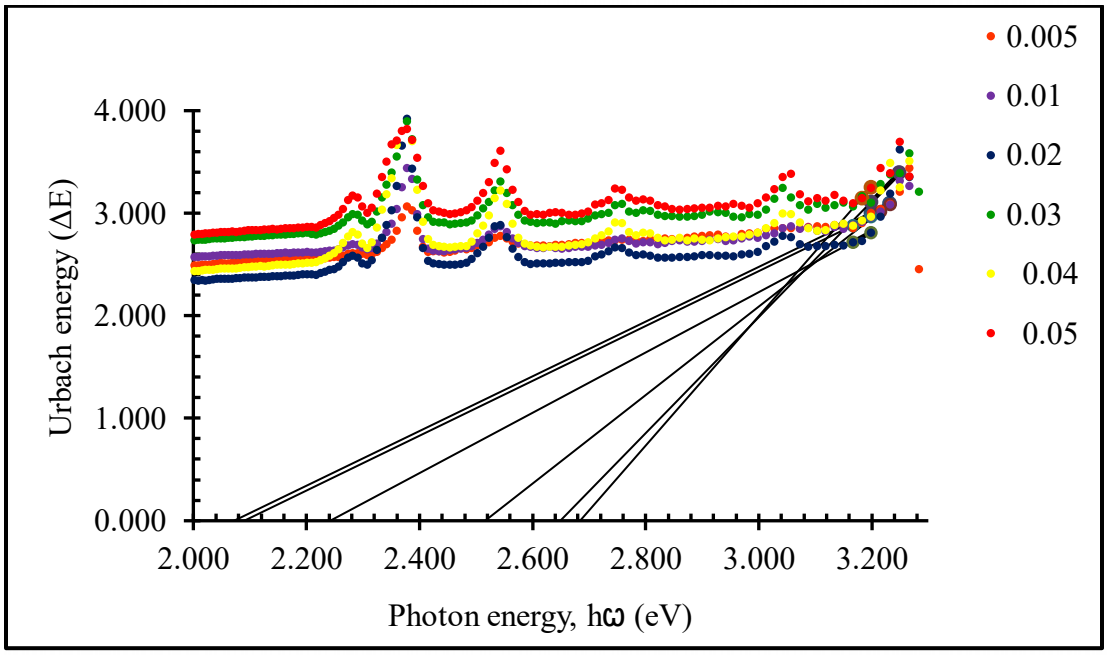


Figure 4.39. Plotted graph of log (α) against photon energy, $\hbar\omega$ of ZBTEr (NPs)-CNTs glasses

05-4506832 pustaka.upsi.edu.my Perpustakaan Tuanku Bainun Kampus Sultan Abdul Jalil Shah PustakaTBainun ptbupsi

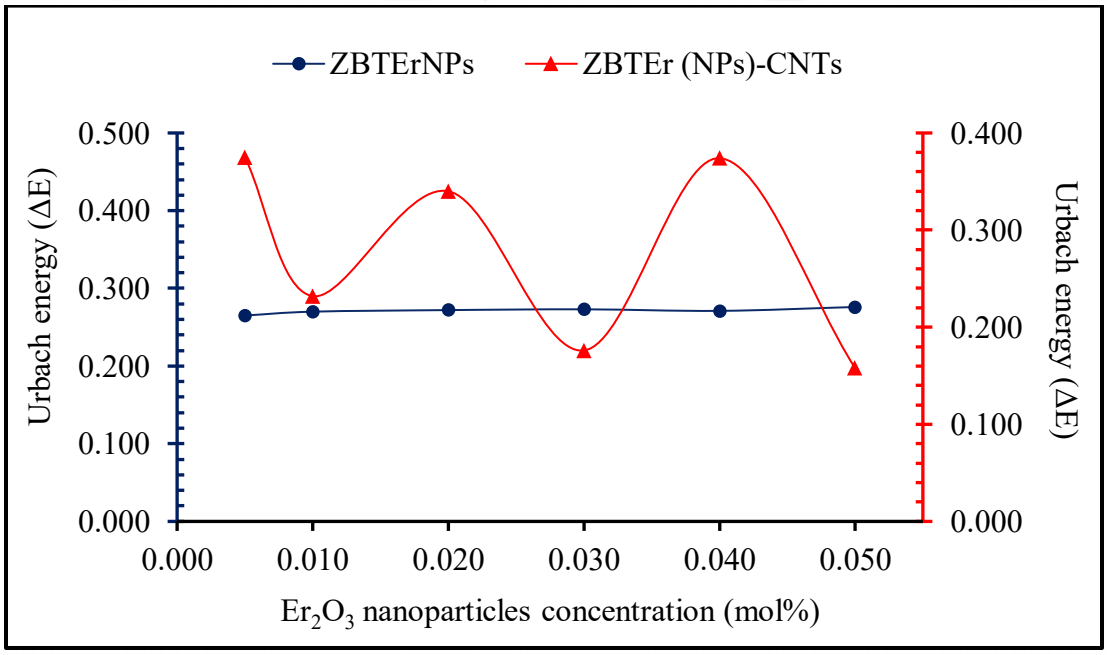


Figure 4.40. Variation of Urbach energy as a function of Er_2O_3 nanoparticles concentration for ZBTEr (NPs)-uncoated and ZBTEr (NPs)-CNTs glasses

05-4506832 pustaka.upsi.edu.my Perpustakaan Tuanku Bainun Kampus Sultan Abdul Jalil Shah PustakaTBainun ptbupsi

05-4506832 pustaka.upsi.edu.my Perpustakaan Tuanku Bainun Kampus Sultan Abdul Jalil Shah PustakaTBainun ptbupsi

Table 4.24

Comparison of Urbach energy (ΔE) value between ZBTEr (NPs)-uncoated and ZBTEr (NPs)-CNTs glasses

Er_2O_3 nanoparticles concentration (mol%)	Urbach energy, Δ*E* (eV) (±0.100)
ZBTEr (NPs)-uncoated	
0.005	0.265
0.010	0.270
0.020	0.272
0.030	0.273
0.040	0.271
0.050	0.276
ZBTEr (NPs)-CNTs	
0.005	0.375
0.010	0.232
0.020	0.340
0.030	0.176
0.040	0.374
0.050	0.158

05-4506832 pustaka.upsi.edu.my Perpustakaan Tuanku Bainun Kampus Sultan Abdul Jalil Shah PustakaTBainun ptbupsi

05-4506832 pustaka.upsi.edu.my Perpustakaan Tuanku Bainun Kampus Sultan Abdul Jalil Shah PustakaTBainun ptbupsi

4.6.4 Refractive Index

The refractive index data can be used to determine the capability of the glasses in optoelectronics devices and in various optical applications, specifically in the optical fiber and laser. Typically, it was found that the refractive index of the ZBTEr (NPs)-CNTs glasses can be calculated by using the given Equation 2.13 that has been described in subsection 2.13.4.

Figure 4.41 shows the ZBTEr (NPs)-CNTs glasses exhibited the increasing trend of refractive index with approximately in the range of 2.432 – 2.542, as compared to the ZBTEr (NPs)-uncoated glasses. It can be concluded that the CNTs coating may improve the refractive index value due to the that the light energy was excited by the CNTs coating layer to the cladding and then, may interact with the glass surfaces thoroughly, which results in the improvement of refractive index in the ZBTEr (NPs)-CNTs glasses.

Nevertheless, the CNTs coating may absorb more light energy whereby, some of the light cannot be returned back which limits the interaction between the CNTs coating layer and tellurite-based glass surfaces and thus, strengthening the refractive index stability in the ZBTEr (NPs)-CNTs glasses. According to Zhang et al., (2018), the cladding structure part in the optical fiber will have the changes of refractive index by affecting the propagation of light inside the fiber directly, which means that the refractive index of the multiple modes is changed. These changes may bring the light wave energy to redistribute

05-4506832 pustaka.upsi.edu.my Perpustakaan Tuanku Bainun Kampus Sultan Abdul Jalil Shah PustakaTBainun ptbupsi

05-4506832 pustaka.upsi.edu.my Perpustakaan Tuanku Bainun Kampus Sultan Abdul Jalil Shah PustakaTBainun ptbupsi

that may cause the movement of the interference spectrum to alter the changes in the surrounding refractive index.

Meanwhile, the effect of CNTs coating on the obtained data of refractive index of the ZBTEr (NPs)-CNTs glasses was effectively correlated to CNTs density due to the highly anisotropic nanoscale structures of CNTs, as tabulated in Table 4.25. The previous studies reported that many attempts were investigated to control the CNTs density for modification of refractive index which is useful for further optical applications (Park et al., 2018). It can be observed that the CNTs have the ability to tune the refractive index value and thus, leading to a direct proportionality between the refractive index value and density in the present work. Nonetheless, the relationship was not linearly increase but showed a slight decrease at 0.05 mol% of Er_2O_3 nanoparticles concentration, considerably due to the inhomogeneous top surface morphology of CNTs onto glass surfaces and hence, the stability of CNTs coating is impressively introduces the changes in the refractive index measurement.

Moreover, the refractive index was influenced by the high polarity of Er^{3+} that exists in the host TeO_2 glass network system which breaks up the Te-O-Te bridging bonds (BOs) into the formation of non-bridging oxygens (NBOs) and structural rearrangement in the glass lattice network. Thus, the increase of NBOs may create more ionic characteristics that influences the polarizability of ions and thereby, result in an improvement in refractive index value (Khan et al., 2019).

05-4506832 pustaka.upsi.edu.my Perpustakaan Tuanku Bainun Kampus Sultan Abdul Jalil Shah PustakaTBainun ptbupsi

05-4506832 pustaka.upsi.edu.my Perpustakaan Tuanku Bainun Kampus Sultan Abdul Jalil Shah PustakaTBainun ptbupsi

In the present work, it can be inferred that the ZBTEr (NPS)-CNTs glass sample with 0.04 mol% of Er_2O_3 nanoparticles concentration exhibited a highest refractive index value of 2.542 which can be used for high-performance in fiber optics. Consequently, these findings show a great improvement in refractive index by strongly interaction bonding between the CNTs coating layer and tellurite-based glasses.

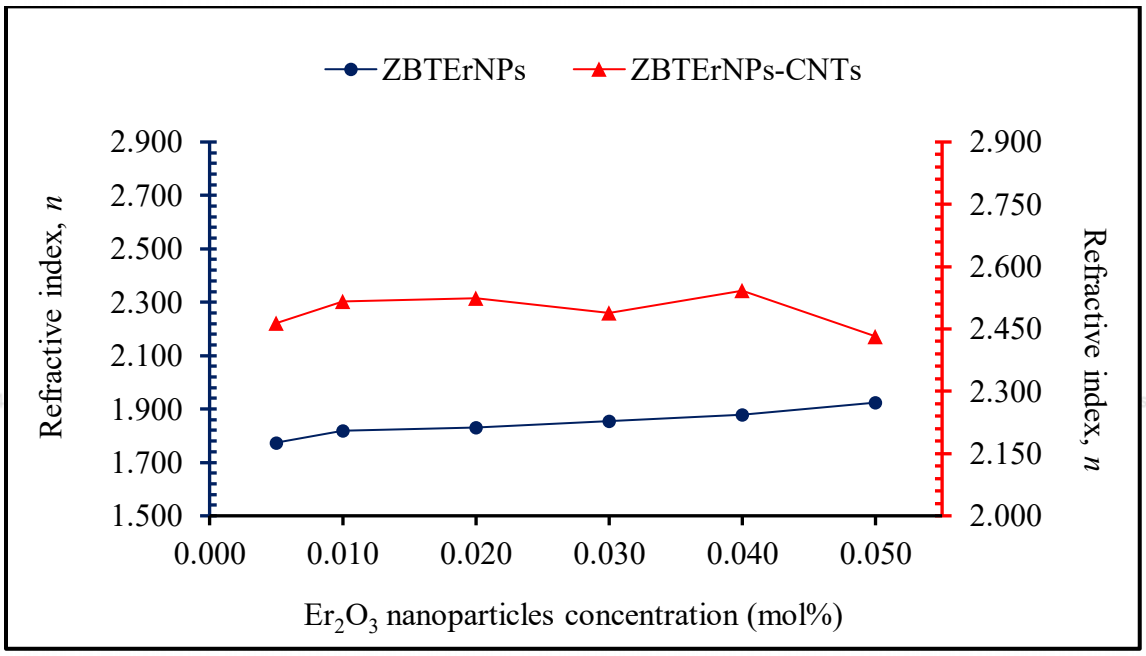


Figure 4.41. Variation of refractive index as a function of Er_2O_3 nanoparticles concentration for ZBTEr (NPs)-uncoated and ZBTEr (NPs)-CNTs glasses

05-4506832 pustaka.upsi.edu.my Perpustakaan Tuanku Bainun Kampus Sultan Abdul Jalil Shah PustakaTBainun ptbupsi

05-4506832 pustaka.upsi.edu.my Perpustakaan Tuanku Bainun Kampus Sultan Abdul Jalil Shah PustakaTBainun ptbupsi

Table 4.25

Comparison of refractive index (n) values between ZBTEr (NPs)-uncoated and ZBTEr (NPs)-CNTs glasses

Er_2O_3 nanoparticles concentration (mol%)	Refractive index (*n*) (±0.100)
ZBTEr (NPs)-uncoated	
0.005	1.774
0.010	1.818
0.020	1.830
0.030	1.855
0.040	1.878
0.050	1.924
ZBTEr (NPs)-CNTs	
0.005	2.463
0.010	2.516
0.020	2.524
0.030	2.489
0.040	2.542
0.050	2.432

05-4506832 pustaka.upsi.edu.my Perpustakaan Tuanku Bainun Kampus Sultan Abdul Jalil Shah PustakaTBainun ptbupsi

05-4506832 pustaka.upsi.edu.my Perpustakaan Tuanku Bainun Kampus Sultan Abdul Jalil Shah PustakaTBainun ptbupsi

4.6.5 Reflection Loss, Transmission Coefficient, and Dielectric Constant

For further studies of the optical properties of the ZBTEr (NPs)-CNTs glassy matrix, the optical parameters such as; reflection loss (R_L), transmission coefficient (T), and dielectric constant (ϵ) were calculated from the refractive index value and by using the given Equations 2.14, 2.15, and 2.16 which has been described in subsection 2.13.5.

As can be referred to Figure 4.42, it can be observed that the variation of reflection loss, transmission coefficient, and dielectric constant of the ZBTEr (NPs)-CNTs glasses along with the Er_2O_3 nanoparticles concentration. Moreover, it can be clearly noted that these optical parameter values showed a non-linear trend whereby, the reflection loss, transmission coefficient, and dielectric constant values in the range of (0.174 – 0.189), (0.681 – 0.703), and (5.915 – 6.462), respectively as tabulated in Table 4.26.

05-4506832 pustaka.upsi.edu.my Perpustakaan Tuanku Bainun Kampus Sultan Abdul Jalil Shah PustakaTBainun ptbupsi

05-4506832 pustaka.upsi.edu.my Perpustakaan Tuanku Bainun Kampus Sultan Abdul Jalil Shah PustakaTBainun ptbupsi

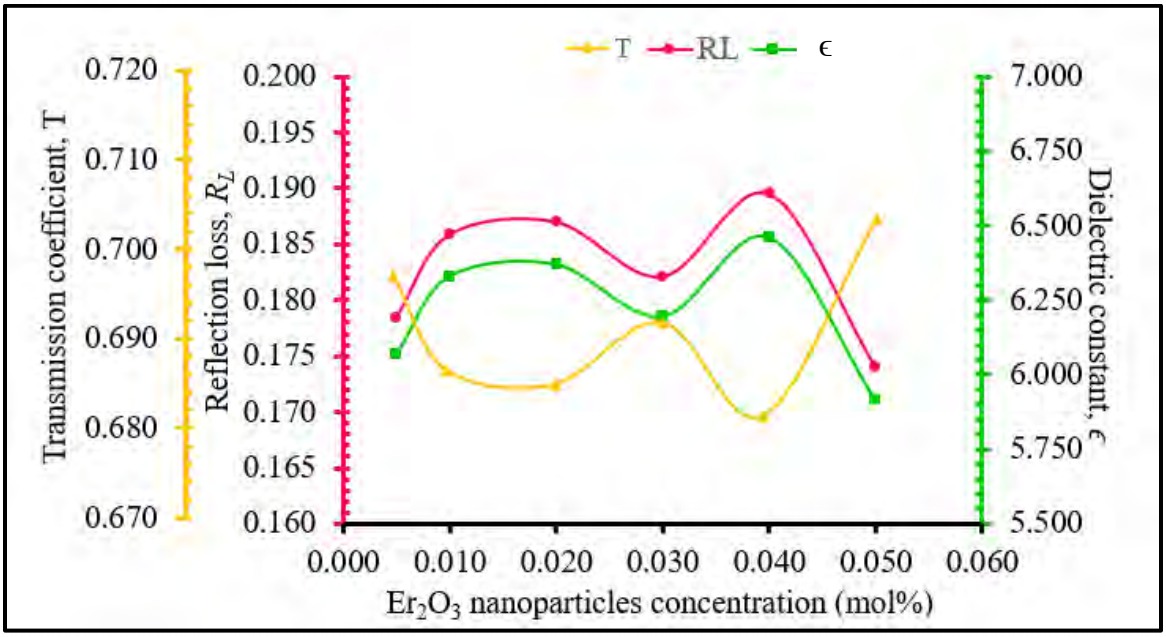


Figure 4.42. Variation of reflection loss, transmission coefficient, and dielectric constant as a function of Er_2O_3 nanoparticles concentration for ZBTEr (NPs)-CNTs glasses

05-4506832 pustaka.upsi.edu.my Perpustakaan Tuanku Bainun Kampus Sultan Abdul Jalil Shah PustakaTBainun ptbupsi

Table 4.26

Variation of reflection loss (R_L), transmission coefficient (T), and dielectric constant (ϵ) for ZBTEr (NPs)-CNTs glasses

Er_2O_3 nanoparticles concentration (mol%)	R_L (±0.004)	T (±0.005)	ϵ (±0.129)
0.005	0.179	0.697	6.066
0.010	0.186	0.687	6.330
0.020	0.187	0.685	6.371
0.030	0.182	0.692	6.195
0.040	0.189	0.681	6.462
0.050	0.174	0.703	5.915

05-4506832 pustaka.upsi.edu.my Perpustakaan Tuanku Bainun Kampus Sultan Abdul Jalil Shah PustakaTBainun ptbupsi

05-4506832 pustaka.upsi.edu.my Perpustakaan Tuanku Bainun Kampus Sultan Abdul Jalil Shah PustakaTBainun ptbupsi

4.6.6 Electronegativity

The electronegativity of an atom refers to its relative ability to attract the electrons in a bond towards itself (Thombre, 2016). The studies on electronegativity become the main concept in understanding the chemical bond and material properties that can be applied in any practical application. It is well known that Pauling initially proposed the methods for the early study concept of electronegativity by which to qualitatively characterize the transition from ionic to covalent bonds (Pauling, 1932). Afterward, the electronegativities of the main group elements, such as the concept of average electronegativity were introduced by Asokamani & Manjula, (1989).

The Pauling electronegativity, average electronegativity, and average electronegativity-based oxide ion polarizability of the TeO_2, B_2O_3, ZnO, and Er_2O_3 oxides in the ZBTEr (NPs)-CNTs glass system were determined by using the Equations 2.17, 2.18, 2.19, and 2.20, respectively which has been stated in subsection 2.13.6 and tabulated in Table 4.27. Therefore, these results simultaneously verify a good agreement with the previously reported studies (Al-Harbi et al., 2021).

05-4506832 pustaka.upsi.edu.my Perpustakaan Tuanku Bainun Kampus Sultan Abdul Jalil Shah PustakaTBainun ptbupsi

05-4506832 pustaka.upsi.edu.my Perpustakaan Tuanku Bainun Kampus Sultan Abdul Jalil Shah PustakaTBainun ptbupsi

Table 4.27

Pauling electronegativity (χ_i), average electronegativity (χ_{av}), and average electronegativity-based oxide ion polarizability $\alpha_0^{2-}(\chi_{nav})$, n = 1, 2, 3 of the ZBTEr (NPs)-CNTs glasses

Oxides	$\boldsymbol{\chi_i}$	$\boldsymbol{\chi_{av}}$	$\boldsymbol{\alpha_0^{2-}(\chi_{1av})}$	$\boldsymbol{\alpha_0^{2-}(\chi_{2av})}$	$\boldsymbol{\alpha_0^{2-}(\chi_{3av})}$
TeO_2	Te = 2.100	2.993	2.358	2.295	1.377
B_2O_3	B = 2.040	2.880	2.444	2.334	1.417
ZnO	Zn = 1.650	2.545	2.698	2.448	1.604
Er_2O_3	Er = 1.240	2.536	2.705	2.451	1.611
	O = 3.440				

05-4506832 pustaka.upsi.edu.my Perpustakaan Tuanku Bainun Kampus Sultan Abdul Jalil Shah PustakaTBainun ptbupsi

A similar approach was applied to ZBTEr (NPs)-CNTs glass system whereby, the average electronegativity-based oxide ion polarizability, $\alpha_0^{2-}(\chi_{av})$ values were presented along with the increase of Er^{3+} nanoparticles concentration, as illustrated in Table 4.28. It can be clearly noted that the average electronegativity-based oxide ion polarizability values exhibited the increasing trend along with the increase of Er^{3+} nanoparticles concentration meanwhile, the obtained values of refractive index-based oxide ion polarizability in the range of 3.332 – 3.403 which ascribes from the higher refractive index values, as stated in previously Table 4.25. The increment of refractive index values may be correlated to the high functional groups existing in CNTs nanostructures and thereby, may shift the refractive index-based oxide ion polarizability values in the glassy matrix.

05-4506832 pustaka.upsi.edu.my Perpustakaan Tuanku Bainun Kampus Sultan Abdul Jalil Shah PustakaTBainun ptbupsi

05-4506832 pustaka.upsi.edu.my Perpustakaan Tuanku Bainun Kampus Sultan Abdul Jalil Shah PustakaTBainun ptbupsi

Table 4.28

Average electronegativity (χ_{av}), average electronegativity-based oxide ion polarizability, α_0^{2-} (χ_{nav}), n = 1, 2, 3, and refractive index-based oxide ion polarizability, $\alpha_0^{2-}(n)$ of ZBTEr (NPs)-CNTs glasses

Er_2O_3 nanoparticles concentration (mol%)	$\boldsymbol{\chi_{av}}$	$\boldsymbol{\alpha_0^{2-}(\chi_{1av})}$	$\boldsymbol{\alpha_0^{2-}(\chi_{2av})}$	$\boldsymbol{\alpha_0^{2-}(\chi_{3av})}$	$\boldsymbol{\alpha_0^{2-}(n)}$
0.005	2.834	2.479	2.349	1.435	3.383
0.010	2.832	2.481	2.349	1.436	3.401
0.020	2.829	2.483	2.351	1.437	3.383
0.030	2.826	2.485	2.352	1.439	3.348
0.040	2.823	2.487	2.353	1.439	3.403
0.050	2.820	2.489	2.354	1.441	3.332

05-4506832 pustaka.upsi.edu.my Perpustakaan Tuanku Bainun Kampus Sultan Abdul Jalil Shah PustakaTBainun ptbupsi

05-4506832 pustaka.upsi.edu.my Perpustakaan Tuanku Bainun Kampus Sultan Abdul Jalil Shah PustakaTBainun ptbupsi

Figure 4.43 shows a least-square plot graph that presents the correlation between the average electronegativity-based oxide ion polarizability, $\alpha_0^{2-}(\chi_{1av})$ and refractive index-based oxide ion polarizability, $\alpha_0^{2-}(n)$ in the ZBTEr (NPs)-CNTs glass system. Herein, the plotted graph from the average electronegativity values does not give reliable results. Due to these findings, the correlation between these two variables was improved as the optical electronegativity is introduced (refer to Table 4.29), whereby the obtained results are more reliable as compared to the average electronegativity values. Hence, these findings may be considered satisfactory results for ZBTEr (NPs)-CNTs glasses.

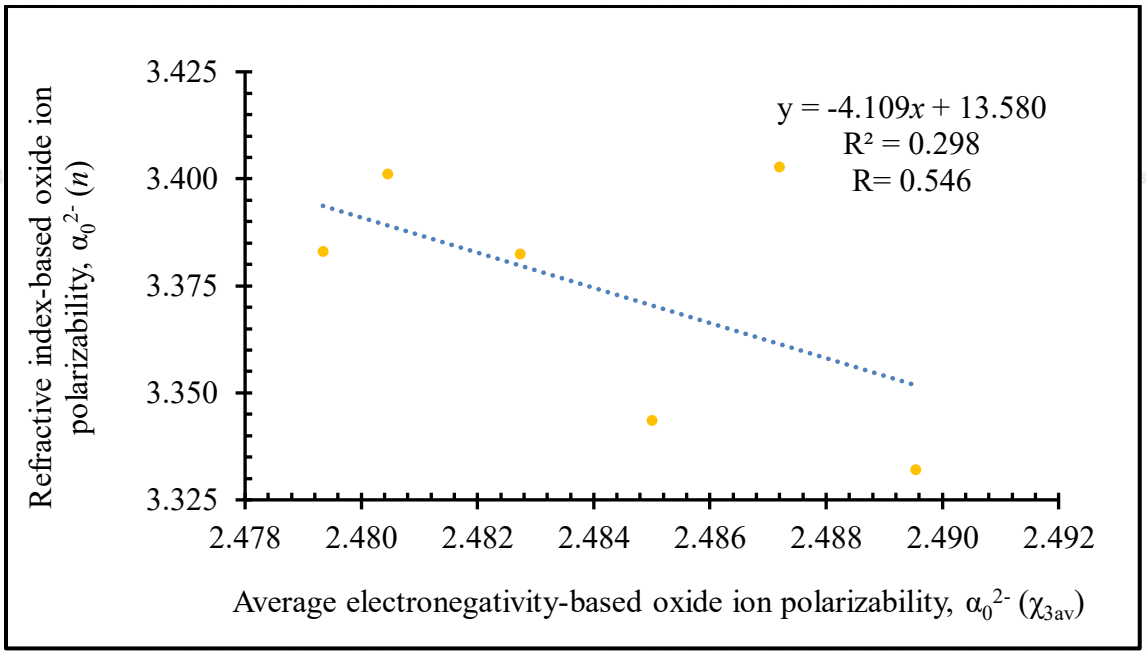


Figure 4.43. Least square plot of refractive index-based oxide ion polarizability, $\alpha_0^{2-}(n)$ against average electronegativity-based oxide ion polarizability, $\alpha_0^{2-}(\chi_{3av})$ of ZBTEr (NPs)-CNTs glasses

05-4506832 pustaka.upsi.edu.my Perpustakaan Tuanku Bainun Kampus Sultan Abdul Jalil Shah PustakaTBainun ptbupsi

05-4506832 pustaka.upsi.edu.my Perpustakaan Tuanku Bainun Kampus Sultan Abdul Jalil Shah PustakaTBainun ptbupsi

Table 4.29

Optical energy bandgap-based optical electronegativity $\Delta\chi^*(E_{opt})$, refractive index-based optical electronegativity $\Delta\chi^*$ (n), energy bandgap optical electronegativity-based oxide ion polarizability $\alpha_0^{2-}(\Delta\chi^*(E_{opt}))$, and refractive index optical electronegativity-based oxide ion polarizability $\alpha_0^{2-}(\Delta\chi^*(n))$ of ZBTEr (NPs)-CNTs glasses

Er_2O_3 nanoparticles concentration (mol%)	$\Delta\chi^*(E_{opt})$	$\Delta\chi^*$ (n)	$\boldsymbol{\alpha_0^{2-}}(\Delta\chi^*(E_{opt}))$	$\boldsymbol{\alpha_0^{2-}}(\Delta\chi^*(n))$
0.005	0.744	0.835	2.831	2.749
0.010	0.698	0.792	2.872	2.788
0.020	0.690	0.785	2.879	2.793
0.030	0.720	0.813	2.852	2.768
0.040	0.676	0.771	2.892	2.806
0.050	0.773	0.861	2.805	2.725

05-4506832 pustaka.upsi.edu.my Perpustakaan Tuanku Bainun Kampus Sultan Abdul Jalil Shah PustakaTBainun ptbupsi

05-4506832 pustaka.upsi.edu.my Perpustakaan Tuanku Bainun Kampus Sultan Abdul Jalil Shah PustakaTBainun ptbupsi

Briefly, it can be noticed that a relation subjected to more approximation comparable to average electronegativity, Zhao et al., (2008) then introduced the concept of optical electronegativity, $\Delta\chi^*$ and suggested the empirical relation for binary oxide glass by using the given Equations 2.21, 2.22, and 2.23, respectively which has been mentioned in the subsection 2.13.6. The least-square plot of energy bandgap optical electronegativity-based oxide ion polarizability, $\alpha_0^{2-}(\Delta\chi^*(E_{opt}))$, and energy bandgap-oxide ion polarizability, $\Delta\chi^*(E_{opt})$ of ZBTEr (NPs)-CNTs glass system were calculated and summarized, as shown in Figure 4.44 and Table 4.29, respectively.

Meanwhile, Figure 4.45 shows the obtained least-square plot of $\alpha_0^{2-}(\Delta\chi^*(n))$ which ascribes the high accuracy to the refractive index data. Therefore, $\alpha_0^{2-}(\Delta\chi^*(n))$ demonstrates reliable results for oxide ion polarizability as compared results to the obtained of $\alpha_0^{2-}(\Delta\chi^*(E_{opt}))$ which has less accuracy of fitting in the ZBTEr (NPs)-CNTs glasses. The difference between $\alpha_0^{2-}(\Delta\chi^*(n))$ and $\alpha_0^{2-}(\Delta\chi^*(E_{opt}))$ could be attributed due to the existence of localized density of states in the energy bandgap according to Davis-Mott's theory for the conduction band that exists in a non-crystalline system (Mott et al., 1972).

05-4506832 pustaka.upsi.edu.my Perpustakaan Tuanku Bainun Kampus Sultan Abdul Jalil Shah PustakaTBainun ptbupsi

05-4506832 pustaka.upsi.edu.my Perpustakaan Tuanku Bainun Kampus Sultan Abdul Jalil Shah PustakaTBainun ptbupsi

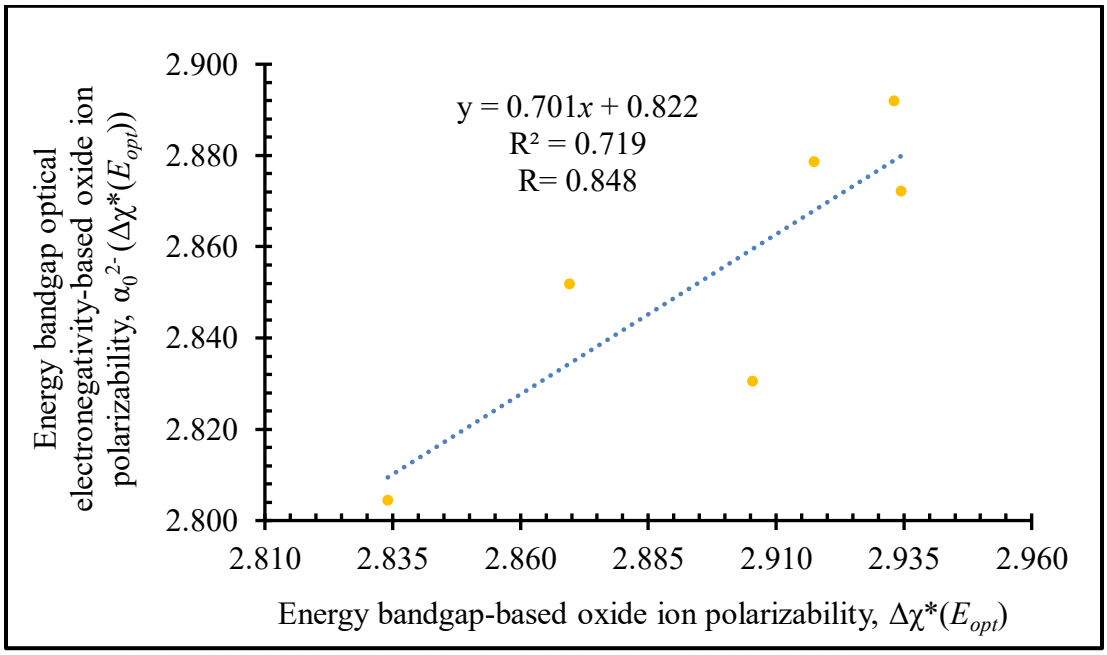


Figure 4.44. Least-square plot of energy bandgap optical electronegativity-based oxide ion polarizability, $\alpha_0^{2-}(\Delta\chi^*(E_{opt}))$ with energy bandgap-based oxide ion polarizability, $\Delta\chi^*(E_{opt})$ of ZBTEr (NPs)-CNTs glasses

05-4506832 pustaka.upsi.edu.my Perpustakaan Tuanku Bainun Kampus Sultan Abdul Jalil Shah PustakaTBainun ptbupsi

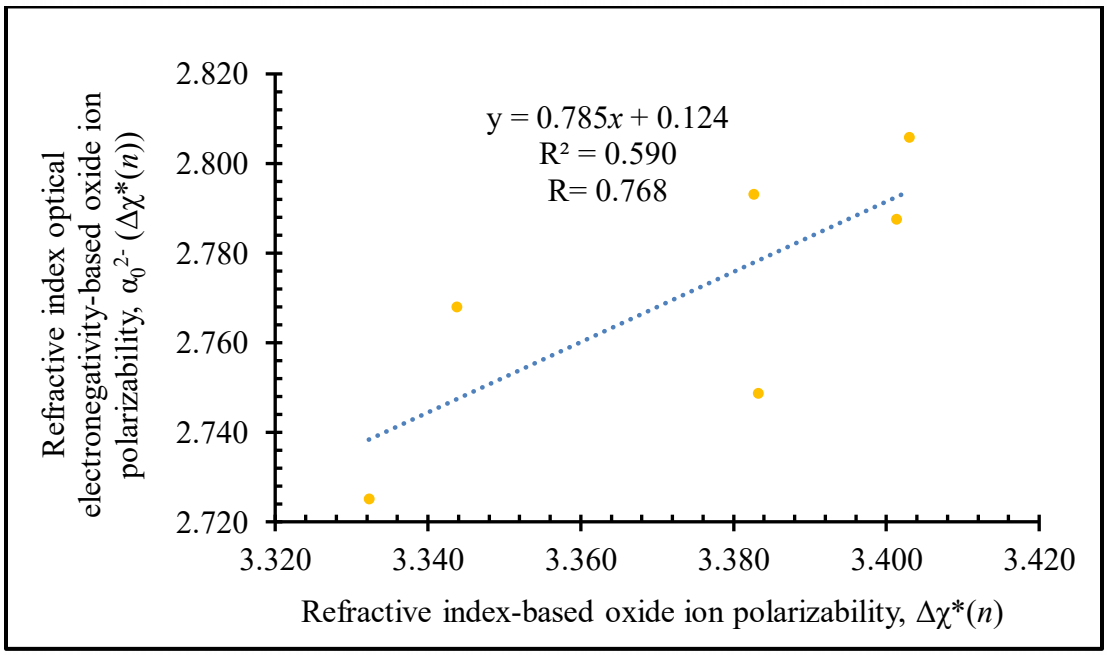


Figure 4.45. Least-square plot of refractive index optical electronegativity-based oxide ion polarizability, $\alpha_0^{2-}(\Delta\chi^*(n))$ with refractive index-based oxide ion polarizability, $\Delta\chi^*(n)$ of ZBTEr (NPs)-CNTs glasses

05-4506832 pustaka.upsi.edu.my Perpustakaan Tuanku Bainun Kampus Sultan Abdul Jalil Shah PustakaTBainun ptbupsi

05-4506832 pustaka.upsi.edu.my Perpustakaan Tuanku Bainun Kampus Sultan Abdul Jalil Shah PustakaTBainun ptbupsi

Apart from that, it can be noticed that the obtained results indicate the stronger covalency of the ligand bonds which is caused by the differences in electronegativity values. Due to these, the tendency of bonding electrons is attracted towards more electronegativities between the two atoms of different electronegativities in a covalent bond.

4.6.7 Judd-Ofelt's Analysis

Judd-Ofelt's theory is vital in physical chemistry which ascribes the intensity of electron transitions occur in the *4f* shell of REIs either in the solids or liquids (Marzouk et al., 2021). By fitting the experimental and theoretical oscillator strength of the absorption transitions, Judd-Ofelt's theory offers a great approach for analyzing the oscillator strengths in the absorption, transition probabilities, branching ratios, and radiative lifetime via the empirical Judd-Ofelt's spectral intensity parameters, (Ω_λ = 2, 4, 6). The experimental oscillator strength (f_{exp}) values of each observed transition state of excitation for different concentrations of Er^{3+} ions can be evaluated by analyzing the total area under absorption band spectra (refer to Figure 4.37) by using the given Equations 2.24, 2.25, 2.26, 2.27, and 2.28, respectively which has been described in subsection 2.13.7.

The experimental oscillator strengths (f_{exp}) and calculated oscillator strengths (f_{cal}) along with the root mean square deviation (δ_{rms}) values, are summarized in Table 4.30. The Judd-Ofelt's analysis of ZBTEr (NPs)-CNTs glasses comprises a higher value of

05-4506832 pustaka.upsi.edu.my Perpustakaan Tuanku Bainun Kampus Sultan Abdul Jalil Shah PustakaTBainun ptbupsi

05-4506832 pustaka.upsi.edu.my Perpustakaan Tuanku Bainun Kampus Sultan Abdul Jalil Shah PustakaTBainun ptbupsi

oscillator strength which indicates the lower symmetry and thus, attribute to the covalent nature between Er^{3+} ions at the excited state level of $^4F_{5/2}$ transition. These results are similar to the previous ZBTEr (NPs)-rGO glasses (refer to subsection 4.4.7) due to the $^4I_{15/2} \rightarrow {}^4F_{5/2}$ transition band demonstrating a highly intense than other transitions which relate to the hypersensitive transitions (HST) (Jørgensen & Judd, 1964). Hence, the known HST which obey the selection rules of $|\Delta J| \leq 2$, $|\Delta L| \leq 2$, and $\Delta S = 0$ can be treated as the characteristics of the host glass network system due to these HST are very responsive to the environment (Buddhudu & Bryant, 1989; Taherunnisa et al., 2019). Among all the prepared ZBTEr (NPs)-CNTs glasses, it can be noticed that the highest experimental oscillator strength (f_{exp}) value at the 0.02 mol% Er^{3+} ions nanoparticles concentration which is located in the $^4I_{15/2} \rightarrow {}^4F_{5/2}$ transition band.

05-4506832 pustaka.upsi.edu.my Perpustakaan Tuanku Bainun Kampus Sultan Abdul Jalil Shah PustakaTBainun ptbupsi

Referring to Table 4.31, it is clearly observed that the small values of (δ_{rms}) approximately in the range of $(0.025 - 0.700) \times 10^{-20}$ represent the reliability of the fitting procedure and verifies a good quality fit that exists between experimental and oscillator strengths of Er^{3+} ions doped tellurite glasses. Furthermore, these obtained findings were supported by previous studies such as Er^{3+}/ Tm^{3+}- doped tellurite (Pepe et al., 2019), Er^{3+}-doped oxychloroborotellurite (Sailaja et al., 2021), and Er^{3+}-doped borozincate (Marzouk et al., 2021) glasses.

05-4506832 pustaka.upsi.edu.my Perpustakaan Tuanku Bainun Kampus Sultan Abdul Jalil Shah PustakaTBainun ptbupsi

05-4506832 pustaka.upsi.edu.my Perpustakaan Tuanku Bainun Kampus Sultan Abdul Jalil Shah PustakaTBainun ptbupsi

Table 4.30

The experimental (f_{exp} ×10^{-6}) and calculated oscillator strength (f_{cal} ×10^{-6}) along with the root mean square deviation (δ_{rms} ×10^{-6}) of ZBTEr (NPs)-CNTs glasses

Absorption transition	ZBTEr (NPs)-CNTs glasses											
	0.005 Er (NPs)		0.010 Er (NPs)		0.020 Er (NPs)		0.030 Er (NPs)		0.040 Er (NPs)		0.050 Er (NPs)	
Ground state ($^4I_{15/2}$)	f_{exp}	f_{cal}	f_{exp}	f_{cal}	f_{exp}	f_{cal}	f_{exp}	f_{cal}	f_{exp}	f_{cal}	f_{exp}	f_{cal}
$^4I_{15/2} \rightarrow {}^4F_{5/2}$	1.182	1.001	1.031	1.005	8.804	7.199	1.666	3.938	1.535	2.638	1.126	3.239
$^4I_{15/2} \rightarrow {}^4F_{7/2}$	0.095	0.059	0.266	0.166	0.263	0.123	0.391	0.247	0.590	0.395	1.751	1.369
$^4I_{15/2} \rightarrow {}^4H_{11/2}$	0.399	0.567	0.550	0.569	2.575	4.077	4.376	2.232	6.584	0.149	3.855	1.852
$^4I_{15/2} \rightarrow {}^4S_{3/2}$	0.071	0.079	0.085	0.108	0.256	0.279	0.337	0.384	0.391	0.443	2.064	2.165
RMS deviation δ_{rms} (×10^{-20})	0.057		0.025		0.479		0.700		0.329		0.691	

05-4506832 pustaka.upsi.edu.my Perpustakaan Tuanku Bainun Kampus Sultan Abdul Jalil Shah PustakaTBainun ptbupsi

05-4506832 pustaka.upsi.edu.my Perpustakaan Tuanku Bainun Kampus Sultan Abdul Jalil Shah PustakaTBainun ptbupsi

According to the obtained optical absorption bands (Figure 4.34) that has been discussed earlier in subsection 4.6.1, Judd-Ofelt's theory (Judd, 1962; Ofelt, 1962) was used in which the experimental and calculated oscillator strengths with a least-square fitting can be proposed to determine the spectral intensity parameters Ω_t(t =2, 4, 6). Additionally, Judd-Ofelt's intensity parameters may imply analyzing the local network structure around the REIs (Sailaja et al., 2021). Particularly, the Ω_2 intensity parameter can be correlated to the glass structure such as the asymmetry of the ligand field inside the host glass and, is most sensitive to the covalent bonding between REIs and the ligand environment of the host glass (Pepe et al., 2019). Meanwhile, both the Ω_4 and Ω_6 intensity parameters are concerned with the rigidity, viscosity, basicity, and dielectrics media in which these characteristics depict the bond between ligand atoms and erbium ions, as well as the vibronic transitions around the host amorphous glass matrix (Gaafar & Marzouk, 2017; Jørgensen & Reisfeld, 1983).

In the current work, Figure 4.46 presents a graphical relation between three intensity parameters (Ω_2, Ω_4, and Ω_6) for the Er^{3+} ions concentration which follows the trend of Ω_2> Ω_4> Ω_6, whereby, the higher value of the Ω_2 indicates the strong covalency and high asymmetry of local surroundings of Er^{3+} ions sites. The increase of Ω_2 intensity parameter can be ascribed to the effects of the CNTs coating layer on glass surfaces. Consequently, these results create the non-covalent functionalization of CNTs caused by the SDS surfactant (Eom et al., 2019) which resulted from the weak van der Waals and π-π interactions existing in the CNTs nanostructures and thereby, suggesting to improve the value of Judd-Ofelt intensity parameters for all the Er^{3+} nanoparticles concentration.

05-4506832 pustaka.upsi.edu.my Perpustakaan Tuanku Bainun Kampus Sultan Abdul Jalil Shah PustakaTBainun ptbupsi

05-4506832 pustaka.upsi.edu.my Perpustakaan Tuanku Bainun Kampus Sultan Abdul Jalil Shah PustakaTBainun ptbupsi

Meanwhile, the lowest value of Ω_6 was found to decrease which correlated to the decrement of rigidity between Er^{3+} ions and ligand bonds. The high functionalization that existed in CNTs nanostructures promotes to improve the value of Judd-Ofelt intensity parameters by the factor of the high degree of agglomeration structures (Belosludtseva et al., 2021; Rathinavel et al., 2021), as proved by SEM and EDX analyses that have been discussed in the subsection 4.5.1. Nevertheless, it can be noticed at 0.01 mol% Er^{3+} ions concentration indicates the value of the Ω_6 intensity parameter which was slightly increased than the Ω_4 intensity parameter. As a result, the glass sample with 0.01 mol% Er^{3+} ions possessed a relatively long-range structural network and high rigidity of the glass matrix which was strongly affected by the CNTs coating layer onto tellurite-based glass surfaces. In comparison, the increment of Ω_6 intensity parameter for the ZBTEr (NPs)-CNTs glass with 0.01 mol% Er^{3+} ions concentration may be correlated to the high functional groups in CNTs structures and thereby, resulting in the shift of Judd-Ofelt's intensity parameters value in the glass matrix.

The spectroscopic quality factor (χ) can be identified by using the intensity parameters ratio of $\frac{\Omega_4}{\Omega_6}$ as proposed by Jacobs & Weber, (1976). As can be referred to Table 4.32, the calculated (χ) values for all the Er^{3+} ions concentration of the ZBTEr (NPs)-CNTs glass system were found to be in the range of 0.199 to 4.391 whereby, 0.05 mol% Er^{3+} ions concentration for the ZBTEr (NPs)-CNTs glass system exhibited the highest value of χ about 4.391, suggesting that the CNTs-coated glass probably gives a high impact on the emission strength for the laser applications.

05-4506832 pustaka.upsi.edu.my Perpustakaan Tuanku Bainun Kampus Sultan Abdul Jalil Shah PustakaTBainun ptbupsi

05-4506832 pustaka.upsi.edu.my Perpustakaan Tuanku Bainun Kampus Sultan Abdul Jalil Shah PustakaTBainun ptbupsi

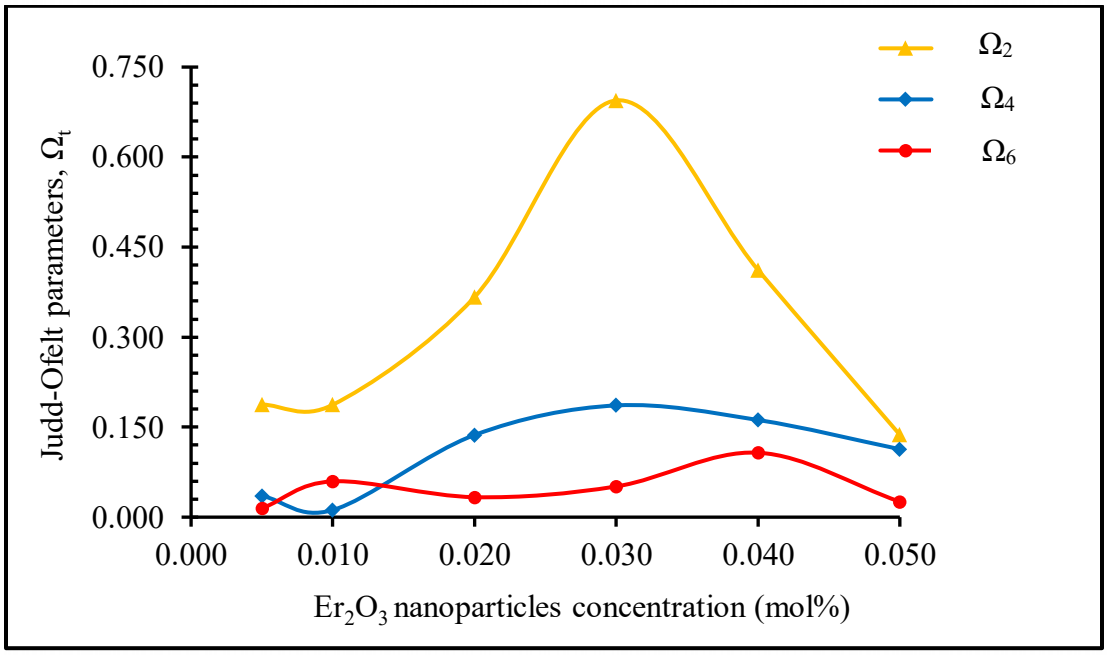


Figure 4.46. Variation of the Judd-Ofelt intensity parameters, Ω_t (t = 2, 4, 6) as a function of Er_2O_3 nanoparticles concentration for ZBTEr (NPs)-CNTs glasses

05-4506832 pustaka.upsi.edu.my Perpustakaan Tuanku Bainun Kampus Sultan Abdul Jalil Shah PustakaTBainun ptbupsi

05-4506832 pustaka.upsi.edu.my Perpustakaan Tuanku Bainun Kampus Sultan Abdul Jalil Shah PustakaTBainun ptbupsi

05-4506832 pustaka.upsi.edu.my Perpustakaan Tuanku Bainun Kampus Sultan Abdul Jalil Shah PustakaTBainun ptbupsi

Table 4.31

Judd-Ofelt's intensity parameter ($\Omega_\lambda \times 10^{-20}$ cm^2) and spectroscopic quality factor $\chi = \frac{\Omega_4}{\Omega_6}$ *of ZBTEr (NPs)-CNTs glasses*

Er_2O_3 nanoparticles concentration (mol%)	Ω_2	Ω_4	Ω_6	$\chi = \frac{\Omega_4}{\Omega_6}$	Ω_i Trends
0.005	0.188	0.036	0.015	2.415	$\Omega_2 > \Omega_4 > \Omega_6$
0.010	0.187	0.012	0.059	0.199	$\Omega_2 > \Omega_6 > \Omega_4$
0.020	0.367	0.137	0.033	4.111	$\Omega_2 > \Omega_4 > \Omega_6$
0.030	0.695	0.186	0.051	3.637	$\Omega_2 > \Omega_4 > \Omega_6$
0.040	0.412	0.162	0.107	1.507	$\Omega_2 > \Omega_4 > \Omega_6$
0.050	0.137	0.113	0.026	4.391	$\Omega_2 > \Omega_4 > \Omega_6$

05-4506832 pustaka.upsi.edu.my Perpustakaan Tuanku Bainun Kampus Sultan Abdul Jalil Shah PustakaTBainun ptbupsi

05-4506832 pustaka.upsi.edu.my Perpustakaan Tuanku Bainun Kampus Sultan Abdul Jalil Shah PustakaTBainun ptbupsi

By using the Judd-Ofelt's intensity parameters, the radiative properties including, radiative transition probability (A_τ), branching ratio (β_R), and radiative lifetime (τ_{rad}) can be determined for all the Er^{3+} nanoparticles concentration of the ZBTEr (NPs)-CNTs glasses by using the given Equations 2.30, 2.31, 2.32, 2.33, and 2.34, respectively, as has been described in subsection 2.13.7 and the obtained data are summarized in Table 4.32 – Table 4.37, respectively. As can be seen from Table 4.36, the calculated radiative transition probability (A_{ed}) for $^4I_{13/2} \rightarrow {}^4I_{15/2}$ transition of 0.04 mol% Er^{3+} nanoparticles concentration of the ZBTEr (NPs)-CNTs glass system was found in the value of 52.74 s^{-1}, indicating a higher value compared to the other Er^{3+} nanoparticles concentrations. As a result, the obtained higher (A_{ed}) value was influenced by the higher refractive index value (2.542) at 0.04 mol% Er^{3+} nanoparticles concentration in the ZBTEr (NPs)-CNTs glass system, as previously stated in Table 4.25. Moreover, it was believed that the higher value of the refractive index was definitely caused by the increment of the (A_{ed}) value for the ZBTEr (NPs)-CNTs glass matrix, which is beneficial for achieving the strong characteristics of the fiber optics.

Branching ratio (β_R) refers to the fraction of total photon flux from the upper manifold to a lower manifold for the determination of the stimulated emission in an excitation (Jlassi et al., 2010; Walsh et al., 1998). The obtained branching ratio at the $^2H_{11/2} \rightarrow {}^4I_{15/2}$ transition located in the wavelength of 522 nm, ranging from 0.950 – 0.960 for all the Er^{3+} ions concentration of the ZBTEr (NPs)-CNTs glass system. Consequently, these results are useful for the strong green emission which can be implemented for continuous laser action.

05-4506832 pustaka.upsi.edu.my Perpustakaan Tuanku Bainun Kampus Sultan Abdul Jalil Shah PustakaTBainun ptbupsi

05-4506832 pustaka.upsi.edu.my Perpustakaan Tuanku Bainun Kampus Sultan Abdul Jalil Shah PustakaTBainun ptbupsi

The radiative lifetime (τ_{rad}) values of the emission bands for the $^2H_{11/2} \rightarrow {}^4I_{15/2}$ transition level of the ZBTEr (NPs)-CNTs glass system were found approximately in the range value from 0.212 – 0.900 ms that caused by the strong effects of the CNTs coating layer on the glass surfaces. Additionally, the decrement of (τ_{rad}) value correlates to the non-radiative decay process which is proportional to the radiative decay rate, as reported by Aarts et al., (2011). Meanwhile, the longer (τ_{rad}) in the ZBTEr (NPs)-CNTs glass system provides an advantage over the stated transition levels which attributes to the optical laser and amplifier applications (Zhang et al., 2015). As can be referred to Table 4.32, the (τ_{rad}) of the $^4H_{9/2}$ transition level was found to be 40.807 ms which demonstrates the highest value of a radiative lifetime. Consequently, it can be concluded that the (τ_{rad}) of the $^4H_{9/2} \rightarrow {}^4I_{15/2}$ transition level at 0.005 mol% Er^{3+} nanoparticles concentration of the ZBTEr (NPs)-CNTs glass system can be a suitable material for fiber laser due to the longer emission of a radiative lifetime.

05-4506832 pustaka.upsi.edu.my Perpustakaan Tuanku Bainun Kampus Sultan Abdul Jalil Shah PustakaTBainun ptbupsi

05-4506832 pustaka.upsi.edu.my Perpustakaan Tuanku Bainun Kampus Sultan Abdul Jalil Shah PustakaTBainun ptbupsi

Table 4.32

The magnetic dipole and electric dipole radiative transition probabilities (A_{MD}, A_{ED}), emission branching ratio (β_R), and radiative lifetime (t_r) of 0.005 mol% ZBTEr (NPs)-CNTs glass

Er_2O_3 nanoparticles concentration (mol%)	Transition	λ (nm)	A_{MD} (s^{-1})	A_{ED} (s^{-1})	β_R	t_r (ms)
0.005	$^4I_{13/2} \rightarrow {}^4I_{15/2}$	1530	137.120	7.410	1.000	6.919
	$^4I_{11/2} \rightarrow {}^4I_{13/2}$	2804	26.840	1.380	0.696	
	$^4I_{15/2}$	990		12.300	0.304	24.682
	$^4I_{9/2} \rightarrow {}^4I_{11/2}$	4168	5.580	0.090	0.231	
	$^4I_{13/2}$	1676		3.000	0.123	
	$^4I_{15/2}$	800		15.840	0.646	40.807
	$^4F_{9/2} \rightarrow {}^4I_{9/2}$	3771	9.010	0.590	0.059	
	$^4I_{11/2}$	1980	24.880	5.390	0.186	
	$^4I_{13/2}$	1161		6.910	0.043	
	$^4I_{15/2}$	660		115.610	0.712	6.158
	$^4S_{3/2} \rightarrow {}^4I_{9/2}$	1710		4.210	0.043	
	$^4I_{11/2}$	1212		2.230	0.023	
	$^4I_{13/2}$	846		27.030	0.275	
	$^4I_{15/2}$	545		64.670	0.659	10.189
	$^2H_{11/2} \rightarrow {}^4F_{9/2}$	2497		4.760	0.004	
	$^4I_{9/2}$	1502		14.420	0.012	
	$^4I_{11/2}$	1104		9.690	0.008	
	$^4I_{13/2}$	792		15.670	0.013	
	$^4I_{15/2}$	522		1129.780	0.962	0.852
	$^4F_{7/2} \rightarrow {}^4F_{9/2}$	1942		0.810	0.003	
	$^4I_{9/2}$	1282		9.730	0.035	
	$^4I_{11/2}$	980		20.990	0.076	
	$^4I_{13/2}$	726		50.280	0.182	
	$^4I_{15/2}$	493		194.320	0.704	3.622
	$^2G_{9/2} \rightarrow {}^4F_{7/2}$	2439		1.950	0.006	
	$^2H_{11/2}$	1907		2.460	0.007	
	$^4F_{9/2}$	1081		2.740	0.084	
	$^4I_{9/2}$	840		6.600	0.020	
	$^4I_{11/2}$	699		47.510	0.140	
	$^4I_{13/2}$	560		176.820	0.522	
	$^4I_{15/2}$	410		74.670	0.221	2.955

05-4506832 pustaka.upsi.edu.my Perpustakaan Tuanku Bainun Kampus Sultan Abdul Jalil Shah PustakaTBainun ptbupsi

05-4506832 pustaka.upsi.edu.my Perpustakaan Tuanku Bainun Kampus Sultan Abdul Jalil Shah PustakaTBainun ptbupsi

Table 4.33

The magnetic dipole and electric dipole radiative transition probabilities (A_{MD}, A_{ED}), emission branching ratio (β_R), and radiative lifetime (t_r) of 0.01 mol% ZBTEr (NPs)-CNTs glass

Er_2O_3 nanoparticles concentration (mol%)	Transition	λ (nm)	A_{MD} (s^{-1})	A_{ED} (s^{-1})	β_R	t_r (ms)
0.01	$^4I_{13/2} \rightarrow {}^4I_{15/2}$	1530	146.170	25.330	1.000	5.831
	$^4I_{11/2} \rightarrow {}^4I_{13/2}$	2804	28.610	3.880	0.483	
	$^4I_{15/2}$	990		34.820	0.517	14.856
	$^4I_{9/2} \rightarrow {}^4I_{11/2}$	4168	5.950	0.170	0.234	
	$^4I_{13/2}$	1676		12.800	0.489	
	$^4I_{15/2}$	800		7.270	0.278	38.184
	$^4F_{9/2} \rightarrow {}^4I_{9/2}$	3771	9.610	0.670	0.045	
	$^4I_{11/2}$	1980	26.520	16.270	0.189	
	$^4I_{13/2}$	1161		7.160	0.032	
	$^4I_{15/2}$	660		165.750	0.733	4.425
	$^4S_{3/2} \rightarrow {}^4I_{9/2}$	1710		11.310	0.027	
	$^4I_{11/2}$	1212		8.780	0.021	
	$^4I_{13/2}$	846		119.580	0.281	
	$^4I_{15/2}$	545		286.150	0.672	2.348
	$^2H_{11/2} \rightarrow {}^4F_{9/2}$	2497		5.140	0.004	
	$^4I_{9/2}$	1502		19.590	0.016	
	$^4I_{11/2}$	1104		9.160	0.007	
	$^4I_{13/2}$	792		19.240	0.016	
	$^4I_{15/2}$	522		1183.290	0.957	0.809
	$^4F_{7/2} \rightarrow {}^4F_{9/2}$	1942		0.860	0.001	
	$^4I_{9/2}$	1282		24.750	0.039	
	$^4I_{11/2}$	980		23.920	0.037	
	$^4I_{13/2}$	726		18.390	0.029	
	$^4I_{15/2}$	493		574.740	0.894	1.556
	$^2G_{9/2} \rightarrow {}^4F_{7/2}$	2439		2.110	0.003	
	$^2H_{11/2}$	1907		2.420	0.004	
	$^4F_{9/2}$	1081		4.010	0.042	
	$^4I_{9/2}$	840		7.290	0.011	
	$^4I_{11/2}$	699		64.560	0.095	
	$^4I_{13/2}$	560		297.210	0.436	
	$^4I_{15/2}$	410		279.130	0.410	1.468

05-4506832 pustaka.upsi.edu.my Perpustakaan Tuanku Bainun Kampus Sultan Abdul Jalil Shah PustakaTBainun ptbupsi

05-4506832 pustaka.upsi.edu.my Perpustakaan Tuanku Bainun Kampus Sultan Abdul Jalil Shah PustakaTBainun ptbupsi

Table 4.34

The magnetic dipole and electric dipole radiative transition probabilities (A_{MD}, A_{ED}), emission branching ratio (β_R), and radiative lifetime (t_r) of 0.02 mol% ZBTEr (NPs)-CNTs glass

Er_2O_3 nanoparticles concentration (mol%)	Transition	λ (nm)	A_{MD} (s^{-1})	A_{ED} (s^{-1})	β_R	t_r (ms)
0.02	$^4I_{13/2} \rightarrow {}^4I_{15/2}$	1530	147.570	20.090	1.000	5.964
	$^4I_{11/2} \rightarrow {}^4I_{13/2}$	2804	28.890	3.850	0.532	
	$^4I_{15/2}$	990		28.760	0.468	16.261
	$^4I_{9/2} \rightarrow {}^4I_{11/2}$	4168	6.000	0.290	0.078	
	$^4I_{13/2}$	1676		7.680	0.095	
	$^4I_{15/2}$	800		66.760	0.827	12.387
	$^4F_{9/2} \rightarrow {}^4I_{9/2}$	3771	9.700	1.290	0.021	
	$^4I_{11/2}$	1980	26.770	12.840	0.077	
	$^4I_{13/2}$	1161		24.620	0.048	
	$^4I_{15/2}$	660		438.570	0.854	1.946
	$^4S_{3/2} \rightarrow {}^4I_{9/2}$	1710		13.690	0.055	
	$^4I_{11/2}$	1212		6.050	0.024	
	$^4I_{13/2}$	846		67.560	0.271	
	$^4I_{15/2}$	545		161.670	0.649	4.016
	$^2H_{11/2} \rightarrow {}^4F_{9/2}$	2497		10.380	0.004	
	$^4I_{9/2}$	1502		33.130	0.012	
	$^4I_{11/2}$	1104		29.260	0.010	
	$^4I_{13/2}$	792		44.210	0.016	
	$^4I_{15/2}$	522		2672.950	0.958	0.358
	$^4F_{7/2} \rightarrow {}^4F_{9/2}$	1942		2.330	0.002	
	$^4I_{9/2}$	1282		28.070	0.030	
	$^4I_{11/2}$	980		80.290	0.086	
	$^4I_{13/2}$	726		213.940	0.229	
	$^4I_{15/2}$	493		609.040	0.652	1.071
	$^2G_{9/2} \rightarrow {}^4F_{7/2}$	2439		4.540	0.005	
	$^2H_{11/2}$	1907		7.900	0.009	
	$^4F_{9/2}$	1081		8.490	0.033	
	$^4I_{9/2}$	840		15.300	0.018	
	$^4I_{11/2}$	699		127.770	0.150	
	$^4I_{13/2}$	560		459.900	0.539	
	$^4I_{15/2}$	410		208.830	0.245	1.173

05-4506832 pustaka.upsi.edu.my Perpustakaan Tuanku Bainun Kampus Sultan Abdul Jalil Shah PustakaTBainun ptbupsi

05-4506832 pustaka.upsi.edu.my Perpustakaan Tuanku Bainun Kampus Sultan Abdul Jalil Shah PustakaTBainun ptbupsi

Table 4.35

The magnetic dipole and electric dipole radiative transition probabilities (A_{MD}, A_{ED}), emission branching ratio (β_R), and radiative lifetime (t_r) of 0.03 mol% ZBTEr (NPs)-CNTs glass

Er_2O_3 nanoparticles concentration (mol%)	Transition	λ (nm)	A_{MD} (s^{-1})	A_{ED} (s^{-1})	β_R	t_r (ms)
0.03	$^4I_{13/2} \rightarrow {}^4I_{15/2}$	1530	141.510	29.120	1.000	5.861
	$^4I_{11/2} \rightarrow {}^4I_{13/2}$	2804	27.700	5.610	0.420	
	$^4I_{15/2}$	990		46.030	0.580	12.604
	$^4I_{9/2} \rightarrow {}^4I_{11/2}$	4168	5.760	0.390	0.060	
	$^4I_{13/2}$	1676		11.100	0.108	
	$^4I_{15/2}$	800		85.980	0.833	9.687
	$^4F_{9/2} \rightarrow {}^4I_{9/2}$	3771	9.300	2.290	0.017	
	$^4I_{11/2}$	1980	25.670	20.210	0.069	
	$^4I_{13/2}$	1161		33.720	0.050	
	$^4I_{15/2}$	660		576.590	0.863	1.498
	$^4S_{3/2} \rightarrow {}^4I_{9/2}$	1710		18.610	0.052	
	$^4I_{11/2}$	1212		8.610	0.024	
	$^4I_{13/2}$	846		98.190	0.272	
	$^4I_{15/2}$	545		234.960	0.652	2.775
	$^2H_{11/2} \rightarrow {}^4F_{9/2}$	2497		18.450	0.004	
	$^4I_{9/2}$	1502		56.570	0.012	
	$^4I_{11/2}$	1104		43.610	0.009	
	$^4I_{13/2}$	792		67.670	0.014	
	$^4I_{15/2}$	522		4538.120	0.961	0.212
	$^4F_{7/2} \rightarrow {}^4F_{9/2}$	1942		3.560	0.003	
	$^4I_{9/2}$	1282		40.640	0.032	
	$^4I_{11/2}$	980		106.030	0.084	
	$^4I_{13/2}$	726		275.040	0.218	
	$^4I_{15/2}$	493		835.010	0.663	0.793
	$^2G_{9/2} \rightarrow {}^4F_{7/2}$	2439		7.760	0.006	
	$^2H_{11/2}$	1907		11.400	0.009	
	$^4F_{9/2}$	1081		12.290	0.022	
	$^4I_{9/2}$	840		26.240	0.020	
	$^4I_{11/2}$	699		199.770	0.155	
	$^4I_{13/2}$	560		724.170	0.560	
	$^4I_{15/2}$	410		294.480	0.228	0.774

05-4506832 pustaka.upsi.edu.my Perpustakaan Tuanku Bainun Kampus Sultan Abdul Jalil Shah PustakaTBainun ptbupsi

05-4506832 pustaka.upsi.edu.my Perpustakaan Tuanku Bainun Kampus Sultan Abdul Jalil Shah PustakaTBainun ptbupsi

Table 4.36

The magnetic dipole and electric dipole radiative transition probabilities (A_{MD}, A_{ED}), emission branching ratio (β_R), and radiative lifetime (t_r) of 0.04 mol% ZBTEr (NPs)-CNTs glass

Er_2O_3 nanoparticles concentration (mol%)	Transition	λ (nm)	A_{MD} (s^{-1})	A_{ED} (s^{-1})	β_R	t_r (ms)
0.04	$^4I_{13/2} \rightarrow {}^4I_{15/2}$	1530	150.750	52.740	1.000	4.914
	$^4I_{11/2} \rightarrow {}^4I_{13/2}$	2804	29.510	8.740	0.360	
	$^4I_{15/2}$	990		68.010	0.640	9.411
	$^4I_{9/2} \rightarrow {}^4I_{11/2}$	4168	6.130	0.520	0.058	
	$^4I_{13/2}$	1676		24.470	0.214	
	$^4I_{15/2}$	800		83.180	0.728	8.748
	$^4F_{9/2} \rightarrow {}^4I_{9/2}$	3771	9.910	1.550	0.014	
	$^4I_{11/2}$	1980	27.350	31.800	0.074	
	$^4I_{13/2}$	1161		34.310	0.043	
	$^4I_{15/2}$	660		693.720	0.869	1.252
	$^4S_{3/2} \rightarrow {}^4I_{9/2}$	1710		29.320	0.036	
	$^4I_{11/2}$	1212		17.690	0.022	
	$^4I_{13/2}$	846		224.270	0.278	
	$^4I_{15/2}$	545		536.660	0.664	1.238
	$^2H_{11/2} \rightarrow {}^4F_{9/2}$	2497		12.010	0.004	
	$^4I_{9/2}$	1502		45.670	0.014	
	$^4I_{11/2}$	1104		37.190	0.011	
	$^4I_{13/2}$	792		61.360	0.018	
	$^4I_{15/2}$	522		3173.010	0.953	0.300
	$^4F_{7/2} \rightarrow {}^4F_{9/2}$	1942		3.030	0.002	
	$^4I_{9/2}$	1282		59.110	0.032	
	$^4I_{11/2}$	980		117.570	0.064	
	$^4I_{13/2}$	726		260.420	0.142	
	$^4I_{15/2}$	493		1393.470	0.760	0.545
	$^2G_{9/2} \rightarrow {}^4F_{7/2}$	2439		5.450	0.003	
	$^2H_{11/2}$	1907		10.440	0.007	
	$^4F_{9/2}$	1081		13.090	0.018	
	$^4I_{9/2}$	840		18.540	0.012	
	$^4I_{11/2}$	699		184.310	0.117	
	$^4I_{13/2}$	560		746.080	0.474	
	$^4I_{15/2}$	410		580.230	0.369	0.636

05-4506832 pustaka.upsi.edu.my Perpustakaan Tuanku Bainun Kampus Sultan Abdul Jalil Shah PustakaTBainun ptbupsi

05-4506832 pustaka.upsi.edu.my Perpustakaan Tuanku Bainun Kampus Sultan Abdul Jalil Shah PustakaTBainun ptbupsi

Table 4.37

The magnetic dipole and electric dipole radiative transition probabilities (A_{MD}, A_{ED}), emission branching ratio (β_R), and radiative lifetime (t_r) of 0.05 mol% ZBTEr (NPs)-CNTs glass

Er_2O_3 nanoparticles concentration (mol%)	Transition	λ (nm)	A_{MD} (s^{-1})	A_{ED} (s^{-1})	β_R	t_r (ms)
0.05	$^4I_{13/2} \rightarrow {}^4I_{15/2}$	1530	132.010	12.920	1.000	6.900
	$^4I_{11/2} \rightarrow {}^4I_{13/2}$	2804	25.840	2.400	0.656	
	$^4I_{15/2}$	990		14.840	0.344	23.211
	$^4I_{9/2} \rightarrow {}^4I_{11/2}$	4168	5.370	0.190	0.095	
	$^4I_{13/2}$	1676		5.130	0.088	
	$^4I_{15/2}$	800		47.560	0.816	17.168
	$^4F_{9/2} \rightarrow {}^4I_{9/2}$	3771	8.680	0.430	0.025	
	$^4I_{11/2}$	1980	23.950	6.950	0.085	
	$^4I_{13/2}$	1161		16.140	0.044	
	$^4I_{15/2}$	660		309.210	0.846	2.737
	$^4S_{3/2} \rightarrow {}^4I_{9/2}$	1710		9.490	0.057	
	$^4I_{11/2}$	1212		4.090	0.025	
	$^4I_{13/2}$	846		45.090	0.271	
	$^4I_{15/2}$	545		107.900	0.648	6.003
	$^2H_{11/2} \rightarrow {}^4F_{9/2}$	2497		3.440	0.003	
	$^4I_{9/2}$	1502		13.070	0.012	
	$^4I_{11/2}$	1104		16.310	0.015	
	$^4I_{13/2}$	792		23.480	0.021	
	$^4I_{15/2}$	522		1054.360	0.949	0.900
	$^4F_{7/2} \rightarrow {}^4F_{9/2}$	1942		1.240	0.002	
	$^4I_{9/2}$	1282		17.500	0.027	
	$^4I_{11/2}$	980		55.860	0.086	
	$^4I_{13/2}$	726		152.520	0.236	
	$^4I_{15/2}$	493		420.080	0.649	1.545
	$^2G_{9/2} \rightarrow {}^4F_{7/2}$	2439		1.750	0.004	
	$^2H_{11/2}$	1907		4.710	0.010	
	$^4F_{9/2}$	1081		5.100	0.059	
	$^4I_{9/2}$	840		5.840	0.012	
	$^4I_{11/2}$	699		64.900	0.135	
	$^4I_{13/2}$	560		232.960	0.485	
	$^4I_{15/2}$	410		141.820	0.295	2.081

05-4506832 pustaka.upsi.edu.my Perpustakaan Tuanku Bainun Kampus Sultan Abdul Jalil Shah PustakaTBainun ptbupsi

05-4506832 pustaka.upsi.edu.my Perpustakaan Tuanku Bainun Kampus Sultan Abdul Jalil Shah PustakaTBainun ptbupsi

4.6.8 Luminescence Analysis

Figures 4.47 and 4.48 show the luminescence spectra of Er^{3+} nanoparticles for ZBTEr (NPs)-CNTs and ZBTEr (NPs)-uncoated glasses excited by excitation at 357 nm with an average range of 500 – 600 nm and corresponding to the room temperature. Referring to Figure 4.47, it was clearly presented that the luminescence spectra of the ZBTEr (NPs)-CNTs glasses shows two prominent emission peaks at 530 nm and 551 nm range which was corresponded to $^2H_{11/2} \rightarrow {}^4I_{15/2}$ and $^4S_{3/2} \rightarrow {}^4I_{15/2}$ transitions, respectively. In comparison, Figure 4.48 presents only one prominent peak in the range of 550 – 560 nm for the ZBTEr (NPs)-uncoated glasses. Moreover, the highest luminescence intensity generated by the green emission at 551 nm can be associated with the excited state of oxygen-vacancy and defect-level of emission that occurred in the ZBTEr (NPs)-CNTs phase, as shown in Figure 4.47.

Additionally, the ZBTEr (NPs)-CNTs glasses with 0.005 and 0.01 mol% of Er^{3+} nanoparticles concentration presented a higher intensity peak, as compared to the other concentration of glasses. As a result, these findings are proved by Judd-Ofelt's analysis whereby, the intensity parameters and spectroscopic quality are particularly important for improving the ZBTEr (NPs)-CNTs glasses than the ZBTEr (NPs)-uncoated glasses. Other than that, it can be concluded that the luminescence intensity decreases as the increase of Er^{3+} nanoparticles in the ZBTEr (NPs)-CNTs glass system. Consequently, these results attribute to the luminescence concentration quenching (LCQ) that is caused by the non-radiative energy transfer via the cross-relaxation (CR) process in the amorphous matrix

05-4506832 pustaka.upsi.edu.my Perpustakaan Tuanku Bainun Kampus Sultan Abdul Jalil Shah PustakaTBainun ptbupsi

05-4506832 pustaka.upsi.edu.my Perpustakaan Tuanku Bainun Kampus Sultan Abdul Jalil Shah PustakaTBainun ptbupsi

system. Besides, the decreasing luminescence intensity can be attributed to the effects of CNTs whereby, the ZBTEr (NPs) glass surfaces are fully covered with CNTs layers and thus, creating the formation of C-O and C=O bonds on the glass surfaces.

Other than that, the ZBTEr (NPs)-CNTs glasses implied that the electrons supposedly jumped from the valence band to the conduction band however, the excited electrons decreased from the conduction band and thus, releasing the photon energy which tend to undergo the non-radiative relaxation process (Chan et al., 2021). The energy exciton states were generated via the strong electron-electron interactions between the CNTs coating layers and tellurite-based glass surfaces, attributing to an improved luminescence excitation in the ZBTEr (NPs)-CNTs glasses. Furthermore, the formation of carbon bonds on the tellurite-based glass surfaces exhibits the high performance of luminescence excitation, resulting in the enhancement of luminescence intensity.

The influence of CNTs coating on luminescence characteristics of ZBTEr (NPs)-CNTs glasses was compared with the ZBTEr (NPs)-uncoated glasses, as reported by (Azlan, et al., 2015). It was worth noting that the luminescence intensity was improved by coating the tellurite-based glass surfaces with CNTs.

05-4506832 pustaka.upsi.edu.my Perpustakaan Tuanku Bainun Kampus Sultan Abdul Jalil Shah PustakaTBainun ptbupsi

05-4506832 pustaka.upsi.edu.my Perpustakaan Tuanku Bainun Kampus Sultan Abdul Jalil Shah PustakaTBainun ptbupsi

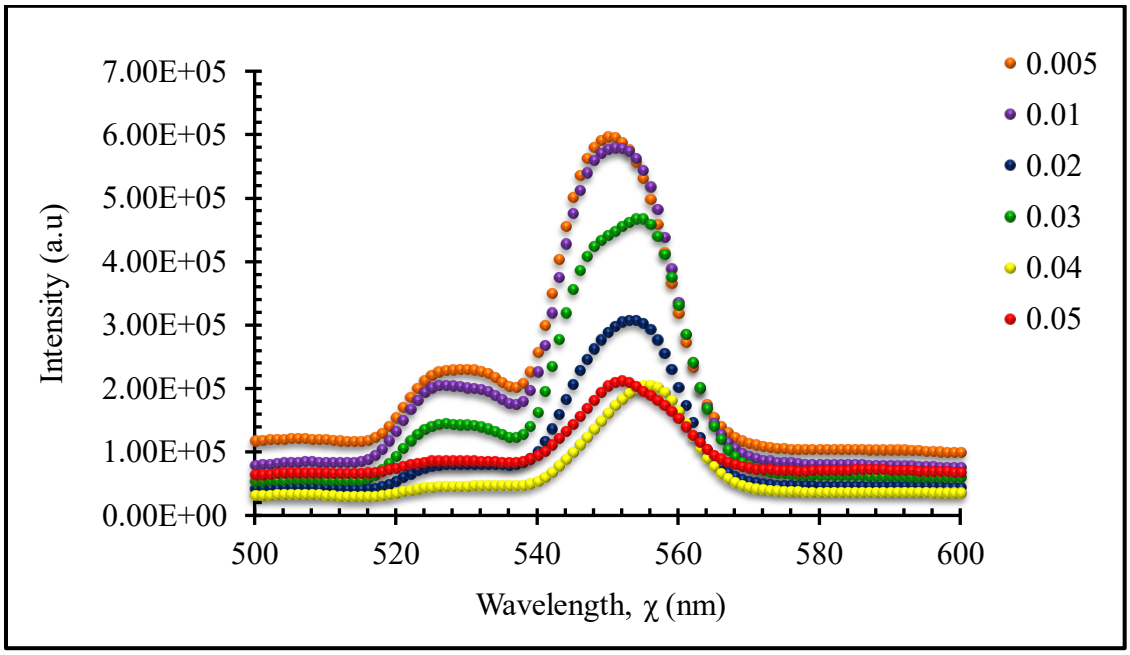


Figure 4.47. Luminescence spectra of ZBTEr (NPs)-CNTs glasses

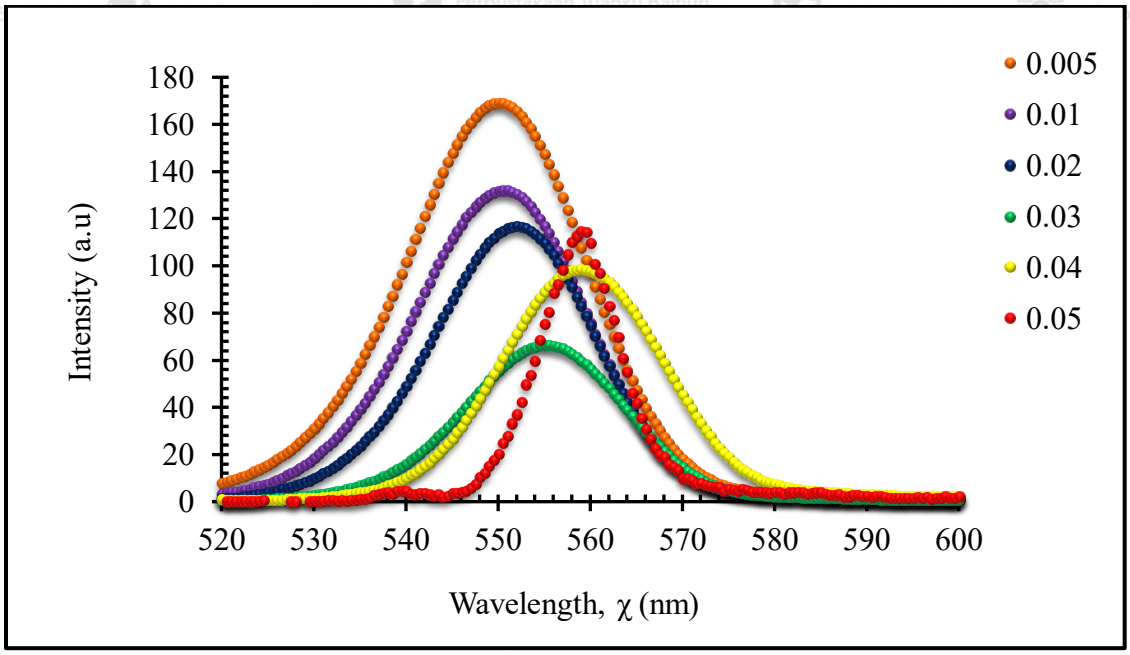


Figure 4.48. Luminescence spectra of ZBTEr (NPs)-uncoated glasses (Azlan, Halimah, Suriani, Azlina, Umar, et al., 2019)

05-4506832 pustaka.upsi.edu.my Perpustakaan Tuanku Bainun Kampus Sultan Abdul Jalil Shah PustakaTBainun ptbupsi

05-4506832 pustaka.upsi.edu.my Perpustakaan Tuanku Bainun Kampus Sultan Abdul Jalil Shah PustakaTBainun ptbupsi

Figure 4.49 displays the electronic configuration schematic energy level diagram of the ZBTEr (NPs)-CNTs and ZBTEr (NPs)-uncoated glasses under the excitation at 375 nm wavelength for determination of emission and energy transfer (ET) mechanism. As presented in Figure 4.49, the Er^{3+} nanoparticles are then observed to be excited by absorbing a photon from the ground state level $^4I_{15/2}$ to the excited state level $^4G_{11/2}$ through the ground state absorption (GSA) process. Afterward, the electrons are sequentially raised from the $^4G_{11/2}$ level to undergo the decay non-radiatively (NR) process through multi-phonon relaxation (MPR) in order to populate to $^2H_{9/2}$, $^4F_{5/2}$, and $^4F_{7/2}$ transition levels. Furthermore, the electrons located at the $^4F_{7/2}$ level are relaxed non-radiatively (NR) and ultimately populate at the $^2H_{11/2}$ level in which the present state level is located in a thermal equilibrated population with the excited state $^4S_{3/2}$ level. These resulting states are observed whereby, the electrons decay radiatively (R) to produce the green emission state at $^2H_{11/2}$ + $^4S_{3/2}$ levels to the ground state $^4I_{15/2}$ level in the ZBTEr (NPs)-CNTs glasses.

The possible causes of the red emission mechanism could be ascribed via the energy transfer (ET) process between two distances of Er^{3+} ions in the ZBTEr (NPs)-CNTs glasses. The red emission peaks are strongly influenced by the energy transfer (ET) process through the effect of Er^{3+} ions nanoparticles in the amorphous matrix system, as follows:

$$ET_1: Er^{3+}(^4I_{13/2}) + Er^{3+}(^4I_{11/2}) \rightarrow Er^{3+}(^4F_{9/2}) + Er^{3+}(^4I_{15/2})$$

$$ET_2: Er^{3+}(^4I_{11/2}) + Er^{3+}(^4I_{13/2}) \rightarrow Er^{3+}(^4F_{9/2}) + Er^{3+}(^4I_{15/2})$$

05-4506832 pustaka.upsi.edu.my Perpustakaan Tuanku Bainun Kampus Sultan Abdul Jalil Shah PustakaTBainun ptbupsi

05-4506832 pustaka.upsi.edu.my Perpustakaan Tuanku Bainun Kampus Sultan Abdul Jalil Shah PustakaTBainun ptbupsi

Nonetheless, it can be seen that the red emission peak disappears in the present ZBTEr (NPs)-CNTs glasses along with the increase of Er^{3+} ions nanoparticles, as shown in Figure 4.47. It was believed that due to the low concentration of Er^{3+} ions nanoparticles that exist in the ZBTEr (NPs)-CNTs glasses. Besides, the green emission bands as illustrated in Figure 4.49 may be attributed to the cross-relaxation (CR) process, as follows:

$$CR_1: {}^4S_{3/2} + {}^4I_{15/2} \rightarrow {}^4I_{9/2} + {}^4I_{13/2}$$

$$CR_2: {}^4S_{9/2} + {}^4I_{15/2} \rightarrow {}^4I_{11/2} + {}^4I_{13/2}$$

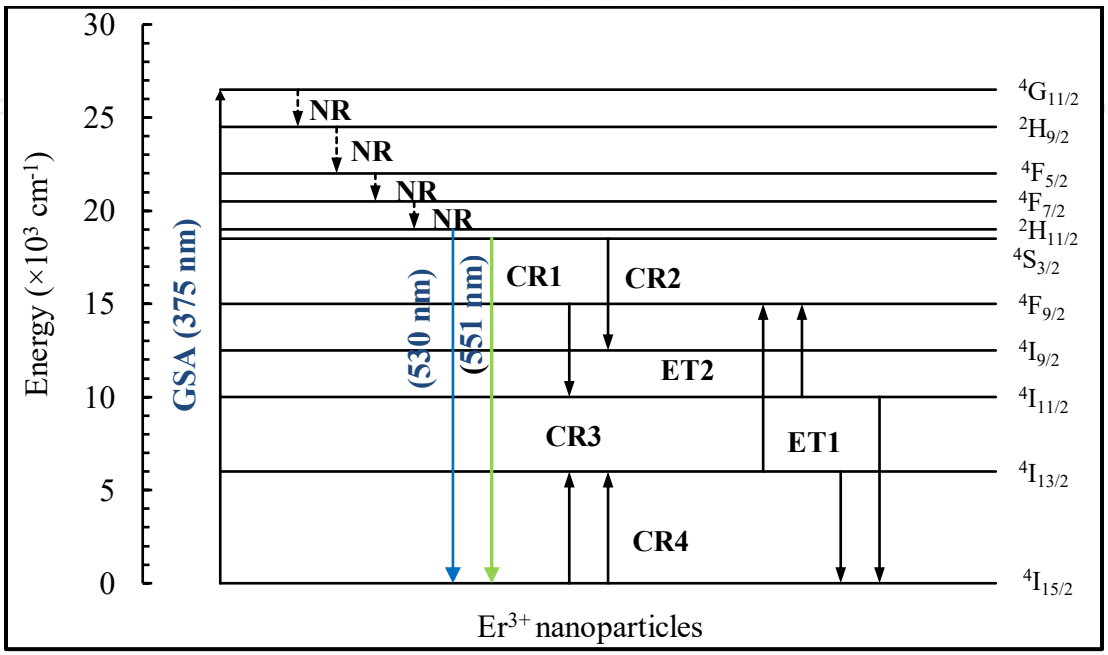


Figure 4.49. Schematic energy levels diagram of Er^{3+} nanoparticles of the ZBTEr (NPs)-CNTs and ZBTEr (NPs)-uncoated glasses

05-4506832 pustaka.upsi.edu.my Perpustakaan Tuanku Bainun Kampus Sultan Abdul Jalil Shah PustakaTBainun ptbupsi

05-4506832 pustaka.upsi.edu.my Perpustakaan Tuanku Bainun Kampus Sultan Abdul Jalil Shah PustakaTBainun ptbupsi

4.7 Comparative Studies of the ZBTEr (NPs)-rGO and ZBTEr (NPs)-CNTs Glasses

The comparative studies of the ZBTEr (NPs)-rGO and ZBTEr (NPs)-CNTs glasses have been studied to further investigate the effects and correlation between the rGO or CNTs coating layer and tellurite-based glass. This analysis provides a discussion of the comparative studies between the present study with the previous studies which can be related to this work. Additionally, this section comprises the optical properties including, optical bandgap energy, refractive index, and Judd-Ofelt's analysis, as presented in next subsection 4.7.1.

4.7.1 Optical Properties Characterization

05-4506832 pustaka.upsi.edu.my Perpustakaan Tuanku Bainun Kampus Sultan Abdul Jalil Shah PustakaTBainun ptbupsi

Generally, this section provides the discussion on the two fundamental optical properties including, optical bandgap energy and refractive index along with the supported data, as has been tabulated previously in Table 4.6, 4.8, 4.23, and 4.25, respectively. The ZBTEr (NPs)-rGO and ZBTEr (NPs)-CNTs glasses were successfully presented which demonstrated the optimum value for optical bandgap energy and refractive index. Importantly, it can be noticed that the correlation between optical bandgap energy and refractive index is vital for many applications especially in wide bandgap semiconductors. Afterward, the detail of the analytical comparative studies between the optical bandgap energy and refractive index will be discussed in this section.

05-4506832 pustaka.upsi.edu.my Perpustakaan Tuanku Bainun Kampus Sultan Abdul Jalil Shah PustakaTBainun ptbupsi

05-4506832 pustaka.upsi.edu.my Perpustakaan Tuanku Bainun Kampus Sultan Abdul Jalil Shah PustakaTBainun ptbupsi

As has been presented earlier in subsections 4.4.2, 4.4.4, 4.6.2, and 4.6.4, it can be noticed that the ZBTEr (NPs)-rGO glass at 0.04 mol% of Er-NPs concentration demonstrated the optical bandgap energy value, E_{opt} = 2.980 eV and refractive index value, n = 2.402. Meanwhile, the ZBTEr (NPs)-CNTs glass at 0.05 mol% of Er-NPs concentration presented the optical bandgap energy value, E_{opt} = 2.875 eV and refractive index, n = 2.432. It was noted that a higher value of optical bandgap energy was demonstrated to enhance the refractive index value which in turn both of these values are suitable to be applied in fiber optics technology (Lalla et al., 2020). From this point of view, Gomaa et al., (2021) proposed that the relation between the optical bandgap energy and the refractive index was strongly dependent on the optical absorption of the material whereby, the atoms absorb and emit electromagnetic radiation. The high optical absorption in the ZBTEr (NPs)-rGO glasses were significantly produced a high refractive index value due to the existing electronic transitions. Furthermore, the optical refractive index was utilized in various fields of optoelectronic devices including, optical lasers, light-emitting diodes (LEDs), as well as linear and non-linear optics.

Additionally, it is crucial to understand the correlation between bandgap energy and refractive index in this study whereby, these optical properties are vital among the other properties especially for fiber optics. Moreover, these two fundamental properties are critical that can be applied for the estimation of the choice of semiconductor devices primarily in fiber optics communication (Lamichhane & Ravindra, 2020).

05-4506832 pustaka.upsi.edu.my Perpustakaan Tuanku Bainun Kampus Sultan Abdul Jalil Shah PustakaTBainun ptbupsi

05-4506832 pustaka.upsi.edu.my Perpustakaan Tuanku Bainun Kampus Sultan Abdul Jalil Shah PustakaTBainun ptbupsi

Therefore, an analytical comparison was presented on the optical properties of the ZBTEr (NPs)-rGO and ZBTEr (NPs)-CNTs glasses showing the different values of optical bandgap energy and refractive index between the present study and previous studies, as stated in the summarized results in Table 4.38. Particularly, it can be clearly seen that the ZBTEr (NPs)-rGO and ZBTEr (NPs)-CNTs glasses in the present study demonstrate the lower value of optical bandgap energy at approximately, 2.875 eV and 2.890 eV and high refractive index value in the range 2.402 and 2.432 compared to the ZBTEr (NPs)-uncoated and Er^{3+} doped chloroborotellurite (OCBTEr) (Sailaja et al., 2021). Consequently, these results were believed due to the stronger bonding interaction between the rGO or CNTs coating layer on the tellurite-based glass surfaces. In addition, the high functionalization of the rGO and CNTs layers that are attached on the glass surfaces may alter the forbidden energy gap between the valence band (VB) and conduction band (CB) in the electronic transition and thereby, resulting in the decreasing optical bandgap energy value. Nevertheless, it was concluded that the obtained range values of bandgap energy for the coated glasses in the present work is good for semiconductor properties especially in the field of fiber optics.

Moreover, the optical bandgap energy values of the ZBTEr (NPs)-rGO and ZBTEr (NPs)-CNTs glasses were slightly higher than in the previous studies as proposed in the Er^{3+} doped nanoparticles bio-silica borotellurite (TBSEr (NPs)) (Halimah et al., 2019) and Er^{3+} doped alkali bismuth borate (BLKEr) (Mariyappan et al., 2019) glasses. In comparison, the previous works suggested that the obtained bandgap energy values were probably due to the incorporation of Er^{3+} nanoparticles in the amorphous glass system, as

05-4506832 pustaka.upsi.edu.my Perpustakaan Tuanku Bainun Kampus Sultan Abdul Jalil Shah PustakaTBainun ptbupsi

05-4506832 pustaka.upsi.edu.my Perpustakaan Tuanku Bainun Kampus Sultan Abdul Jalil Shah PustakaTBainun ptbupsi

well as the presence of the borate oxide, B_2O_3 as the glass modifier which possesses higher phonon energy compared to other oxides. Notably, the high optical bandgap energy values are categorized in the semiconductor properties and useful for optical laser applications.

Nevertheless, it was noticed that the uncoated glass samples displayed higher optical bandgap energy values which correlated to the effects of particle size of dopant. In comparison, the increase of optical bandgap energy was caused by the smaller particle size in which the Er^{3+} nanoparticles were added into the host glass matrix. As a result, the smaller size of particles resulted in the widening of the optical bandgap energy value in the glass system.

Based on the optical bandgap energy, it can be noticed that the refractive index value of the ZBTEr (NPs)-rGO and ZBTEr (NPs)-CNTs glasses exhibited an increasing trend than the other previous studies, as tabulated in Table 4.39. Generally, the increasing refractive index value can be ascribed to the density factor of the rGO and CNTs layers on the glass surfaces and subsequently, caused to the shift of optical absorption spectra. In addition to this, it was noticed that the intensity in the optical absorption spectra of the ZBTEr (NPs)-rGO and ZBTEr (NPs)-CNTs glasses were found improved, as the rGO and CNTs coating materials were deposited on the glass surfaces. Therefore, it can be concluded that the deposition of rGO and CNTs demonstrates higher refractive index in the amorphous glass system.

05-4506832 pustaka.upsi.edu.my Perpustakaan Tuanku Bainun Kampus Sultan Abdul Jalil Shah PustakaTBainun ptbupsi

05-4506832 pustaka.upsi.edu.my Perpustakaan Tuanku Bainun Kampus Sultan Abdul Jalil Shah PustakaTBainun ptbupsi

Table 4.38

The summarized results of optical bandgap energy, E_{opt} and refractive index, n for ZBTEr (NPs)-rGO, ZBTEr (NPs)-CNTs, and previous studies

Glass systems	Er_2O_3 nanoparticles concentration (mol%)	Optical bandgap energy, E_{opt} (eV)	Refractive index, n	Literature
ZBTEr (NPs)-rGO	0.040	2.980	2.402	Present work
ZBTEr (NPs)-CNTs	0.050	2.875	2.432	Present work
ZBTEr (NPs)	0.050	3.840	1.924	(Azlan et al., 2017)
TBSEr (NPs)	0.100	2.890	2.297	(Halimah et al., 2019)
OCBTEr	2.500	3.800	2.224	(Sailaja et al., 2021)
BLKEr	0.050	2.619	1.641	(Mariyappan et al., 2019)

05-4506832 pustaka.upsi.edu.my Perpustakaan Tuanku Bainun Kampus Sultan Abdul Jalil Shah PustakaTBainun ptbupsi

05-4506832 pustaka.upsi.edu.my Perpustakaan Tuanku Bainun Kampus Sultan Abdul Jalil Shah PustakaTBainun ptbupsi

As can be referred to Table 4.39, it can be clearly noticed that the ZBTEr (NPs)-rGO glass with 0.01 mol% of Er_2O_3 nanoparticles concentration showed the $\Omega_2 > \Omega_6 > \Omega_4$ trend meanwhile, the ZBTEr (NPs)-CNTs glass with 0.04 mol% of Er_2O_3 nanoparticles concentration followed the $\Omega_2 > \Omega_4 > \Omega_6$ trend. These results indicate that the higher value of the Ω_2 intensity parameter that may be correlated to the strong covalency and symmetry around Er^{3+} ions sites along with the deposition of the rGO and CNTs layers on the glass surfaces. Similarly, it can be seen that the previous studies demonstrated the higher value of the Ω_2 intensity parameter which has been proved by 0.2 mol% and 0.5 mol% Er^{3+} doped sodium zinc-tellurite (Zhang et al., 2021) and Er^{3+} doped halageno-antimonate (Iezid et al., 2021) glasses.

In contrast, it can be clearly seen that the Er^{3+} doped fluoroindate glass system (Liu et al., 2021) showed a high value of Ω_6 intensity parameter as compared with the present study. As a result, the increasing value of the Ω_6 intensity parameter was influenced by the overlap integral of the 5*d* and 4*f* orbital electrons around Er^{3+} ligand bonds and thus, the Ω_6 intensity parameter was indicated to be less dependent on the environment (Tanabe et al., 1993; Yang et al., 2004). Furthermore, it is worth noting that the lower value of Ω_4 and Ω_6 intensity parameters correlate to relatively low ionicity, rigidity, and viscosity as well as, favorable to be used in the luminescence properties (Sailaja et al., 2021; Yusof, Ghoshal, & Azlan, 2017).

05-4506832 pustaka.upsi.edu.my Perpustakaan Tuanku Bainun Kampus Sultan Abdul Jalil Shah PustakaTBainun ptbupsi

05-4506832 pustaka.upsi.edu.my Perpustakaan Tuanku Bainun Kampus Sultan Abdul Jalil Shah PustakaTBainun ptbupsi

Table 4.39

The summarized results of Judd-Ofelt's intensity parameters, Ω_t (t = 2, 4, 6) for ZBTEr (NPs)-rGO, ZBTEr (NPs)-CNTs, and previous studies

Glass systems	Er_2O_3 concentration nanoparticles (mol%)	Ω_2	Ω_4	Ω_6	$\chi = \frac{\Omega_4}{\Omega_6}$	Ω_i Trend	Literature
ZBTEr (NPs)-rGO	0.010	0.145	0.065	0.070	0.923	$\Omega_2 > \Omega_6 > \Omega_4$	Present work
ZBTEr (NPs)-CNTs	0.040	0.412	0.162	0.107	1.507	$\Omega_2 > \Omega_4 > \Omega_6$	Present work
TZNaEr	0.200	5.600	2.110	0.730	2.890	$\Omega_2 > \Omega_4 > \Omega_6$	(Zhang et al., 2021)
TZNaEr	0.500	4.820	1.510	0.850	1.776	$\Omega_2 > \Omega_4 > \Omega_6$	(Zhang et al., 2021)
IZSB-1Er	0.200	1.360	0.670	2.100	0.319	$\Omega_6 > \Omega_2 > \Omega_4$	(Liu et al., 2021)
SZNEr	0.200	3.270	1.240	1.880	0.660	$\Omega_2 > \Omega_6 > \Omega_4$	(Iezid et al., 2021)

05-4506832 pustaka.upsi.edu.my Perpustakaan Tuanku Bainun Kampus Sultan Abdul Jalil Shah PustakaTBainun ptbupsi

05-4506832 pustaka.upsi.edu.my Perpustakaan Tuanku Bainun Kampus Sultan Abdul Jalil Shah PustakaTBainun ptbupsi

Besides that, both the refractive index and Judd-Ofelt's intensity parameters are dependent on the wavelength of the obtained absorption spectra (Lalla et al., 2020). Furthermore, it can be noticed that the refractive index value of the ZBTEr (NPs)-rGO and ZBTEr (NPs)-CNTs glasses are considerably higher than the ZBTEr (NPs)-uncoated glasses, as proved in Table 4.8 and 4.26, respectively. According to Richards & Jha, (2017), the higher value of the refractive index (above ~1.800) and low multi-phonon decay rates may increase the radiative transition probabilities. Therefore, it was concluded that the refractive index value plays an important role in Judd-Ofelt's intensity parameters of both coated glasses in this present work. Additionally, the higher refractive index value of both ZBTEr (NPs)-rGO and ZBTEr (NPs)-CNTs demonstrates larger stark splitting effects (Raouf El-Mallawany, 2017; Richards & Jha, 2017) which have been presented in subsections 4.4.8 and 4.6.8, respectively.

Moreover, it can be noted that the radiative lifetime of both the ZBTEr (NPs)-rGO and ZBTEr (NPs)-CNTs glasses estimated by Judd-Ofelt's studies showed a longer value (higher than ~10^{-5} s) which significantly supported by previous studies (Lalla et al., 2019; Mariyappan et al., 2019; Marzouk et al., 2021).

Apart from that, Judd-Ofelt's intensity parameters can be correlated with the chemical nature of the metal-ligand bonds whereby, these ligands are part of the structural complexity of the glassy matrix and thus, resulting in the hypersensitive transition of Ω_2 dependency (Lalla et al., 2020). Additionally, the tellurite host glassy matrix which has been used in the present work offers a large compositional space that varies due to its

05-4506832 pustaka.upsi.edu.my Perpustakaan Tuanku Bainun Kampus Sultan Abdul Jalil Shah PustakaTBainun ptbupsi

05-4506832 pustaka.upsi.edu.my Perpustakaan Tuanku Bainun Kampus Sultan Abdul Jalil Shah PustakaTBainun ptbupsi

advantages in the glass transition, melting temperature, as well as crystallization temperature and hence, these important factors cause the variation of the Judd-Ofelt's intensity parameters. In this regard, it was concluded that the calculated Judd-Ofelt's intensity parameters of the ZBTEr (NPs)-rGO and ZBTEr (NPs)-CNTs glasses showed satisfactory values including, oscillator strengths and low root mean square deviation, δ_{rms} as can be observed similarly in the previous studies (Amiar Rodin & Sahar, 2018; Hasim & Rohani, 2017; Jupri et al., 2018; Lachheb et al., 2018).

Moreover, the REIs of Er^{3+} ions presenting in the Judd-Ofelt's intensity parameters of the ZBTEr (NPs)-rGO and ZBTEr (NPs)-CNTs glasses demonstrated a good agreement value due to the absorption spectra possessing intense and non-overlapping absorption bands from the UV region, as proved by the obtained optical absorption spectra (refer to Figures 4.13 and 4.37) which in turn allowing more accurate estimation of oscillator strengths and Judd-Ofelt's intensity parameters values.

4.8 Summary

In summary, it was concluded that the physical, structural, and optical properties of the ZBTEr (NPs)-rGO, ZBTEr (NPs)-CNTs, and ZBTEr (NPs)-uncoated had been investigated in this work. The optical properties of both ZBTEr (NPs)-rGO and ZBTEr (NPs)-CNTs glasses were increased than the ZBTEr (NPs)-uncoated glasses which ascribed to the effects of rGO and CNTs coating layer on the glass surfaces. Afterward, the

05-4506832 pustaka.upsi.edu.my Perpustakaan Tuanku Bainun Kampus Sultan Abdul Jalil Shah PustakaTBainun ptbupsi

05-4506832 pustaka.upsi.edu.my Perpustakaan Tuanku Bainun Kampus Sultan Abdul Jalil Shah PustakaTBainun ptbupsi

morphological studies of both ZBTEr (NPs)-rGO and ZBTEr (NPs)-CNTs glasses clearly proved the rGO and CNTs structures that are attached on the glass surfaces with the supported EDX and micro-Raman analyses. Meanwhile, the Judd-Ofelt's analysis and luminescence properties were successfully accomplished which acts as the important parameters for improving the ZBTEr (NPs) glasses. Thus, the deposition of rGO and CNTs coating layer on the ZBTEr (NPs) glass surfaces was believed to be potentially improved the optical properties of glass materials as well as, may be utilized for future fiber optics applications.

05-4506832 pustaka.upsi.edu.my Perpustakaan Tuanku Bainun Kampus Sultan Abdul Jalil Shah PustakaTBainun ptbupsi
05-4506832 pustaka.upsi.edu.my Perpustakaan Tuanku Bainun Kampus Sultan Abdul Jalil Shah PustakaTBainun ptbupsi

05-4506832 pustaka.upsi.edu.my Perpustakaan Tuanku Bainun Kampus Sultan Abdul Jalil Shah PustakaTBainun ptbupsi

CHAPTER 5

CONCLUSION AND FUTURE WORKS

05-4506832 pustaka.upsi.edu.my Perpustakaan Tuanku Bainun Kampus Sultan Abdul Jalil Shah PustakaTBainun ptbupsi

5.1 Introduction

This chapter reviewed a summary of the related findings from the experimental investigation of the ZBTEr (NPs)-rGO and ZBTEr (NPs)-CNTs glasses in this work, which are in accordance to the research objectives as mentioned in Chapter 1. Remarkably, it is important to conclude that the objectives were successfully achieved based on the overall physical, structural, and optical properties which can be used as a benchmark for the fabrication of the glass coatings. The scientific contribution is well-emphasized throughout this study with the presented prospective tasks for future outlooks.

05-4506832 pustaka.upsi.edu.my Perpustakaan Tuanku Bainun Kampus Sultan Abdul Jalil Shah PustakaTBainun ptbupsi

05-4506832 pustaka.upsi.edu.my Perpustakaan Tuanku Bainun Kampus Sultan Abdul Jalil Shah PustakaTBainun ptbupsi

5.2 Conclusion

In summary, the two sets of glass series, namely as the ZBTEr (NPs)-rGO and ZBTEr (NPs)-CNTs glasses were successfully fabricated by utilizing the conventional melt-quenching and spray coating techniques. To achieve the objectives in this work, the physical, structural, and optical properties of the ZBTEr (NPs)-rGO and ZBTEr (NPs)-CNTs glass samples were studied. The optical properties of coated glasses were principally influenced by the effects of the rGO and CNTs coating layers attached on the glass surfaces.

In the present work, the density and molar volume of the ZBTEr (NPs)-rGO and ZBTEr (NPs)-CNTs glasses were found to increase along with the increase of Er_2O_3 nanoparticles concentration approximately from 4.588 kg/m^3 to 4.881 kg/m^3 and 25.868 m^3/mol to 26.737 m^3/mol, respectively. It can be concluded that the increased value of both density and molar volume was correlated to the higher atomic mass and atomic radius of the Er_2O_3 nanoparticles compared to the tellurite oxide, TeO_2. The decreased value of polaron radius resulted from the increased value of erbium ion concentration. Meanwhile, the oxygen packing density (OPD) and field strength were found to increase due to the greater atomic mass and ionic radius in the glass system.

SEM micrographs displayed the existence of rGO and CNTs structures on the glass surfaces and TEM images confirmed the average size of erbium nanoparticles in the range of ~23.530 nm. The XRD spectra proved the amorphous nature for ZBTEr (NPs)-rGO and ZBTEr (NPs)-CNTs glass samples. The transmission bands demonstrated the presence of

05-4506832 pustaka.upsi.edu.my Perpustakaan Tuanku Bainun Kampus Sultan Abdul Jalil Shah PustakaTBainun ptbupsi

05-4506832 pustaka.upsi.edu.my Perpustakaan Tuanku Bainun Kampus Sultan Abdul Jalil Shah PustakaTBainun ptbupsi

stretching vibrations mode of TeO_4, TeO_3, and BO_3 structural units, showing the formation of non-bridging oxygens (NBOs) in the host glassy matrix. Meanwhile, the Raman spectra demonstrated the high-quality with the better dispersion obtained for rGO and CNTs solutions.

The optical absorption bands spectra from UV-Vis analysis were presented for all the ZBTEr (NPs)-rGO and ZBTEr (NPs)-CNTs glass samples whereby, the obtained peaks are recognized to 4*f*-4*f* transition from the ground state level, $^4G_{11/2}$ to various excited state levels ($^2H_{9/2}$, $^4F_{5/2}$, $^4F_{7/2}$, $^2H_{11/2}$, $^4S_{3/2}$, $^4F_{9/2}$, $^4I_{11/2}$, and $^4I_{9/2}$). Based on the obtained absorption spectra in this work, it was shown that the optical bandgap energy value of the ZBTEr (NPs)-rGO glasses was found to improve approximately from 1.913 eV to 2.980 eV meanwhile, from 2.513 eV to 2.875 eV for the ZBTEr (NPs)-CNTs glasses. The improved value of optical bandgap energy was ascribed to the shift of optical absorption which resulted from the effects of high functionalization of rGO and CNTs structures. Apart from that, the Urbach energy value was found in a non-linear trend approximately from 0.118 eV to 0.408 eV for the ZBTEr (NPs)-rGO glasses meanwhile, from 0.158 eV to 0.375 eV for the ZBTEr (NPs)-CNTs glasses. Consequently, the Urbach energy value was correlated to the phonon-assisted transition, indicating high defects in the amorphous glass matrix.

The obtained finding of refractive index value was found to increase along with the increase of Er_2O_3 nanoparticles concentration approximately from 2.402 to 2.775 for the ZBTEr (NPs)-rGO glasses meanwhile, from 2.432 to 2.542 for the ZBTEr (NPs)-CNTs glasses. As a result, it was noticed that the presence of a high degree number of

05-4506832 pustaka.upsi.edu.my Perpustakaan Tuanku Bainun Kampus Sultan Abdul Jalil Shah PustakaTBainun ptbupsi

05-4506832 pustaka.upsi.edu.my Perpustakaan Tuanku Bainun Kampus Sultan Abdul Jalil Shah PustakaTBainun ptbupsi

functionalized groups from the high agglomeration structures attached on the glass surfaces may enhance the refractive index value. Additionally, the obtained results of reflection loss, transmission coefficient, and dielectric constant values were found in a non-linear trend along with the increase of Er_2O_3 nanoparticles concentration ranging from (0.169 – 0.221), (0.638 – 0.709), and (5.769 – 7.701), respectively for the ZBTEr (NPs)-rGO glasses meanwhile, (0.174 – 0.189), (0.681 – 0.703), and (5.915 – 6.462), respectively for the ZBTEr (NPs)-CNTs glasses due to the changes in the optical absorption. It can be concluded that these optical parameters were clearly deduced based on the refractive index value of the ZBTEr (NPs)-rGO and ZBTEr (NPs)-CNTs glasses.

The refractive index optical electronegativity-based oxide ion polarizability, $\alpha_0^{2-}(\Delta\chi^*(n))$ value demonstrates the reliable results of oxide ion polarizability value than the obtained results of energy bandgap optical electronegativity-based oxide ion polarizability, $\alpha_0^{2-}(\Delta\chi^*(E_{opt}))$ value for the ZBTEr (NPs)-rGO and ZBTEr (NPs)-CNTs glass samples. Hence, it can be described that the obtained results of optical electronegativity indicate the stronger covalency of the ligand bond that exists in the glassy matrix system.

The Judd-Ofelt's intensity parameters showed the $\Omega_2>\Omega_6>\Omega_4$ trend for 0.005, 0.01, and 0.02 mol% Er_2O_3 nanoparticles concentration samples of the ZBTEr (NPs)-rGO glasses whereby, these results showed the higher value of Ω_2 which was correlated due to the effects of the rGO coating layer on the glass surfaces, resulting in a high covalency and asymmetry around Er^{3+} ions sites. Besides, the findings showed the lowest value of Ω_2 from 0.03, 0.04, and 0.05 mol% Er_2O_3 nanoparticles concentration samples which can be

05-4506832 pustaka.upsi.edu.my Perpustakaan Tuanku Bainun Kampus Sultan Abdul Jalil Shah PustakaTBainun ptbupsi

05-4506832 pustaka.upsi.edu.my Perpustakaan Tuanku Bainun Kampus Sultan Abdul Jalil Shah PustakaTBainun ptbupsi

ascribed to the weaker bonding around Er^{3+} and thus, demonstrating the long-range effects of amorphous glassy matrix and strong ionicity between the Er-O bonds. Meanwhile, the Judd-Ofelt's intensity parameters followed the $\Omega_2>\Omega_4>\Omega_6$ trend for the ZBTEr (NPs)-CNTs glasses except 0.01 mol% Er_2O_3 nanoparticles concentration sample whereby, these findings corresponded to the strong covalency and high asymmetry of local surroundings around Er^{3+} ions sites. Nonetheless, the sample of 0.01 mol% exhibits the lowest Ω_6 value which correlates to the less rigidity between Er^{3+} ions and ligand bonds in the glassy matrix. Hence, it can be concluded that the high functionalization of rGO and CNTs structures on the glass surfaces promotes altering the Judd-Ofelt's intensity parameters value. As a result, the improved value of Judd-Ofelt's intensity parameters may beneficial for improving the current fiber optics technology.

05-4506832 pustaka.upsi.edu.my Perpustakaan Tuanku Bainun Kampus Sultan Abdul Jalil Shah PustakaTBainun ptbupsi

Furthermore, it was noticed that the radiative parameters, branching ratio, and radiative lifetime were calculated based on the input data from the different absorption bands. Similarly, the ZBTEr (NPs)-rGO and ZBTEr (NPs)-CNTs glasses demonstrated the radiative parameters and branching ratio at the $^2H_{11/2}\rightarrow{}^4I_{15/2}$ transition which presented the highest radiative transition value and thereby, suggesting a strong green emission. As a result, it was found that the branching ratio is relevant for $^2H_{11/2}\rightarrow{}^4I_{15/2}$ transition with approximately (0.900 – 0.970) and the radiative lifetime showed a value ranging from (0.245 – 0.819 ms), respectively for all the ZBTEr (NPs)-rGO glass samples. Meanwhile, the obtained value of branching ratio falls into the range of (0.950 – 0.960) and radiative lifetime showed the value approximately from (0.212 – 0.900 ms), respectively. These

05-4506832 pustaka.upsi.edu.my Perpustakaan Tuanku Bainun Kampus Sultan Abdul Jalil Shah PustakaTBainun ptbupsi

05-4506832 pustaka.upsi.edu.my Perpustakaan Tuanku Bainun Kampus Sultan Abdul Jalil Shah PustakaTBainun ptbupsi

findings indicate the significant lifetime values that caused by the effects of rGO and CNTs coating layer and show a good improvement in Judd-Ofelt's analysis.

Meanwhile, this presented work was supported by luminescence analysis which showed two strong emission peaks at 375 nm excitation for both the ZBTEr (NPs)-rGO and ZBTEr (NPs)-CNTs glasses. As a result, these findings showed that the luminescence spectra correspond to the $^2H_{11/2} \rightarrow {}^4I_{15/2}$ and $^4S_{3/2} \rightarrow {}^4I_{15/2}$ transitions whereby, the luminescence intensity for a green laser is dominant for the ZBTEr (NPs)-rGO and ZBTEr (NPs)-CNTs glasses. Nevertheless, it was observed that the absence of red emission can be ascribed to the effects of a small concentration of Er_2O_3 nanoparticles dopant in the host glassy matrix. Importantly, the luminescence mechanism is demonstrated by using the energy level diagram of Er^{3+} ions nanoparticles of the ZBTEr (NPs)-rGO and ZBTEr (NPs)-CNTs glasses. Consequently, it was noticed that the electrons decay radiatively (R) to generate a green emission at ($^2H_{11/2} + {}^4S_{3/2}$) excited state levels to the ground state level ($^4I_{15/2}$).

Overall, it can be summarized that 0.005 mol% Er_2O_3 nanoparticles concentration of the ZBTEr (NPs)-rGO glass sample shows the optimal concentration based on the characteristics including, the lower optical bandgap energy (1.913 eV) and higher refractive index (2.775) values. Meanwhile, the optimal concentration for the ZBTEr (NPs)-CNTs glasses is 0.04 mol% Er_2O_3 nanoparticles concentration glass sample which was due to the lower optical bandgap energy (2.513 eV) and higher refractive index (2.542) values. Nevertheless, both of the glasses show a lower emission lifetime value of 0.245 ms

05-4506832 pustaka.upsi.edu.my Perpustakaan Tuanku Bainun Kampus Sultan Abdul Jalil Shah PustakaTBainun ptbupsi

05-4506832 pustaka.upsi.edu.my Perpustakaan Tuanku Bainun Kampus Sultan Abdul Jalil Shah PustakaTBainun ptbupsi

for ZBTEr (NPs)-rGO and 0.300 ms for ZBTEr (NPs)-CNTs glass system which was correlated to the effects of rGO and CNTs coating layers on the glass surfaces. In addition, the decreasing value of emission lifetime was caused by the non-radiative process, as has been discussed in the luminescence analysis. Therefore, it can be concluded that 0.005 mol% ZBTEr (NPs)-rGO and 0.04 mol% ZBTEr (NPs)-CNTs glass samples are prominent to be used for further characteristics in the fiber optics applications due to the lower optical bandgap energy, high refractive index, and lower emission lifetime than the current fiber optics applications.

Lastly, the present work has been well-investigated to achieve the research objectives; to synthesize the two sets of glass series namely, the ZBTEr (NPs)-rGO and ZBTEr (NPs)-CNTs glasses via the melt-quenched and spray-coated methods, to investigate the morphological, particle size, as well as bonding parameters of the ZBTEr (NPs)-rGO and ZBTEr (NPs)-CNTs glasses, to determine the optical properties including, optical absorption, optical bandgap energy, refractive index, as well as Urbach energy of the ZBTEr (NPs)-rGO and ZBTEr (NPs)-CNTs glasses, and to analyze the Judd-Ofelt's intensity parameters, emission lifetime, as well as investigating the luminescence properties. As a result, the research objectives as has been outlined in Chapter 1 were achieved, and hence, this research was successfully accomplished and completed.

05-4506832 pustaka.upsi.edu.my Perpustakaan Tuanku Bainun Kampus Sultan Abdul Jalil Shah PustakaTBainun ptbupsi

05-4506832 pustaka.upsi.edu.my Perpustakaan Tuanku Bainun Kampus Sultan Abdul Jalil Shah PustakaTBainun ptbupsi

5.3 Suggestions for Future Outlook

Prior to the previous discussion, the objective of investigating the rGO and CNTs coating materials that are attached on the tellurite-based glass surfaces had been completely fulfilled. Therefore, the obtained results in this study were successfully investigated in order to provide the fundamental data on the glass coatings field by the fabrication of the ZBTEr (NPs)-rGO and ZBTEr (NPs)-CNTs glasses. Consequently, it was demonstrated that the coating materials including, rGO and CNTs were highly attached with the tellurite-based glasses. These findings greatly encourage the researchers for further investigation as well as, to continue and expand for the improvement in more detail. Thus, the recommendations for future outlooks are stated as follows:

05-4506832 pustaka.upsi.edu.my Perpustakaan Tuanku Bainun Kampus Sultan Abdul Jalil Shah PustakaTBainun ptbupsi

i. The present work only studied three different properties including, physical, structural, and optical properties of the coated glasses. Further investigation of the electrical properties would assist to further elucidate, design, and achieve the outstanding improvement in fiber optics.

ii. Improved coating techniques must be further explored in order to produce a high distribution of coating materials on the glass surfaces. The improved technique of the glass coatings should consider the advantage to optimize the cost-effective and advanced coating technique, for instance, the electrophoretic deposition (EPD) method.

05-4506832 pustaka.upsi.edu.my Perpustakaan Tuanku Bainun Kampus Sultan Abdul Jalil Shah PustakaTBainun ptbupsi

05-4506832 pustaka.upsi.edu.my Perpustakaan Tuanku Bainun Kampus Sultan Abdul Jalil Shah PustakaTBainun ptbupsi

iii. Further work should consider the combination of rGO/CNTs composite in order to explore the possibility of performance of glass coatings, suggesting the excellent optical and mechanical properties for contribution to fiber optics applications.

iv. The present work has been carried out to investigate the improvement of optical properties in the glass system by using glass coatings. In the future, graphene-based materials (GBNs) probably consider to be doped into the glass system in order to further investigate the structural properties, including the structural arrangement of the glass network. This would be useful due to the strong characteristics of GBNs especially, the mechanical properties.

v. Another key factor for future study is to expand the investigation analysis by using the Mc-Cumber's theory in order to support the obtained results from the Judd-Ofelt's theory as well as, for evaluating the comparison findings between Judd-Ofelt and Mc-Cumber analyses. Other than that, the Mc-Cumber's theory can be applied for the estimation of the high-performance lasing medium in the operating laser of optical applications.

05-4506832 pustaka.upsi.edu.my Perpustakaan Tuanku Bainun Kampus Sultan Abdul Jalil Shah PustakaTBainun ptbupsi

05-4506832 pustaka.upsi.edu.my Perpustakaan Tuanku Bainun Kampus Sultan Abdul Jalil Shah PustakaTBainun ptbupsi

REFERENCES

Aarts, L., Jaeqx, S., Ende, B. M. Van Der, & Meijerink, A. (2011). Downconversion for the Er^{3+}, Yb^{3+} couple in KPb_2Cl —A low-phonon frequency host. *Journal of Luminescence*, *131*, 608–613.

Abdel-Baki, M., & El-Diasty, F. (2007). Optical properties of oxide glasses containing transition metals : Case of titanium- and chromium-containing glasses. *Current Opinion in Solid State and Materials Science*, *10*(5–6), 217–229.

Abid, Sehrawat, P., Islam, S. S., Mishra, P., & Ahmad, S. (2018). Reduced graphene oxide (rGO) based wideband optical sensor and the role of Temperature , Defect States and Quantum Efficiency. *Scientific Reports*, *8*(1).

Afroozeh, A. (2021). Dependence of linear and non-linear optical properties to sp^3 domains level and edges length in graphene-based nanomaterials. *Optik*, *226*, 165903.

Ahmadi, F., Hussin, R., & Ghoshal, S. K. (2016). Judd-Ofelt intensity parameters of samarium-doped magnesium zinc sulfophosphate glass. *Journal of Non-Crystalline Solids*, *448*, 43–51.

Ahmed, E. M., Youssif, M. I., & Elzelaky, A. A. (2019). Structural, thermal and photoemission properties of erbium doped phosphate glass. *Ceramics International*, *45*(18), 24014–24021.

Akbari, E., Akbari, I., & Ebrahimi, M. R. (2019). sp^2/ sp^3 bonding ratio dependence of the band-gap in graphene oxide. *The European Physical Journal B*, *92*(4).

Al-azzawi, A. A., Almukhtar, A. A., Hamida, B. A., Das, S., Dhar, A., & Paul, M. C. (2019). Wideband and flat gain series erbium doped fiber amplifier using hybrid active fiber with backward pumping distribution technique. *Results in Physics*, *13*, 102186.

Al-Gaashani, R., Najjar, A., Zakaria, Y., Mansour, S., & Atieh, M. A. (2019). XPS and structural studies of high quality graphene oxide and reduced graphene oxide prepared by different chemical oxidation methods. *Ceramics International*, *45*, 14439–14448.

Al-Hadeethi, Y., Sayyed, M. I., & Rammah, Y. S. (2019). Investigations of the physical, structural, optical and gamma-rays shielding features of B_2O_3 – Bi_2O_3 – ZnO – CaO glasses. *Ceramics International*, *45*(16), 20724–20732.

Al-Harbi, N., Sayyed, M. I., Al-Hadeethi, Y., Kumar, A., Elsafi, M., Mahmoud, K. A., Khandaker, M. U., & Bradley, D. A. (2021). A novel $CaO–K_2O–Na_2O–P_2O_5$ glass systems for radiation shielding applications. *Radiation Physics and Chemistry*, *188*,

05-4506832 pustaka.upsi.edu.my Perpustakaan Tuanku Bainun Kampus Sultan Abdul Jalil Shah PustakaTBainun ptbupsi

05-4506832 pustaka.upsi.edu.my Perpustakaan Tuanku Bainun Kampus Sultan Abdul Jalil Shah PustakaTBainun ptbupsi

109645.

Alalawi, A., Al-Buriahi, M. S., Sayyed, M. I., Akyildirim, H., Arslan, H., Zaid, M. H. M., & Tonguc, B. T. (2020). Influence of lead and zinc oxides on the radiation shielding properties of tellurite glass systems. *Ceramics International*, *46*(11), 17300–17306.

Ali, E., Hadis, D., Hamzeh, K., Mohammad, K., Nosratollah, Z., Abolfazl, A., Mozhgan, A., Younes, H., & Woo, J. S. (2014). Carbon nanotubes: properties, synthesis, purification, and medical applications. *Nanoscale Research Letters*, *9*, 393.

Alvarez-Ramos, M. E., Alvarado-Rivera, J., Zayas, M. E., Caldiño, U., & Hernández-Paredes, J. (2018). Yellow to orange-reddish glass phosphors: Sm^{3+}, $Tb^{3+}$and Sm^{3+}/Tb^{3+} in zinc tellurite-germanate glasses. *Optical Materials*, *75*, 88–93.

Amiar Rodin, N. L., & Sahar, M. R. (2018). Erbium doped sodium magnesium boro-tellurite glass: Stability and Judd-Ofelt analysis. *Materials Chemistry and Physics*, *216*, 177–185.

Amjad, R. J., Sahar, M. R., Ghoshal, S. K., Dousti, M. R., & Arifin, R. (2013). Synthesis and characterization of Dy^{3+} doped zinc-lead-phosphate glass. *Optical Materials*, *35*, 1103–1108.

Antidormi, A., Roche, S., & Colombo, L. (2020). Impact of oxidation morphology on reduced graphene oxides upon thermal annealing. *JPhys Materials*, *3*(1).

Aradhana, D. M., Dissanayake, S., Cifuentes, M. P., & Humphrey, M. G. (2018). Optical limiting properties of (reduced) graphene oxide covalently functionalized by coordination complexes. *Coordination Chemistry Reviews*, *375*, 489–513.

Arora, N., & Sharma, N. N. (2014). Arc discharge synthesis of carbon nanotubes: Comprehensive review. *Diamond and Related Materials*, *50*, 135–150.

Arranz-Mascarós, P., Godino-Salido, M. L., López-Garzón, R., García-Gallarín, C., Chamorro-Mena, I., López-Garzón, F. J., Fernández-García, E., & Gutiérrez-Valero, M. D. (2020). Non-covalent Functionalization of Graphene to Tune Its Band Gap and Stabilize Metal Nanoparticles on Its Surface. *ACS Omega*, *5*(30), 18849–18861.

Asokamani, R., & Manjula, R. (1989). Correlation between electronegativity and superconductivity. *Physica Review B*, *39*(7), 4217–4221.

Augustine, S., Singh, J., Srivastava, M., Sharma, M., Das, A., & D. Malhotra, B. (2017). Biomaterials Science Recent advances in carbon based nanosystems for cancer theranostics. *Biomaterials Science*, *5*, 901–952.

Awang, A., Ghoshal, S. K., Sahar, M. R., & Arifin, R. (2015). Gold nanoparticles assisted structural and spectroscopic modification in Er^{3+}-doped zinc sodium

05-4506832 pustaka.upsi.edu.my Perpustakaan Tuanku Bainun Kampus Sultan Abdul Jalil Shah PustakaTBainun ptbupsi

05-4506832 pustaka.upsi.edu.my Perpustakaan Tuanku Bainun Kampus Sultan Abdul Jalil Shah PustakaTBainun ptbupsi

tellurite glass. *Optical Materials*, *42*, 495–505.

Azizighannad, S., & Mitra, S. (2018). Stepwise reduction of Graphene Oxide (GO) and its effects on chemical and colloidal properties. *Scientific Reports*, *8*, 10083.

Azlan, M. N., & Halimah, M. K. (2018). Role of Nd^{3+} nanoparticles on enhanced optical efficiency in borotellurite glass for optical fiber. *Results in Physics*, *11*, 58–64.

Azlan, M. N., Halimah, M. K., Baki, S. O., & Mohamad, D. W. (2015). Green Emission of Tellurite Based Glass Containing Erbium Oxide Nanoparticles. *Journal of Nanomaterials*.

Azlan, M. N., Halimah, M. K., El-Mallawany, R., Faznny, M. F., & Eevon, C. (2017). Optical properties of zinc borotellurite glass system doped with erbium and erbium nanoparticles for photonic applications. *Journal of Materials Science: Materials in Electronics*, *28*(5), 4318–4327.

Azlan, M. N., Halimah, M. K., Shafinas, S. Z., & Daud, W. M. (2015). Electronic polarizability of zinc borotellurite glass system containing erbium nanoparticles. *Materials Express*, *5*(3), 211–218.

Azlan, M. N., Halimah, M. K., Suriani, A. B., Azlina, Y., & El-mallawany, R. (2019). Electronic polarizability and third-order nonlinearity of Nd^{3+} doped borotellurite glass for potential optical fiber. *Materials Chemistry and Physics*, *236*.

Azlan, M. N., Halimah, M. K., Suriani, A. B., Azlina, Y., Umar, S. A., & El-Mallawany, R. (2019). Upconversion properties of erbium nanoparticles doped tellurite glasses for high efficient laser glass. *Optics Communications*, *448*, 82–88.

Ba, H., Sutter, C., Papaefthimiou, V., Zafeiratos, S., Bahouka, A., Lafue, Y., Nguyen-Dinh, L., Romero, T., & Pham-Huu, C. (2020). Foldable flexible electronics based on few-layer graphene coated on paper composites. *Carbon*, *167*, 169–180.

Bachvarova-nedelcheva, A., Iordanova, R., Ganev, S., & Dimitriev, Y. (2018). Glass formation and structural studies of glasses in the TeO-ZnO-Bi_2O_3–NbO_5 system. *Journal of Non-Crystalline Solids*.

Bacon, R. (1960). Growth, structure, and properties of graphite whiskers. *Journal of Applied Physics*, *31*(2), 283–290.

Balda, R., Hakmeh, N., Barredo-zuriarrain, M., Merdrignac-Conacec, O., García-Revilla, S., Arriandiaga, M. A., & Fernández, J. (2016). Influence of Upconversion Processes in the Optically-Induced Inhomogeneous Thermal Behavior of Erbium-Doped Lanthanum Oxysulfide Powders. *Materials*, *9*(5), 353.

05-4506832 pustaka.upsi.edu.my Perpustakaan Tuanku Bainun Kampus Sultan Abdul Jalil Shah PustakaTBainun ptbupsi

05-4506832 pustaka.upsi.edu.my Perpustakaan Tuanku Bainun Kampus Sultan Abdul Jalil Shah PustakaTBainun ptbupsi

Becerril, H. A., Mao, J., Liu, Z., Stoltenberg, R. M., Bao, Z., & Chen, Y. (2008). Evaluation of solution-processed reduced graphene oxide films as transparent conductors. *ACS Nano*, *2*(3), 463–470.

Belosludtseva, A. A., Bobenko, N. G., Egorushkin, V. E., Korusenko, P. M., Melnikova, N. V., & Nesov, S. N. (2021). Oxygen functionalization and electronic band gap control in the disordered multi-walled carbon nanotubes. *Synthetic Metals*, *280*, 116866.

Bengisu, M. (2015). Borate glasses for scientific and industrial applications: a review. *Journal of Materials Science*, *51*, 2199–2242.

Bhardwaj, S., Shukla, R., Sanghi, S., Agarwal, A., & Pal, I. (2014). Spectroscopic properties of Sm^{3+} doped lead bismosilicate glasses using Judd-Ofelt theory. *Spectrochimica Acta - Part A: Molecular and Biomolecular Spectroscopy*, *117*, 191–197.

Bhatia, B., Meena, S. L., Parihar, V., & Poonia, M. (2015). Optical Basicity and Polarizability of Nd^{3+}-Doped Bismuth Borate Glasses. *New Journal of Glass and Ceramics*, *5*, 44–52.

Bodelot, L., Pavić, L., Hallais, S., Charliac, J., & Lebental, B. (2019). Aggregate-driven reconfigurations of carbon nanotubes in thin networks under strain: in-situ characterization. *Scientific Reports*, *9*(1), 5513.

Bonaccorso, F., Sun, Z., Hasan, T., & Ferrari, A. C. (2010). Graphene photonics and optoelectronics. *Nature Photonics*, *4*(9), 611–622.

Brodie, B. C. (1859). On the atomic weight of graphite. *Philosophical Transactions of the Royal Society of London*, *149*(0), 249–259.

Buddhudu, S., & Bryant, F. J. (1989). OPTICAL TRANSITIONS OF Er^{3+}:La_2O_2S AND Er^{3+}:Y_2O_2S. *Journal of the Less-Common Metals*, *147*, 213–225.

Bulus, I., Hussin, R., Ghoshal, S. K., Tamuri, A. R., & Jupri, S. A. (2019). Enhanced elastic and optical attributes of boro-telluro-dolomite glasses : Role of CeO_2 doping. *Ceramics International*, *45*, 18648–18658.

Bunaciu, A. A., Udriştioiu, E. gabriela, & Aboul-Enein, H. Y. (2015). X-Ray Diffraction: Instrumentation and Applications. *Critical Reviews in Analytical Chemistry*, *45*(4), 289–299.

Bunch, J. S., Verbridge, S. S., Alden, J. S., Zande, A. M. Van Der, Parpia, J. M., Craighead, H. G., & Mceuen, P. L. (2008). Impermeable Atomic Membranes from 2008. *Nano Letters*, *8*(8), 2458–2462.

05-4506832 pustaka.upsi.edu.my Perpustakaan Tuanku Bainun Kampus Sultan Abdul Jalil Shah PustakaTBainun ptbupsi

05-4506832 pustaka.upsi.edu.my Perpustakaan Tuanku Bainun Kampus Sultan Abdul Jalil Shah PustakaTBainun ptbupsi

Câmara, J. G., da Silva, D. M., Kassab, L. R. P., de Araújo, C. B., & Gomes, A. S. L. (2021). Random laser emission from neodymium doped zinc tellurite glass-powder presenting luminescence concentration quenching. *Journal of Luminescence*, *233*, 117936.

Cao, R., Lu, Y., Tian, Y., Huang, F., Guo, Y., Xu, S., & Zhang, J. (2016). 2 μm emission properties and nonresonant energy transfer of Er^{3+} and Ho^{3+} codoped silicate glasses. *Scientific Reports*, *6*(1), 1–11.

Carnall, W. T., Fields, P. R., & Rajnak, K. (1968). Electronic Energy Levels in the Trivalent Lanthanide Aquo Ions. I. Pr^{3+}, Nd^{3+}, Pm^{3+}, Sm^{3+}, Dy^{3+}, Ho^{3+}, Er^{3+}, and Tm^{3+}. *The Journal of Chemical Physics*, *49*(10), 4424–4442.

Chan, K. F., Mohd Zaid, M. H., Liza, S., Mamat, M. S., Matori, K. A., Endot, N. A., Tanemura, M., & Yaakob, Y. (2021). Tuning the optical bandgap of multi-walled carbon nanotube-modified zinc silicate glass-ceramic composites. *Ceramics International*, *47*(14), 20108–20116.

Chaudhary, K. T., Rizvi, Z. H., Bhatti, K. A., Ali, J., & Yupapin, P. P. (2013). Multiwalled carbon nanotube synthesis using arc discharge with hydrocarbon as feedstock. *Journal of Nanomaterials*, 1–13.

Cheng, C., Li, S., Thomas, A., Kotov, N. A., & Haag, R. (2017). Functional Graphene Nanomaterials Based Architectures: Biointeractions, Fabrications, and Emerging Biological Applications. *Chemical Reviews*, *117*(3), 1826–1914.

Chien, C. T., Li, S. S., Lai, W. J., Yeh, Y. C., Chen, H. A., Chen, I. S., Chen, L. C., Chen, K. H., Nemoto, T., Isoda, S., Chen, M., Fujita, T., Eda, G., Yamaguchi, H., Chhowalla, M., & Chen, C. W. (2012). Tunable photoluminescence from graphene oxide. *Angewandte Chemie - International Edition*, *51*(27), 6662–6666.

Chimalawong, P., Kirdsiri, K., Kaewkhao, J., & Limsuwan, P. (2012). Investigation on the physical and optical properties of Dy^{3+} doped soda-lime-silicate glasses. *Procedia Engineering*, *32*, 690–698.

Chopra, N., Kaur, S., Kaur, M., Singla, S., Marwaha, R., Sharma, G., & Heer, M. S. (2018). Optical, Physical and Structural Properties of Er^{3+} Doped Low-Phonon Energy Vitreous Matrix: ZnO-B_2O_3-TeO_2. *Physica Status Solidi (A)*, *215*(13), 1700934.

Chua, C. K., & Pumera, M. (2014). Chemical reduction of graphene oxide: A synthetic chemistry viewpoint. *Chemical Society Reviews*, *43*(1), 291–312.

Dato, A., & Frenklach, M. (2010). Substrate-free microwave synthesis of graphene: experimental conditions and hydrocarbon precursors. *New Journal of Physics*, *12*(12), 125013.

05-4506832 pustaka.upsi.edu.my Perpustakaan Tuanku Bainun Kampus Sultan Abdul Jalil Shah PustakaTBainun ptbupsi

05-4506832 pustaka.upsi.edu.my Perpustakaan Tuanku Bainun Kampus Sultan Abdul Jalil Shah PustakaTBainun ptbupsi

De Silva, K. K. H., Huang, H. H., Joshi, R. K., & Yoshimura, M. (2017). Chemical reduction of graphene oxide using green reductants. *Carbon*, *119*, 190–199.

Deopa, N., & Rao, A. S. (2017). Spectroscopic studies of Sm^{3+} ions activated lithium lead alumino borate glasses for visible luminescent device applications. *Optical Materials*, *72*, 31–39.

Devreese, J. T. (2003). Polarons. *Digital Encyclopedia of Applied Physics*, 383–412.

Dideikin, A. T., & Vul', A. Y. (2019). Graphene oxide and derivatives: The place in graphene family. *Frontiers in Physics*, *6*.

Dimitrov, V., & Komatsu, T. (2013). Electronic polarizability, optical basicity and single bond strength of oxide glasses. *Journal of Chemical Technology and Metallurgy*, *48*(6), 549–554.

Dimitrov, V., & Sakka, S. (1996). Linear and nonlinear optical properties of simple oxides. II. *Journal of Applied Physics*, *79*(3), 1741–1745.

Ding, N., Diao, J., Zhang, D., Zheng, T., & Lv, J. (2020). Spectroscopic properties of Yb^{3+} and Nd^{3+} co-doped tellurite glass for 1.0 μm laser application. *Ceramics International*, *46*, 25633–25637.
05-4506832 pustaka.upsi.edu.my Perpustakaan Tuanku Bainun Kampus Sultan Abdul Jalil Shah PustakaTBainun ptbupsi
Divina, R., Marimuthu, K., Sayyed, M. I., Tekin, H. O., & Agar, O. (2019). Physical, structural, and radiation shielding properties of B_2O_3–MgO–K_2O–Sm_2O_3 glass network modified with TeO_2. *Radiation Physics and Chemistry*, *160*, 75–82.

Dreyer, D. R., Ruoff, R. S., & Bielawski, C. W. (2010). From Conception to Realization : An Historial Account of Graphene and Some Perspectives for Its Future. *Angewandte Chemie International Edition*, *49*(49), 9336–9344.

Dubois, S. M., Zanolli, Z., Declerck, X., & Charlier, J. (2009). Electronic properties and quantum transport in Graphene-based nanostructures. *The European Physical Journal B*, *72*(1), 1–24.

Edwards, R. S., & Coleman, K. S. (2013). Graphene synthesis : relationship to applications. *Nanoscale*, *5*(1), 38–51.

Effendy, N., Sidek, H. A. A., Halimah, M. K., & Zaid, M. H. M. (2021). Enhancement on thermal , elastic and optical properties of new formulation tellurite glasses : Influence of ZnO as a glass modifier. *Materials Chemistry and Physics*, *273*, 125156.

El-diasty, F., Wahab, F. A. A., & Abdel-baki, M. (2006). Optical band gap studies on lithium aluminum silicate glasses doped with Cr^{3+} ions. *Journal of Applied Physics*, *100*, 093511.
05-4506832 pustaka.upsi.edu.my Perpustakaan Tuanku Bainun Kampus Sultan Abdul Jalil Shah PustakaTBainun ptbupsi

05-4506832 pustaka.upsi.edu.my Perpustakaan Tuanku Bainun Kampus Sultan Abdul Jalil Shah PustakaTBainun ptbupsi

El-Mallawany, R., El Adawy, A., Gamal, A., & Rammah, Y. S. (2021). Experimental and theoretical elastic moduli of sodium–zinc–tellurite glasses. *Optik*, *243*, 167330.

El-Mallawany, Raouf. (2017). Introduction to tellurite glasses. *Springer Series in Materials Science*, *254*, 1–13.

Elkhoshkhany, N., Essam, O., & Embaby, A. M. (2018). Optical, thermal and antibacterial properties of tellurite glass system doped with ZnO. *Materials Chemistry and Physics*, *214*, 489–498.

Elkhoshkhany, N., Marzouk, S., El-Sherbiny, M., & Ahmed, A. (2019). Properties of tellurite glass doped with ytterbium oxide for optical applications. *Journal of Materials Science: Materials in Electronics*, *30*(7), 6963–6976.

Emiru, T. F., & Ayele, D. W. (2016). Controlled synthesis , characterization and reduction of graphene oxide : A convenient method for large scale production. *Egyptian Journal of Basic and Applied Sciences*, *4*(1), 74–79.

Eom, G., Oh, C., Moon, J., Kim, H., Kim, M. K., Kim, K., Seo, J. W., Kang, T., & Lee, H. J. (2019). Highly sensitive and selective detection of dopamine using overoxidized polypyrrole/sodium dodecyl sulfate-modified carbon nanotube electrodes. *Journal of Electroanalytical Chemistry*, *848*, 113295.
05-4506832 pustaka.upsi.edu.my Perpustakaan Tuanku Bainun Kampus Sultan Abdul Jalil Shah PustakaTBainun ptbupsi
Fang, M., Xiong, X., Hao, Y., Zhang, T., & Wang, H. (2019). Preparation of highly conductive graphene-coated glass fibers by sol-gel and dip-coating method. *Journal of Materials Science & Technology*, *35*(9), 1989–1995.

Fang, M., Xiong, X., Hao, Y., Zhang, T., Wang, H., Cheng, H., & Zeng, Y. (2019). Preparation of Highly Conductive Graphene-coated Glass Fibers by Sol-gel and Dip-coating Method. *Journal of Materials Science & Technology*, *35*(9), 1989–1995.

Fatemi, S. M., & Foroutan, M. (2015). Recent developments concerning the dispersion of carbon nanotubes in surfactant/polymer systems by MD simulation. *Journal of Nanostructure in Chemistry*, *6*(1), 29–40.

Faznny, M. F., Halimah, M. K., & Azlan, M. N. (2016). Effect of Lanthanum Oxide on Optical Properties of Zinc Borotellurite Glass System. *Journal of Optoelectronics and Biomedical Materials*, *8*(2), 49–59.

Fitzpatrick, M. E., Fry, A. T., Holdway, P., Kandil, F. A., Shackleton, J., & Suominen, L. (2005). Determination of Residual Stresses by X-ray Diffraction. *National Physical Laboratory*, *1309*(52).

Gaafar, M. S., & Marzouk, S. Y. (2017). Judd–Ofelt analysis of spectroscopic properties of Er^{3+} doped TeO_2-BaO-ZnO glasses. *Journal of Alloys and Compounds*, *723*,

05-4506832 pustaka.upsi.edu.my Perpustakaan Tuanku Bainun Kampus Sultan Abdul Jalil Shah PustakaTBainun ptbupsi

05-4506832 pustaka.upsi.edu.my Perpustakaan Tuanku Bainun Kampus Sultan Abdul Jalil Shah PustakaTBainun ptbupsi

1070–1078.

Ganesh, E. N. (2013). Single Walled and Multi Walled Carbon Nanotube Structure. *Synthesis and Applications*, *2*(4), 311–320.

Gangwar, H., Singh, V., Tewari, B. S., Gupta, H., & Purohit, L. P. (2019). Study of zinc doped tellurite glasses using XRD, UV-Vis and FTIR. *Materials Today: Proceedings*, *17*, 329–337.

Gao, W., Alemany, L. B., Ci, L., & Ajayan, P. M. (2009). New insights into the structure and reduction of graphite oxide. *Nature Chemistry*, *1*(5), 403–408.

Gaur, M., Misra, C., Yadav, A. B., Swaroop, S., Maolmhuaidh, F. O., Bechelany, M., & Barhoum, A. (2021). Biomedical Applications of Carbon Nanomaterials: Fullerenes, Quantum Dots, Nanotubes, Nanofibers, and Graphene. *Materials*, *14*, 5978.

Geim, A. K., & Novoselov, K. S. (2007). The rise of graphene. *Nature Materials*, *6(3)*, 183–191.

Gifford, B. J., He, X., Kim, M., Kwon, H., Saha, A., Sifain, A. E., Wang, Y., Htoon, H., Kilina, S., Doorn, S. K., & Tretiak, S. (2019). Optical Effects of Divalent Functionalization of Carbon Nanotubes. *Chemistry of Materials*, *31*(17), 6950–6961.
05-4506832 pustaka.upsi.edu.my Perpustakaan Tuanku Bainun Kampus Sultan Abdul Jalil Shah PustakaTBainun ptbupsi
Goh, S. X. L., Goh, E. X. Y., & Lee, H. K. (2021). Sodium dodecyl sulfate-multi-walled carbon nanotubes-coated-membrane solid phase extraction of glucocorticoids in aqueous matrices. *Talanta*, *221*, 121624.

Gomaa, H. M., Yahia, I. S., & Zahran, H. Y. (2021). Correlation between the static refractive index and the optical bandgap: Review and new empirical approach. *Physica B: Physics of Condensed Matter*, *620*, 413246.

Gomes, J. F., Lima, A. M. O., Sandrini, M., Medina, A. N., Steimacher, A., Pedrochi, F., & Barboza, M. J. (2017). Optical and spectroscopic study of erbium doped calcium borotellurite glasses. *Optical Materials*, *66*, 211–219.

Greenwood, G. . (1956). The growth of dispersed precipitates in solutions. *Acta Metallurgica*, *4*(3), 243–248.

Grobert, N. (2007). Carbon nanotubes – importance of clean CNT material for the success of future applications . *Review Literature And Arts Of The Americas*, *10*(1–2), 28–35.

Guo, J., Qi, H., Song, Z., Ni, J., Wang, C., Wang, W., & Peng, G. (2020). A Comparative Study of Thermal Impact on Erbium Doped Distributed Feedback Fiber Laser Output Power. *IEEE Photonics Journal*, *12*(2), 1502009.

05-4506832 pustaka.upsi.edu.my Perpustakaan Tuanku Bainun Kampus Sultan Abdul Jalil Shah PustakaTBainun ptbupsi

05-4506832 pustaka.upsi.edu.my Perpustakaan Tuanku Bainun Kampus Sultan Abdul Jalil Shah PustakaTBainun ptbupsi

Gupta, N., Khanna, A., Hirdesh, Dippel, A. C., & Gutowski, O. (2020). Structure of bismuth tellurite and bismuth niobium tellurite glasses and $Bi_2Te_4O_{11}$ anti-glass by high energy X-ray diffraction. *RSC Advances*, *10*(22), 13237–13251.

Gupta, V., Sharma, N., Singh, U., Arif, M., & Singh, A. (2017). Synthesis and characterization of graphene oxide. *Optik*.

Halimah, M. K., Faznny, M. F., Azlan, M. N., & Sidek, H. A. A. (2017). Optical basicity and electronic polarizability of zinc borotellurite glass doped La^{3+} ions. *Results in Physics*, *7*, 581–589.

Halimah, M. K., Hamza, A. M., Muhammad, F. D., Chan, K. T., Umar, S. A., Umaru, I., & Geidam, I. G. (2019). Effect of erbium nanoparticles on structural and spectroscopic properties of bio-silica borotellurite glasses containing silver oxide. *Materials Chemistry and Physics*, *236*, 121795.

Hamza, A. M., Halimah, M. K., Muhammad, F. D., & Chan, K. T. (2019). Physical properties, ligand field and Judd-Ofelt intensity parameters of bio-silicate borotellurite glass system doped with erbium oxide. *Journal of Luminescence*, *207*, 497–506.

Hamza, A. M., Halimah, M. K., Muhammad, F. D., Chan, K. T., Usman, A., Faznny, M. F., Zaitizila, I., & Tafida, R. A. (2019). Structural, optical and thermal properties of Er^{3+}-Ag codoped bio-silicate borotellurite glass. *Results in Physics*, *14*, 102457.

Han, Z., & Fina, A. (2011). Thermal conductivity of carbon nanotubes and their polymer nanocomposites: A review. *Progress in Polymer Science*, *36*(7), 914–944.

Hasan, T., Senger, B. J., Ryan, C., Culp, M., Gonzalez-rodriguez, R., Coffer, J. L., & Naumov, A. V. (2017). Optical Band Gap Alteration of Graphene Oxide via Ozone Treatment. *Scientific Reports*, *7*(1).

Hasim, N., & Rohani, M. S. (2017). The effect of Nd^{3+} composition on Judd-ofelt analysis of lithium niobate tellurite glasses codoped with Er^{3+}. *Solid State Phenomena*, *268 SSP*, 191–197.

Huang, Y., Sutter, E., Shi, N. N., Zheng, J., Yang, T., Englund, D., Gao, H., & Sutter, P. (2015). Reliable Exfoliation of Large-Area High-Quality Flakes of Graphene and Other Two-Dimensional Materials. *ACS Nano*, *9*(11), 10612–10620.

Hummers, W. S., & Offeman, R. E. (1958). Preparation of Graphitic Oxide. *Journal of the American Chemical Society*, *80*(6), 1339.

Hussein, K. I., Alqahtani, M. S., Alzahrani, K. J., Alqahtani, F. F., Zahran, H. Y., Alshehri, A. M., Yahia, I. S., Reben, M., & Yousef, E. S. (2022). The Effect of ZnO, MgO, TiO_2, and Na_2O Modifiers on the Physical, Optical, and Radiation Shielding

05-4506832 pustaka.upsi.edu.my Perpustakaan Tuanku Bainun Kampus Sultan Abdul Jalil Shah PustakaTBainun ptbupsi

05-4506832 pustaka.upsi.edu.my Perpustakaan Tuanku Bainun Kampus Sultan Abdul Jalil Shah PustakaTBainun ptbupsi

Properties of a TeTaNb Glass System. *Materials*, *15*(5).

Ibrahim, A., Klopocinska, A., Horvat, K., & Hamid, Z. A. (2021). Graphene-based nanocomposites: Synthesis, mechanical properties, and characterizations. *Polymers*, *13*(17).

Iezid, M., Goumeidane, F., Abidi, A., Poulain, M., Legouera, M., Syam Prasad, P., Środa, M., & Venkateswara Rao, P. (2021). Judd-Ofelt analysis and luminescence studies of Er^{3+} doped halogeno-antimonate glasses. *Optical Materials*, *120*, 111422.

Iijima, S. (1991). Helical microtubules of graphitic carbon. *Nature*, *354*(6348), 56–58.

Iijima, S., & Ichihashi, T. (1993). Single-shell carbon nanotubes of 1-nm diameter. *International Journal of Environmental Science and Technology*, *363*(6430), 603–605.

Ikram, R., Jan, B. M., & Ahmad, W. (2020). An overview of industrial scalable production of graphene oxide and analytical approaches for synthesis and characterization. *Journal of Materials Research and Technology*, *9*(5), 11587–11610.

Ishtiaq, U., Aref, A., Muhsan, A. S., Rashid, A., & Hamdi, S. S. (2022). High strength glass beads coated with CNT/rGO incorporated urethane coating for improved crush resistance for effective hydraulic fracturing. *Journal of Petroleum Exploration and Production Technology*.

Jacobs, R. R., & Weber, M. J. (1976). Dependence of the $^4F_{3/2} \rightarrow {}^4I_{11/2}$ Induced-Emission Cross Section for Nd^{3+} on Glass Composition. *IEEE Journal of Quantum Electronics*, *12*(2), 102–111.

Jia, C., Zhang, X., Matras-Postolek, K., Huang, B., & Yang, P. (2018). Z-scheme reduced graphene oxide/TiO_2-Bronze/$W_{18}O_{49}$ ternary heterostructure towards efficient full solar-spectrum photocatalysis. *Carbon*, *139*, 415–426.

Jiménez-pérez, J. L., Gutiérrez-fuentes, R., López-gamboa, G., & Sánchez-ramírez, J. F. (2018). Measurement of optical nonlinear refractive index response of graphene nanoparticles dispersed in an aqueous solution by Z scan technique. *Optical Materials*, *84*, 236–241.

Jimenez, J. A., Sendova, M., & Manchini, M. (2020). Thermal and spectroscopic characterization of copper and erbium containing aluminophosphate glass. *Spectrochimica Acta Part A: Molecular and Biomolecular Spectroscopy*, *226*, 117546.

Jin, Y., Zheng, Y., Podkolzin, S. G., & Lee, W. (2020). Band gap of reduced graphene oxide tuned by controlling functional groups. *Journal of Materials Chemistry C*,

05-4506832 pustaka.upsi.edu.my Perpustakaan Tuanku Bainun Kampus Sultan Abdul Jalil Shah PustakaTBainun ptbupsi

05-4506832 pustaka.upsi.edu.my Perpustakaan Tuanku Bainun Kampus Sultan Abdul Jalil Shah PustakaTBainun ptbupsi

8(14), 4885–4894.

Jlassi, I., Elhouichet, H., & Ferid, M. (2011). Thermal and optical properties of tellurite glasses doped erbium. *Journal of Materials Science*, *46*(3), 806–812.

Jlassi, I., Elhouichet, H., Ferid, M., & Barthou, C. (2010). Judd–Ofelt analysis and improvement of thermal and optical properties of tellurite glasses by adding P_2O_5. *Journal of Luminescence*, *130*(12), 2394–2401.

Johari, P., & Shenoy, V. B. (2011). Modulating optical properties of graphene oxide: Role of prominent functional groups. *ACS Nano*, *5*(9), 7640–7647.

Jørgensen, Chr Klixbüll, & Judd, B. R. (1964). Hypersensitive pseudoquadrupole transitions in lanthanides. *Molecular Physics: An International Journal at the Interface Between Chemistry and Physics*, *8*(3), 281–290.

Jørgensen, Christian K., & Reisfeld, R. (1983). Judd-Ofelt parameters and chemical bonding. *Journal of The Less-Common Metals*, *93*, 107–112.

Judd, B. R. (1962). Optical absorption intensities of rare-earth ions. *Physical Review*, *127*(3), 750–761.

Julien, C., Massot, M., Balkanski, W., Krol, A., & Nazarewicz, W. (1989). Infrared studies of the structure of borate glasses. *Materials Science and Engineering B*, *3*(3), 307–312.

Jupri, S. A., Ghoshal, S. K., Omar, M. F., & Yusof, N. N. (2018). Spectroscopic traits of holmium in magnesium zinc sulfophosphate glass host: Judd-Ofelt evaluation. *Journal of Alloys and Compounds*, *753*, 446–456.

Kasik, I., Matejec, V., Hayer, M., Kamradek, M., Podrazky, O., Mrazek, J., Peterka, P., & Honzatko, P. (2020). Glass materials for optical fibers. *Ceramics - Silikaty*, *64*(1), 29–34.

Kaur, S., Pandey, O. P., Jayasankar, C. K., & Chopra, N. (2021). Effect of gamma irradiation on physical, optical, spectroscopic and structural properties of Er^{3+}-doped vitreous zinc borotellurite. *Journal of Luminescence*, *235*, 118031.

Khan, M. A., Amjad, R. J., Ahmad, M. A., Sattar, A., Hussain, S., Yasmeen, S., & Dousti, M. R. (2019). Structural and Optical Study of Erbium Doped Borophosphate Glasses. *Optik - International Journal for Light and Electron Optics*, 163707.

Khan, S., Ali, J., Harsh, Husain, M., & Zulfequar, M. (2016). Synthesis of reduced graphene oxide and enhancement of its electrical and optical properties by attaching Ag nanoparticles. *Physica E: Low-Dimensional Systems and Nanostructures*, *81*, 320–325.

05-4506832 pustaka.upsi.edu.my Perpustakaan Tuanku Bainun Kampus Sultan Abdul Jalil Shah PustakaTBainun ptbupsi

05-4506832 pustaka.upsi.edu.my Perpustakaan Tuanku Bainun Kampus Sultan Abdul Jalil Shah PustakaTBainun ptbupsi

Khosravi, M., Badehian, H. A., & Habibinejad, M. (2021). Optical properties of double walled carbon nanotubes. *Journal of Electron Spectroscopy and Related Phenomena*, *248*, 147058.

Kim, C. Bin, Lee, J., Cho, J., & Goh, M. (2018). Thermal conductivity enhancement of reduced graphene oxide via chemical defect healing for efficient heat dissipation. *Carbon*, *139*, 386–392.

Kochmann, S., Hirsch, T., & Wolfbeis, O. S. (2012). The pH dependence of the total fluorescence of graphite oxide. *Journal of Fluorescence*, *22*(3), 849–855.

Konstantinidis, M., Lalla, E. A., Lopez-reyes, G., Rodríguez-mendoza, U. R., Lymer, E. A., Freemantle, J., & Daly, M. G. (2021). Statistical learning for the estimation of Judd-Ofelt parameters : A case study of Er^{3+} : Doped tellurite glasses. *Journal of Luminescence*, *235*, 118020.

Krupke, W. F. (1966). Optical absorption and fluorescence intensities in several rare-earth-doped Y_2O_3 and LaF_3 single crystals. *Physical Review*, *145*(1), 325–337.

Kruskopf, M., Pierz, K., Pakdehi, D. M., Stosch, R., Bakin, A., & Schumacher, H. W. (2018). A morphology study on the epitaxial growth of graphene and its buffer layer. *Thin Solid Films*.

05-4506832 pustaka.upsi.edu.my Perpustakaan Tuanku Bainun Kampus Sultan Abdul Jalil Shah PustakaTBainun ptbupsi

Kudin, K. N., Ozbas, B., Schniepp, H. C., Prud'homme, R. K., Aksay, I. A., & Car, R. (2008). Raman spectra of graphite oxide and functionalized graphene sheets. *Nano Letters*, *8*(1), 36–41.

Kurzen, H., Bovigny, L., Bulloni, C., & Daul, C. (2013). Electronic structure and magnetic properties of lanthanide^{3+} cations. *Chemical Physics Letters*, *574*, 129–132.

Labhane, P. K., Patle, L. B., Huse, V. R., Sonawane, G. H., & Sonawane, S. H. (2016). Synthesis of reduced graphene oxide sheets decorated by zinc oxide nanoparticles: Crystallographic, optical, morphological and photocatalytic study. *Chemical Physics Letters*, *661*, 13–19.

Lachheb, R., Herrmann, A., Assadi, A. A., Damak, K., Rüssel, C., & Maâlej, R. (2018). Judd Ofelt analysis and experimental spectroscopic study of erbium doped phosphate glasses. *Journal of Luminescence*.

Lakshmi, Y. A., Swapna, K., Rama, K. S., Reddy, K., Venkateswarlu, M., Mahamuda, S., & Rao, A. S. (2019). Structural, optical and NIR studies of Er^{3+} ions doped bismuth boro tellurite glasses for luminescence materials applications. *Journal of Luminescence*, *211*, 39–47.

05-4506832 pustaka.upsi.edu.my Perpustakaan Tuanku Bainun Kampus Sultan Abdul Jalil Shah PustakaTBainun ptbupsi

05-4506832 pustaka.upsi.edu.my Perpustakaan Tuanku Bainun Kampus Sultan Abdul Jalil Shah PustakaTBainun ptbupsi

Lalla, E. A., Konstantinidis, M., De Souza, I., Daly, M. G., Martín, I. R., Lavín, V., & Rodríguez-Mendoza, U. R. (2020). Judd-Ofelt parameters of RE^{3+}-doped fluorotellurite glass (RE^{3+}= Pr^{3+}, Nd^{3+}, Sm^{3+}, Tb^{3+}, Dy^{3+}, Ho^{3+}, Er^{3+}, and Tm^{3+}). *Journal of Alloys and Compounds*, *845*, 156028.

Lalla, E. A., Lozano-Gorrín, A. D., Konstantinidis, M., Daly, M., Leon-Luis, S. F., Lavín, V., & Rodríguez-Mendoza, U. R. (2019). Optical temperature sensor based on Sm^{3+} emissions in a fluorotellurite glass. *Optical Fiber Technology*, *47*, 178–186.

Lamichhane, A., & Ravindra, N. M. (2020). Energy gap-refractive index relations in perovskites. *Materials*, *13*(8), 1–16.

Lee, X. J., Hiew, B. Y. Z., Lai, K. C., Lee, L. Y., Gan, S., Thangalazhy-Gopakumar, S., & Rigby, S. (2018). Review on graphene and its derivatives : Synthesis methods and potential industrial implementation. *Journal of the Taiwan Institute of Chemical Engineers*, *18*, 13.

Lee, K. H., Kim, T. H., Kim, Y. S., Jung, Y. J., Na, Y. H., & Ryu, B. K. (2008). Structural Modification of Alkali Tellurite Binary Glass System and Its Characterization. *Korean Journal of Materials Research*, *18*(5), 235–240.

Lesniak, M., Mach, G., Starzyk, B., Baranowska, A., Bik, M., Kochanowicz, M., Zmojda, J., Miluski, P., Sitarz, M., & Dorosz, D. (2020). Investigation of the structure in oxyfluoride TeO_2–P_2O_5 based glasses with the various BaF_2 content. *Journal of Molecular Structure*, *1217*, 128452.

Leśniak, M., Szal, R., Starzyk, B., Gajek, M., Kochanowicz, M., Żmojda, J., Miluski, P., Dorosz, J., Sitarz, M., & Dorosz, D. (2019). Influence of barium oxide on glass-forming ability and glass stability of the tellurite–phosphate oxide glasses. *Journal of Thermal Analysis and Calorimetry*, *138*(6), 4295–4302.

Li, Z., Zhang, W., & Xing, F. (2019). Graphene Optical Biosensors. *International Journal of Molecular Sciences*, *20*(10), 2461.

Liang, L., Mo, Z., Ju, B., Xia, C., Hou, Z., & Zhou, G. (2021). Visible and Near-Infrared emission properties of Yb^{3+}/Pr^{3+} co-doped lanthanum aluminum silicate glass. *Journal of Non-Crystalline Solids*, *557*, 120578.

Linda, D., Duclére, J. R., Hayakawa, T., Dutreilh-Colas, M., Cardinal, T., Mirgorodsky, A., Kabadou, A., & Thomas, P. (2013). Optical properties of tellurite glasses elaborated within the TeO_2-Ti_2O-Ag_2O and TeO_2-ZnO-Ag_2O ternary systems. *Journal of Alloys and Compounds*, *561*, 151–160.

Liu, W., & Speranza, G. (2021). Tuning the Oxygen Content of Reduced Graphene Oxide and Effects on Its Properties. *ACS Omega*, *6*(9), 6195–6205.

05-4506832 pustaka.upsi.edu.my Perpustakaan Tuanku Bainun Kampus Sultan Abdul Jalil Shah PustakaTBainun ptbupsi

05-4506832 pustaka.upsi.edu.my Perpustakaan Tuanku Bainun Kampus Sultan Abdul Jalil Shah PustakaTBainun ptbupsi

Liu, X., Li, S., Tan, C., Gao, C., Liu, Y., Ye, H., & Zhang, G. (2022). Coalescence kinetics and microstructure evolution of Cu nanoparticles sintering on substrates: a molecular dynamics study. *Journal of Materials Research and Technology*, *17*, 1132–1145.

Liu, Z., She, J., & Peng, B. (2021). Spectroscopic properties of Er^{3+}-doped fluoroindate glasses. *Journal of Rare Earths*.

Lundie, M., Sljivancanin, Z., & Tomic, S. (2015). Electronic and optical properties of reduced graphene oxide. *Journal of Materials Chemistry C*, *3*, 7632–7641.

Lunt, A. J. G., Chater, P., & Korsunsky, A. M. (2018). On the origins of strain inhomogeneity in amorphous materials. *Scientific Reports*, *8*(1).

Ma, C., Wang, C., Gao, B., Adams, J., Wu, G., & Zhang, H. (2019). Recent progress in ultrafast lasers based on 2D materials as a saturable absorber. *Applied Physics Reviews*, *6*(4), 041304.

Machado, T. M., Falci, R. F., Silva, I. L., Anjos, V., Bell, M. J. V, & Silva, M. A. P. (2019). Erbium 1.55 μm luminescence enhancement due to copper nanoparticles plasmonic activity in tellurite glasses Tamires. *Materials Chemistry and Physics*, *224*, 73–78.
05-4506832 pustaka.upsi.edu.my Perpustakaan Tuanku Bainun Kampus Sultan Abdul Jalil Shah PustakaTBainun ptbupsi
Madani, S. Y., Mandel, A., & Seifalian, A. M. (2013). A concise review of carbon nanotube's toxicology. *Nano Reviews*, *4*, 21521.

Maheshvaran, K., Arunkumar, S., Sudarsan, V., Natarajan, V., & Marimuthu, K. (2013). Structural and luminescence studies on Er^{3+}/Yb^{3+} co-doped boro-tellurite glasses. *Journal of Alloys and Compounds*, *561*, 142–150.

Mahmood, H., Vanzetti, L., Bersani, M., & Pegoretti, A. (2018). Mechanical properties and strain monitoring of glass-epoxy composites with graphene-coated fibers. *Composites Part A: Applied Science and Manufacturing*, *107*, 112–123.

Mandal, S. K., Dutta, K., Pal, S., Mandal, S., Naskar, A., Pal, P. K., Bhattacharya, T. S., Singha, A., Saikh, R., De, S., & Jana, D. (2019). Engineering of ZnO/rGO nanocomposite photocatalyst towards rapid degradation of toxic dyes. *Materials Chemistry and Physics*, *223*, 456–465.

Manning, S., Ebendorff-heidepriem, H., & Monro, T. M. (2012). Ternary tellurite glasses for the fabrication of nonlinear optical fibres. *Optical Materials Express*, *2*(2), 305–308.

Mao, X., Zhu, L., Liu, H., Chen, H., Li, W., Cao, R., & Li, W. (2021). Cu/graphene composite coatings electrodeposited in a directly dispersed graphene solution after electrochemical exfoliation with enhanced oxidation resistance. *Journal of Alloys*
05-4506832 pustaka.upsi.edu.my Perpustakaan Tuanku Bainun Kampus Sultan Abdul Jalil Shah PustakaTBainun ptbupsi

05-4506832 pustaka.upsi.edu.my Perpustakaan Tuanku Bainun Kampus Sultan Abdul Jalil Shah PustakaTBainun ptbupsi

and Compounds, *882*, 160706.

Marcano, D. C., Kosynkin, D. V, Berlin, J. M., Sinitskii, A., Sun, Z., Slesarev, A., Alemany, L. B., Lu, W., & Tour, J. M. (2010). Improved Synthesis of Graphene Oxide. *ACS Nano*, *4*(8).

Marczewska, A., & Środa, M. (2018). Spectroscopic and thermal study of a new glass from TeO_2–Ga_2O_3–GeO_2 system. *Journal of Molecular Structure*, *1164*, 100–108.

Mariyappan, M., Arunkumar, S., & Marimuthu, K. (2019). Judd-Ofelt analysis and NIR luminescence investigations on Er^{3+} ions doped B_2O_3–Bi_2O_3–Li_2O–K_2O glasses for photonic applications. *Physica B: Condensed Matter*, *572*, 27–35.

Mariyappan, M., Arunkumar, S., & Marimuthu, K. (2019). Physical, structural and optical studies on Er^{3+} ions doped zinc bismuth borate glasses for photonic applications. *AIP Conference Proceedings*, *2115*, 1–5.

Marturi, N. (2013). Vision and visual servoing for nanomanipulation and nanocharacterization in scanning electron microscope. *Micro and Nanotechnologies/Microelectronics. Université de Franche-Comté,*.

Marzouk, S. Y., Azooz, M. A., & Batal, H. A. El. (2021). Judd-Ofelt analysis of spectroscopic measurements of Er^{3+} doped boro-zincate glasses. *Journal of Molecular Structure*, *1243*, 130925.

Maslov, V. G., Svitenkov, A. I., & Krzhizhanovskaya, V. V. (2016). Abnormally high oscillator strengths of the graphene nanoribbons electronic spectrum: quantum chemistry calculations. *RSC Advances*.

Mawlud, S. Q., Ameen, M. M., Sahar, R., Ashur, Z., Mahraz, S., & Ahmed, K. F. (2017). Spectroscopic properties of Sm^{3+} doped sodium-tellurite glasses : Judd-Ofelt analysis. *Optical Materials*, *69*, 318–327.

Mclaughlin, J. C., Tagg, S. L., Zwanziger, J. W., & Hae, D. R. (2000). The structure of tellurite glass : a combined NMR , neutron diffraction , and X-ray diffraction study. *Journal of Non-Crystalline Solids*, *274*, 1–8.

McSherry, M., Fitzpatrick, C., & Lewis, E. (2004). An optical fiber sensor for the detection of germicidal UV irradiation using narrowband luminescent coatings. *IEEE Sensors Journal*, *4*(5), 619–626.

Meyyappan, M., Delzeit, L., Cassell, A., & Hash, D. (2003). Carbon nanotube growth by PECVD: A review. *Plasma Sources Science and Technology*, *12*(2), 205–216.

Minitha, C. R., Anithaa, V. S., Subramaniam, V., & Rajendra Kumar, R. T. (2018). Impact of Oxygen Functional Groups on Reduced Graphene Oxide-Based Sensors

05-4506832 pustaka.upsi.edu.my Perpustakaan Tuanku Bainun Kampus Sultan Abdul Jalil Shah PustakaTBainun ptbupsi

05-4506832 pustaka.upsi.edu.my Perpustakaan Tuanku Bainun Kampus Sultan Abdul Jalil Shah PustakaTBainun ptbupsi

for Ammonia and Toluene Detection at Room Temperature. *ACS Omega*, *3*(4), 4105–4112.

Mohammed, H., Kumar, A., Bekyarova, E., Al-Hadeethi, Y., Zhang, X., Chen, M., Ansari, M. S., Cochis, A., & Rimondini, L. (2020). Antimicrobial Mechanisms and Effectiveness of Graphene and Graphene-Functionalized Biomaterials. A Scope Review. *Frontiers in Bioengineering and Biotechnology*, *8*.

Mohan, V. B., Souri, H., Jayaraman, K., & Bhattacharyya, D. (2018). Mechanical properties of thin films of graphene materials: A study on their structural quality and functionalities. *Current Applied Physics*.

Moon, I. K., Lee, J., Ruoff, R. S., & Lee, H. (2010). Reduced graphene oxide by chemical graphitization. *Nature Communications*, *1*(6), 1–6.

Morigaki, K., & Ogihara, C. (2006). Amorphous Semiconductors: Structure, Optical, and Electrical Properties. *Springer Handbook of Electronic and Photonic Materials*, 565–580.

Mott, N. F., Davis, E. A., & Weiser, K. (1972). Electronic Processes in Non-Crystalline Materials. *Physics Today*, *25*(12), 55.

Mu, J., Gao, F., Cui, G., Wang, S., Tang, S., & Li, Z. (2021). A comprehensive review of anticorrosive graphene-composite coatings. *Progress in Organic Coatings*, *157*(66), 106321.

Mun, S. C., Park, J. J., Park, Y. T., Kim, D. Y., Lee, S. W., Cobos, M., Ye, S. J., Macosko, C. W., & Park, O. O. (2017). High electrical conductivity and oxygen barrier property of polymer- stabilized graphene thin films. *Carbon*, *125*, 492–499.

Munisudhakar, B., Raju, C. N., Babu, M. R., Reddy, N. M., & Moorthy, L. R. (2019). Materials Today : Proceedings Luminescence characteristics of Nd^{3+} doped bismuth borate glasses for photonic applications. *Materials Today: Proceedings*.

Muruganandi, G., Saravanan, M., Vinitha, G., Jessie Raj, M. B., & Sabari Girisun, T. C. (2018). Barium borate nanorod decorated reduced graphene oxide for optical power limiting applications. *Optical Materials*, *75*, 612–618.

Narayan, R., & Kim, S. O. (2015). Surfactant mediated liquid phase exfoliation of graphene. *Nano Convergence*, *2*(1), 20.

Naumov, A. V. (2017). Graphene Oxide: Fundamentals and Applications. *John Wiley & Sons*.

Nazhirah, S. N. M., Ghoshal, S. K., Arifin, R., & Hamzah, K. (2021). Effects of bimetallic nanoparticles Ag and TiO_2 embedment on tellurite zinc–silicate glass:

05-4506832 pustaka.upsi.edu.my Perpustakaan Tuanku Bainun Kampus Sultan Abdul Jalil Shah PustakaTBainun ptbupsi

05-4506832 pustaka.upsi.edu.my Perpustakaan Tuanku Bainun Kampus Sultan Abdul Jalil Shah PustakaTBainun ptbupsi

Self-cleaning characteristics. *Surfaces and Interfaces*, *25*, 101236.

Nazrin, S. N., Halimah, M. K., Muhammad, F. D., Yip, J. S., Hasnimulyati, L., Faznny, M. F., Hazlin, M. A., & Zaitizila, I. (2018). The effect of erbium oxide in physical and structural properties of zinc tellurite glass system. *Journal of Non-Crystalline Solids*, *490*, 35–43.

Necolau, M. I., & Pandele, A. M. (2020). Recent advances in graphene oxide-based anticorrosive coatings: An overview. *Coatings*, *10*, 1149.

Noguera, O., Mirgorodsky, A. P., Smirnov, M. B., & Thomas, P. (2003). Vibrational and structural properties of glass and crystalline phases of TeO_2. *Journal of Non-Crystalline Solids*, *330*, 50–60.

Norizan, M. N., Moklis, M. H., Ngah Demon, S. Z., Halim, N. A., Samsuri, A., Mohamad, I. S., Knight, V. F., & Abdullah, N. (2020). Carbon nanotubes: Functionalisation and their application in chemical sensors. *RSC Advances*, *10*(71), 43704–43732.

Nourbakhsh, A., Cantoro, M., Vosch, T., Pourtois, G., Clemente, F., Veen, M. H. Van Der, Hofkens, J., Heyns, M. M., Gendt, S. De, & Sels, B. F. (2010). Bandgap opening in oxygen plasma-treated graphene. *Nanotechnology*, *21*(43), 435203.

Novoselov, K. S., Geim, A. K., Morozov, S. V, Jiang, D., Zhang, Y., Dubonos, S. V, Grigorieva, I. V, & Firsov, A. A. (2004). Electric Field Effect in Atomically Thin Carbon Films. *Science*, *306*(5696), 666–669.

Nurhafizah, M. D., Suriani, A. B., Mohamed, A., & Soga, T. (2020). Effect of voltage applied for graphene oxide/latex nanocomposites produced via electrochemical exfoliation and its application as conductive electrodes. *Diamond & Related Materials*, *101*(107624).

Ofelt, G. S. (1962). Intensities of crystal spectra of rare-earth ions. *The Journal of Chemical Physics*, *37*(3), 511–520.

Omidvar, A., RashidianVaziri, M. R., & Jaleh, B. (2018). Enhancing the nonlinear optical properties of graphene oxide by repairing with palladium nanoparticles. *Physica E: Low-Dimensional Systems and Nanostructures*, *103*, 239–245.

Pach-Zawada, K., Leśniak, M., Filipecka, K., Golis, E., Yousef, E. S., Pawlik, P., Dorosz, D., Sitarz, M., & Filipecki, J. (2021). Structural studies of tellurite glasses from the $70TeO_2$-5XO-$10P_2O_5$–10ZnO–$5PbF_2$ system (X = Ba, W, Sr, Cd) doped with erbium ions. *Journal of Molecular Structure*, *1224*, 128787.

Papadakis, I., Bakandritsos, A., Swain, A. K., Szabo, T., & Couris, S. (2020). Effects of Size and Oxidation on the Nonlinear Optical Response and Optical Limiting of

05-4506832 pustaka.upsi.edu.my Perpustakaan Tuanku Bainun Kampus Sultan Abdul Jalil Shah PustakaTBainun ptbupsi

05-4506832 pustaka.upsi.edu.my Perpustakaan Tuanku Bainun Kampus Sultan Abdul Jalil Shah PustakaTBainun ptbupsi

Graphene Oxide Sheets. *Journal of Physical Chemistry C*, *124*, 11265–11273.

Park, S. J., Ok, J. G., Park, H. J., Lee, K. T., Lee, J. H., Kim, J. D., Cho, E., Baac, H. W., Kang, S., Guo, L. J., & Hart, A. J. (2018). Modulation of the effective density and refractive index of carbon nanotube forests via nanoimprint lithography. *Carbon*, *129*, 8–14.

Park, S., & Ruoff, R. S. (2009). Chemical methods for the production of graphenes. *Nature Nanotechnology*, *4*, 45–47.

Pauling, L. (1932). THE NATURE OF THE CHEMICAL BOND. IV. THE ENERGY OF SINGLE BONDS AND THE RELATIVE ELECTRONEGATIVITY OF ATOMS. *J. Am. Chem. Soc.*, *54*(9), 3570–3582.

Pavani, P. G., Sadhana, K., & Mouli, V. C. (2011). Optical , physical and structural studies of boro-zinc tellurite glasses. *Physica B: Physics of Condensed Matter*, *406*(6–7), 1242–1247.

Pei, S., & Cheng, H. M. (2012). The reduction of graphene oxide. *Carbon*, *50*(9), 3210–3228.

Pepe, Y., Erdem, M., Sennaroglu, A., & Eryurek, G. (2019). Enhanced gain bandwidth of Tm^{3+} and Er^{3+} doped tellurite glasses for broadband optical amplifier. *Journal of Non-Crystalline Solids*, *522*, 119501.

Perebeinos, V., Tersoff, J., & Avouris, P. (2005). Effect of exciton-phonon coupling in the calculated optical absorption of carbon nanotubes. *Physical Review Letters*, *94*(2), 3–6.

Piao, Y., Tondare, V. N., Davis, C. S., Gorham, J. M., Petersen, E. J., Gilman, J. W., Scott, K., Vladár, A. E., & Hight Walker, A. R. (2021). Comparative study of multiwall carbon nanotube nanocomposites by Raman, SEM, and XPS measurement techniques. *Composites Science and Technology*, *208*, 108753.

Pirouz, A. A., Karjiban, R. A., Bakar, F. A., & Selamat, J. (2018). A novel adsorbent magnetic graphene oxide modified with Chitosan for the simultaneous reduction of mycotoxins. *Toxins*, *10*(9), 361.

Pisarski, W. A., Kowalska, K., Kuwik, M., Polak, J., Pietrasik, E., Goryczka, T., & Pisarska, J. (2020). Novel multicomponent titanate-germanate glasses: Synthesis, structure, properties, transition metal, and rare earth doping. *Materials*, *13*(19), 1–13.

Prabhu, N. S., Hegde, V., Sayyed, M. I., Şakar, E., & Kamath, S. D. (2019). Investigations on the physical, structural, optical and photoluminescence behavior of Er^{3+} ions in lithium zinc fluoroborate glass system. *Infrared Physics and*

05-4506832 pustaka.upsi.edu.my Perpustakaan Tuanku Bainun Kampus Sultan Abdul Jalil Shah PustakaTBainun ptbupsi

05-4506832 pustaka.upsi.edu.my Perpustakaan Tuanku Bainun Kampus Sultan Abdul Jalil Shah PustakaTBainun ptbupsi

Technology, *98*, 7–15.

Price, R. J., Ladislaus, P. I., Smith, G. C., & Davies, T. J. (2019). A novel 'bottom-up' synthesis of few- and multi-layer graphene platelets with partial oxidation via cavitation. *Ultrasonics - Sonochemistry*, *56*, 466–473.

Purkait, T., Singh, G., Kumar, D., Singh, M., & Dey, R. S. (2018). High-performance flexible supercapacitors based on electrochemically tailored three-dimensional reduced graphene oxide networks. *Scientific Reports*, *8*(640), 1–13.

Qian, L., Xie, Y., Zhang, S., & Zhang, J. (2020). Band Engineering of Carbon Nanotubes for Device Applications. *Matter*, *3*(3), 664–695.

Queiroz, M. N., Dantas, N. F., Brito, D. R. N., Barboza, M. J., Steimacher, A., & Pedrochi, F. (2019). Optical and Spectroscopic Investigation of Sm^{3+}-Doped Calcium Borotellurite Glasses. *Journal of Electronic Materials*.

Rathinavel, S., Priyadharshini, K., & Panda, D. (2021). A review on carbon nanotube: An overview of synthesis, properties, functionalization, characterization, and the application. *Materials Science and Engineering B: Solid-State Materials for Advanced Technology*, *268*, 115095.

Reddy, R. R., & Nazeer, A. Y. (1995). Relationship between refractive index, optical electronegativities and electronic polarizability in alkali halides, III–V, II–VI group semiconductors. *Crystal Research and Technology*, *30*(2), 263–266.

Reddy, R. R., Nazeer Ahammed, Y., Abdul Azeem, P., Rama Gopal, K., & Rao, T. V. R. (2001). Electronic polarizability and optical basicity properties of oxide glasses through average electronegativity. *Journal of Non-Crystalline Solids*, *286*(3), 169–180.

Renteria, J. D., Ramirez, S., Malekpour, H., Alonso, B., Centeno, A., Zurutuza, A., Cocemasov, A. I., Nika, D. L., & Balandin, A. A. (2015). Strongly Anisotropic Thermal Conductivity of Free-Standing Reduced Graphene Oxide Films Annealed at High Temperature. *Advanced Functional Materials*, *25*(29), 4664–4672.

Richards, B. D. O., & Jha, A. (2017). Lasers utilising tellurite glass-based gain media. *Springer Series in Materials Science*, *254*, 101–130.

Rodríguez-González, J. A., Rubio-González, C., & Pérez-Sánchez, A. (2021). Deposition of carbon nanotubes onto glass fibers using ultrasound standing waves. *Frontiers of Materials Science*, *15*(3), 471–475.

Ronda, C. (2007). *Luminescence (From Theory to Applications)*.

05-4506832 pustaka.upsi.edu.my Perpustakaan Tuanku Bainun Kampus Sultan Abdul Jalil Shah PustakaTBainun ptbupsi

05-4506832 pustaka.upsi.edu.my Perpustakaan Tuanku Bainun Kampus Sultan Abdul Jalil Shah PustakaTBainun ptbupsi

Ronda, C., & Srivastava, A. (2006). Luminescence science and display materials. *Electrochemical Society Interface*, *15*(1), 55–57.

Sadik, S. A., Durak, F. E., & Altuncu, A. (2020). Widely tunable erbium doped fiber ring laser based on loop and double-pass EDFA design. *Optics and Laser Technology*, *124*, 105979.

Sahoo, S., Sahoo, G., Mun, S., & Sekhar, C. (2022). Review article A review on supercapacitors based on plasma enhanced chemical vapor deposited vertical graphene arrays. *Journal of Energy Storage*, *53*(April), 105212.

Sahu, S., & Rout, G. C. (2017). Band gap opening in graphene : a short theoretical study. *International Nano Letters*, *7*(2), 81–89.

Said Mahraz, Z. A., Sahar, M. R., & Ghoshal, S. K. (2015). Enhanced luminescence from silver nanoparticles integrated Er^{3+}-doped boro-tellurite glasses: Impact of annealing temperature. *Journal of Alloys and Compounds*, *649*, 1102–1109.

Saifuddin, N., Raziah, A. Z., & Junizah, A. R. (2013). Carbon nanotubes: A review on structure and their interaction with proteins. *Journal of Chemistry*.

Sailaja, P., Mahamuda, S., Swapna, K., Venkateswarlu, M., Gupta, M., & Rao, A. S. (2021). Broadband NIR emission at 1.53 μm in trivalent erbium ions doped SrO-Al_2O_3-B_2O_3-$BaCl_2$-10TeO_2 glasses for optical fiber and NIR laser applications. *Journal of Non-Crystalline Solids*, *567*, 120937.

Sajna, M. S., Perumbilavil, S., Prakashan, V. P., Sanu, M. S., Joseph, C., Biju, P. R., & Unnikrishnan, N. V. (2018). Enhanced resonant nonlinear absorption and optical limiting in Er^{3+} ions doped multicomponent tellurite glasses. *Materials Research Bulletin*.

Saraswati, A., Marzuki, A., Fausta, D. E., Suryanti, V., & Singgih, G. A. (2021). Borate Glasses for Low Loss Optical Fibre. *Journal of Physics: Conference Series*, *1912*(1).

Sayyed, M. I., Zaid, M. H. M., Effendy, N., Matori, K. A., Sidek, H. A. A., Lacomme, E., Mahmoud, K. A., & AlShammari, M. M. (2020). The influence of PbO and Bi_2O_3 on the radiation shielding and elastic features for different glasses. *Journal of Materials Research and Technology*, *9*(4), 8429–8438.

Schniepp, H. C., Li, J., Mcallister, M. J., Sai, H., Herrera-alonso, M., Adamson, D. H., Prud, R. K., Car, R., Saville, D. A., & Aksay, I. A. (2006). Functionalized Single Graphene Sheets Derived from Splitting Graphite Oxide. *The Journal of Physical Chemistry B Letetrs*, *2*, 8535–8539.

Shakeri, M. S., & Rezvani, M. (2011). Optical band gap and spectroscopic study of lithium alumino silicate glass containing Y^{3+} ions. *Spectrochimica Acta Part A:*

05-4506832 pustaka.upsi.edu.my Perpustakaan Tuanku Bainun Kampus Sultan Abdul Jalil Shah PustakaTBainun ptbupsi

05-4506832 pustaka.upsi.edu.my Perpustakaan Tuanku Bainun Kampus Sultan Abdul Jalil Shah PustakaTBainun ptbupsi

Molecular and Biomolecular Spectroscopy, *79*, 1920–1925.

Shang, J., Ma, L., Li, J., Ai, W., Yu, T., & Gurzadyan, G. G. (2012). The origin of fluorescence from graphene oxide. *Scientific Reports*, *2*, 1–8.

Sharma, N., Arif, M., Monga, S., Shkir, M., Mishra, Y. K., & Singh, A. (2020). Investigation of bandgap alteration in graphene oxide with different reduction routes. *Applied Surface Science*, *513*, 145396.

Sharma, N., Tomar, S., Shkir, M., Kant Choubey, R., & Singh, A. (2019). Study of Optical and Electrical Properties of Graphene Oxide. *Materials Today: Proceedings*, *36*, 730–735.

Shen, C., Jia, Y., Yan, X., Zhang, W., Li, Y., Qing, F., & Li, X. (2018). Effects of Cu contamination on system reliability for graphene synthesis by chemical vapor deposition method. *Carbon*, *127*, 676–680.

Shen, X., Cheng, G., Zhang, L., & Wei, W. (2020). Fabrication of a hybrid-cladding tellurite glass fiber doped with Tm^{3+} and Ho^{3+}. *Journal of Luminescence*, *227*, 117540.

Shin, D. S., Kim, H. G., Ahn, H. S., Jeong, H. Y., Kim, Y., Odkhuu, D., Tsogbadrakh, N., Lee, H., & Kim, B. H. (2017). Distribution of oxygen functional groups of graphene oxide obtained from low-temperature atomic layer deposition of titanium oxide. *Royal Society of Chemistry*, *7*, 13979–13984.

Shin, H. J., Kim, K. K., Benayad, A., Yoon, S. M., Park, H. K., Jung, I. S., Jin, M. H., Jeong, H. K., Kim, J. M., Choi, J. Y., & Lee, Y. H. (2009). Efficient reduction of graphite oxide by sodium borohydride and its effect on electrical conductance. *Advanced Functional Materials*, *19*(12), 1987–1992.

Silva, A. A., Pinheiro, R. A., Rodrigues, A. C., Baldan, M. R., Trava-Airoldi, V. J., & Corat, E. J. (2018). Graphene sheets produced by carbon nanotubes unzipping and their performance as supercapacitor. *Applied Surface Science*.

Silva, L. M. C., Gonçalves, B. S., Braga, J. de O., de Souza, T. C., de Castro, V. G., Silva, G. G., Lacerda, G. R. B. S., Matencio, T., Barbosa, T. C., Viana, C. M., Houmard, M., & Nunes, E. H. M. (2021). Preparation of titania-reduced graphene oxide composite coatings with electro- and photosensitive properties. *Applied Surface Science*, *538*, 148029.

Singh, V., Seshadri, M., Singh, N., & Mohapatra, M. (2019). Radiative properties of Er^{3+} doped and Er^{3+}/Yb^{3+} co-doped $Sr_3Al_2O_6$ phosphors : exploring the usefulness as a phosphor material. *Journal of Materials Science: Materials in Electronics*.

05-4506832 pustaka.upsi.edu.my Perpustakaan Tuanku Bainun Kampus Sultan Abdul Jalil Shah PustakaTBainun ptbupsi

05-4506832 pustaka.upsi.edu.my Perpustakaan Tuanku Bainun Kampus Sultan Abdul Jalil Shah PustakaTBainun ptbupsi

Singh V , Joung D , Zhai L , Das S , Khondaker SI, S. S. (2011). Graphene based materials : Past , present and future. *Progress in Materials Science*, *56*, 1178–1271.

Slobodian, O. M., Lytvyn, P. M., Nikolenko, A. S., Naseka, V. M., Khyzhun, O. Y., Vasin, A. V., Sevostianov, S. V., & Nazarov, A. N. (2018). Low-Temperature Reduction of Graphene Oxide: Electrical Conductance and Scanning Kelvin Probe Force Microscopy. *Nanoscale Research Letters*, *13*.

Smith, A. T., Marie, A., Zeng, S., Liu, B., & Sun, L. (2019). Synthesis , properties , and applications of graphene oxide/ reduced graphene oxide and their nanocomposites. *Nano Materials Science*.

Smith, K. C. A., Wells, O. C., & McMullan, D. (2008). The fiftieth anniversary of the first applications of the scanning electron microscope in materials research. *Physics Procedia*, *1*(1), 3–12.

Sreedhar, V. B., Krishnaiah, K. V., Rasool, S. K. N., Venkatramu, V., & Jayasankar, C. K. (2019). Raman and photoluminescence studies of europium doped zinc-fluorophosphate glasses for photonic applications. *Journal of Non-Crystalline Solids*, *505*, 115–121.

Sreeja, V. G., & Anila, E. I. (2019). Studies on the effect of reduced graphene oxide on nonlinear absorption and optical limiting properties of potassium doped zinc oxide thin film by Z - scan technique. *Thin Solid Films*, *685*, 161–167.

Sreeja, V. G., Vinitha, G., Reshmi, R., Anila, E. I., & Jayaraj, M. K. (2017). Effect of reduction time on third order optical nonlinearity of reduced graphene oxide. *Optical Materials*, *66*, 460–468.

Stambouli, W., Elhouichet, H., & Ferid, M. (2012). Study of thermal, structural and optical properties of tellurite glass with different TiO_2 composition. *Journal of Molecular Structure*, *1028*, 39–43.

Stankovich, S., Dikin, D. A., Piner, R. D., Kohlhaas, K. A., Kleinhammes, A., Jia, Y., Wu, Y., Nguyen, S. B. T., & Ruoff, R. S. (2007). Synthesis of graphene-based nanosheets via chemical reduction of exfoliated graphite oxide. *Carbon*, *45*(7), 1558–1565.

Stanworth, J. E. (1952). Tellurite Glasses. *Nature*, *169*(4301), 581–582.

Staudenmaier, L. (1898). Verfahren zur Darstellung der Graphitsäure. *Berichte Der Deutschen Chemischen Gesellschaft*.

Sun, G. (2010). Intersubband approach to silicon based lasers-circumventing the indirect bandgap limitation. *Advances in Optics and Photonics*, *3*(1), 53.

05-4506832 pustaka.upsi.edu.my Perpustakaan Tuanku Bainun Kampus Sultan Abdul Jalil Shah PustakaTBainun ptbupsi

05-4506832 pustaka.upsi.edu.my Perpustakaan Tuanku Bainun Kampus Sultan Abdul Jalil Shah PustakaTBainun ptbupsi

Sundaram, R. S., Burghard, M., Gómez-Navarro, C., Chuvilin, A., Kaiser, U., Kurasch, S., Meyer, J. C., & Kern, K. (2010). Atomic Structure of Reduced Graphene Oxide. *Nano Letters*, *10*(4), 1144–1148.

Suriani, A. B., Nurhafizah, M. D., Mohamed, A., Masrom, A. K., Mamat, M. H., Malek, M. F., Ahmad, M. K., Rosmi, M. S., & Tanemura, M. (2017). Electrical enhancement of radiation-vulcanized natural rubber latex added with reduced graphene oxide additives for supercapacitor electrodes. *Journal of Materials Science*, *52*(11), 6611–6622.

Taherunnisa, S. K., Krishna Reddy, D V SambasivaRao, T Rudramamba, K S Zhydachevskyy, Y A Suchocki, A., Piasecki, M., & Rami Reddy, M. (2019). Effect of up-conversion luminescence in Er^{3+} doped phosphate glasses for developing Erbium-Doped Fibre Amplifiers (EDFA) and G-LED's. *Optical Materials: X*, 100034.

Tanabe, S., Ohyagi, T., Soga, N., & Hanada, T. (1992). Compositional dependence of Judd-Ofelt parameters of Er^{3+} ions in alkali-metal borate glasses. *Physical Review B*, *46*(6), 3305–3310.

Tanabe, S., Ohyagi, T., Todoroki, S., Hanada, T., & Soga, N. (1993). Relation between the Ω_6 intensity parameter of Er^{3+} ions and the 151Eu isomer shift in oxide glasses. *Journal of Applied Physics*, *73*(12), 8451–8454.

Tang, S., Wu, W., Xie, X., Li, X., & Gu, J. (2017). Band gap opening of bilayer graphene by graphene oxide support doping. *Royal Society of Chemistry*, *7*, 9862–9871.

Tarcan, R., Todor-Boer, O., Petrovai, I., Leordean, C., Astilean, S., & Botiz, I. (2020). Reduced graphene oxide today. *Journal of Materials Chemistry C*, *8*, 1198–1224.

Thombre, D. B. (2016). The Estimation of Oxide Polarizability and Basicity using Electronegativity for B_2O_3 : M_2O Glass System (M = Li , Na , K , Rb). *International Journal of Innovative Research in Science, Engineering and Technology*, *5*(2), 1230–1236.

Tian, J., Wu, S., Yin, X., & Wu, W. (2019). Novel preparation of hydrophilic graphene/graphene oxide nanosheets for supercapacitor electrode. *Applied Surface Science*, *496*, 143696.

Tiedje, T., Colbow, K. M., Gao, Y., Dahn, J. R., Reimers, J. N., & Houghton, D. C. (1992). Role of Coulomb repulsion in 4*f* orbitals in electrical excitation of rare-earth impurities in semiconductors. *Applied Physics Letters*, *61*(11), 1296–1297.

Tiwari, H., & Dhondiyal, C. C. (2021). Physical and optical analysis of Sm^{3+} doped zinc phosphate glass. *Materials Today: Proceedings*.

05-4506832 pustaka.upsi.edu.my Perpustakaan Tuanku Bainun Kampus Sultan Abdul Jalil Shah PustakaTBainun ptbupsi

05-4506832 pustaka.upsi.edu.my Perpustakaan Tuanku Bainun Kampus Sultan Abdul Jalil Shah PustakaTBainun ptbupsi

Tzounis, L., Zappalorto, M., Panozzo, F., Tsirka, K., Maragoni, L., Paipetis, A. S., & Quaresimin, M. (2019). Highly conductive ultra-sensitive SWCNT-coated glass fiber reinforcements for laminate composites structural health monitoring. *Composites Part B: Engineering*, *169*, 37–44.

Umar, S. A., Halimah, M. K., Chan, K. T., & Latif, A. A. (2017). Polarizability , optical basicity and electric susceptibility of Er^{3+} doped silicate borotellurite glasses. *Journal of Non-Crystalline Solids*.

Ural, N. (2021). The significance of scanning electron microscopy (SEM) analysis on the microstructure of improved clay: An overview. *Open Geosciences*, *13*(1), 197–218.

Usman, A., Halimah, M. K., Latif, A. A., Diana, F., & Abubakar, A. I. (2018). Influence of Ho^{3+} ions on structural and optical properties of zinc borotellurite glass system. *Journal of Non-Crystalline Solids*.

Walsh, B. M., Barnes, N. P., Bartolo, B. Di, & Walsh, B. M. (1998). Branching ratios, cross sections, and radiative lifetimes of rare earth ions in solids: Application to Tm^{3+} and Ho^{3+} ions in $LiYF_4$. *Journal of Applied Physics*, *83*(5), 2772–2787.

Wan, Q., Wang, H., Li, S., & Wang, J. (2018). Journal of Colloid and Interface Science 3 , 3-tetramethylurea solution. *Journal of Colloid And Interface Science*, *526*, 167–173.

Wan, R., Wang, P., Li, S., & Ma, Y. (2021). 2.86 μm emission and fluorescence enhancement through controlled precipitation of ZnTe nanocrystals in DyF_3 doped multicomponent tellurite oxyfluoride glass. *Journal of Non-Crystalline Solids*, *564*, 120842.

Wang, J., Mu, X., Sun, M., & Mu, T. (2019). Optoelectronic properties and applications of graphene-based hybrid nanomaterials and van der Waals heterostructures. *Applied Materials Today*, *16*, 1–20.

Wang, M., Li, Z., Hou, K., Wang, J., & Yang, S. (2020). Balancing oxygen-containing groups and structural defects for optimizing macroscopic tribological properties of graphene oxide coating. *Applied Surface Science*, *516*, 146122.

Wang, Q., Wen, J., Luo, Y., Peng, G.-D., Pang, F., Chen, Z., & Wang, T. (2020). Enhancement of lifetime in Er-doped silica optical fiber by doping Yb ions via atomic layer deposition. *Optical Materials Express*, *10*(2), 397.

Wang, W., Tuo, T., & Jiang, C. (2020). Enhancing near-infrared luminescence of Ln^{3+} (Yb^{3+}/Er^{3+})-doped germanium tellurite glasses by coating with graphene. *Optical and Quantum Electronics*, *52*(6), 1–8.

05-4506832 pustaka.upsi.edu.my Perpustakaan Tuanku Bainun Kampus Sultan Abdul Jalil Shah PustakaTBainun ptbupsi

05-4506832 pustaka.upsi.edu.my Perpustakaan Tuanku Bainun Kampus Sultan Abdul Jalil Shah PustakaTBainun ptbupsi

Wang, X. Y., Narita, A., & Müllen, K. (2017). Precision synthesis versus bulk-scale fabrication of graphenes. *Nature Reviews Chemistry*, *2*(1).

Wang, X., Zhi, L., & Mullen, K. (2008). Transparent, Conductive Graphene Electrodes for Dye-Sensitized Solar Cells. *Nano Letters*, *8*(1), 323–327.

Watt, M. R., & Gerhardt, R. A. (2020). Factors that affect network formation in carbon nanotube composites and their resultant electrical properties. *Journal of Composites Science*, *4*(3), 100.

Wei, C., Hu, J., & Menyuk, C. R. (2016). Comparison of Loss in Silica and Chalcogenide Negative Curvature Fibers as the Wavelength Varies. *Frontiers in Physics*, *4*(30).

Wen, H., Zhang, J., Yao, Q., Liu, L., Dong, W., Li, J., & Wang, J. (2019). Thermal, Optical Characterization and Judd-Ofelt Analyis of Nd^{3+}-Doped $BaO-TeO_2-B_2O_3$ Glasses. *Materials and Technology*, *53*(3), 305–309.

Woehrle, G. H., Hutchison, J. E., Özkar, S., & Finke, R. G. (2006). Analysis of nanoparticle transmission electron microscopy data using a public- domain image-processing program, Image. *Turkish Journal of Chemistry*, *30*(1), 1–13.

Woo, Y. S. (2019). Transparent conductive electrodes based on graphene-related materials. *Micromachines*, *10*(1), 24–28.

Xiao, J., Zhan, H., Wang, X., Xu, Z. Q., Xiong, Z., Zhang, K., Simon, G. P., Liu, J. Z., & Li, D. (2020). Electrolyte gating in graphene-based supercapacitors and its use for probing nanoconfined charging dynamics. *Nature Nanotechnology*, *15*(8), 683–689.

Xie, S., Li, W., Pan, Z., Chang, B., & Lianfeng, S. (2000). Mechanical and physical properties on carbon nanotube. *Journal of Physics and Chemistry of Solids*, *61*(7), 1153–1158.

Yan, S., Pu, S., Zhang, Y., Yuan, M., & Zhang, C. (2021). Sensing properties of graphene-oxide-functionalized single-mode–no-core–single-mode fiber structure. *Results in Physics*, *25*, 104310.

Yang, S., Lohe, M. R., Müllen, K., & Feng, X. (2016). New-Generation Graphene from Electrochemical Approaches: Production and Applications. *Advanced Materials*, *28*(29), 6213–6221.

Yang, Y., Liu, R., Wu, J., Jiang, X., Cao, P., Hu, X., & Pan, T. (2015). Bottom-up Fabrication of Graphene on Silicon/ Silica Substrate via a Facile Soft-hard Template Approach. *Scientific Reports*, *5*(1).

Yang, Zhongmin, Xu, S., Hu, L., & Jiang, Z. (2004). Thermal analysis and optical properties of Yb^{3+}/Er^{3+}-codoped oxyfluoride germanate glasses. *Journal of the*

05-4506832 pustaka.upsi.edu.my Perpustakaan Tuanku Bainun Kampus Sultan Abdul Jalil Shah PustakaTBainun ptbupsi

05-4506832 pustaka.upsi.edu.my Perpustakaan Tuanku Bainun Kampus Sultan Abdul Jalil Shah PustakaTBainun ptbupsi

Optical Society of America B, *21*(5), 951.

Yang, Zhoufei, Tian, J., Yin, Z., Cui, C., Qian, W., & Wei, F. (2019). Carbon nanotube- and graphene-based nanomaterials and applications in high-voltage supercapacitor: A review. *Carbon*, *141*, 467–480.

Yanmaz, E., Doğan, M., & Turhan, Y. (2021). Effect of sodium dodecyl sulfate on thermal properties of polyvinyl alcohol (PVA)/modified single-walled carbon nanotube (SWCNT) nanocomposites. *Diamond and Related Materials*, *115*.

Yao, J. H., Elder, K. R., Guo, H., & Grant, M. (1993). Theory and simulation of Ostwald ripening. *Physical Review B*, *47*(21).

Yilbas, B. S., Ibrahim, A., Ali, H., Khaled, M., & Laoui, T. (2018). Hydrophobic and optical characteristics of graphene and graphene oxide films transferred onto functionalized silica particles deposited glass surface. *Applied Surface Science*, *442*, 213–223.

Yu, F., Song, P., Wu, D., Birks, T., Bird, D., & Knight, J. (2019). Attenuation limit of silica-based hollow-core fiber at mid-IR wavelengths. *APL Photonics*, *4*(8), 080803.

Yu, M. F., Files, B. S., Arepalli, S., & Ruoff, R. S. (2000). Tensile loading of ropes of single wall carbon nanotubes and their mechanical properties. *Physical Review Letters*, *84*(24), 5552–5555.

Yuan, J., Zheng, G., Ye, Y., Chen, Y., Deng, T., Xiao, P., Ye, Y., & Wang, W. (2021). Enhanced 1.5 μm emission from Yb^{3+}/Er^{3+}-codoped tungsten tellurite glasses for broadband near-infrared optical fiber amplifiers and tunable fiber lasers. *RSC Advances*, *11*(45), 27992–27999.

Yuliantini, L., Djamal, M., Hidayat, R., Boonin, K., Yasaka, P., & Kaewnuam, E. (2019). Optical and X-ray induced luminescence of Sm^{3+} -doped borotellurite and fluoroborotellurite glasses : A comparative study. *Journal of Luminescence*, *213*, 19–28.

Yusof, N. N., Ghoshal, S. K., Ari, R., Awang, A., Tewari, H. S., & Hamzah, K. (2017). Self-cleaning and spectral attributes of erbium doped sodium-zinc-tellurite glass : Role of titania nanoparticles. *Journal of Non-Crystalline Solids*.

Yusof, N. N., Ghoshal, S. K., & Azlan, M. N. (2017). Optical properties of titania nanoparticles embedded Er^{3+}-doped tellurite glass: Judd-Ofelt analysis. *Journal of Alloys and Compounds*, *724*, 1083–1092.

Zachariasen, W. H. (1932). The Atomic Arrangement in Glass. *Journal of the American Chemical Society*, *54*(10), 3841–3851.

05-4506832 pustaka.upsi.edu.my Perpustakaan Tuanku Bainun Kampus Sultan Abdul Jalil Shah PustakaTBainun ptbupsi

05-4506832 pustaka.upsi.edu.my Perpustakaan Tuanku Bainun Kampus Sultan Abdul Jalil Shah PustakaTBainun ptbupsi

Zaitizila, I., Halimah, M. K., Muhammad, F. D., & Nurisya, M. S. (2018). Influence of manganese doping on elastic and structural properties of silica borotellurite glass. *Journal of Non-Crystalline Solids*, *492*, 50–55.

Zanane, H., Velázquez, M., Denux, D., Duclère, J. R., Cornette, J., Kermaoui, A., Kellou, H., Lahaye, M., & Buffière, S. (2020). Judd-Ofelt analysis and crystal field calculations of Er^{3+} ions in new oxyfluorogermanotellurite glasses and glass-ceramics. *Optical Materials*, *100*, 109640.

Zaytseva, O., & Neumann, G. (2016). Carbon nanomaterials: Production, impact on plant development, agricultural and environmental applications. *Chemical and Biological Technologies in Agriculture*, *3*(1), 1–26.

Zhang, F., Bi, Z., Huang, A., & Xiao, Z. (2015). Luminescence and Judd-Ofelt analysis of the Pr^{3+} doped fluorotellurite glass. *Journal of Luminescence*, *160*(37), 85–89.

Zhang, L., Xia, Y., Shen, X., Yang, R., & Wei, W. (2018). Investigations on the effects of the Stark splitting on the fluorescence behaviors in Yb^{3+}-doped silicate, tellurite, germanate, and phosphate glasses. *Optical Materials*, *75*, 1–6.

Zhang, X., Shao, X., & Liu, S. (2012). Dual Fluorescence of Graphene Oxide: A Time-Resolved Study. *The Journal of Physical Chemistry A*, *116*(27), 7308–7313.
05-4506832 pustaka.upsi.edu.my Perpustakaan Tuanku Bainun Kampus Sultan Abdul Jalil Shah PustakaTBainun ptbupsi
Zhang, Ya nan, Xie, W. ge, Wang, J., & Wang, P. (2018). Study on the effect of carbon nanotube coating on the refractive index sensing sensitivity of fiber modal interferometer. *Optical Materials*, *75*, 666–672.

Zhang, Yifan, Sheng, L., Fang, Y., An, K., Yu, L., Liu, Y., & Zhao, X. (2017). Synthesis of 3C-SiC nanowires from a graphene / Si configuration obtained by arc discharge method Abstract SiC nanowires were fabricated by heat-treating a graphene/ Si configuration without. *Chemical Physics Letters*.

Zhang, Yu, Xia, L., Li, C., Ding, J., Li, J., & Zhou, Y. (2021). Enhanced 2.7 μm mid-infrared emission in Er^{3+}/Ho^{3+} co-doped tellurite glass. *Optics and Laser Technology*, *138*, 106913.

Zhang, Yu, Xia, L., Shen, X., Li, J., Yang, G., & Zhou, Y. (2021). Broadband mid-infrared emission in Dy^{3+}/Er^{3+} co-doped tellurite glass. *Journal of Luminescence*, *236*, 118078.

Zhao, G., Liu, H. Y., Du, X., Zhou, H., Mai, Y. W., Jia, Y. Y., & Yan, W. (2021). Glass fibres coated with flame synthesised carbon nanotubes to enhance interface properties. *Composites Communications*, *24*, 100623.

Zhao, X., Wang, X., Lin, H., & Wang, Z. (2008). Average electronegativity, electronic polarizability and optical basicity of lanthanide oxides for different coordination

05-4506832 pustaka.upsi.edu.my Perpustakaan Tuanku Bainun Kampus Sultan Abdul Jalil Shah PustakaTBainun ptbupsi

05-4506832 pustaka.upsi.edu.my Perpustakaan Tuanku Bainun Kampus Sultan Abdul Jalil Shah PustakaTBainun ptbupsi

numbers. *Physica B: Condensed Matter*, *403*(10–11), 1787–1792.

Zhou, M., Wang, Y., Zhai, Y., Zhai, J., Ren, W., Wang, F., & Dong, S. (2009). Controlled synthesis of large-area and patterned electrochemically reduced graphene oxide films. *Chemistry - A European Journal*, *15*(25), 6116–6120.

Zhou, Y., Cheng, X., Huang, F., Sha, Z., Han, Z., Chen, J., Yang, W., Yu, Y., Zhang, J., Peng, S., Wu, S., Rider, A., Dai, L., & Wang, C. H. (2021). Hierarchically structured electrodes for moldable supercapacitors by synergistically hybridizing vertical graphene nanosheets and MnO_2. *Carbon*, *172*, 272–282.

Zhu, Y., Shen, X., Su, X., Zhou, M., Zhou, Y., Li, J., & Yang, G. (2019). Concentration dependent structural , thermal and luminescence properties in Er^{3+} /Tm^{3+} doped tellurite glasses. *Journal of Non-Crystalline Solids*, *507*, 19–29.

Zimmermann, H. M. (2010). Basics of Optical Emission and Absorption. *[Springer Series in Optical Sciences] Integrated Silicon Optoelectronics*, *148*.

05-4506832 pustaka.upsi.edu.my Perpustakaan Tuanku Bainun Kampus Sultan Abdul Jalil Shah PustakaTBainun ptbupsi

05-4506832 pustaka.upsi.edu.my Perpustakaan Tuanku Bainun Kampus Sultan Abdul Jalil Shah PustakaTBainun ptbupsi

05-4506832 pustaka.upsi.edu.my Perpustakaan Tuanku Bainun Kampus Sultan Abdul Jalil Shah PustakaTBainun ptbupsi

APPENDIX A

ACADEMIC JOURNALS:

[1] **Y. Azlina**, M. N. Azlan, A. B. Suriani, H. R. Shaari, Imed Boukhris, Imen Kebaili, N. M. Al-Hada, S. A. Umar, B. K. Kenzhaliyev, M. H. M. Zaid, R. Hisam, S. M. Iskandar, S. N. Nazrin, N. N. Yusof, M. K. Khadijah, Z. A. Alrowaili, M. S. Al-Buriahi, R. A. Tafida, and F. Fika (2022). Emission Properties of Reduced Graphene Oxide-coated Er^{3+}-tellurite Glass for Fiber Optics. *Journal of Materials Science: Materials in Electronics (JMSE)* Vol. 33, No. 36, pp. 26915-26930

[2] **Y. Azlina,** M. N. Azlan, A. B. Suriani, H. R. Shaari, Imed Boukhris, Imen Kebaili, N. M. Al-Hada, S. A. Umar, B. K. Kenzhaliyev, M. H. M. Zaid, R. Hisam, S. M. Iskandar, S. N. Nazrin, N. N. Yusof, M. K. Khadijah, Z. A. Alrowaili, and M. S. Al-Buriahi (2022). Carbon Nanotubes-coated Tellurite-based Amorphous Glass: Structural and Optical Investigations for Potential Optical Fibers. *(Submitted to Ceramics International)*

[3] **Y. Azlina**, M. N. Azlan, H. R. Shaari, and A. B. Suriani (2022). Optical Properties of Reduced Graphene Oxide-coated Tellurite Glass Doped at Different Erbium Composition. *Sains Malaysiana*. Vol. 52, No. 1, pp. 261-269

05-4506832 pustaka.upsi.edu.my Perpustakaan Tuanku Bainun Kampus Sultan Abdul Jalil Shah PustakaTBainun ptbupsi

05-4506832 pustaka.upsi.edu.my Perpustakaan Tuanku Bainun Kampus Sultan Abdul Jalil Shah PustakaTBainun ptbupsi

[4] **Y. Azlina,** M. N. Azlan, S. S. Hajer, M. K. Halimah, A. B. Suriani, S. A. Umar, R. Hisam, M. H. M. Zaid, S. M. Iskandar, B. K. Kenzhaliyev, A. V. Nitsenko, N. N. Yusof, and Boukhris Imed (2021). Graphene Oxide Deposition on Neodymium Doped Zinc Borotellurite Glass Surface: Optical and Polarizability Study for Future Fiber Optics. *Optical Materials.* Vol. 117, pp. 111138

[5] **Y. Azlina,** M. N. Azlan, H. R. Shaari, S. N. Nazrin, N. M. Al-Hada, S. A. Umar, M. H. M. Zaid, R. Hisam, S. M. Iskandar, B. K. Kenzhaliyev, G. K. Kassymova, and Boukhris Imed (2021). Polarizability of Erbium-doped Zinc-tellurite Glasses Coated with Graphene Oxide for Telecommunication Devices. *Chalcogenide Letters.* Vol. 18, No. 9, pp. 525-534

05-4506832 pustaka.upsi.edu.my Perpustakaan Tuanku Bainun Kampus Sultan Abdul Jalil Shah PustakaTBainun ptbupsi

[6] M. N. Azlan, **Y. Azlina**, H. R. Shaari, S. N. Nazrin, N. M. Al-Hada, Imed Boukhris, S. A. Umar, M. H. M. Zaid, R. Hisam, S. M. Iskandar, and B. K. Kenzhaliyev (2021). Red Emission, Upconversion and Intensity Parameters of Erbium Oxide Doped Tellurite Glass for Laser Glass. *Journal of Materials Science: Materials in Electronics.* Vol. 32, No. 19, pp. 24415-24428

[7] H. R. Shaari, M. N. Azlan, **Y. Azlina**, N. M. Al-Hada, S. A. Umar, B. K. Kenzhaliyev, M. H. M. Zaid, R. Hisam, and N.N. Yusof (2022). Oxide Ion Polarizability, Optical Basicity, and Metallization Criterion of GO-coated Nd_2O_3 (NPs)-TeO_2 Glass for Linear Optical Fiber. *Chalcogenide Letters.* Vol. 19, No. 8, pp. 565-577

05-4506832 pustaka.upsi.edu.my Perpustakaan Tuanku Bainun Kampus Sultan Abdul Jalil Shah PustakaTBainun ptbupsi

05-4506832 pustaka.upsi.edu.my Perpustakaan Tuanku Bainun Kampus Sultan Abdul Jalil Shah PustakaTBainun ptbupsi

[8] H. R. Shaari, M. N. Azlan, **Y. Azlina**, S. S. Hajer, S. N. Nazrin, S. A. Umar, B. K. Kenzhaliyev, Imed Boukhris, and N. M. Al-Hada (2021). Investigation of Structural and Optical Properties of Graphene Oxide-coated Neodymium Nanoparticles Doped Zinc-Tellurite Glass for Glass Fiber. *Journal of Inorganic and Organometallic Polymers and Materials.* Vol. 31, No. 11, pp. 4349-4359

[9] H. R. Shaari, M. N. Azlan, A. B. Suriani, and **Y. Azlina**. (2022). The Effect of rGO on Optical Properties of Neodymium Nanoparticles Doped Tellurite Glass System. *Journal of Mechanical Engineering.* Vol. SI 11(1), pp. 273-288

[10] M. N. Azlan, M. K. Halimah, A. B. Suriani, **Y. Azlina**, and S. A. Umar. (2021). The Optical Performance of Holmium Oxide Doped Tellurite Glass for Potential Optical Fiber. *Solid State Phenomena.* Vol. 317, pp. 95-99

05-4506832 pustaka.upsi.edu.my Perpustakaan Tuanku Bainun Kampus Sultan Abdul Jalil Shah PustakaTBainun ptbupsi

05-4506832 pustaka.upsi.edu.my Perpustakaan Tuanku Bainun Kampus Sultan Abdul Jalil Shah PustakaTBainun ptbupsi

APPENDIX B

PRESENTATIONS:

[1] **Y. Azlina**, M. N. Azlan, H. R. Shaari and A. B. Suriani. Spectroscopic Characteristics and Judd-Ofelt Analysis of Reduced Graphene Oxide-coated Borotellurite Glass for Potential Fiber Optics. Presented at 1st World Integrated Chemical and Material Engineering Technology Conference **(WiCMETC 2023)** held at Avana Grand Hotel, Bangkok, Thailand, 4th – 5th February 2023 **(Oral Presentation)**

[2] **Y. Azlina**, M. N. Azlan, H. R. Shaari and A. B. Suriani. Carbon Nanotubes-coated Tellurite Glass: Optical Properties and Judd-Ofelt Theory Analysis for Future Fiber Optics. Presented at Invention, Innovation & Design Exposition **(IIDEX 2022)** via Virtual Platform, 21st – 25th November 2022 **(Video Presentation)**

[3] **Y. Azlina**, M. N. Azlan, A. B. Suriani, and H. R. Shaari. Judd-Ofelt Intensity Parameters and Luminescence Analysis of Reduced Graphene Oxide-coated Tellurite Glass for Fiber Optics. Presented at 31st Regional Conference on Solid State Science and Technology 2022 (31st RCSSST 2022) held at Hotel Perdana, Kota Bharu, Kelantan, 6th – 8th September 2022 **(Poster Presentation)**

05-4506832 pustaka.upsi.edu.my Perpustakaan Tuanku Bainun Kampus Sultan Abdul Jalil Shah PustakaTBainun ptbupsi

05-4506832 pustaka.upsi.edu.my Perpustakaan Tuanku Bainun Kampus Sultan Abdul Jalil Shah PustakaTBainun ptbupsi

[4] **Y. Azlina**, M. N. Azlan, and H. R. Shaari. Optical Properties of Carbon Nanotubes-coated Tellurite Glass: Judd-Ofelt Analysis for Future Fiber Optics. Presented at 3rd Bionanotechnology Research Seminar & Conference 2022 **(3rd BioNanoSem 2022)** held at The Everly Hotel, Putrajaya, 4th August 2022 **(Oral Presentation)**

[5] **Y. Azlina,** M. N. Azlan, and A. B. Suriani. Structural and Optical Properties of Reduced Graphene Oxide-coated Tellurite Glass Doped with Erbium Nanoparticles. Presented at 8th International Conference on Solid State Science and Technology 2021 **(8th ICSSST 2021)** via Virtual Conference, 1st – 3rd November 2021 **(Oral Presentation)**

05-4506832 pustaka.upsi.edu.my Perpustakaan Tuanku Bainun Kampus Sultan Abdul Jalil Shah PustakaTBainun ptbupsi
05-4506832 pustaka.upsi.edu.my Perpustakaan Tuanku Bainun Kampus Sultan Abdul Jalil Shah PustakaTBainun ptbupsi

05-4506832 pustaka.upsi.edu.my Perpustakaan Tuanku Bainun Kampus Sultan Abdul Jalil Shah PustakaTBainun ptbupsi

APPENDIX C

AWARDS:

[1] **Y. Azlina,** M. N. Azlan, H. R. Shaari, and A. B. Suriani. Optical Properties of Carbon Nanotubes-coated Tellurite Glass: Judd-Ofelt Analysis for Future Fiber Optics. **The Best Project Award.** Presented at 3rd Bionanotechnology Research Seminar & Conference 2022 **(3rd BioNanoSem 2022),** held at The Everly Hotel, Putrajaya, 4th August 2022.

[2] **Y. Azlina** and M. N. Azlan, **Bronze Award.** Structural and Optical Properties of Reduced Graphene Oxide-coated Tellurite Glass Doped with Erbium Nanoparticles. Presented at 5th Materials Technology Challenges (MTC 5.0): A Virtual Competition at 8th International Conference on Solid State Science and Technology 2021 **(8th ICSSST 2021)** via Virtual Competition, 1st – 3rd November 2021.

[3] **Y. Azlina,** M. N. Azlan, H. R. Shaari, and A. B. Suriani. Optical Properties of Carbon Nanotubes-coated Tellurite Glass: Judd-Ofelt Theoretical Analysis for Future Fiber Optics. **Bronze Award**. Presented at Invention, Innovation & Design Exposition **(IIDEX 2022)** via Virtual Competition, 21st – 25th November 2022.

05-4506832 pustaka.upsi.edu.my Perpustakaan Tuanku Bainun Kampus Sultan Abdul Jalil Shah PustakaTBainun ptbupsi

05-4506832 pustaka.upsi.edu.my Perpustakaan Tuanku Bainun Kampus Sultan Abdul Jalil Shah PustakaTBainun ptbupsi

[4] H. R. Shaari, M. N. Azlan, A. B. Suriani, and **Y. Azlina.** A Novelty Technique in Enhancing Optical Fiber Properties through Fusion Graphene Oxide and Tellurite Glass. **Gold Award.** Presented at Invention, Innovation & Design Exposition **(IIDEX 2022)** via Virtual Competition, 21st – 25th November 2022.

05-4506832 pustaka.upsi.edu.my Perpustakaan Tuanku Bainun Kampus Sultan Abdul Jalil Shah PustakaTBainun ptbupsi

05-4506832 pustaka.upsi.edu.my Perpustakaan Tuanku Bainun Kampus Sultan Abdul Jalil Shah PustakaTBainun ptbupsi

J Mater Sci: Mater Electron

Emission properties of reduced graphene oxide-coated Er^{3+}-tellurite glass for fiber optics

Y. Azlina[1], M. N. Azlan[1,*], A. B. Suriani[1], H. R. Shaari[1], Imed Boukhris[2,3], Imen Kebaili[2,4], Naif Mohammed Al-Hada[5], S. A. Umar[6], B. K. Kenzhaliyev[7], M. H. M. Zaid[8], R. Hisam[9], S. M. Iskandar[10], S. N. Nazrin[8], N. N. Yusof[10], Khadijah Mohammedsaleh Katubi[11], Z. A. Alrowaili[12], M. S. Al-Buriahi[13], R. A. Tafida[14], and Fika Fauzi[15]

[1] *Physics Department, Faculty of Science and Mathematics, University Pendidikan Sultan Idris, 35900 Tanjong Malim, Perak, Malaysia*
[2] *Department of Physics, Faculty of Science, King Khalid University, P.O. Box 9004, Abha, Saudi Arabia*
[3] *Laboratoire Des Matériaux Composites Céramiques Et Polymères (LaMaCoP), Faculté Des Sciences de Sfax, BP 805, 3000 Sfax, Tunisia*
[4] *Laboratoire de Physique Appliquée, Groupe de Physique Des Matériaux Luminescents, Faculté Des Sciences de Sfax, Département de Physique, Université de Sfax, BP 1171, 3018 Sfax, Tunisie*
[5] *Shandong Key Laboratory of Biophysics, Institute of Biophysics, Dezhou University, Dezhou 253023, China*
[6] *Department of Physics, Faculty of Science, Federal University Lafia, Lafia, Nasarawa State, Nigeria*
[7] *Institute of Metallurgy and Ore Beneficiation, Satbayev University, Almaty, Kazakhstan*
[8] *Department of Physics, Faculty of Science, Universiti Putra Malaysia, 43400 Serdang, Selangor, Malaysia*
[9] *Faculty of Applied Sciences, Universiti Teknologi MARA, 40450 Shah Alam, Selangor, Malaysia*
[10] *School of Physics, Universiti Sains Malaysia, 11800 USM Penang, Malaysia*
[11] *Department of Chemistry, College of Science, Princess Nourah Bint Abdulrahman University, P .O. Box 84428, Riyadh 11671, Saudi Arabia*
[12] *Department of Physics, College of Science, Jouf University, P.O.Box 2014, Sakaka, Saudi Arabia*
[13] *Department of Physics, Sakarya University, Sakarya, Turkey*
[14] *Physics Department, Nigerian Defence Academy, Kaduna, Nigeria*
[15] *Physics Education Department, Faculty of Mathematics and Natural Sciences, Universitas Negeri Yogyakarta, Yogyakarta 55281, Indonesia*

Received: 1 August 2022
Accepted: 15 October 2022

© The Author(s), under exclusive licence to Springer Science+Business Media, LLC, part of Springer Nature 2022

ABSTRACT

In this work, reduced graphene oxide-coated zinc borotellurite doped with erbium oxide nanoparticles denoted as ZBTEr (NPs)-rGO was studied as an approach to enhance the optical properties of glass materials. Herein, a melt-quenched technique was used to prepare the ZBTEr (NPs) glasses. A simple and inexpensive spray-coated technique was employed to deposit the rGO onto the glass surfaces directly. The morphological studies of ZBTEr (NPs)-rGO glass surfaces were investigated by scanning electron microscope (SEM) and high-resolution transmission electron microscopy (HR-TEM) meanwhile, the structural investigation of ZBTEr (NPs) glasses was revealed by X-ray diffraction

Address correspondence to E-mail: azlanmn@fsmt.upsi.edu.my

https://doi.org/10.1007/s10854-022-09356-6
Published online: 09 November 2022

05-4506832 pustaka.upsi.edu.my Perpustakaan Tuanku Bainun Kampus Sultan Abdul Jalil Shah PustakaTBainun ptbupsi

Sains Malaysiana 52(1)(2023): 261-269
http://doi.org/10.17576/jsm-2023-5201-21

Optical Properties of Reduced Graphene Oxide-Coated Tellurite Glass Doped at Different Erbium Composition

(Sifat Optik Kaca Telurit Bersalut Graphene Oksida Terkurang Didop pada Komposisi Erbium Berbeza)

AZLINA YAHYA, MUHAMMAD NOORAZLAN ABD AZIS* & SURIANI ABU BAKAR

Physics Department, Faculty of Science and Mathematics, Universiti Pendidikan Sultan Idris, 35900 Tanjung Malim, Perak Darul Ridzuan, Malaysia

Received: 31 May 2022/Accepted: 11 October 2022

ABSTRACT

Graphene-based nanomaterials have significant potential to be used as coating materials for glass performance. In this work, reduced graphene oxide (rGO)-coated tellurite glass was synthesized via melt-quenching and low-cost spray coating techniques for improving the optical properties in the glassy matrix. The structural properties investigated using X-Ray Diffraction (XRD) confirmed the structural arrangement of an amorphous nature phase meanwhile, Scanning Electron Microscopy (SEM) analysis proved the morphological structure images of rGO onto the tellurite glass surface. The refractive index value of rGO-coated glass was found higher in the range of 2.402 - 2.775 due to the graphene-based effects. The optical bandgap energy value of rGO-coated glass was improved from 1.913 - 2.980 eV which correlated to the changes in rGO absorption characteristics. The Urbach energy showed a high number of defects in absorption with the presence of rGO structures. By virtue of improved optical properties, the rGO-coated glass may be beneficial to be used as a glass coating material for high optical performance of fiber optics.

Keywords: Erbium nanoparticles; rGO; tellurite glass

05-4506832 pustaka.upsi.edu.my Perpustakaan Tuanku Bainun Kampus Sultan Abdul Jalil Shah PustakaTBainun ptbupsi

ABSTRAK

Bahan nano berasaskan grafin mempunyai potensi ketara untuk digunakan sebagai bahan salutan untuk prestasi kaca. Dalam kajian ini, kaca tellurit disalut grafin oksida terkurang (rGO) telah disintesis melalui teknik lebur lindap dan salutan semburan kos rendah untuk meningkatkan sifat optik dalam kaca matriks. Sifat struktur yang dijalankan menggunakan pembelauan sinar-X (XRD) mengesahkan susunan struktur fasa sifat amorfus manakala, analisis mikroskop pengimbasan elektron (SEM) membuktikan imej struktur morfologi rGO pada permukaan kaca tellurit. Nilai indeks biasan kaca disaluti rGO didapati lebih tinggi dalam julat 2.402 - 2.775 disebabkan oleh kesan berasaskan grafin. Nilai tenaga jurang jalur optik kaca disaluti rGO telah meningkat dari 1.913 - 2.980 eV yang dikaitkan dengan perubahan dalam ciri penyerapan rGO. Tenaga Urbach menunjukkan bilangan kekurangan yang tinggi dalam penyerapan dengan kehadiran struktur rGO. Berdasarkan sifat optik yang dipertingkatkan, kaca disaluti rGO bermanfaat untuk digunakan sebagai bahan salutan kaca untuk prestasi tinggi gentian optik.

Kata kunci: Kaca telurit; nanozarah erbium; rGO

INTRODUCTION

Graphene oxide (GO) is oxidized from graphene derivative that possesses an atomic arrangement similar to the graphene sheet due to its oxygenated carbon backbone and adhered mostly with hydroxyl, carboxyl, carbonyl, and epoxide groups on nanosheets (Al-Gaashani et al. 2019). GO has attracted attention as a unique material and solution-possessable multifunction carbon platform via modifying the electronically conducting sp^2 to insulating sp^3 carbon atoms and may tune the bandgap of GO sheets which in turn also affects nonlinear optical (NLO) properties of GO (Abozied et al. 2021; Aradhana et al. 2018). The tuning of bandgap caused by the existence of various oxygen-containing functional groups localized at the edges enables GO as a promising prospect in the field of optoelectronics, sensors, electrodes, as well as lithium-ion batteries (Bhuyan et al. 2016; Cao et al. 2017). However, the higher graphitic structure defects

05-4506832 pustaka.upsi.edu.my Perpustakaan Tuanku Bainun Kampus Sultan Abdul Jalil Shah PustakaTBainun ptbupsi

05-4506832 pustaka.upsi.edu.my Perpustakaan Tuanku Bainun Kampus Sultan Abdul Jalil Shah PustakaTBainun ptbupsi

Optical Materials 117 (2021) 111138

Contents lists available at ScienceDirect

Optical Materials

journal homepage: www.elsevier.com/locate/optmat

Research Article

Graphene oxide deposition on neodymium doped zinc borotellurite glass surface: Optical and polarizability study for future fiber optics

Y. Azlina [a], M.N. Azlan [a,*], S.S. Hajer [b], M.K. Halimah [c], A.B. Suriani [a], S.A. Umar [d], R. Hisam [e], M. H.M. Zaid [c], S.M. Iskandar [f], B.K. Kenzhaliyev [g], A.V. Nitsenko [g], N.N. Yusof [h], Boukhris Imed [i,j]

[a] Physics Department, Faculty of Science and Mathematics, University Pendidikan Sultan Idris, 35900, Tanjong Malim, Perak, Malaysia
[b] Physics Department, Faculty of Science, Elmergib University, Port Street Al Khums, 40414, Elmergib, Libya
[c] Department of Physics, Faculty of Science, Universiti Putra Malaysia, 43400, Serdang, Selangor, Malaysia
[d] Department of Physics, Faculty of Science, Federal University Lafia, Lafia, Nasarawa State, Nigeria
[e] Faculty of Applied Sciences, Universiti Teknologi MARA, 40450, Shah Alam, Selangor, Malaysia
[f] School of Physics, Universiti Sains Malaysia, 11800, USM, Penang, Malaysia
[g] Institute of Metallurgy and Ore Beneficiation, Satbayev University, Almaty, Kazakhstan
[h] Physics Department, AOMRG & Laser Centre, Faculty of Science, Universiti Teknologi Malaysia, 81310, Johor Bahru, Johor, Malaysia
[i] Department of Physics, Faculty of Science, King Khalid University, P.O. Box 9004, Abha, Saudi Arabia
[j] Université de Sfax, Faculté des Sciences de Sfax, Département de Physique, Laboratoire des matériaux composites céramiques et polymères (LaMaCoP) Faculté des sciences de Sfax BP 805, Sfax 3000, Tunisie

ARTICLE INFO

Keywords:
Optical bandgap
Refractive index
Oxide ion polarizability

ABSTRACT

Neodymium oxide doped tellurite-based glass has been widely documented for potential uses in optoelectronics, but graphene oxide (GO)-coated tellurite-based glass has rarely been reported. In this work, we compare two sets of glass series which were GO-coated and uncoated tellurite-based glass series denoted as ZBTNd-GO and ZBTNd, respectively. The two sets of glasses were fabricated via melt-quenched process. A set of glass was coated with GO using low-cost spray coating method. The structural and morphological properties of the glass samples were investigated to confirm the type of structure in glass and formation of graphene oxide on glass surface. The X-ray diffraction (XRD) pattern confirmed the amorphous structural arrangement in both sets of glass series. The morphological study proved the existence of GO layers on top of the ZBTNd-GO surface. The optical bandgap energy of ZBTNd-GO glass was found in the range of 3.253 eV–3.381 eV which was higher than ZBTNd glass. Meanwhile, the refractive index of ZBTNd-GO glass varies from 2.301 to 2.332 which was higher than ZBTNd glass due to the presence of functionalized oxygenated groups in GO structure. The oxide ion polarizability of ZBTNd-GO glass was found decreased due to the shift of optical band gap when coated with GO. This work offers a new form of glass that could be used as a new strategy to upgrade the current photonic materials.

1. Introduction

Graphene oxide (GO) is oxidized from a graphene derivative that can be described as a carbon-based substance composed primarily of an abundant content of oxygen-containing functionality groups found at the edges of GO structures [1,2]. The excellent properties in GO have an extraordinary interest to be included in the optoelectronics application [3,4], super-capacitors [5,6], or as an energy charge storage like GO-based lithium ion battery [7], respectively as well as suitable to be applied in the enhancement of sensing [8] and solar cells [9] applications.

In particular, the widening of band gap energy in GO structures which due to the pristine graphene through the transformation from sp^2 to sp^3 hybrid via an oxidation process, can be considered to be beneficial for enhancing the optical properties in the glass materials [10,11]. The tuning of GO band gap energy implies, in particular, the presence of higher functional groups of oxygen, which can be correlated with the effect of oxidation in GO structures [12]. The integration of graphene oxide and tellurite glass is therefore a way to further enhance the optical properties of the glass network system, as the inclusion of GO itself would perform as an ideal candidate for the production of excellent glass coatings.

* Corresponding author.
E-mail address: azlanmn@fsmt.upsi.edu.my (M.N. Azlan).

https://doi.org/10.1016/j.optmat.2021.111138
Received 22 December 2020; Received in revised form 13 April 2021; Accepted 27 April 2021
Available online 13 May 2021
0925-3467/© 2021 Elsevier B.V. All rights reserved.

05-4506832 pustaka.upsi.edu.my Perpustakaan Tuanku Bainun Kampus Sultan Abdul Jalil Shah PustakaTBainun ptbupsi

05-4506832 pustaka.upsi.edu.my Perpustakaan Tuanku Bainun Kampus Sultan Abdul Jalil Shah PustakaTBainun ptbupsi

Chalcogenides Letters Vol. 18, No. 9, September 2021, p. 525 - 534

Polarizability of erbium-doped zinc-tellurite glasses coated with graphene oxide for telecommunication devices

Y. Azlina[a], M. N. Azlan[a,*], H. R. Shaari[a], S. N. Nazrin[b], N. M. Al-Hada[c], S. A. Umar[d], M. H. M. Zaid[b], R. Hisam[e], S. M. Iskandar[f], B. K. Kenzhaliyev[g], G. K. Kassymova[g], I. Boukhris[h,i]

[a]*Physics Department, Faculty of Science and Mathematics, University Pendidikan Sultan Idris, 35900 Tanjong Malim, Perak, Malaysia*

[b]*Department of Physics, Faculty of Science, Universiti Putra Malaysia, 43400, Serdang, Selangor, Malaysia*

[c]*Shandong Key Laboratory of Biophysics, Institute of Biophysics, Dezhou University, Dezhou 253023, China*

[d]*Department of Physics, Faculty of Science, Federal University Lafia, Lafia, Nasarawa State, Nigeria*

[e]*Faculty of Applied Sciences, Universiti Teknologi MARA, 40450 Shah Alam, Selangor, Malaysia*

[f]*School of Physics, Universiti Sains Malaysia, 11800 USM, Penang, Malaysia;*

[g]*Institute of Metallurgy and Ore Beneficiation, Satbayev University, Almaty, Kazakhstan*

[h]*Department of Physics, Faculty of Science, King Khalid University; P.O. Box 9004, Abha, Saudi Arabia.*

[i]*Université de Sfax, Faculté des Sciences de Sfax, Département de Physique, Laboratoire des matériaux composites céramiques et polymères (LaMaCoP) Faculté des sciences de Sfax BP 805, Sfax 3000, Tunisie*

Graphene-based nanomaterials offer superior properties especially in optical performance. The existence of oxygen functionalized group in graphene active layers is beneficial to enhance the optical properties of current tellurite glass. In this work, two series of glasses denoted as ZBTEr (uncoated) and ZBTEr-GO (coated) were successfully prepared using melt-quenching and low-cost spray coating techniques. X-ray diffraction analysis was done on both glass series and confirmed the amorphous structural arrangement in the glass system. Morphological study was investigated by using Scanning Electron Microscopy (SEM) and revealed the distribution of graphene layers on the glass surface. The UV-Vis spectroscopy was carried out and several absorption bands were determined for both series of glasses. The computation of oxide ion polarizability and optical basicity were investigated based on Lorentz-Lorentz equation. The oxide ion polarizability and optical basicity for ZBTEr-GO (coated) glasses were found higher than ZBTEr (uncoated) glasses due to the existence of sp^2 graphitic attached on the oxygenic functional groups in GO layers. The metallization criterion values for ZBTEr-GO (coated) glasses were found decreased and tend to be more metallic. Hence, the deposition of graphene layers on the tellurite glasses offer a new strategy to improve the current telecommunication devices.

(Received June 21, 2021; Accepted September 10, 2021)

Keywords: Oxide ion polarizability, Optical basicity, Metallization criterion, Graphene oxide, Tellurite glass

1. Introduction

Graphene is a two-dimensional of single-atom-thick sheet with sp^2 bonded carbon atoms in a hexagonal structure. The use of graphene in broad optical applications display their remarkable usefulness in the field of optics, photonics, and optoelectronics devices for instance,

* Corresponding author: azlanmn@fsmt.upsi.edu.my

05-4506832 pustaka.upsi.edu.my Perpustakaan Tuanku Bainun Kampus Sultan Abdul Jalil Shah PustakaTBainun ptbupsi

J Mater Sci: Mater Electron (2021) 32:24415–24428

Red emission, upconversion and intensity parameters of erbium oxide doped tellurite glass for laser glass

M. N. Azlan[1,*], Y. Azlina[1], H. R. Shaari[1], S. N. Nazrin[2], Naif Mohammed Al-Hada[3], Imed Boukhris[4,5], S. A. Umar[6], M. H. M. Zaid[2], R. Hisam[7], S. M. Iskandar[8], and B. K. Kenzhaliyev[9]

[1] *Physics Department, Faculty of Science and Mathematics, University Pendidikan Sultan Idris, 35900 Tanjong Malim, Perak, Malaysia*
[2] *Department of Physics, Faculty of Science, Universiti Putra Malaysia, 43400 Serdang, Selangor, Malaysia*
[3] *Shandong Key Laboratory of Biophysics, Institute of Biophysics, Dezhou University, Dezhou 253023, China*
[4] *Department of Physics, Faculty of Science, King Khalid University, P.O. Box 9004, Abha, Saudi Arabia*
[5] *Laboratoire des Matériaux Composites Céramiques et Polymères (LaMaCoP), Faculté des Sciences de Sfax, Département de Physique, Université de Sfax, BP 805, 3000 Sfax, Tunisie*
[6] *Department of Physics, Faculty of Science, Federal University Lafia, Lafia, Nasarawa, Nigeria*
[7] *Faculty of Applied Sciences, Universiti Teknologi MARA, 40450 Shah Alam, Selangor, Malaysia*
[8] *School of Physics, Universiti Sains Malaysia (USM), 11800 Penang, Malaysia*
[9] *Institute of Metallurgy and Ore Beneficiation, Satbayev University, Almaty, Kazakhstan*

05-4506832 pustaka.upsi.edu.my Perpustakaan Tuanku Bainun Kampus Sultan Abdul Jalil Shah PustakaTBainun ptbupsi

Received: 24 July 2021
Accepted: 25 August 2021
Published online: 1 September 2021

© The Author(s), under exclusive licence to Springer Science+Business Media, LLC, part of Springer Nature 2021

ABSTRACT

This work presents the effect of erbium oxide in tellurite glass on the intensity parameters, emission and upconversion to be used as laser glass. We select 0.04 mol fraction of erbium oxide in tellurite glass as it gives the optimum results for glass stability, luminescence and intensity parameters. The structural arrangement of glass matrices was revealed by XRD analysis. The amorphous structural arrangement was found and there was no crystalline structure existed in the glass matrix. The FTIR analysis revealed the existence of TeO_3 non-bridging oxygen which has important role in the shifting of the optical parameters. The Judd–Ofelt analysis (intensity parameters, $\Omega_\lambda = 2, 4, 6$) were studied by applying nine transition states obtained from UV–Vis-NIR absorption spectrum which were $^4G_{11/2} + {}^2H_{9/2} + {}^4F_{5/2} + {}^4F_{7/2} + {}^2H_{11/2} + {}^4S_{3/2} + {}^4F_{9/2} + {}^4I_{9/2} + {}^4I_{11/2}$. The obtained results for the intensity parameters were in accordance by the following trends $\Omega_2 > \Omega_4 > \Omega_6$. A broad red emission at 648 nm was found with excitation state of 380 nm. Four emission peaks were found from upconversion emission spectrum as follows; 381 nm, 420 nm, 466 nm and 560 nm which correspond to $^4G_{11/2} \rightarrow {}^4I_{15/2}$, $^4F_{3/2} \rightarrow {}^4I_{15/2}$, $^4F_{7/2} \rightarrow {}^4I_{15/2}$ and $^4S_{3/2} \rightarrow {}^4I_{15/2}$. The prominent emission for upconversion was 560 nm which produce yellow emission. Based on these results, erbium doped boro-tellurite glass is capable to be utilized as red, blue and green glass lasers.

Address correspondence to E-mail: azlanmn@fsmt.upsi.edu.my

https://doi.org/10.1007/s10854-021-06917-z

05-4506832 pustaka.upsi.edu.my Perpustakaan Tuanku Bainun Kampus Sultan Abdul Jalil Shah PustakaTBainun ptbupsi

05-4506832 pustaka.upsi.edu.my Perpustakaan Tuanku Bainun Kampus Sultan Abdul Jalil Shah PustakaTBainun ptbupsi

Chalcogenide Letters Vol. 19, No. 8, August 2022, p. 565 - 577

Oxide ion polarizability, optical basicity, and metallization criterion of GO-coated Nd_2O_3 (NPs) - TeO_2 glass for linear optical fibre

H. R. Shaari[a], M. N. Azlan[a,*], Y. Azlina, N. M. Al-Hada[b], S. A. Umar[c], B. K. Kenzhaliyev[d], M. H. M. Zaid[e], R. Hisam[f], N. N. Yusof[g]

[a]*Physics Department, Faculty of Science and Mathematics, University Pendidikan Sultan Idris, 35900 Tanjong Malim, Perak, Malaysia;*
[b]*Shandong Key Laboratory of Biophysics, Institute of Biophysics, Dezhou University, Dezhou 253023, China*
[c]*Department of Physics, Faculty of Science, Federal University Lafia, Lafia, Nasarawa State, Nigeria*
[d]*Institute of Metallurgy and Ore Beneficiation, Satbayev University, Almaty, Kazakhstan;*
[e]*Department of Physics, Faculty of Science, Universiti Putra Malaysia, 43400, Serdang, Selangor, Malaysia;*
[f]*Faculty of Applied Sciences, Universiti Teknologi MARA, 40450 Shah Alam, Selangor, Malaysia;*
[g] *School of Physics, Universiti Sains Malaysia, 11800 USM, Penang, Malaysia*

The versatility of graphene oxide (GO) as coating materials on the glass surface is a new revolution in the advanced glass era. In this work, GO liquid solution was prepared by using electrochemical exfoliation in an electrolyte solution assisted by different surfactants. Meanwhile, a glass series was prepared by using the conventional melt-quenched technique. A low-cost and simple spray deposition technique was used to deposit the GO on the glass sample. The obtained glass series was denoted as GO coated TNd (NPs), meanwhile, the uncoated glass was labelled as uncoated TNd (NPs). The linear optical properties of GO coated TNd (NPs) glass series was determined using UV-Vis spectrophotometer and utilizing the Lorentz-Lorentz equation to determine the value of polarizability. X-ray diffraction spectra revealed the amorphous structural characteristics of the glass series. The SEM morphological image revealed the variation of GO distribution on the glass surface due to the agglomeration and inhomogeneity of GO distribution on the glass surface. The homogeneity of GO distribution on the glass surface is negligible in this work as we focus solely on the effect of GO on glass properties. According to the observations, the value of GO-coated TNd (NPs) is in the range 3.4531-3.8549 Å and uncoated TNd (NPs) is in the range 2.709- 2.774 Å. Meanwhile, the optical basicity value ranges from 1.220 to 1.262. These results demonstrate that the polarizability of oxide ions and optical basicity values of the GO coated TNd (NPs) glass series was higher than the uncoated TNd (NPs) glass. The metallization criterion for the GO-coated TNd (NPs) glass system is in the range of $0.3 < M < 0.4$. Based on these results, the obtained glasses are promising in linear optical glass fibre.

(Received May 17, 2022; Accepted August 30, 2022)

Keywords: Graphene oxide, Neodymium-doped, Tellurite, Glasses coating, Optical basicity, Metallization criterion

1. Introduction

The discovery and availability of nanomaterials such as graphene oxide (GO) have exceptional mechanical, electrical, thermal, optical, and physical characteristics [1]. The excellent properties of GO have been attracted the interest of many applications [2], [3] such as optoelectronics, supercapacitors, energy storage devices such as GO-based lithium rechargeable

* Corresponding author: azlanmn@fsmt.upsi.edu.my
https://doi.org/10.15251/CL.2022.198.565

05-4506832 pustaka.upsi.edu.my Perpustakaan Tuanku Bainun Kampus Sultan Abdul Jalil Shah PustakaTBainun ptbupsi

05-4506832 pustaka.upsi.edu.my Perpustakaan Tuanku Bainun Kampus Sultan Abdul Jalil Shah PustakaTBainun ptbupsi

Journal of Inorganic and Organometallic Polymers and Materials (2021) 31:4349–4359
https://doi.org/10.1007/s10904-021-02061-7

Investigation of Structural and Optical Properties of Graphene Oxide-Coated Neodymium Nanoparticles Doped Zinc-Tellurite Glass for Glass Fiber

H. R. Shaari[1] · M. N. Azlan[1] · Y. Azlina[1] · S. S. Hajer[2] · S. N. Nazrin[3] · S. A. Umar[4] · B. K. Kenzhaliyev[5] · Imed Boukhris[6,7] · Naif Mohammed Al-Hada[8]

Received: 14 April 2021 / Accepted: 24 June 2021 / Published online: 2 July 2021
© The Author(s), under exclusive licence to Springer Science+Business Media, LLC, part of Springer Nature 2021

Abstract

Carbon-based materials such as graphene oxide are known as attractive candidate to improve the current optoelectronic and laser devices. In this work, neodymium nanoparticles doped zinc-tellurite glass coated with graphene oxide (GO) denoted as ZBTNd (NPs)-GO was prepared via low-cost melt-quenching method and simple spray coating method. The structural properties of the glass system had been carried out by using X-ray diffraction (XRD) and confirmed its amorphous structural arrangement with non-existence of crystalline structure. The TeO3 and BO3 structural units were found dominant in tellurite glass network as determined by Fourier transforms infrared spectrometer (FTIR). High number of oxygen functional groups and stacked of graphene layers on the glass surface were revealed by field scanning electron microscopy (FESEM) and Raman spectroscopy. The optical band gap energy values were found to decrease in the range of 2.665–2.405 eV along with dopant concentration. In the meantime, the refractive index values were found more than $n > 2.00$ and fall in the range of 2.12 to 2.20. The electronic polarization was calculated by using Lorentz-Lorentz equation and found in the range of 6.516 to 7.211 $Å^3$. Based on these results, the improvements on optical properties of tellurite glass have been made to be used in laser application.

Keywords Tellurite glasses · Graphene oxide · Band gap · Refractive index · Laser application

✉ M. N. Azlan
azlanmn@fsmt.upsi.edu.my

1 Physics Department, Faculty of Science and Mathematics, University Pendidikan Sultan Idris, 35900 Tanjong Malim, Perak, Malaysia

2 Physics Department, Faculty of Science, Elmergib University, Port Street Al Khums, 40414, Elmergib, Libya

3 Department of Physics, Faculty of Science, Universiti Putra Malaysia, 43400 Serdang, Selangor, Malaysia

4 Department of Physics, Faculty of Science, Federal University Lafia, Lafia, Nasarawa State, Nigeria

5 Institute of Metallurgy and Ore Beneficiation, Satbayev University, Almaty, Kazakhstan

6 Department of Physics, Faculty of Science, King Khalid University, P.O. Box 9004, Abha, Saudi Arabia

7 Département de Physique, Laboratoire des Matériaux Composites Céramiques et Polymères (LaMaCoP), Faculté des Sciences de Sfax, Université de Sfax, BP 805, Sfax 3000, Tunisia

8 Shandong Key Laboratory of Biophysics, Institute of Biophysics, Dezhou University, Dezhou 253023, China

1 Introduction

The role of graphene in optoelectronics application especially on laser glass has been actively investigated in recent years. Novoselov reported graphene-based materials to have outstanding properties such as excellent electrical conductivity, flexibility, and hardness properties [1]. The interest of graphene oxide (GO) in optoelectronic devices has increased extensively due to its low-cost production and high electrical performance. Graphene oxide consists of stacked layers and abundant of oxygen functional group. Graphene oxide is also significant in the application of optics, photonics, and optoelectronic devices [2]. The significant impacts of GO on tellurite glass for optical fiber have been reported by Azlina et.al [3] which found the improvement of optical properties due to the presence of oxygen-containing functional groups in GO layers.

Glass materials with outstanding optical properties is essential to improve the current optical application such as optical switches, sensors, solar cells, and

05-4506832 pustaka.upsi.edu.my Perpustakaan Tuanku Bainun Kampus Sultan Abdul Jalil Shah PustakaTBainun ptbupsi

05-4506832 pustaka.upsi.edu.my Perpustakaan Tuanku Bainun Kampus Sultan Abdul Jalil Shah PustakaTBainun ptbupsi

The Effect of rGO On Optical Properties of Neodymium Nanoparticles Doped Tellurite Glass System

Hafizah Rajaa Shaari, Muhammad Noorazlan, Suriani Abu Bakar, Azlina Yahya*
Nanotechnology Research Centre, Physics Department,
Faculty of Science and Mathematics, Universiti Pendidikan Sultan Idris,
35900 Tanjung Malim, Perak, Malaysia
** azlanmn@fsmt.upsi.edu.my*

ABSTRACT

Nanomaterials based on graphene have outstanding properties, particularly in terms of optical performance. Using melt-quenching and low-cost spray coating procedures, we effectively generated a series of reduced graphene oxide-coated tellurite glasses doped with neodymium nanoparticles, denoted as rGO-ZBTNd (NPs) glasses. An X-ray diffraction study of glass samples validated the glass system's amorphous structure. FESEM morphological analysis was used to evaluate the appearance of rGO on the glass substrate and revealed the dispersion of rGO. UV-Vis spectroscopy was used to determine different absorption bands. The refractive index value calculated using the Dimitrov and Sakka equation was found to be more than n > 2.000 and in the range of 2.339 to 2.657 when compared to uncoated samples. On the basis of these findings, a new method involving rGO deposited on tellurite glass has been developed to improve the tellurite glass currently utilised in laser applications.

Keywords: *Tellurite Glass; Reduced Graphene Oxide; Optical Parameter; Refractive Index*

Introduction

Tellurium oxide is a potential glass forming that has been shown to be useful in current technological applications. Because of its unique qualities, tellurite

ISSN 1823-5514, eISSN 2550-164X
Received for review: 2022-08-23
Accepted for publication: 2022-10-11
Published: 2022-11-15
© 2022 College of Engineering,
Universiti Teknologi MARA (UiTM), Malaysia.

05-4506832 pustaka.upsi.edu.my Perpustakaan Tuanku Bainun Kampus Sultan Abdul Jalil Shah PustakaTBainun ptbupsi

Solid State Phenomena
ISSN: 1662-9779, Vol. 317, pp 95-99
doi:10.4028/www.scientific.net/SSP.317.95
© 2021 Trans Tech Publications Ltd, Switzerland
Submitted: 2020-01-06
Revised: 2020-07-30
Accepted: 2020-07-30
Online: 2021-05-10

The Optical Performance of Holmium Oxide Doped Tellurite Glass for Potential Optical Fiber

MUHAMMAD NOORAZLAN Abd Azis[1,2,a*], HALIMAH Mohamed Kamari[3,b], SURIANI Abu Bakar[1,2,c], AZLINA Yahya[1,2,d] and UMAR Saad Aliyu[4,e]

[1]Physics Department, Universiti Pendidikan Sultan Idris, 43400, Tanjung Malim, Perak, Malaysia

[2]Nanotechnology Research Center, Faculty of Science and Mathematics, Universiti Pendidikan Sultan Idris, 35900 Tanjung Malim, Perak, Malaysia

[3]Physics Department, Universiti Putra Malaysia, 35900, Serdang, Selangor, Malaysia

[4]Department of Physics, Faculty of Science, Federal University Lafia, Nigeria

[a]azlanmn@fsmt.upsi.edu.my, [b]halimahmk@upm.edu.my, [c]suriani@fsmt.upsi.edu.my, [d]azlinayahya15@gmail.com, [e]usaltilde@yahoo.com

Keywords: Tellurite glass, holmium oxide, optical fiber materials List the keywords covered in your paper.

Abstract. Borotellurite glass had been widely applied in the field of optical communications and devices. In this work, holmium oxides doped borotellurite glass had been successfully fabricated via conventional melt-quenched technique. The structural properties of holmium doped tellurite glass were found using x-ray diffraction (XRD) method. The nonexistence of sharp peaks in XRD pattern shows that the inclusion of holmium tellurite glass leads to the formation long range of disorderness. The optical properties of the glass system such as refractive index and optical band gap energy are investigated using UV-Vis spectrophotometer. The value of refractive index is found in nonlinear trend along with holmium oxides concentration. It is found that the refractive index is more than 2 at 0.01, 0.03 and 0.04 of holmium concentrations. The optical band gap energy was found in similar trend with refractive index which is in nonlinear pattern.

Introduction

The extensive research on optical glass materials had been done to produce the high optical ability in glass materials for optoelectronics applications. Among the heavy metal oxides, tellurite oxide shows outstanding optical properties such as high refractive index, high dielectric constants, a wide band infrared transmittance and large third order non-linear optical susceptibility [1]. It is known that tellurite glass has high potential to be used in core clad fiber optics [1]. However, the current materials for fiber optics are made from silicate oxide which has numerous weaknesses for fiber optics [2]. Hence, it is highly important to introduce tellurite oxide as the novel materials for fiber optics.

The single component of tellurite glass has low stability and prone to fractures. The multi-component glass system is the best solution to increase the glass forming stability and to enhance the structural properties. Boron and zinc oxides had been chosen in this research due to several reasons as follows [2]:

a. Boron oxide: Excellent materials to increase the hardness properties and phonon energy (from 770 to 1335 cm^{-1})
b. Zinc oxide: Outstanding materials to reduce the melting temperature and may act as former glass

The introduction of rare earth oxides as dopants in glass materials had been widely investigated. Rare earth oxides are known to have sharp spectral properties which is beneficial to be used in wide optoelectronics applications. Erbium oxide are the well-known dopant which had been used in many glass materials. However, there are few more rare-earth oxides which have high potential to be used in optical glass materials. Holmium oxide is one of the rare-earth oxides which have high potential to improve the optical performance of tellurite glass.

All rights reserved. No part of contents of this paper may be reproduced or transmitted in any form or by any means without the written permission of Trans Tech Publications Ltd, www.scientific.net. (#590096533-27/05/22,18:05:00)

Organizer

UNIVERSITI MALAYSIA PERLIS

Special Interest Group (SIG)
Faculty of Chemical Engineering & Technology
Universiti Malaysia Perlis

Co-Organizer

THE PAPUA NEW GUINEA UNIVERSITY OF TECHNOLOGY

King Mongkut's University of Technology Thonburi

CERTIFICATE

OF PARTICIPATION

AZLINA YAHYA

as

PRESENTER

at the

WORLD INTEGRATED CHEMICAL & MATERIAL ENGINEERING TECHNOLOGY CONFERENCE (WiCMETC 2023)

4 - 5th February 2023
Avana Grand Hotel, Bangkok, Thailand

PROF. TS. DR. MOHD MUSTAFA AL BAKRI BIN ABDULLAH
Dean
Faculty of Chemical Engineering & Technology
Universiti Malaysia Perlis

#UniMAPMantap #UniMAP4Society #Engineering4Society

Ilmu I Keikhlasan I Kecemerlangan

#UniversitiMalaysiaPerlis

#gemilangbersamaunimap

www.unimap.edu.my

Universiti Teknologi MARA | Pejabat Timbalan Naib Canselor Penyelidikan dan Inovasi

iidex2022

Invention, Innovation & Design Exposition

DISRUPTIVE . SUSTAINABLE . UNITY

Certificate of PARTICIPATION

This certificate is presented to

AZLINA BINTI YAHYA

Title: CARBON NANOTUBES-COATED TELLURITE GLASS: OPTICAL PROPERTIES AND JUDD-OFELT THEORY ANALYSIS FOR FUTURE FIBER OPTICS

in recognition of participation in iidex2022

PROFESSOR TS. DR NORAZAH ABD RAHMAN
Deputy Vice-Chancellor (Research & Innovation)
Universiti Teknologi MARA

Main Sponsor :

BANK ISLAM

UNIVERSITI TEKNOLOGI MARA

UNIVERSITI MALAYSIA KELANTAN

THE MALAYSIAN SOLID STATE SCIENCE AND TECHNOLOGY SOCIETY
MASS



Certificate OF PARTICIPATION

THIS CERTIFICATE IS AWARDED TO

MISS AZLINA YAHYA

AS

E-POSTER PRESENTER

IN

2022 RCSST

31st REGIONAL CONFERENCE
ON SOLID STATE SCIENCE AND TECHNOLOGY 2022
6 - 8 SEPTEMBER 2022

Ts. DR. NOR HAKIMIN BIN ABDULLAH
CHAIRMAN
31st RCSSST 2022

PROFESSOR DR. ABDUL HALIM BIN SHAARI
PRESIDENT
THE MALAYSIAN SOLID STATE SCIENCE AND TECHNOLOGY SOCIETY (MASS)

ENTREPRENEURSHIP IS OUR THRUST

Cert. ID: 184

BioNanoSem
BIONANOTECHNOLOGY RESEARCH

Certificate of Award

This is certify that

AZLINA YAHYA

has been awarded as

Presenter (Physical)

for the project entitled

Optical Properties of Carbon Nanotubes-coated Tellurite Glass: Judd-Ofelt Analysis for Future Fiber Optics

at the 3rd Bionanotechnology Research Seminar and Conference (BioNanoSem 2022)

held on 4th August 2022 at The Everly Putrajaya Hotel, Putrajaya, Malaysia and online platform.

Assoc. Prof. Ts. ChM. Dr. Nik Ahmad Nizam bin Nik Malek
Director
Centre for Sustainable Nanomaterials (CSNano)
Universiti Teknologi Malaysia (UTM)

Assoc. Prof. Dr. Ruslinda A. Rahim
Director
National Nanotechnology Centre (NNC)
Ministry of Science, Technology & Innovation (MOSTI)

Prof. Dr. Ismail Zainol
President
Malaysian Biomaterial Society (MBS)

Organized by UTM UNIVERSITI TEKNOLOGI MALAYSIA csnano Co-organized by KEMENTERIAN SAINS, TEKNOLOGI DAN INOVASI MALAYSIAN BIOmaterials SOCIETY Persatuan Biobahan Malaysia

"Prospering Bionanotechnology Research, Innovation and Commercialization"

Universiti Teknologi MARA Cawangan Perlis Kampus Arau

i-IDeA 2020 THE 5TH INTERNATIONAL INNOVATION, DESIGN AND ARTICULATION

ICSSST 2021 8TH INTERNATIONAL CONFERENCE ON SOLID STATE SCIENCE & TECHNOLOGY

CERTIFICATE *OF* PRESENTATION

This is to certify that

AZLINA YAHYA

in the

8th International Conference on Solid State Science and Technology (ICSSST 2021)

via

Virtual Conference, 1st-3rd November 2021

at the

5th International Innovation, Design and Articulation (i-IDeA 2020)

Prof. Dr. Hj. Khudzir Hj. Ismail
Rector
Universiti Teknologi MARA Perlis Branch, Malaysia

Prof. Ts. Dr. Mohd Azlan Mohd Ishak
Chairman of ICSSST 2021
Universiti Teknologi MARA Perlis Branch, Malaysia

Prof. Dr. Abdul Halim Shaari
President
The Malaysian Solid State Science and Technology Society

"Empowering Research, Innovation Ideas and Entrepreneurship Towards Sustainable Economy"

Strategic partners :

Sponsors :

BioNanoSem
BIONANOTECHNOLOGY RESEARCH

Certificate of Award

This is certify that

AZLINA YAHYA

has been awarded as

Best Project Award (Physical)

for the project entitled

Optical Properties of Carbon Nanotubes-coated Tellurite Glass: Judd-Ofelt Analysis for Future Fiber Optics

at the 3rd Bionanotechnology Research Seminar and Conference (BioNanoSem 2022)

held on 4th August 2022 at The Everly Putrajaya Hotel, Putrajaya, Malaysia and online platform.

Assoc. Prof. Ts. ChM. Dr. Nik Ahmad Nizam bin Nik Malek
Director
Centre for Sustainable Nanomaterials (CSNano)
Universiti Teknologi Malaysia (UTM)

Assoc. Prof. Dr. Ruslinda A. Rahim
Director
National Nanotechnology Centre (NNC)
Ministry of Science, Technology & Innovation (MOSTI)

Prof. Dr. Ismail Zainol
President
Malaysian Biomaterial Society (MBS)

Organized by | UTM UNIVERSITI TEKNOLOGI MALAYSIA csnano

Co-organized by | KEMENTERIAN SAINS, TEKNOLOGI DAN INOVASI | MALAYSIAN BIOmaterials SOCIETY Persatuan Biobahan Malaysia

"Prospering Bionanotechnology Research, Innovation and Commercialization"

Universiti Teknologi MARA Cawangan Perlis Kampus Arau

i-IDeA 2020 THE 5TH INTERNATIONAL INNOVATION, DESIGN AND ARTICULATION

ICSSST 2021 8TH INTERNATIONAL CONFERENCE ON SOLID STATE SCIENCE & TECHNOLOGY

CERTIFICATE OF AWARD

This is to certify that

Azlina Yahya, Ts. Dr. Muhammad Noorazlan Abd Azis

with the project

Optical Properties of Reduced Graphene Oxide-Coated Tellurite Glass for Fiber Optics Technology

have been awarded

Bronze Award

in the

5th Materials Technology Challenge (MTC5.0): A Virtual Competition

at the

8th International Conference on Solid State Science and Technology (ICSSST 2021)

Prof. Dr. Hj. Khudzir Hj. Ismail
Rector
Universiti Teknologi MARA Perlis Branch, Malaysia

Prof. Ts. Dr. Mohd Azlan Mohd Ishak
Chairman of ICSSST 2021
Universiti Teknologi MARA Perlis Branch, Malaysia

Prof. Dr. Abdul Halim Shaari
President
The Malaysian Solid State Science and Technology Society

"Empowering Research, Innovation Ideas and Entrepreneurship Towards Sustainable Economy"

Strategic partners

Sponsors

UNIVERSITI TEKNOLOGI MARA

Pejabat
Timbalan Naib Canselor
Penyelidikan dan Inovasi

iidex2022

Invention, Innovation & Design Exposition

DISRUPTIVE . SUSTAINABLE . UNITY

Certificate of AWARD

Heartiest Congratulations to

AZLINA BINTI YAHYA

on the successful achievement of

Title: CARBON NANOTUBES-COATED TELLURITE GLASS: OPTICAL PROPERTIES AND JUDD-OFELT THEORY ANALYSIS FOR FUTURE FIBER OPTICS

for being awarded the iidex2022

BRONZE AWARD

PROFESSOR TS. DR NORAZAH ABD RAHMAN
Deputy Vice-Chancellor (Research & Innovation)
Universiti Teknologi MARA

UNIVERSITI TEKNOLOGI MARA

Main Sponsor :

BANK ISLAM

Pejabat
Timbalan Naib Canselor
Penyelidikan dan Inovasi

UNIVERSITI TEKNOLOGI MARA

iidex2022

Invention, Innovation & Design Exposition

DISRUPTIVE . SUSTAINABLE . UNITY

Certificate of AWARD

Heartiest Congratulations to

HAFIZAH RAJAA BINTI SHAARI
MUHAMMAD NOORAZLAN BIN ABD AZIS
AZLINA BT YAHYA
SURIANI BT ABU BAKAR

on the successful achievement of

Title: A NOVELTY TECHNIQUE IN ENHANCING OPTICAL FIBER PROPERTIES THROUGH FUSION GRAPHENE OXIDE AND TELLURITE GLASS

for being awarded the iidex2022

GOLD AWARD

PROFESSOR TS. DR NORAZAH ABD RAHMAN
Deputy Vice-Chancellor (Research & Innovation)
Universiti Teknologi MARA

UNIVERSITI TEKNOLOGI MARA

Main Sponsor :

BANK ISLAM